Titre: Title:	Analytical and Experimental Evaluation of the Settlement and Volume Variation of Tailings Slurry Deposited in Containment Structures
Auteur: Author:	Jiahao Qin
Date:	2020
Type:	Mémoire ou thèse / Dissertation or Thesis
Référence: Citation:	Qin, J. (2020). Analytical and Experimental Evaluation of the Settlement and Volume Variation of Tailings Slurry Deposited in Containment Structures [Mémoire de maîtrise, Polytechnique Montréal]. PolyPublie. https://publications.polymtl.ca/5247/

POLYTECHNIQUE MONTRÉAL

affiliée à l'Université de Montréal

ANALYTICAL AND EXPERIMENTAL EVALUATION OF THE SETTLEMENT AND VOLUME VARIATION OF TAILINGS SLURRY DEPOSITED IN CONTAINMENT STRUCTURES

JIAHAO QIN

Département de génies civil, géologique et des mines

Mémoire présenté en vue de l'obtention du diplôme de *Maîtrise ès sciences appliquées*

Génie minéral

Mai 2020

POLYTECHNIQUE MONTRÉAL

affiliée à l'Université de Montréal

Ce mémoire intitulé :

ANALYTICAL AND EXPERIMENTAL EVALUATION OF THE SETTLEMENT AND VOLUME VARIATION OF TAILINGS SLURRY DEPOSITED IN CONTAINMENT STRUCTURES

Présenté par **Jiahao QIN**

en vue de l'obtention du diplôme de *Maîtrise ès sciences appliquées*

a été dûment accepté par le jury d'examen constitué de :

Richard SIMON, président

Li LI, membre et directeur de recherche

Pengyu YANG, membre

DEDICATION

To my parents

To my country

ACKNOWLEDGEMENTS

At first, I want to express my sincere appreciation and deepest gratitude to my supervisor Prof. Li Li. It is your support, guidance and understanding that help me to finish all the work including the journal articles and the Master's thesis. The patience, extensive knowledge, rigorous attitude and plenty of discussion time out of your busy schedule helped me to overcome the problems in the project. Moreover, many thanks for your courses given at the beginning of the project and the chance to present my work in some occasions.

I would like to express my grateful thankfulness to Prof. Richard Simon and Dr. Pengyu Yang for your being the jury members of my master's thesis defence. Thanks a lot for your time considering your busy work.

My grateful thanks are also dedicated to Prof. Robert Chapuis, Prof. Adel Hanna and Prof. Biao Li for their courses. I want to specially thank Dr. Jian Zheng and Dr. Feitao Zeng for their spending a lot of time to discuss and comment my articles and thesis. Besides, Noura El-Harrak, Patrick Bernèche, Éric Turgeon and Samuel Chénier are acknowledged for their kind help in my laboratory tests. I also appreciate my colleagues and friends in RIME-IRME research group for your help and suggestions.

I would like to acknowledge the financial support from the Natural Sciences and Engineering Research Council of Canada (NSERC), Fonds de recherche du Québec—Nature et Technologies (FRQNT), and industrial partners of the Research Institute on Mines and the Environment (RIME UQAT-Polytechnique).

Finally, I want to express my appreciations to my parents for their understanding and support to me.

RÉSUMÉ

Les résidus miniers sont des rejets de moulins de concentrateur, qui sont généralement déposés dans des parcs à résidus miniers en surface. En cas d'une gestion inappropriée, les résidus miniers peuvent entraîner des catastrophes à l'environnement et aux vies. L'utilisation des résidus miniers comme un matériau de remblai pour remplir les chantiers miniers souterrains permet de réduire la quantité des résidus miniers déposés en surface. En plus, le remblayage des chantiers souterrains permet d'améliorer la stabilité du terrain et augmenter la récupération du minerai.

Lorsque les résidus miniers sont déposés dans les parcs à résidus miniers, leur volume peut diminuer en raison de la sédimentation, de la consolidation sous poids propre et du retrait par évaporation. Une estimation appropriée de la variation du volume des résidus miniers est nécessaire pour éviter le dépassement de la capacité de stockage conçue des parcs à résidus miniers.

Les trois processus (la sédimentation, la consolidation sous poids propre et le retrait par évaporation) peuvent avoir lieu également au remblai en pulpe lors de sa déposition dans un chantier souterrain. La variation du volume de remblai doit être évaluée correctement pour assurer la stabilité des barricades et un contact serré entre le remblai et les toits des chantiers ou pour éviter de créer des espaces vides importants entre la surface du remblai et le plancher de galerie de niveau supérieur.

Le principal objectif de ce mémoire est d'évaluer l'affaissement et la variation de volume des résidus miniers dans les parcs à résidus miniers ou des remblais en pulpes dans les chantiers souterrains.

Afin d'atteindre l'objectif principal, une compréhension approfondie de la variation du volume des résidus miniers ou des remblais en pulpe associée aux processus de la sédimentation, de la consolidation et du retrait par évaporation est nécessaire. La recherche bibliographique montre que pratiquement tous les travaux de recherche ont porté sur les études de la consolidation des résidus miniers ou des remblais en pulpe. Il y a peu de travaux portant sur la sédimentation. L'indice des vides à la transition entre la sédimentation et la consolidation est un paramètre critique, mais sa détermination reste encore inconnue.

Dans ce mémoire, on a montré que la phase de retrait normal d'une courbe de retrait par évaporation est très similaire au processus de sédimentation. Ainsi, l'indice des vides au début de désaturation

(correspondant à la valeur d'entrée d'air) e_{AEV} sur la courbe de retrait est considéré comme identique à l'indice des vides critique à la fin de sédimentation ou au début de consolidation.

Suite à ces analyses, deux solutions analytiques ont été proposées en considérant la variation de volume des résidus miniers ou des remblais en pulpe associée aux processus de la sédimentation, de la consolidation et du retrait par évaporation. La première a été développée en considérant l'indice des vides final e_f d'une courbe de retrait afin d'estimer l'affaissement ou la variation du volume des résidus miniers dans des parcs à résidus miniers dans des régions arides ou semi-arides. La deuxième a été formulée en utilisant l'indice des vides au début de désaturation e_{AEV} et le coefficient de compression obtenu par un essai de consolidation standard pour évaluer l'affaissement ou la variation de volume des remblais en pulpe dans des chantiers souterrains ou des résidus miniers dans des parcs à résidus miniers dans des régions non-arides. Les deux solutions analytiques proposées ont été validées avec succès par des résultats expérimentaux obtenus par des essais au laboratoire en modèle physique. Les solutions proposées peuvent être utilisées pour calculer l'affaissement et la variation du volume des résidus miniers ou des remblais en pulpe, au moins dans la phrase préliminaire d'un projet.

L'application des solutions proposées pour évaluer l'affaissement ou la variation du volume des résidus miniers ou des remblais en pulpe nécessite de faire des essais de retrait par évaporation. Ce type d'essais est facile à réaliser et assez courant en mécanique des sols. On voit également quelques travaux d'essais au laboratoire pour obtenir les courbes de retrait des résidus miniers non cimentés. Pour le remblayage des chantiers souterrains, les remblais sont souvent cimentés. Ceci est particulièrement vrai pour les remblais en pâte. Or, la revue de littérature montre qu'il n'existe pas de travaux portant sur les essais de retrait par évaporation des remblais en pâtes cimentés. Pour combler cette lacune, une série d'essais de retrait par évaporation a été menée pour acquérir les courbes de retrait d'un remblai en pâte cimenté et non cimenté en considérant différentes teneurs en ciment et teneurs en eau initiales. Leur influence sur les paramètres de retrait, incluant l'indice des vides final e_f, la limite de retrait w_s, l'indice des vides (e_{AEV}) et la teneur en eau (w_{AEV}) au début de désaturation a également été étudiée. Les résultats indiquent que les valeurs de ces paramètres de retrait des remblais cimentés sont beaucoup plus élevées que celles des remblais non cimentés pour une teneur en eau initiale donnée. L'augmentation de la teneur en ciment de 3 à 7% entraîne une légère augmentation des valeurs de ces paramètres de retrait. Pour une teneur en ciment donnée,

les valeurs des paramètres de retrait peuvent varier significativement avec la variation de la teneur en eau initiale.

Les principaux résultats ont été présentés dans deux articles de revues soumis. Des résultats supplémentaires sur les essais de retrait par évaporation et sur les essais de consolidation sont présentés dans les annexes.

ABSTRACT

Tailings are mine wastes produced by milling process, which are conventionally deposited on ground surface in tailings storage facility (TSF). In case of inappropriate management, the surface disposal of tailings can lead to undesirable consequences to the environment and lives. In underground mines, the use of tailings as a filling material to fill underground mined stopes allows reduction of surface disposal of tailings. Stope backfilling also helps improve ground stability and increase ore recovery.

When slurried tailings are deposited in a TSF, the volume of the tailings tends to diminish due to sedimentation, self-weight consolidation and shrinkage by evaporation. An accurate estimation of the volume change of deposited tailings is necessary to help better optimize the life cycle management.

The three processes (sedimentation, self-weight consolidation and shrinkage by evaporation) also take place in backfill slurry, placed in underground mine stopes. The volume variation of the backfill slurry should be correctly evaluated to ensure the stability of barricade and to ensure a tight contact between backfill and stope roof or to avoid excess void space between the top surface of the backfill and the floor of over cut drift.

The main objective of the thesis is to estimate the settlement and volume variation of tailings deposited in TSF or of backfill slurry in underground mine stopes.

In order to reach the main objective, a comprehensive understanding of the volume change of tailings or backfill slurry associated with the processes of sedimentation, consolidation and shrinkage by evaporation is necessary. A literature review showed that the consolidation of tailings or backfill slurry has been largely investigated while the study on the sedimentation of tailings or backfill slurry is almost absent. The void ratio at the transition between sedimentation and consolidation is a critical parameter. Its determination however remains unknown.

In this thesis, one shows that the normal shrinkage stage of shrinkage curve is very similar to the process of sedimentation. Thus, the unsaturation onset (i.e. air entry value) void ratio e_{AEV} on the shrinkage curve can be considered as identical to the critical void ratio at the end of sedimentation or at the beginning of consolidation.

Bases on the above analyses, two analytical solutions have been proposed by considering the volume change of tailings or backfill slurry associated with the processes of sedimentation, consolidation and shrinkage by evaporation. The first one was developed by considering the final void ratio e_f of shrinkage curve in order to estimate the settlement or volume change of tailings deposited in a TSF in arid or semi-arid regions. The second one was formulated by using the unsaturation onset void ratio e_{AEV} and the coefficient of compression obtained by standard consolidation test to evaluate the settlement or volume variation of backfill slurry placed in underground mine stopes or tailings deposited in a TSF in non arid regions. The two proposed analytical solutions have been successfully verified by experimental results obtained by physical model tests. The proposed solutions can thus be used to estimate the settlement and volume variation of tailings or backfill slurry, at least in the preliminary stage of a project.

The application of the proposed solutions for evaluating the settlement or volume variation of tailings or backfill slurry requires to perform shrinkage tests. This type of tests is easy to do and quite common in soil mechanics. One sees a few works published on laboratory tests to obtain shrinkage curves of uncemented tailings. For underground mines, backfills are usually cemented. This is particularly true for paste backfill. The literature review however showed that there is no published work on shrinkage tests of cemented paste backfill. To fill this gap, a series of shrinkage tests has been performed to obtain the shrinkage curves of cemented and uncemented paste backfill by considering different cement contents and initial water contents. Their influence on the shrinkage parameters, including the final void ratio e_f, shrinkage limit w_s, unsaturation onset void ratio (e_{AEV}) and water content (w_{AEV}) has also been evaluated. The results indicate that the values of shrinkage parameters of cemented backfill are much higher than those of uncemented backfill at a given initial water content. An increase of cement content from 3 to 7% results in a slight increase in the values of shrinkage parameters. For a given cement content, the values of shrinkage parameters can significantly vary with the variation of initial water content.

The principal results have been presented in two submitted journal papers. Additional results on shrinkage tests and consolidation tests are presented in the appendices.

TABLE OF CONTENTS

LIST OF TABLES

LIST OF FIGURES

LIST OF SYMBOLS AND ABBREVIATIONS

Symbols

A	cross-section area (m^3)
a_{sh}	minimum void ratio
a_v	coefficient of compressibility (kPa^{-1})
a_{vi}	coefficient of compressibility at layer i (kPa^{-1})
a_{vn}	coefficient of compressibility at nth loading step (kPa^{-1})
B	width of stope (m)
b_{sh}	slope of the line of tangency
C_C	coefficient of curvature
C_c	compression index
C_U	coefficient of uniformity
C_0	initial cement content
c_{sh}	curvature of residual shrinkage stage
c_v	coefficient of consolidation (m^2/s)
c_{vn}	coefficient of consolidation at nth loading step (m^2/s)
D_{10}	grain diameter at 10% passing (μm)
D_{30}	grain diameter at 30% passing (μm)
D_{60}	grain diameter at 60% passing (μm)
d	soil thickness (m)
e	void ratio
e_{AEV}	unsaturation onset void ratio
e_a	absorption shrinkage void ratio
e_c	critical void ratio between sedimentation and consolidation

e_f	final void ratio
e_n	void ratio at nth loading step in consolidation test
e_{n-1}	void ratio at (n-1)th loading step in consolidation test
e_s	saturation void ratio
e_{ca}	capillary shrinkage void ratio
e_{min}	minimum void ratio
e_{ca0}	void ratio at zero water content resulting from capillary shrinkage
e_0	initial void ratio
e_υ	maximum void ratio from the saturated condition to totally dry condition
G_s	specific gravity
H	height of backfill (m)
H_d	height of dirft (m)
H_{50}	drainage path length for 50% primary consolidation (m)
h_{co}	average rise of capillary (m)
h_0	initial height (m)
h_1	height of tailings slurry after sedimentation (m)
K	earth pressure coefficient
k_{sat}	saturated hydraulic conductivity (m/s)
k_{satn}	saturated hydraulic conductivity at nth loading step (m/s)
L	width of stope (m)
L_{BT}	top length of barricade (m)
L_d	width of drift (m)
l_i	thickness of divided layer (m)
M_d	mass of dry soil (kg)

$M_{sf.tot}$	final total mass of solids (kg)
$M_{s0.c}$	initial mass of cement (kg)
$M_{s0.tail}$	initial mass of tailings (kg)
$M_{s0.tot}$	initial total mass of solids (kg)
M_{t0}	initial total mass of each sample (kg)
M_{w0}	initial mass of water (kg)
m	filling rate (m/h)
m_v	coefficient of volume compressibility (kPa^{-1})
m_{vn}	coefficient of volume compressibility at nth loading step (kPa^{-1})
n	porosity
SL'	apparent shrinkage limit
SL	true shrinkage limit
S_a	saturation by adhesion
S_c	settlement by consolidation (m)
S_{ca}	capillary saturation
S_{fs}	settlement induced by full shrinkage (m)
S_{ns}	settlement by normal shrinkage (m)
S_r	degree of saturation
S_t	total settlement induced by sedimentation and consolidation (m)
T_v	time factor
t	desiccation time (s)
u	pore water pressure (kPa)
u'	excess pore water pressure (kPa)
V	volume of wet soil (m^3)

V_c	volume variation by consolidation (m^3)
V_d	volume of dry soil (m^3)
V_{fs}	volume variation by full shrinkage (m^3)
V_{ns}	volume variation by normal shrinkage (m^3)
$V_{s0.tot}$	initial total volume of solids (m^3)
V_t	total volume variation induced by sedimentation and consolidation (m)
V_0	initial volume of slurry (m^3)
w	water content
w_{AEV}	unsaturation onset water content
w_c	cracking water content
w_L	liquid limit
w_p	plastic limit
w_r	residual water content
w_s	shrinkage limit
w_0	initial water content
x	elevation from the bottom of the tailings or backfill slurry (m)
α_1	upstream stope angle (˚)
α_2	downstream stope angle (˚)
γ'	saturated unit weight of backfill (kN/m^3)
γ	unit of dry backfill (kN/m^3)
γ_{sat}	saturated unit weight of tailings (kN/m^3)
γ_w	unit weight of water (kN/m^3)
γ_{wr}	unit weight of waste rock (kN/m^3)
δ	interface friction angle between barricade and drift wall (˚)

ε_v	volume shrinkage rate
θ	volumetric water content
θ_{amax}^{SSC}	maximum adsorption volumetric water content
σ'	effective stress (kPa)
σ_i'	average effective stress at layer *i* (kPa)
σ_h	horizontal total stress (kPa)
σ_v	vertical total stress (kPa)
σ'_h	horizontal effective stress (kPa)
σ'_v	vertical effective stress (kPa)
ρ_{cement}	density of cement (kg/m^3)
$\rho_{tailings}$	density of tailings (kg/m^3)
ρ_w	density of water (kg/m^3)
υ	moisture ratio
υ_{AE}	moisture ratio at suction of air entry value
υ_{SL}	moisture ratio at shrinkage limit
Φ'	effective friction angle of backfill (˚)
ψ	matrix suction (kPa)

Abbreviations

AEV	Air entry value
AMD	Acid mine drainage
ASTM	American Society for Testing and Materials
CHB	Cemented hydraulic backfill
CPB	Cemented paste backfill

CUAPS	Curing under applied pressure system
DEM	Discrete element modelling
HB	Hydraulic backfill
LL	Liquid limit
LVDT	Linear variable differential transformer
PB	Paste backfill
PL	Plastic limit
PWP	Pore water pressure
RH	Relative humidity
SEM	Scanning electron microscope
SICT	Seepage-induced consolidation test
SWRC	Soil water retention curve
TSF	Tailings storage facility
uCPB	Uncemented paste backfill
UCS	Uniaxial compressive strength
USCS	Unified soil classification system
WRB	Waste rock barricade
WRI	Waste rock inclusions

LIST OF APPENDICES

CHAPTER 1 INTRODUCTION

1.1 Statement of the problem

Hard rock mines can produce large amount of solid wastes in terms of tailings and waste rocks, which are usually disposed on the ground surface. The tailings are transported and deposited in tailings pond while the waste rocks are disposed as waste rock piles. These mine wastes must be properly managed due to their potential environmental risks. For instance, the surface disposal of mine wastes is usually accompanied with several geotechnical and geochemical issues, such as the failure of tailings dams and acid mine drainage (AMD).

In recent decades, backfill has been commonly used in underground mines around the world. The application of backfill in underground stopes can lead to improved ground stability, increased ore recovery, and minimized ore dilution. It can also reduce the amount of surface disposed mine wastes and thus minimize the environmental impact.

When a tailings slurry is poured in a tailings pond or when a backfill slurry is deposited in a stope, the slurry has similar hydro-geotechnical behavior. The particles tend to settle down under the effect of gravity. The slurry thus tends to become denser and expel the pore water out of the slurry. As the tailings and backfill contain a large portion of fine particles, their hydraulic conductivity is low. The drainage is limited, quickly resulting in the generation of the excess pore water pressure (PWP). The dissipation of excess PWP takes place with time, accompanied with drainage, volume variation and settlement of the slurry. Depending on the initial water content, the drainage and dissipation of the excess PWP can generally be divided into two stages: sedimentation and consolidation (Imai 1981). In the process of sedimentation, the over saturated slurry is in a state of fluid. The grain-grain contacts are absent and the effective stresses are nil (Dromer et al. 2004). When the drainage and dissipation of the excess PWP proceed to a critical degree at which the grain-grain contacts begin, effective stresses are generated and the process of consolidation starts (Been and Sills 1981). The volume and settlement of the slurry can further change, but mainly due to the variation of the effective stresses.

It is an important task is to evaluate the volume variation and settlement of the tailings or backfill slurry after its placement in a tailings pond or underground mine stope. For tailings ponds, the settlement and volume variation are critical for estimating the storage capacity and optimizing the

life cycle management. For underground mine stopes, understanding the settlement behavior of backfill slurry is important to avoid the creation of excess void between the top surface of the settled backfill and the floor of access drift used as a passing way for vehicles and workers. When the mine stope is filled in two stages (i.e., plug pour and final pour), a “rule of thumb” is to make a plug pour 2 to 3 meters higher than the roof level of the access drift. When the plug pour is much higher than the designed height, the cost will be uselessly increased due to the high cement content of plug. When the plug gains enough strength, the final pour is completed in one stage. If the settled backfill of the plug pour is lower than the drift, an excessive pressure can be applied on the top part of the barricade during the pouring of the final pour, which is usually much higher than the plug pour. The barricade can fail near the upper portion due to internal local instability (Yang et al. 2017), resulting in undesirable consequences.

Over the years, numerous studies have been conducted to investigate the settlement of tailings or backfill slurry by considering self-weight consolidation. A number of analytical solutions have also been proposed to evaluate the settlement and volume variation of tailings or backfill slurry during and after the deposition in a tailings storage facility or a mine stope (Gibson 1958; Gibson et al. 1967; Zheng et al. 2020a). However, the settlement and volume variation associated with the process of sedimentation have never been taken into account, mainly due to the difficulty in determining the critical void ratio of transition between the processes of sedimentation and consolidation (McRoberts and Nixon 1976). The application of the existing solutions tends to largely underestimate the settlement and volume variation of tailings or backfill slurry.

On this study, a detailed analysis presented in Chapter 3 shows that the sedimentation process of a self-weight consolidation test is similar to the normal shrinkage stage of a shrinkage test. In both cases, the volume variation of the settled slurry is only due and equal to the volume reduction of pore water, the former due to the expelled supernatant water and the latter due to the evaporation. The process of sedimentation finishes when the grain-grain contacts begin while the normal shrinkage stage ends when the grain-grain contacts start and unsaturation initiates. The critical void ratio at the end of sedimentation can thus be considered as equal to the unsaturation onset void ratio. The former can then be determined through shrinkage tests.

Shrinkage test is simple and easy to realize. Over the years, a number of studies have been conducted to investigate the shrinkage response of clayey soil. A few studies have also been

performed to investigate the shrinkage behavior of uncemented tailings or the chemical shrinkage associated with the cement hydration of paste backfill. The shrinkage response of cemented paste backfill (CPB) has never been analyzed while paste backfill for underground mines is seldom uncemented. Shrinkage tests on CPB are necessary.

1.2 Objectives of the thesis

The general objective of the thesis is to estimate the settlement and volume variation of tailings or backfill slurry deposited in a containment structure by considering the combined effects of sedimentation, shrinkage and self-weight consolidation. The objective has been reached through the achievement of the following sub-objectives:

1) Understanding the settlement and volume variation of tailings slurry deposited in tailings ponds or underground mine stopes by considering the shrinkage, sedimentation and self-weight consolidation.
    - Analyze the volume variation of a slurry under the processes of shrinkage and sedimentation;
    - Develop analytical solutions to evaluate the settlement and volume variation of the tailings or backfill slurry by considering the combined effects of shrinkage, sedimentation and consolidation;
    - Validate the proposed solutions with laboratory test results.
2) Investigating the shrinkage behavior of cemented and uncemented paste backfill.

1.3 Contributions

The realization of this research project resulted in the submission of two peer-reviewed journal articles:

J1. An analytical solution to estimate the settlement of tailings slurry deposited in a containment structure. Submitted to *Engineering Geology*. This article is presented in Chapter3.

J2. Experimental study of the shrinkage behavior of cemented paste backfill. Submitted to *Construction and Building Materials*. This article is presented in Chapter4.

The completion of the research project contributes to a better understanding of the hydro-geotechnical behavior of tailings or backfill slurry after being placed in a tailings pond or underground mine stope. The proposed analytical solutions can be used to estimate the settlement and volume variation of tailings or backfill slurry after being placed in a tailings pond or mine stope by considering the combined effects of shrinkage, sedimentation and self-weight consolidation. The proposed analytical solutions can be considered as a simple and useful tool for practitioners in the preliminary design of the tailings ponds or underground mine stopes. The shrinkage tests performed on CPB resulted in a better understanding of the influence of cement on the shrinkage response and volume variation of CPB.

1.4 Organizations

The thesis is organized in a paper-based format. It is structured as follows:

Chapter 1 presents a general introduction of the problem proposed in the thesis. The objective, academic contributions and organizations of the thesis are included.

Chapter 2 presents a comprehensive literature review of the state of knowledge, including the geotechnical properties of tailings and backfill, disposal of tailings or backfill in tailings ponds and mine stopes, shrinkage and consolidation behavior of tailings or backfill slurry.

Chapter 3 (Article 1) presents the experimental and analytical studies to estimate the volume and settlement change of tailings slurry deposited in a containment structure. The analytical solutions were verified with experimental results obtained by physical model tests.

Chapter 4 (Article 2) presents an experimental study of the shrinkage behavior of cemented and uncemented paste backfill. The influence of the cement content and initial water content on the shrinkage response and shrinkage parameters was also investigated.

Chapter 5 presents a general discussion on the limitations of the realized works in the thesis.

Chapter 6 presents the main conclusions and recommendations.

CHAPTER 2 LITERATURE REVIEW

2.1 Tailings disposal

Tailings are a by-product of milling process after ore has been subjected several mechanical and chemical processes, such as crushing, grinding, and floatation. Tailings are generally transported by pipelines and deposited to tailings storage facilities (TSF) to eliminate the unfavorable effect of some poisonous chemical compositions. They must be appropriately managed to avoid pollution to the environment (Vick 1990; Bussière 2007). This is particularly true when the tailings are chemically reactive, containing some elements like sulfide, which are source elements for the generation of acid mine drainage (AMD) (Bussière et al. 2004; Edraki et al. 2014). Moreover, TSF can fail and result in serious consequences to the environment, infrastructures and lives (Blight 2009; Burritt and Christ 2018; Byrne et al. 2018; Palu and Julien 2019).

Tailings can also be used as fill material to fill underground mined stopes. This technology has also the advantages of improving the ground stability, increasing ore recovery and reducing the amount of surface disposal of mining wastes (Li 2014). Water and binders are usually added and mixed with tailing to improve the mechanical properties and ensure the flowability necessary for the transpiration by pipes.

2.1.1 Tailings storage facility

Tailings dams are the most commonly used structures constructed to retain the tailings slurry. When the tailings contain acid-generating sulphide minerals, the tailings are generally required to remain below water table to prevent the dust and AMD generations (Kossoff et al. 2014).

The locally available materials like locally derived soils, tailings and waste rocks are usually applied to construct tailings dams (Bussière 2007; Álvarez-Valero 2009). The construction of tailings dams must respect the limitation of the full designed height. The storage capacity for containing tailings is thus limited. Tailings dams can be progressively built to lower the investment at the beginning. Thus, intermediate tailings dams are usually built and gradually elevated with tailings discharge increasing, instead of constructing a determined full storage capacity tailings dam at the beginning (Lottermoser 2003).

Tailings dams can be raised upstream, vertically (center-line), or downstream, as shown in Figure 2-1 once the initial retaining embankment has been constructed (Martin and McRoberts 1999). The upstream tailings dam is designed to place the new coarse tailings as dam material in the finished embankment while the downstream method is to put the new coarse tailings as dam material outside of the existing structures. The centerline method is to place the new coarse tailings as dam material just at the top of the old impoundment.

Among the three methods, the upstream is the most economic one and requires the smallest amount of construction materials (Soares et al. 2000). A layer of sand sized tailings will be put at the bottom of the tailings impoundment to ensure good drainage and avoid excessive settlement (Saad and Mitri 2010).

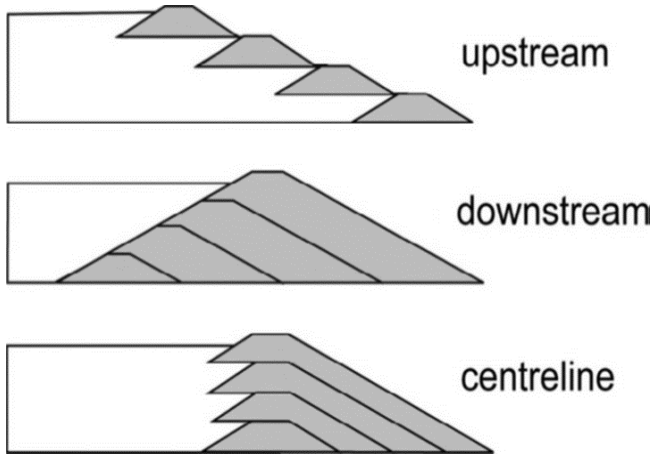

Figure 2-1: Schematic diagrams of three typical tailings dam construction methods (taken from Kossoff et al. 2014).

A tailings dam can fail due to several influencing factors. These include slope and foundation instability, internal erosion (also called piping), overtopping by flooding water, surface erosion, seismic damage and damage to decantation structures (ICOLD 1996). Most of failures happen in the upstream raised dams (Strachan 2002), which are mostly caused by dynamic liquefaction induced by seismic loading like earthquake, mine blasting and other dynamic loadings or static liquefaction (Davies 2002). In addition, internal erosion is also dangerous for the stability of tailings dam. This failure is caused by seepage through the tailings dam. Piping failure during tailings height raising can become more possible when fine-tailings layer lies between two coarse-tailings layers (Van Niekerk and Viljoen 2005). Foundation failure is another significant failure

type (Rico et al. 2008). When the foundation material has a low hydraulic conductivity, the drainage and dissipation of excess pore water pressure (PWP) will be slow, leading to establishment of excessive PWP. However, an excessively high permeability of foundation material may be subjected to piping failure. Finally, it should be kept in mind that the safety of tailings dams not only relies on the design, but also on the maintenance and monitoring as long as they exist (Kossoff et al. 2014).

2.1.2 Co-disposal method

The physical stability of tailings dams is mainly related to tailings' high compressibility while the problem of AMD is closely related to the unsaturated characteristics of waste rocks. The two problems can thus be solved by the co-disposal of tailings and waste rocks (Wickland et al. 2006). This can result in a mixture of the two materials, called paste rocks, having low compressibility (due to the waste rocks) and low permeability (due to the tailings). Wickland and Wilson (2005) investigated the self-weight consolidation behavior of waste rocks and tailings mixture. Three mixtures were put in three column apparatus. The long-term settlement and PWP were measured. As comparison, another column was filled with waste rocks only, as shown in Figure 2-2. Their results showed that a specific mixture ratio of waste rocks and tailings can result in a hydraulic conductivity as low as that of the tailings and a compressibility as low as that of the waste rocks.

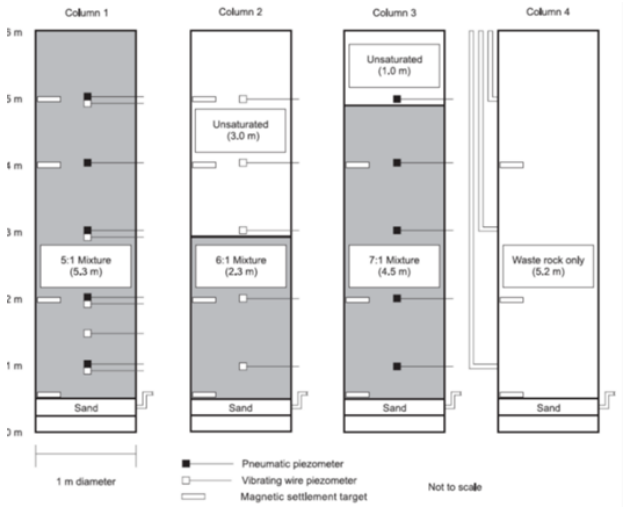

Figure 2-2: Column self-weight consolidation tests of mixtures composed of tailings and waste rocks (taken from Wickland and Wilson 2005).

2.1.3 Waste rock inclusion

Waste rock inclusion (WRI) is a structure built with waste rocks in TSF, which serves as vertical drain to accelerate the consolidation and drainage of tailings. With WRI, the excess PWP of tailings in TSF can dissipate more rapidly due to the horizontal drainage. The potential of liquefaction of tailings can thus be reduced. Bolduc and Aubertin (2014) suggested to place WRI in impoundment at the beginning of the tailings deposition. As a result, the tailings can be stored in the cells formed by WRI. A conceptual diagram of WRI is shown in Figure 2-3.

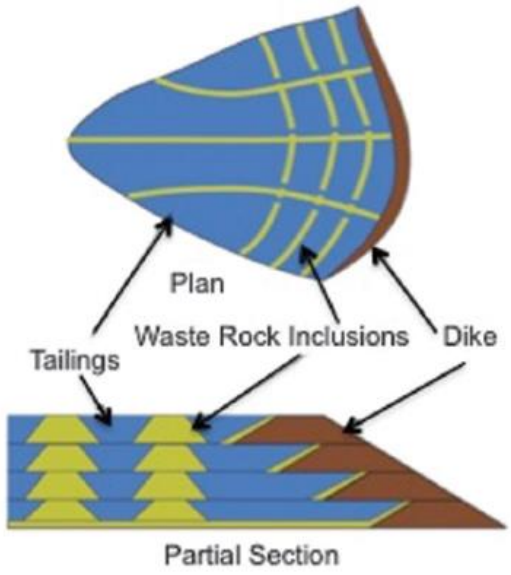

Figure 2-3: Conceptual diagram of WRI in tailings impoundment (taken from Bolduc and Aubertin 2014).

Bolduc and Aubertin (2014) investigated by numerical modeling the dissipation of excess PWP along the base at different positions from inclusions. Their numerical results showed that the WRI can accelerate the dissipation of excess PWP. The excess PWP dissipates faster near the inclusions. Figure 2-4 shows the degrees of consolidation at different positions along the base. The effect of accelerated consolidation by the introduction of WRI is clearly shown.

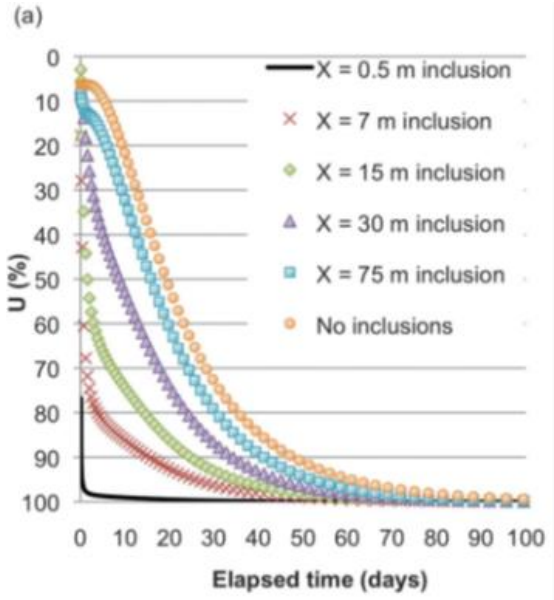

Figure 2-4: Degree of consolidation of tailings with elapsed time at different positions from the inclusion along the base (taken from Bolduc and Aubertin 2014).

Jaouhar et al. (2011) investigated the effect of the spacing, shape and size of WRI through numerical modeling. Their numerical results indicate that the simplified shape has moderate effect on the excess PWP dissipation and degree of consolidation.

2.1.4 Tailings used as fill material to fill underground mine stopes

In underground mining, backfill made of tailings can be used to fill the mined-out stopes. This practice can help to reduce the surface disposal of mine wastes. The application of backfill can also improve the ground stability, reduce ore dilutions and increase ore recovery (Li and Yang 2015).

2.1.4.1 Critical problems in mining with backfill

2.1.4.1.1 Stresses in backfilled stopes

In backfilled stopes, barricades made of waste rocks, timber or concrete should be constructed in the access drift to retain the backfill in the stopes (Hughes et al. 2010; Li and Aubertin 2011). The stresses in the backfilled stopes are critical to the designs of barricades and backfill. The evolution of stresses in backfilled stope is a complicated process. The stresses can be affected by several aspects, including self-weight consolidation, arching effect, and cement hydration (Fahey et al.

2009). For dry and cohesionless backfill, the stresses in backfilled stopes can be estimated by applying the Marston (1930) solution as follows (Aubertin et al. 2003):

$$\sigma_v = \gamma B\left(\frac{1-\exp\left(-\frac{2Kh\tan\phi'}{B}\right)}{2K\tan\phi'}\right) \quad (2\text{-}1)$$

$$\sigma_h = K\sigma_v \quad (2\text{-}2)$$

where, σ_v and σ_h are the vertical and horizontal stresses at depth of h, respectively; γ is the unit weight of backfill; φ' is the effective friction angle of backfill; B is the width of the stope; K represents the earth pressure coefficient. The related parameters are shown in Figure 2-5.

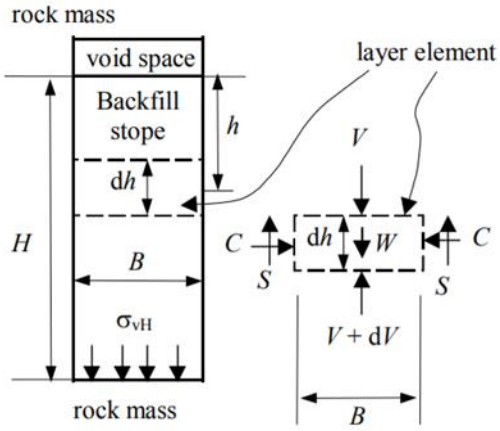

Figure 2-5: Marston's model of arching effect (taken from Aubertin et al. 2003).

The Marston's model involves several limitations. The model is two-dimensional for vertical stopes. The model does not consider the presence of water and cohesion of backfill.

2.1.4.1.2 Barricade stability

Traditionally, barricades are usually made of bricks, reinforced steel with shotcrete and timber (Potvin et al. 2005). The construction of barricades made of waste rocks has become more and more popular in Canada and Australia. The design solution of waste rock barricade (WRB) was firstly proposed by Li and Aubertin (2011) based on limit equilibrium analysis. The WRB was simplified as a rectangular block. Fully drained and submerged conditions were considered. The application of the Li and Aubertin (2011) solution generally leads to overly conservative design of barricades.

Yang et al. (2017) developed a solution by considering a trapezoidal barricade, as shown in Figure 2-6. Both the global stability and internal local stability have been taken into account. In the global stability analysis, the WRB was considered as a stiff block, whose sliding failure is mainly resisted by the frictional shear strength between the WBR and the side walls and floor of drift. In the internal local stability analysis, the sliding failure of upper portion of WRB was considered. The solution of Yang et al. (2017) is given as follows:

$$L_{BT} = \frac{\gamma_b\left(H-\frac{H_d}{2}\right)\left(\frac{FS}{\tan\delta}-\frac{1}{\tan\alpha_1}\right)-\gamma_{wr}H_d\left(\frac{1}{2}+K\frac{H_d}{3L_d}\right)\left(\frac{1}{\tan\alpha_1}+\frac{1}{\tan\alpha_2}\right)}{\gamma_{wr}\left(1+K\frac{H_d}{L_d}\right)}, for\ \delta \le \delta_c \quad (2\text{-}3)$$

$$L_{BT} = \frac{\gamma_b}{\gamma_{wr}}(H-H_d)\left(\frac{C_M \times FS}{\tan\phi'}-\frac{1}{\tan\alpha_1}\right), for\ \delta > \delta_c \quad (2\text{-}4)$$

where L_{BT} is the required top length of barricade; H_d and L_d represent the height and width of the drift, respectively; α_1 and α_2 represent the upstream and downstream slope angles, respectively; H is the height of the paste backfill in the stope (Figure 2-6); γ_b is unit weight of the paste backfill; γ_{wr} is the unit weight of waste rocks; δ is the interface friction angle between the barricade and drift wall; K is the earth pressure coefficient and FS is the factor of safety; C_M is a calibration factor; ϕ' is the internal friction angle of waste rocks.

The analytical solution of Yang et al. (2017) has been partly validated by numerical results obtained with FLAC2D.

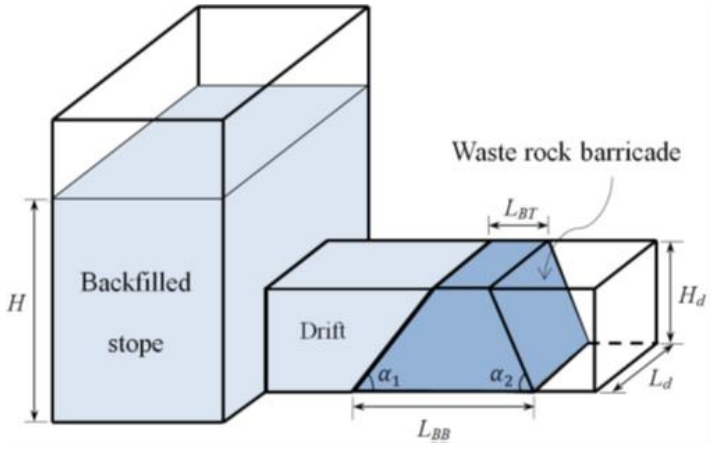

Figure 2-6: Backfilled stope containing a drift and a trapezoidal waste rock barricade (taken from Yang et al. 2017).

2.1.4.1.3 Required strength of exposed backfill

In several cases, cemented backfill has to be used to fill the primary stopes or to build a man-made sill mat. The cemented backfill should remain stable when it is exposed on one side due to the excavation of an adjacent secondary stope or at the bottom due to the excavation of underlying stope. A critical issue is how to estimate the required strength for these cemented backfills.

Figure 2-7 shows a wedge model proposed by Mitchel et al. (1982). By considering very high and narrow stope and assuming that the friction angle of backfill is equal to 0˚ and the cohesion between the backfill and side walls is equal to the cohesion of the backfill, Mitchell et al. (1982) proposed the following equation to determine the minimum (i.e. FS = 1) required strength of side-exposed backfill:

$$UCS = 2c = \frac{\gamma H}{1+H/L} \tag{2-5}$$

where UCS is the minimum required uniaxial compressive strength, γ is the unit weight of backfill, H is the height of backfill and L is the width of stope.

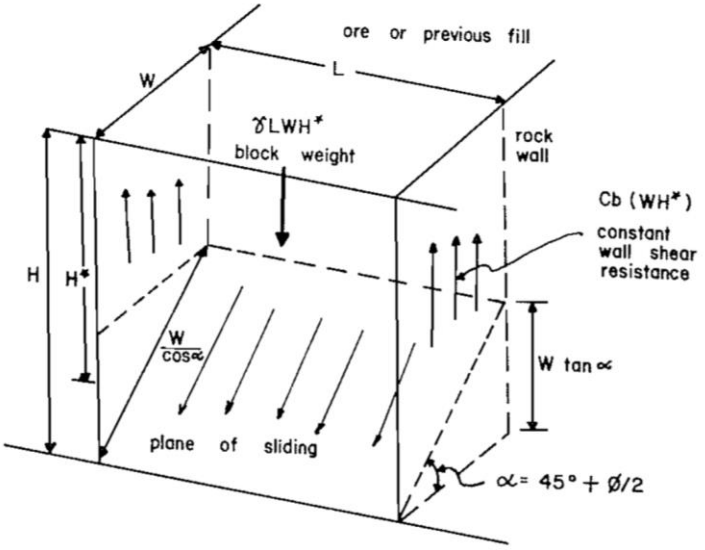

Figure 2-7: Wedge model for side exposed backfill (taken from Mitchel et al. 1982).

Figure 2-8 shows a comparison between the Mitchell et al. (1982) solution and experimental results. Good agreement has been shown between the measured minimum required strengths and those predicted by the solution of Mitchell et al. (1982).

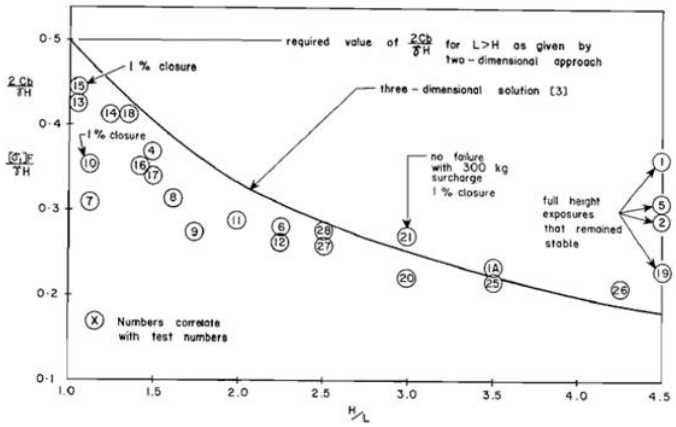

Figure 2-8: Comparison between relationship of $c/\gamma H$ and H/L obtained from Mitchel's model and model test (taken from Mitchel et al. 1982).

The Mitchel et al. (1982) model has been revised by Li and Aubertin (2012). Several improvements have been made by considering more realistic conditions (Li 2014). Yang et al. (2017) performed some numerical modelling and proposed an improved analytical solution after taking into account tension cracks when the backfill is exposed on one side (Yang et al.2017). Liu et al. (2018) proposed an analytical solution for estimating the required strength of cemented backfill exposed on one side and pressured on the opposite side. The proposed solution was partly validated by numerical results obtained with FLAC3D.

2.1.4.2 Mining backfill

Mining backfill is generally divided into three categories: hydraulic backfill (HB), paste backfill (PB) and rockfill. HB and PB are usually made of tailings with the addition of water while rockfill is for most case made of waste rocks. Binder can be added to form cemented HB, PB or rockfill.

2.1.4.2.1 Hydraulic backfill

Hydraulic backfill is a mixture usually composed of classified tailings and water. Binder can be added in some cases to form a cemented hydraulic backfill. The tailings are classified by hydrocyclone and the coarse particles of underflow are used for the fabrication of hydraulic backfill while the fine tailings of overflow are transported to the tailings pond (Rankine et al. 2007). The different grain size distribution curves of the tailings used in hydraulic backfill and paste fill are

shown in Figure 2-9. According to Potvin et al. (2005), a hydraulic backfill should contain au maximum 10% of particles finer than 10 μm.

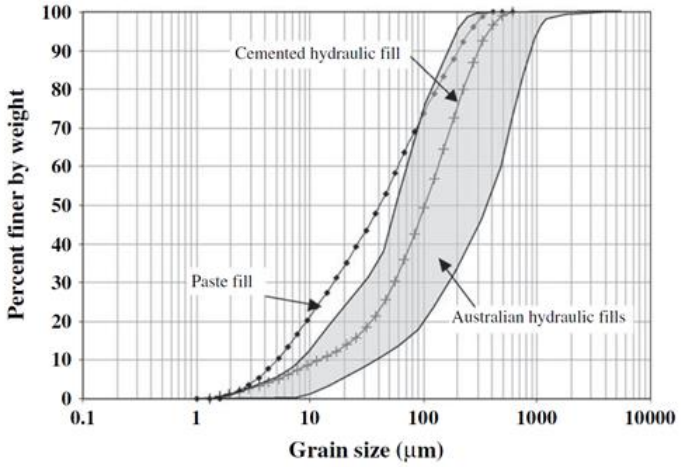

Figure 2-9: Different grain size distribution curves of hydraulic backfill, cemented hydraulic backfill and paste backfill (taken from Rankine et al. 2007).

The hydraulic conductivity of HB generally ranges from 10^{-6} to 10^{-5} m/s with the sandy size to silty size particles. The solid content of hydraulic backfill is about 75 to 80%. Cement can be added to the hydraulic backfill to increase the strength. When HB is transported by pipelines, the flow velocity should be large enough because sedimentation may happen and blocks the pipelines if the flow is not fast enough. Hydraulic conductivity of cemented hydraulic backfill (CHB) is lower than that of uncemented hydraulic backfill since the cementation decreases the effective void ratio for flow. The friction angle of hydraulic backfill with very angular grains are significantly higher than those of granular soils (Sivakugan et al. 2006). The cohesion of cemented hydraulic backfill is mainly influenced by the binder type, binder content and curing time (Grice 2001).

2.1.4.2.2 Paste backfill

Cemented paste backfill (CPB) is a mixture composed by full tailings and water. For underground mines, paste backfill is always cemented. The binder can be Portland cement, slag and fly ash (Yilmaz and Fall 2017). According to Potvin et al. (2005), a paste backfill should contain at least 15% of particles finer than 20 μm.

CPB behaves as a Bingham plastic fluid (Yang and Li 2015). It can flow like a viscous material once its yield shear stress is exceeded. The yield shear stress is generally measured by rheometer or vane tests. It can also be roughly estimated by slump tests (Clayton et al. 2003).

The hydraulic conductivity of paste backfill is much lower than that of hydraulic backfill due to the larger portion of finer particles. The uniaxial compressive strength (UCS) of CPB depends on the type and content of added cement. Generally, the cement content is 3 to 5% in final pour while it ranges from 5 to 7% in plug pour (Yilmaz and Fall 2017). The mechanical properties of CPB including UCS, cohesion and friction angle depend on many factors like binder types, binder contents, curing time. Figure 2-10 shows the UCS of CPB with different binder contents, which increases with *w*/*c* ratio (ratio of water mass to cement mass) and cement content (Fall et al. 2008). The variations of shear strength parameters with curing time shown in Figure 2-11 indicate that the cohesion increases significantly with curing time while friction angle is only slightly affected by the cement hydration with curing time (Ghirian and Fall 2014).

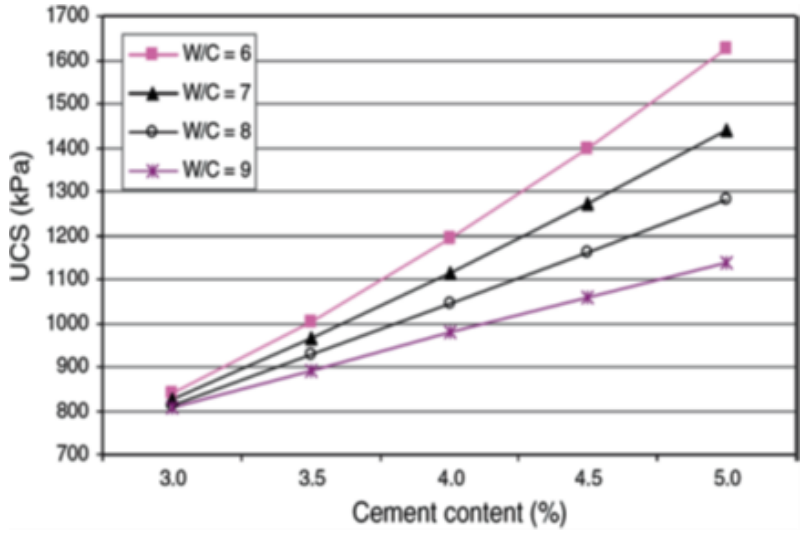

Figure 2-10: Variations of UCS of CPB with cement content under different water/cement (*w*/*c*) ratios (taken from Fall et al. 2008).

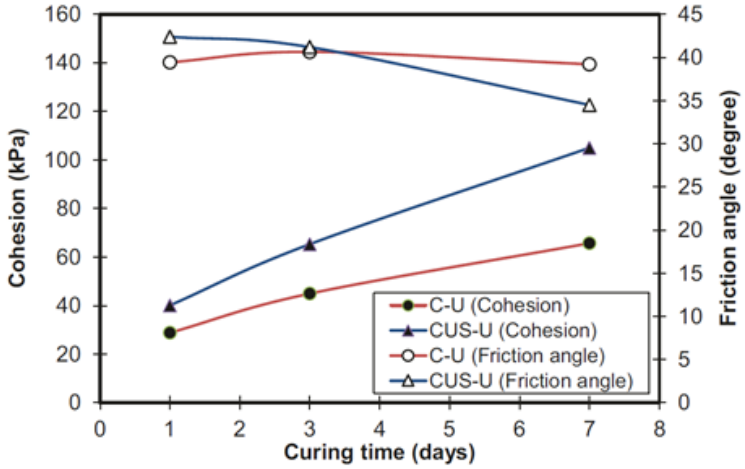

Figure 2-11: Variations of cohesion and friction angle with curing time in load cell experiments (taken from Ghirian and Fall 2014).

Figure 2-12 shows a process of manufacturing CPB. It includes cyclone of mill tailings, storage of tailings, thickening by thickener, mixing with binders. The thickening of tailings is aimed to attain high enough solid concentration of 70 to 85% by dewatering (Landriault 1995). Mixing is an important process to obtain the uniform and workable paste backfill. This process can be done by batch or continuous process. A large-volume cement silo near paste plant is necessary. Cement is poured into paste plant with a conveyor (Bussière 2007).

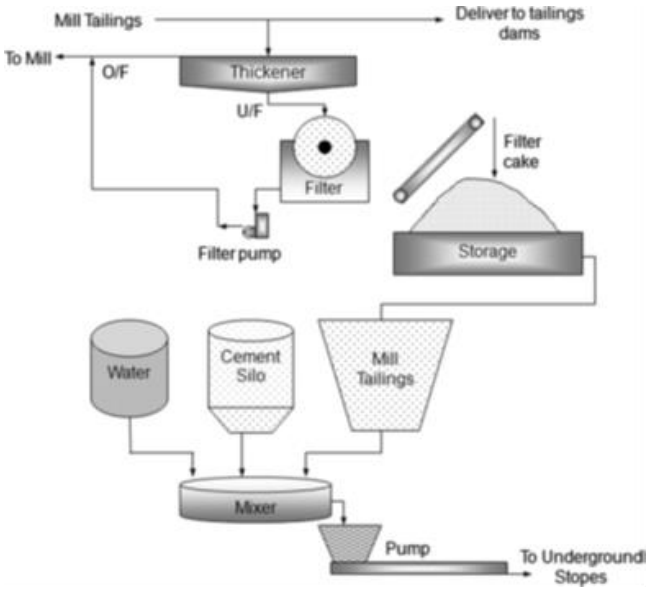

Figure 2-12: Manufacture process of cemented paste backfill (taken from Yilmaz and Fall 2017).

2.1.4.2.3 Rockfill

Rockfill is mainly composed of waste rocks. Tailings and binder can sometimes be added. In general, construction of barricade is not necessary, but installation of fences can sometimes be needed to maintain high slope and even vertical wall. The typical grain size used for rockfill ranges from 1 to 100 mm. The hydraulic conductivity of rockfill can be as high as 4×10^{-2} m/s (Williams 1992) while the friction angle ranges from 35˚ to 55˚ (Potvin et al. 2005). The UCS of cemented rockfill can range from about 1 MPa to 16 MPa while the UCS of uncemented rockfill is close to 0, as shown in Figure 2-13 (Shrestha et al. 2008).

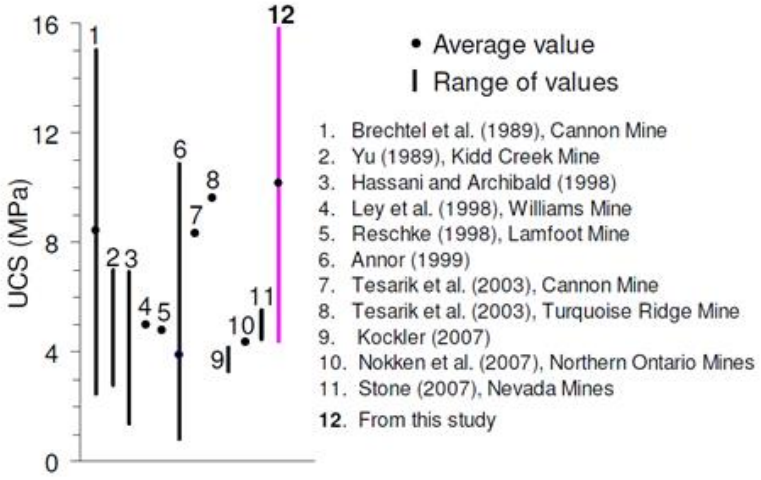

Figure 2-13: Comparison between measured UCS of cemented rockfill (5.5 and 6% cement) and reported values (taken from Shrestha et al. 2008).

2.2 Geotechnical properties of tailings

2.2.1 Physical properties of tailings

Tailings contain particles whose sizes can vary from that of sand to those of silt and clay. Figure 2-14 shows typical grain size distribution curves of hard rock mine tailings in Quebec, Canada (Bussière 2007). The size of 10% passing, D_{10}, of these tailings ranges from 0.001 to 0.004 mm while the size of 60% passing, D_{60}, ranges from 0.01 to 0.05 mm. Therefore, the coefficient of uniformity C_U ranges from 8 to 18. According to the Unified Soil Classification System (USCS), the tailings are categorized as a non-plastic silt (ML) or silty sand (SL).

Previous studies on the Atterberg limits of tailings showed that tailings generally have a liquid limit, w_L lower than 40% and a hardly measurable plastic limit, w_p ranging from 0 to 15% (Mittal and Morgenstern 1976; Barbour et al. 1993; Aubertin et al. 1996; Qiu and Sego 2001), which indicates a slight or non plasticity.

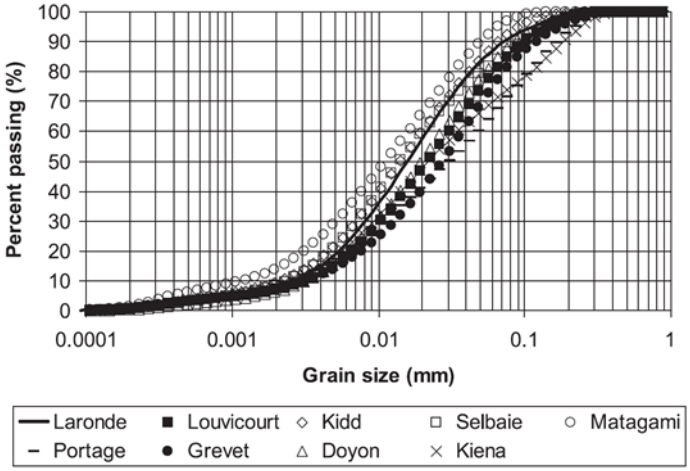

Figure 2-14: Grain size distribution curves of hard rock mine tailings from different mines in Quebec, Canada (taken from Bussière 2007).

2.2.2 Compression properties

The consolidation properties of tailings have been investigated for decades because they are necessary to estimate the settlement of tailings in TSF. Moreover, the consolidation properties of tailings are required to manage the construction process and prevent the possible excessive pressure in the impoundment. The effective stresses for most TSF can range from 0.5 to 100 kPa (Qiu and Sego 2001). When the tailings slurry is poured in tailings pond, the initial effective stress shortly after the deposition is nearly zero. The material is very soft and can exhibit considerable deformation under an applied effective stress. Therefore, the conventional oedometer test is not appropriate for measuring the consolidation properties. In order to overcome the disadvantages of oedometer tests, new experimental methods have been developed. These include seepage induced test (Imai 1979), physical centrifuge modelling (Stone et al. 1994) and slurry consolidometer test (Qiu and Sego 2001).

2.2.3 Hydraulic conductivity

The hydraulic conductivity k_{sat} of tailings is generally measured by performing laboratory odometer test, rigid wall permeability test, or flexible wall permeameter test. The measured k_{sat} of remolded samples ranges from 1×10^{-7} to 1×10^{-4} cm/s for fine particle tailings (Bussière 2007) and from 1×10^{-2} to 1×10^{-4} cm/s for coarse particle tailings.

Figure 2-15 shows the variation of measured k as function of e of four types of tailings (Qiu and Sego (2001). The results show that the gold tailings and copper tailings have a larger saturated hydraulic conductivity (4.5×10^{-5} to 9.8×10^{-5} cm/s) compared to the coal tailings and oil sand tailings, for a given void ratio. This difference can be due to the difference in their grain size characterizations.

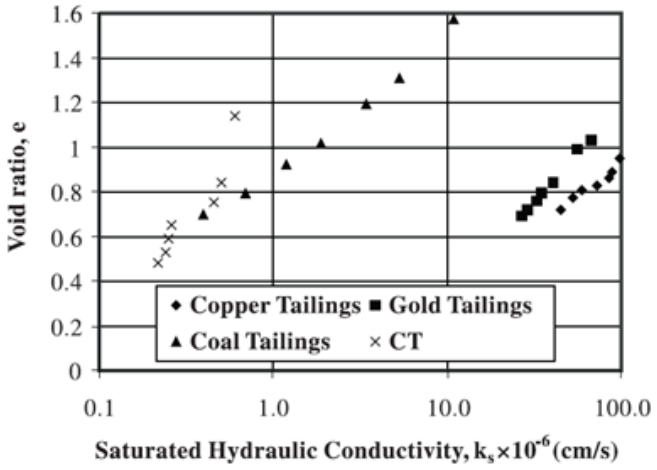

Figure 2-15: Relationship between void ratio and saturated hydraulic conductivity for different types of tailings (taken from Qiu and Sego 2001).

The saturated hydraulic conductivity k_{sat} can be estimated with equations based on some physical properties of tailings, including void ratio e, D_{10} and C_U. Aubertin et al. (1996) developed an equation as follows:

$$k = c\frac{\gamma_w}{\mu}D_{10}^2 C_U^{1/3}\frac{e^{3+x}}{1+e} \tag{2-6}$$

where μ is the fluid viscosity, x and c are two constants, k is the hydraulic conductivity, γ_w is the unit weight of water, D_{10} is the particle size of 10% passing and C_U is coefficient of uniformity.

Figure 2-16 shows a comparison between the calculated and measured values of k_{sat}. The measured k_{sat} of hard rock tailings ranges from 5×10^{-4} to 1×10^{-5} cm/s. A good agreement was obtained between the calculated and measured values of k_{sat}. The hydraulic conductivity can thus be estimated by applying the proposed equation with the basic geotechnical parameters including D_{10} and C_U. According to experimental data of hydraulic conductivity tailings, the average x value is 2.16 while average c is 0.02, which could be used for the estimation of hydraulic conductivity of homogenized tailings.

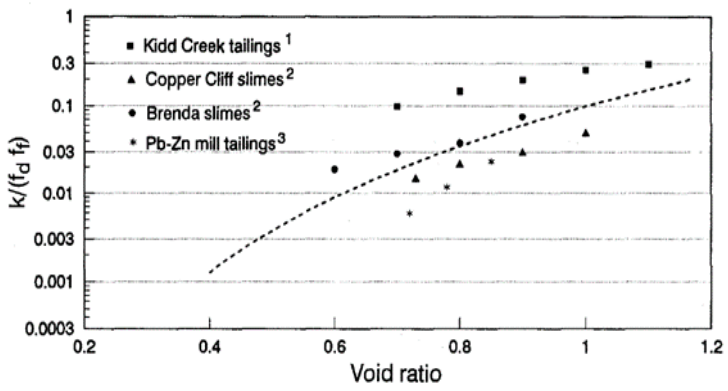

Figure 2-16: Comparison between calculated and measured relationship of saturated hydraulic conductivity and void ratio (taken from Aubertin et al. 1996).

2.2.4 Soil water retention characteristics

Soil water retention curve (SWRC) shows how the matric suction ψ varies with the volumetric water content θ. It is a basic characteristic of soil to link the hydraulic characteristics and mechanical property (Mbonimpa et al. 2006). A typical SWRC is shown in Figure 2-17. Air-entry value (AEV) is the matrix suction where air enters the largest pores of the soil while the residual suction is the suction large enough to expel the residual water in the soil.

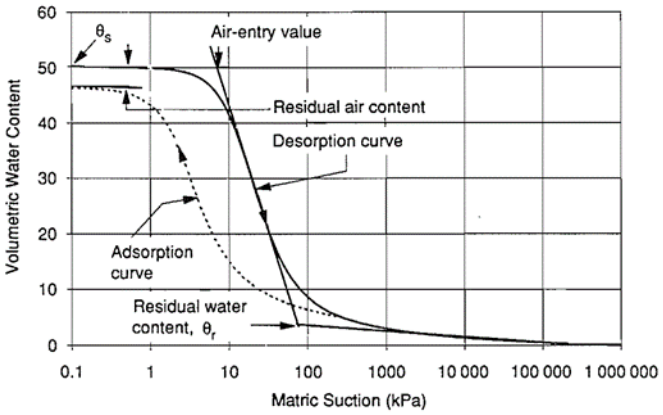

Figure 2-17: A typical soil water retention curve of silty soil (taken from Fredlund and Xing 1994).

The comprehensive understanding of the SWRC is crucial to analyze many issues related to unsaturated strength of soil. For the non-plastic soils like hard rock tailings, the air entry value and residual suctions are important to characterize the water retention properties. The air entry value for fine particles tailings generally ranges from 10 and 70 kPa while the coarse particle tailings have a smaller air entry value (Bussière 2007). The SWRC models proposed by Fredlund and Xing (1994) and Van Genuchten (980) have been proven to describe well the soil water retention curves of tailings. Aubertin et al. (2003) proposed a modified Kovacs (MK) model to predict soil water retention curves with some basic geotechnical parameters:

$$S_r = \frac{\theta}{n} = 1 - \langle 1 - S_a \rangle \langle 1 - S_{ca} \rangle \tag{2-7}$$

where S_r is degree of saturation; θ is volumetric water content; S_a and S_{ca} are the saturation by adhesion and capillary saturation, respectively, described as follows:

$$S_{ca} = 1 - \left[\left(\frac{h_{co}}{\psi}\right)^2 + 1 \right]^m exp[-m(h_{co}/\psi)^2] \tag{2-8}$$

$$S_a = 0.01 \left\{ 1 - \frac{\ln[1+\psi/(0.86 h_{\infty}^{1.2})]}{\ln[1+\psi_0/(0.86 h_{\infty}^{1.2})]} \right\} \frac{\ln(\frac{h_{co}}{\psi_n})^{2/3}}{e^{1/3}(\frac{\psi}{\psi_n})^{1/6}} \tag{2-9}$$

where m is a material parameter equal to $1/C_U$; ψ_n equals to 1 cm if ψ is given in cm; h_{co} is the average rise of capillary calculated with the following equation:

$$h_{co} = \frac{0.75}{eD_0 \times 1.17 \times \log C_u + 1} \tag{2-10}$$

Figure 2-18 shows a comparison between the predictive results and the measured water retention curves. It is seen that the agreement between them is good.

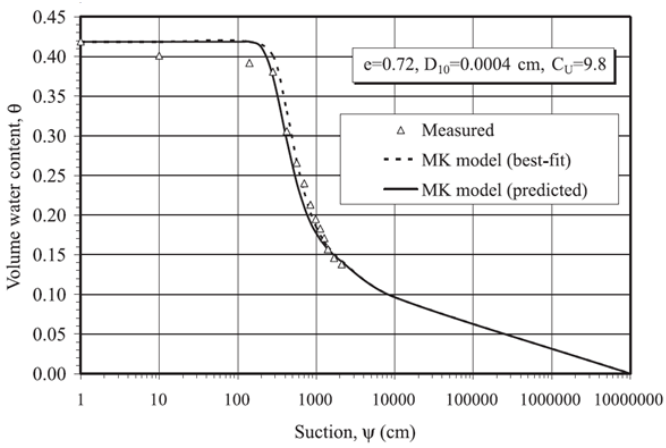

Figure 2-18: Comparison between predicted SWRC using MK model and measured SWRC with given void ratio and gradation characteristic for typical hard rock tailings (taken from Aubertin et al. 2003).

2.2.5 Strength properties

The strength properties of tailings include the cohesion and internal friction angel. Strength properties of tailings significantly affect the stability of tailings storage facilities. Based on undrained shear tests, Vick (1990) reported total cohesion between 0 and 100 kPa and total friction angle between 14˚ and 25˚. By summarizing previously published results obtained on saturated tailings samples, Bussière (2007) reported that the effective cohesion is close to zero while the effective friction angle ranges from 30˚ to 42˚. James et al. (2011) performed direct shear tests on drained tailings. Their results showed an effective friction angle of 36.6˚ but zero effective cohesion. Jehring and Bareither (2016) conducted undrained triaxial tests on copper tailings. Their results showed effective friction angle ranging from 34.0˚ to 36.1˚. The coal tailings and oil sand tailings showed similar effective friction angles of 32˚ to 34˚ but with small cohesions (Qiu and Sego 2001). In addition, the degree of saturation, void ratio of samples and stress path affect the strength properties (Bussière 2007).

2.3 Shrinkage theory of soils

Shrinkage by desiccation is a fundamental process describing the volume change of soils associated with the water loss by evaporation and induced suction (Holts et al. 2011). For swelling soils, the volume change during desiccation is considerable and can induce excessive settlement, desiccation cracks, etc. The cracks of soils affect the strength, permeability and other geotechnical properties (Tang et al. 2011).

Shrinkage characteristics of soils are generally described by the relationship between water content (*w*) and void ratio (*e*). The curve relating *w* and *e* is called shrinkage curve (Fredlund et al. 2002). Figure 2-19 shows typical shrinkage behaviors of non-structured soils in disturbed loose and non-aggregated state and structured soils containing large inter-aggregate pores, respectively.

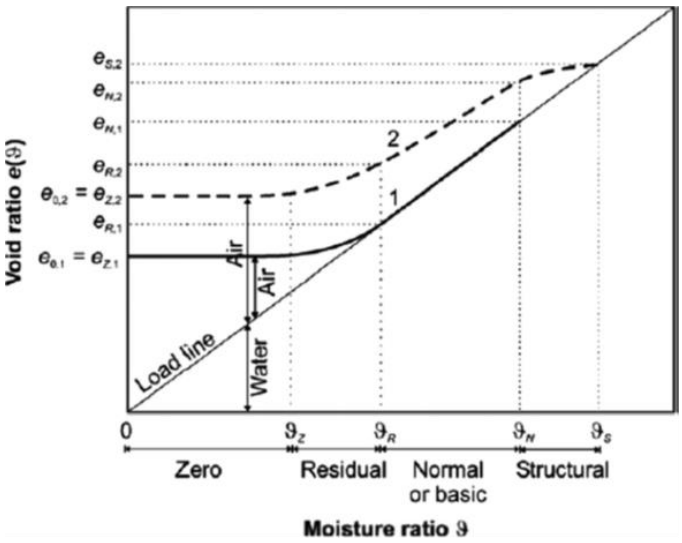

Figure 2-19: Representative shrinkage curve for a non-structured soil and a structured soil (take from Cornelis et al. 2006a).

In Figure 2-19, Curve 2 (dashed line) shows the variation of *e* with *w* of a structured soil. The shrinkage is divided into structural shrinkage, normal shrinkage, residual shrinkage and zero shrinkage. For unstructured soils, Curve 1 (solid line) shows an absence of the structural shrinkage stage, compared to the shrinkage curve of structured soils. In the normal shrinkage stage, the volume variation totally results from loss of water and the volume reduction of the tested soil is equal to the volume of evaporated water. As a result, the variation of void ratio is proportional to the variation of water content in such stage. When the water content decreases to a critical value at

which the grain-grain contacts begin and air enters the largest voids, the unsaturation process starts. The suction corresponding to the onset of unsaturation represents air entry value (Saleh-Mbemba et al. 2011; Saleh-Mbemba et al. 2010). With further water evaporation, the degree of saturation decreases to below 100% and the pace of volume change significantly diminishes. This stage is called residual shrinkage stage. At the end of this stage, the void ratio then becomes constant with more water loss. This stage is called zero shrinkage stage. The water content at the intersection between the normal shrinkage stage and zero shrinkage stage is called apparent shrinkage limit (*SL'* or w_s) (Fredlund et al. 2002; Holtz et al. 2011). The water content at which the volume of soil stops decreasing and keeps constant after the residual shrinkage stage is called true shrinkage limit (*SL*) (Cornelis et al. 2006a).

2.3.1 Shrinkage tests

2.3.1.1 Conventional shrinkage tests

Shrinkage test is usually conducted to obtain the shrinkage curve. This test is simple and easy to realize, only requiring the volume and mass measurements with a Vernier caliper and a balance. The void ratio and water content can after then be calculated. Conventional shrinkage test methods include the method of direct measurement of dimensions and volume replacement method (Upreti and Leong 2018). In volume replacement method, wax, mercury can be used to coat the specimen to obtain the volume (Gapak et al. 2017). The wax and mercury coat will prevent water evaporation from specimen. Therefore, volume replacement method with wax and mercury generally requires duplicate soil specimens with different water contents to determine the whole shrinkage curve. Other encasement materials like PVAc (unibond waterproof polyvinyl acetate) glue can also be used to replace wax or mercury. This is called clod method. The PVAc glue allows the evaporation of specimen from clod. Therefore, we can use only one specimen with clod method to determine the shrinkage curve. The direct volume measurement is easy but not very accurate while the volume replacement method is a destructive method.

Many studies were conducted to investigate the shrinkage properties of plastic soils because the volume change induced by desiccation is important for engineering structures on clayey soil foundations (Marinho 1994). However, there are few researches on the shrinkage of non-plastic

silts (Péron et al. 2009b). Péron et al. (2006) performed shrinkage tests on both silty and clayey soils. Figure 2-20 shows a picture of a mold with a base made of Teflon. The wall friction was largely reduced to avoid cracking. A metal substrate with thin spaced notches was placed at the bottom of the mold in order to generate cracking. The horizontal and vertical deformations were measured at different water contents while the mass was weighed with balance. Figure 2-21 shows the variations of void ratio and strains in three directions with water content. In addition, the suction change with desiccation and crack geometry evolution were also measured with tensiometer and a digital camera. From the cracking onset and suction measurement, cracking was found to start at the beginning of unsaturation for silty soils when the suction approached the air entry value while the water content was also close to the shrinkage limit. The test results showed that the cracking occurs when the moisture distribution is non-uniform and tensile stress increases under restraint boundary.

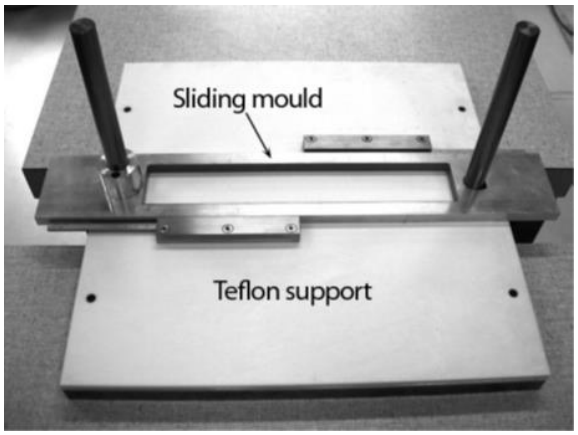

Figure 2-20: Sliding mold with Teflon base in the desiccation tests (taken from Péron et al. 2009b).

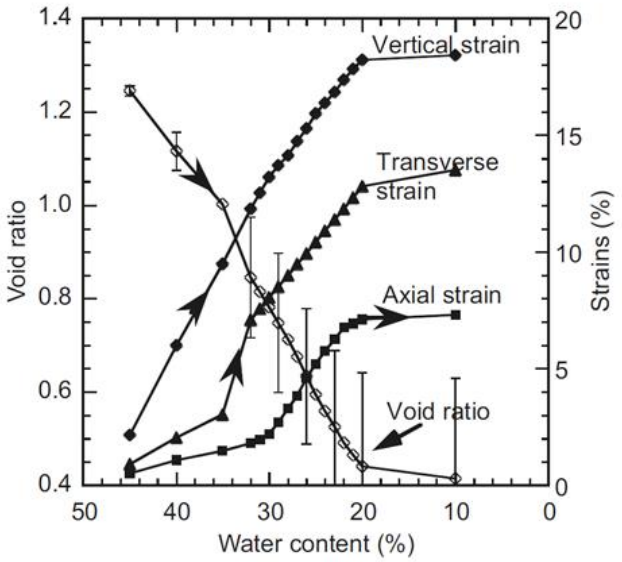

Figure 2-21: Variations of void ratio and strains in three directions with water content (taken from Péron et al. 2009b).

The physical and mechanical properties of hard rock tailings are similar to those of silty soils. So, the methodology to study the shrinkage of non-plastic soils can be applied to hard rock tailings. Saleh-Mbemba et al. (2016) studied the shrinkage of hard rock tailings by considering different water contents. Their experimental setup was similar to that of Péron et al. (2009b). The internal walls of the mold were covered by a plastic film to reduce the resistance of desiccation deformation and ensure a one-dimensional evaporation at the top surface of the sample. Pressure plate tests were conducted to obtain the soil water retention curve (SWRC) of the sample. Figure 2-22 shows the relationship between void ratio (e), degree of saturation (S_r) and volumetric water content (θ) with suction as well as water content, indicating that water content at air entry value (AEV) is close to the shrinkage limit for hard rock tailings. During the constrained shrinkage tests, crack propagations were observed. The water content at cracking onset was close to the water content at AEV. Water content at AEV is a good indicator of crack initiation for tailings. Regarding the effect of initial water content on the shrinkage properties, Figure 2-23 shows that the final void ratio and shrinkage limit increase as the water content increases from 40 to 48%. The final void ratio and shrinkage limit increase as the initial void ratio increases, as shown in Figure 2-24.

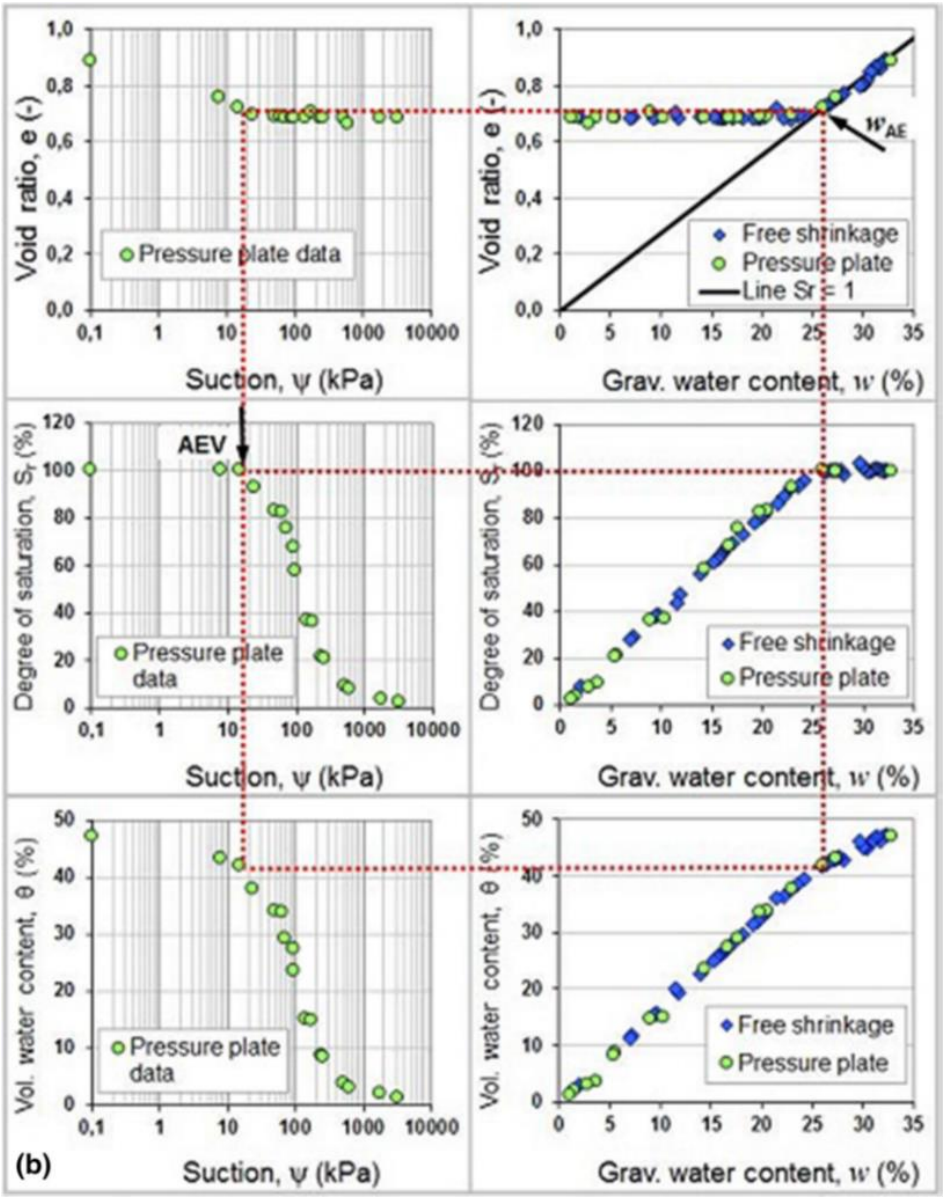

Figure 2-22: Experimental curves of e-ψ, S_r-ψ, θ-ψ, e-w, S_r-w and θ-w (taken from Saleh-Mbemba et al. 2016).

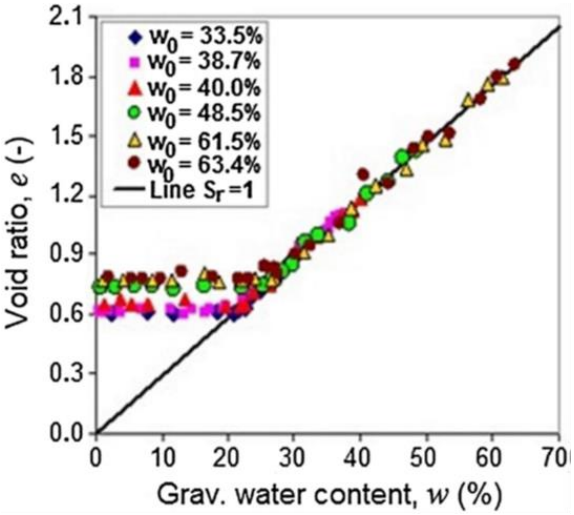

Figure 2-23: Shrinkage curves of hard rock tailings with different initial water contents (taken from Saleh-Mbemba et al. 2016).

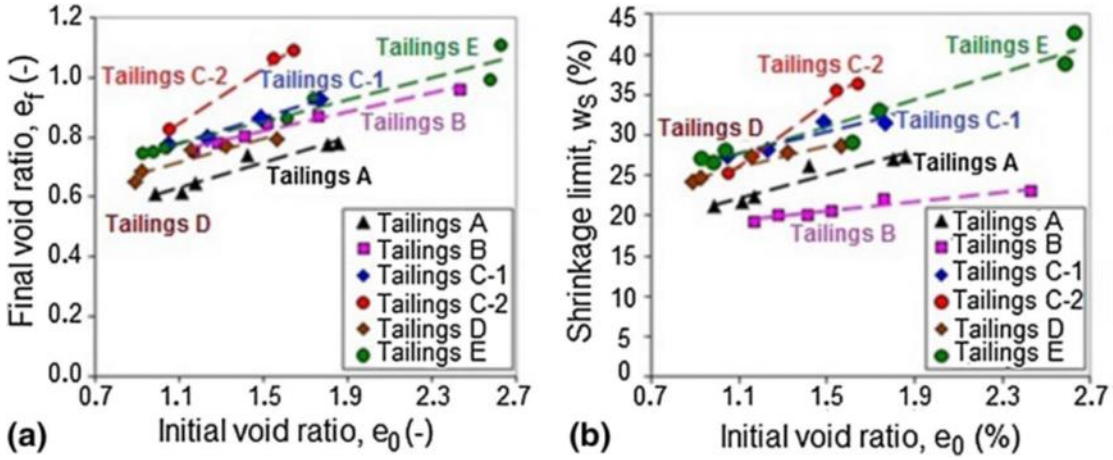

Figure 2-24: Relationship between (a) final void ratio e_f, and (b) shrinkage limit w_s with initial void ratio e_0 for different tailings (taken from Saleh-Mbemba et al. 2016).

The desiccation phenomenon of mine wastes was investigated by Rodríguez (2006). A coupled hydromechanical formulation was considered by considering the conservation of solid and liquid masses and equilibrium equation in total stresses. A constitutive equation between applied stresses, suctions and volumetric strains was proposed. The hydromechanical formulations were programmed in a numerical code based on the finite element method. The mechanical and hydraulic properties were determined through psychrometer tests, constant head tests, oedometer tests, unconfined compression tests and uniaxial tension tests. A series of desiccation tests were

then carried out, some of which were realized with open plates under atmospheric conditions and others in a hermetic container with a control of the inner relative humidity (*RH*). Water loss and vertical contraction were recorded while the crack patterns were photographed. Figure 2-25 shows the relationships of *e*-ψ and *e*-*w* obtained by drying process and drying-wetting process, respectively while the evolution of water loss and vertical strain is shown in Figure 2-26. The numerical results of moisture content and horizontal stresses were obtained. Rodríguez (2006) indicated that crack formation was due to the horizontal stress exceeding the tensile strength of tailings.

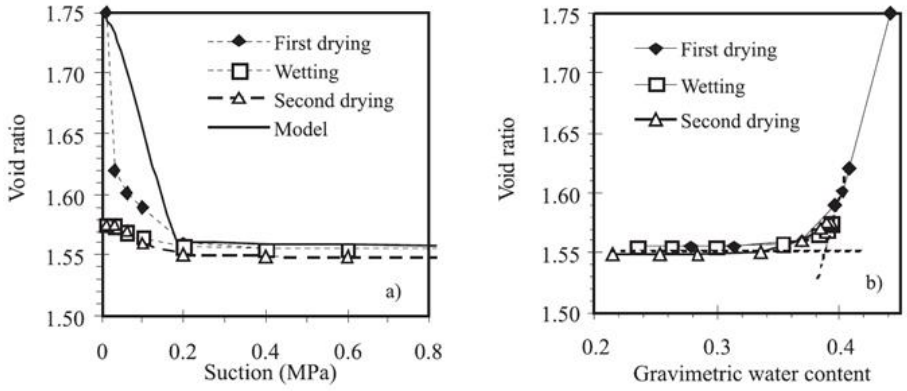

Figure 2-25: (a) *e*-ψ curve, and (b) *e*-*w* curve under different drying and wetting stages (taken from Rodríguez 2006).

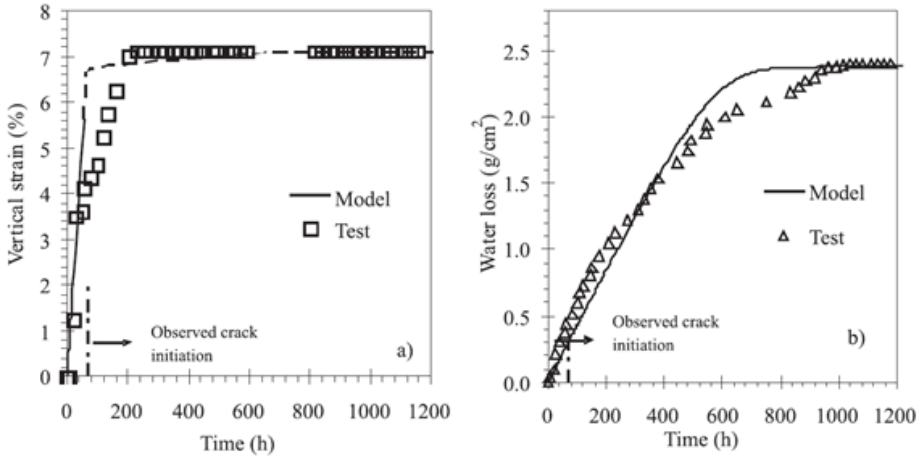

Figure 2-26: Variations of (a) vertical strain, and (b) water loss with desiccated time obtained from desiccation tests and numerical modelling (taken from Rodríguez 2006).

The volume replacement method based on Archimedes' law was used to measure the volume change of soil (Reeve et al. 1980; Krosley et al. 2003). This method is accurate but destructive. The method consists to determine the volume of dry soil immersing in water after the soil surface being coated of some immiscible materials. The mercury replacement method was withdrawn from ASTM recommendation due to the poisonous characterizations of mercury (ASTM 2008) while wax method is considered to be safe to acquire w_s for fine-grained soils. Nevertheless, Prakash et al. (2009) conducted shrinkage tests by using the mercury method and wax method. The volume of coating wax was calculated by considering its density and measured mass. The volume of the tested dry soil sample was obtained as the difference between volume of coated soil sample and the volume of the applied wax. The measured volume of the dry soil sample can be used to calculate the shrinkage limit as follows:

$$SL = \left[w - \left\{\frac{V - V_d}{m_d}\rho_w\right\}\right] \tag{2-11}$$

where, SL is the shrinkage limit; w is the initial water content of soil; V is the volume of wet soil; V_d is the volume of the dry soil; m_d is the mass of dry soil and ρ_w is the density of water.

Figure 2-27 shows the comparisons between the shrinkage limits obtained by wax method and mercury method. The difference is on the order of $\pm$3.8%, which was considered as acceptable in practice.

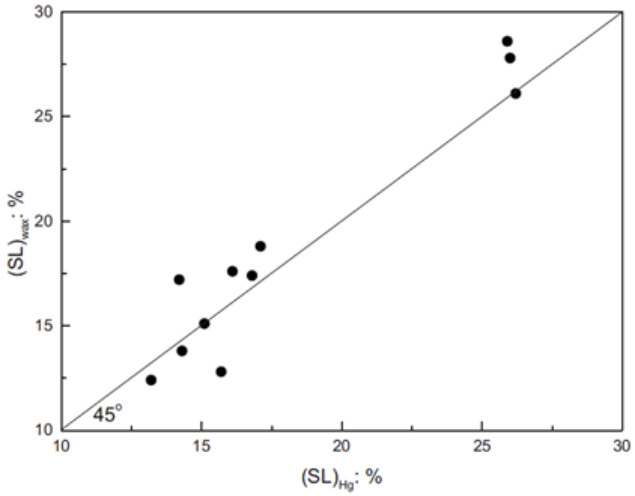

Figure 2-27: Comparison between shrinkage limit determined by wax method and mercury method (taken from Prakash et al. 2009).

Since the volume replacement method using mercury, wax or other materials is not appropriate for the continuous volume measurement of one single simple. The balloon method using balloon covering the soil specimen is developed to measure the volume change with time (Tariq and Durnford 1993; Gapak et al. 2017). Gapak et al (2017) used four kinds of bentonite as experimental materials and studied their shrinkage curves obtained with four conventional methods including wax coated method, clod method, direct volume measurement and balloon method. By using the balloon method, the air flow passing the exit pipe and inlet pipe can help to control ambient air in the shrinkage process while the volume of bentonite sample can be measured with the Archimedes' principle immersing in water. However, errors can be caused by the neglect of the volume of balloon in the volume measurement of bentonite. Figure 2-28 shows the shrinkage curves of all four bentonites with different measurement methods. The difference between the shrinkage curves obtained by balloons and those obtained by other methods indicates that the measured void ratio was largely affected by the errors induced by the neglect of the balloon's volume.

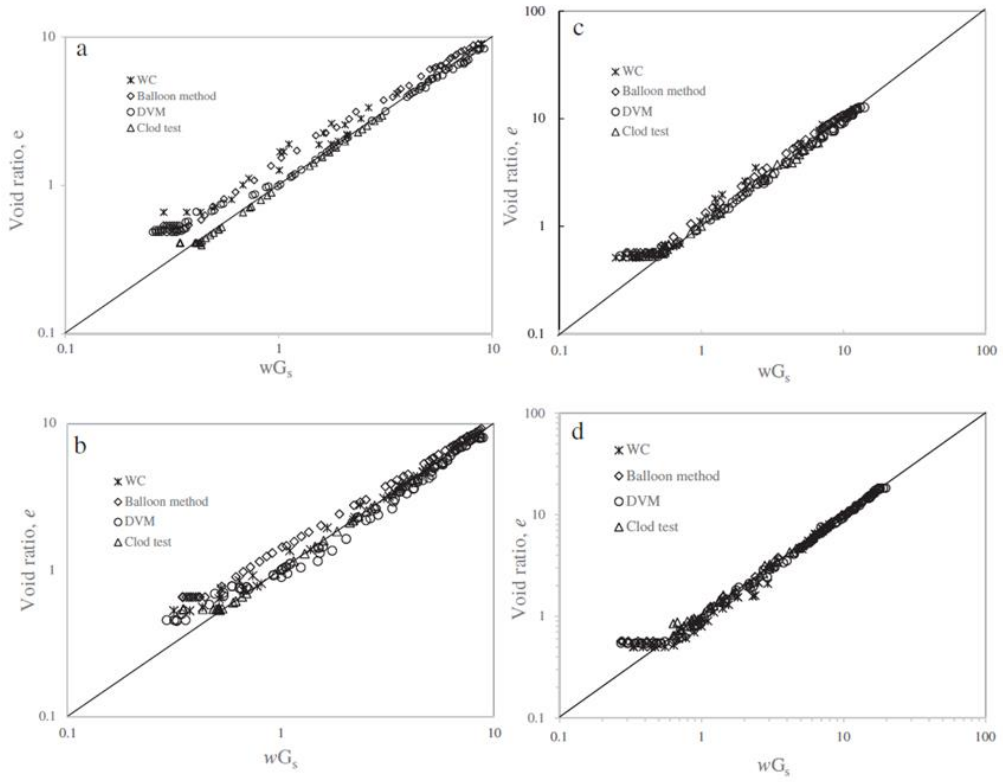

Figure 2-28: Shrinkage curves obtained with different measurement methods for four types of bentonites (taken from Gapak et al. 2017).

Generally, the shrinkage tests need long time to realize. Krisdani et al. (2008) tried to reduce the experiment duration by increasing the evaporation rate. They conducted a series of shrinkage tests under different drying rates and investigated the associated effects. Three different soils including 100% residual soil, 80% residual soil +20% fine soil and 60% residual soil +40% fine soil were tested. The soil samples were respectively put under ambient conditions, a fan and a lamp to achieve different drying rates. The variations of void ratio with elapsed time indicated that only the decrease rates of void ratio were affected by drying rates while final void ratio kept constant. As shown in Figure 2-29, the shrinkage curves were not influenced by the evaporation rates, which demonstrated the possibility of reducing the time duration for shrinkage tests by modifying the drying conditions. Umezakin and Kawamura (2013) thus proposed a vacuum evaporation method to reduce the water content more quickly. A negative pressure was then supplied with a vacuum pump to promote the air evaporation.

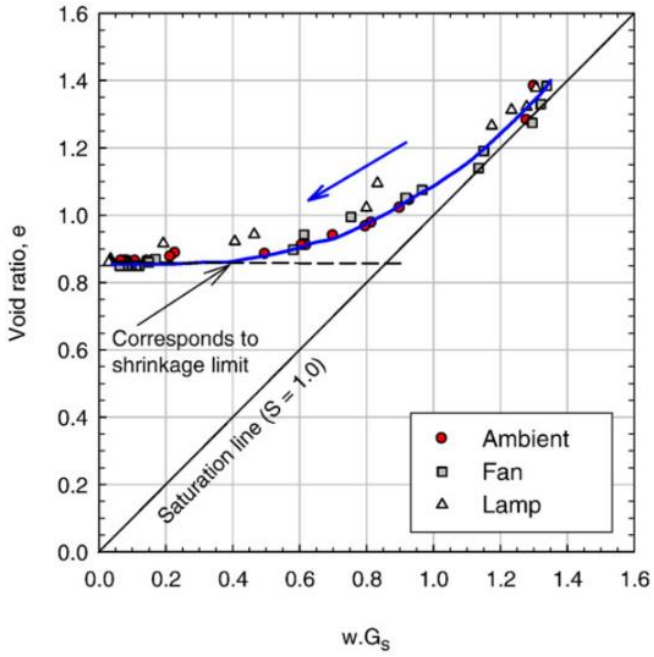

Figure 2-29: Shrinkage curves measured under different evaporation rates (taken from Krisdani et al. 2008).

2.3.1.2 Shrinkage tests of soils with additives

Soil improvement technology was developed and applied in different domains of geotechnical engineering, in which soil is always modified with some additive materials like cement or other binders. The backfill amended with cement is also one form of soil improvement with additives. After the addition of additives, the shrinkage properties of soil may change.

Compacted clays are commonly utilized to construct barriers in waste disposal facilities like nuclear containment facility, tailings ponds and solid waste landfills (Albrecht and Benson 2001). Under the evaporation and desiccation induced by sun, tree roots or other influencing factors, the compacted clays may undergo excessive shrinkage and desiccated cracking, which will immensely increase the hydraulic conductivity of barriers and result in the leakage of unfavorable materials. Therefore, some additives like sand, lime and fibers have been utilized to help control the volume change of compacted clays (Omidi et al, 1996; Tang et al. 2012).

Cement is a conventional material used in soil improvement while the chemical shrinkage and hydration heat sometimes will bring problems to the treated soils. Wang et al. (2011) investigated the shrinkage properties of cement solidified sludge generated from port engineering and channel engineering. The excessive shrinkage of sludge used as a backfill material will lead to cracks and influence the strength, permeability and stability of filled soils. The effects of cement contents, initial water contents and curing time on sludge's strength and volume change properties were studied through uniaxial compression tests and shrinkage tests. Figures 2-30, 2-31 and 2-32 show the varied volume shrinkage ratio (ratio of decreased volume to initial total volume) and strength with different initial water contents, curing periods and cement contents. The increased initial water content significantly increased volume shrinkage ratio but reduced the strength. The longer curing time was found to increase both the measured parameters. The volume shrinkage ratio decreased while the strength increased as the cement content increased. They also studied the effects of lime on the shrinkage properties of sludge (Wang et al. 2012). The results showed that it had a similar effect as cement.

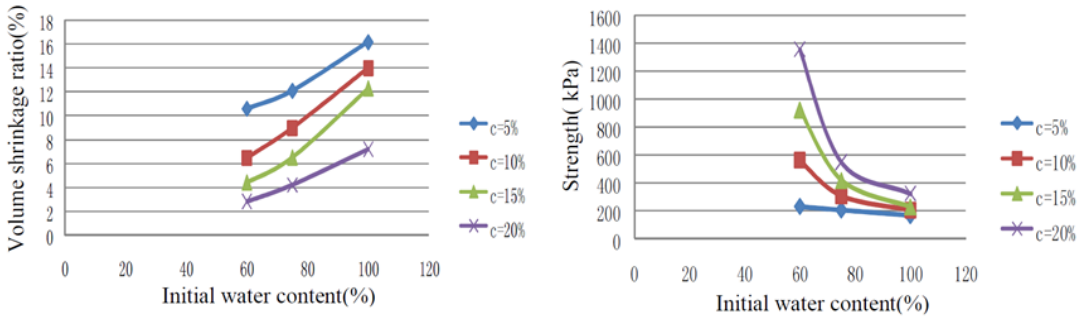

(a) (b)

Figure 2-30: Variations of (a) volume shrinkage ratio, and (b) strength with initial water content under different cement contents (taken from Wang et al. 2011).

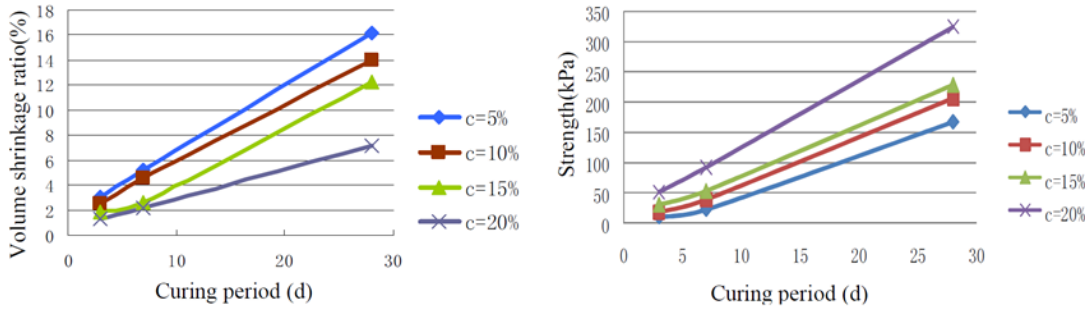

(a) (b)

Figure 2-31: Variations of (a) volume shrinkage ratio, and (b) strength with curing period under different cement contents (taken from Wang et al. 2011).

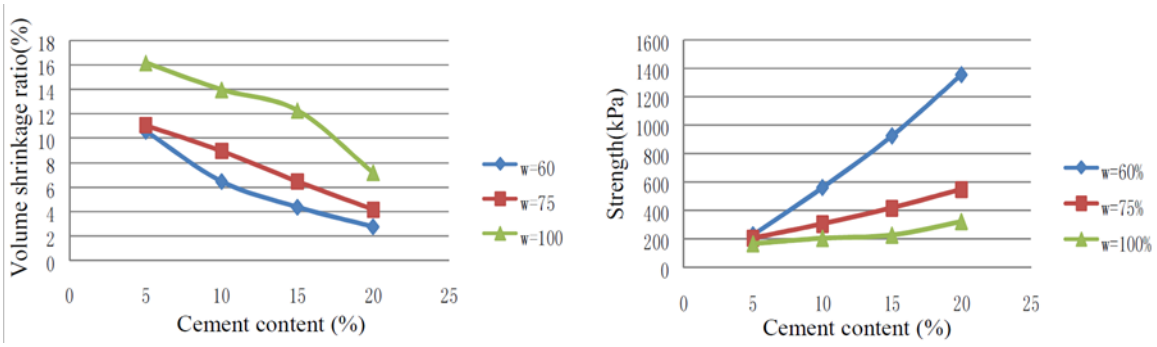

(a) (b)

Figure 2-32: Variations of (a) volumetric shrinkage ratio, and (b) strength with cement content under different initial water contents (taken from Wang et al. 2011).

Dash and Hussain (2015) measured shrinkage properties of lime amended soils. Six different soils with different plastic limits were treated with a wide range of lime contents and cured for different periods. The shrinkage curves of treated samples with different lime contents and curing time were shown in Figure 2-33. In general, the addition of lime helped to reduce the shrinkage of all treated soils while the volumetric shrinkage response of 100% residual soil shown an unobvious change due to its inconsiderable volume change properties.

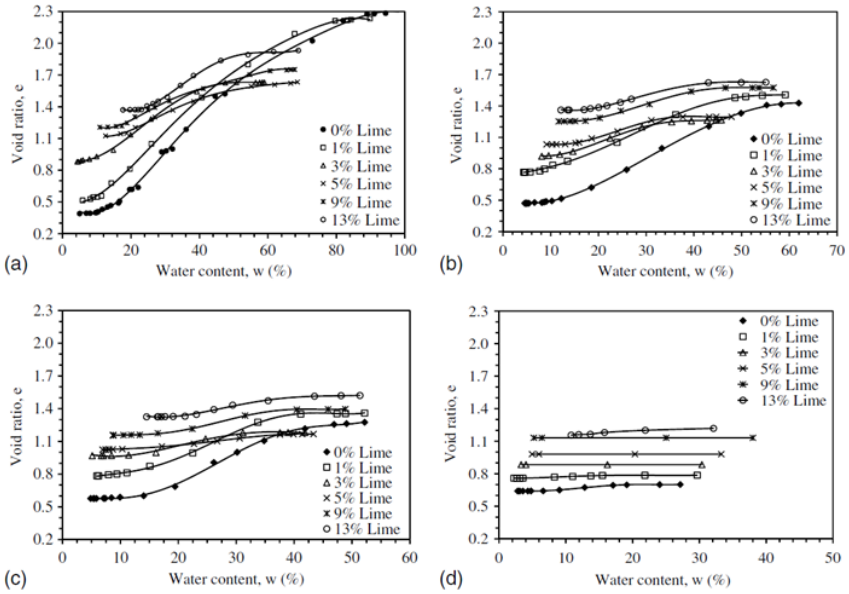

Figure 2-33: Shrinkage curves under different lime contents of different mixed soils (taken from Dash and Hussain 2015).

The effect of the coir waste to reduce desiccated volume change of expansive soils was investigated by Jayasree et al. (2015). Marine clays treated with different contents of coir pith and coir fiber were tested in the shrinkage tests. Figure 2-34 shows the variations of Atterberg parameters with different coir waste contents. For both kinds of coir waste, the shrinkage limits were found to increase with the content of additives.

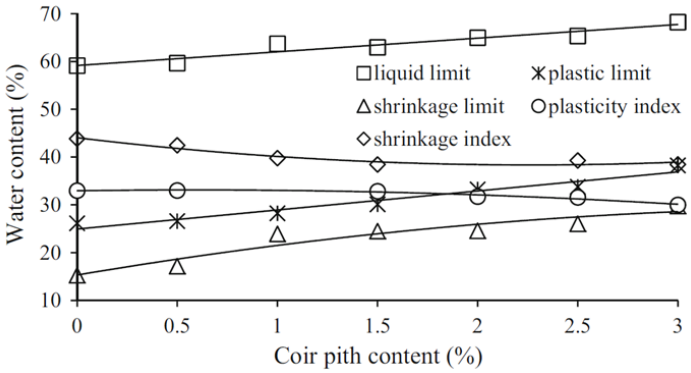

(a)

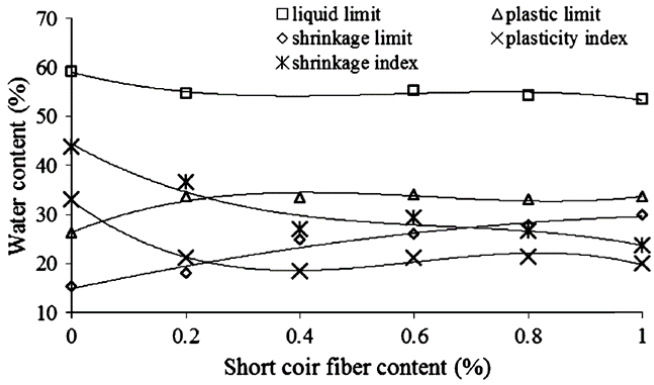

(b)

Figure 2-34: Variations of Atterberg limits with added content of (a) coir pith, and (b) short coir fiber (taken from Jayasree et al. 2015).

The pore fluid salinity has some effects on the volume change properties of soils (Fourie et al. 2001; Tang et al. 2011). Mishra et al. (2019) conducted a series of shrinkage tests with kaolin clay amended with different concentrations of NaCl and KCl. The images of the specimens were photographed to study the surficial morphology. From the images, samples with high pore fluid salinity are found to separate out the flocculated clusters of salt and the cracks will never occur in all samples. The shrinkage tests provided shrinkage curves and the relationship between density and water content under different salinity types and concentrations. Minimum void ratio and shrinkage limit of specimen decreased with increase of salinity concentration for both specimens amended KCl and NaCl as shown in the Figure 2-35. Additionally, the shrinkage limit and minimum void ratio of NaCl amended samples are smaller than those added with KCl. The reduced

thickness of diffused double layers, increased osmatic suction and inter-particle attraction induced by high salty concentration are believed to lead to facilitation of shrinkage.

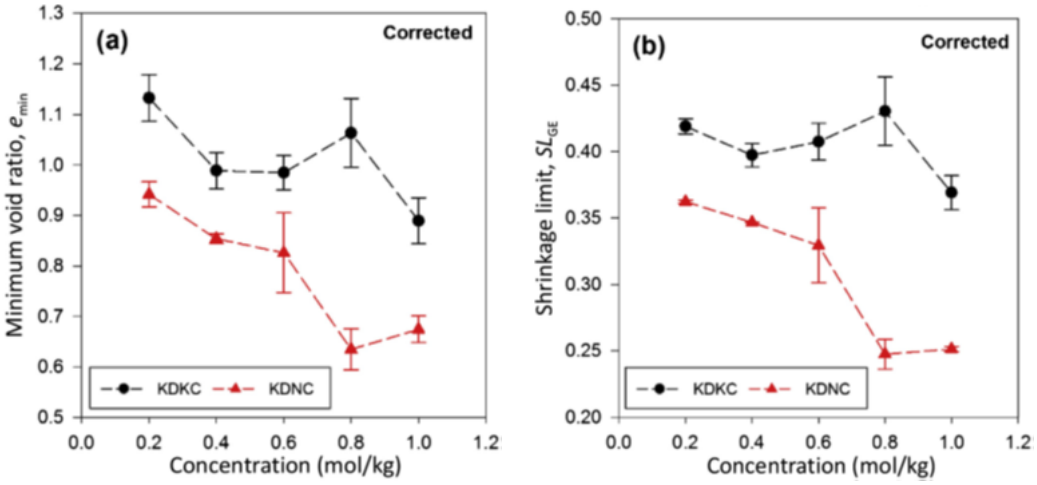

Figure 2-35: Variations of (a) minimum void ratio e_{min}, and (b) shrinkage limit, SL_{GE} for kaolin clays amended with KCl and NaCl (taken from Mishra et al. 2019).

The shrinkage characteristics of low plastic soils polluted with NaCl were investigated by Zhang et al. (2017) and later by Mishra et al. (2019). Soluble salt of 0%, 2% and 5% of mass content was mixed with dry silt powders and then added with distilled water to the water content of 45%. Shrinkage tests with fluid replacement method were conducted while three methods including pressure plate test, filter paper test and vapor equilibrium test were utilized to measure the SWRC of NaCl contaminated soils. The shrinkage curves for three NaCl contaminated soils were shown in Figure 2-36 and indicated that the soluble salt had no influence on shrinkage curves of samples. Then two shrinkage models were applied to describe the shrinkage curves (McGarry and Malafant 1987; Cornelis et al. 2006b). With the SWRCs of the three kinds of polluted soils, the relationships between void ratio and matrix suction were built as shown in Figure 2-37. It can be seen that the curve can be divided into three parts based on the degree of saturation and void ratio change.

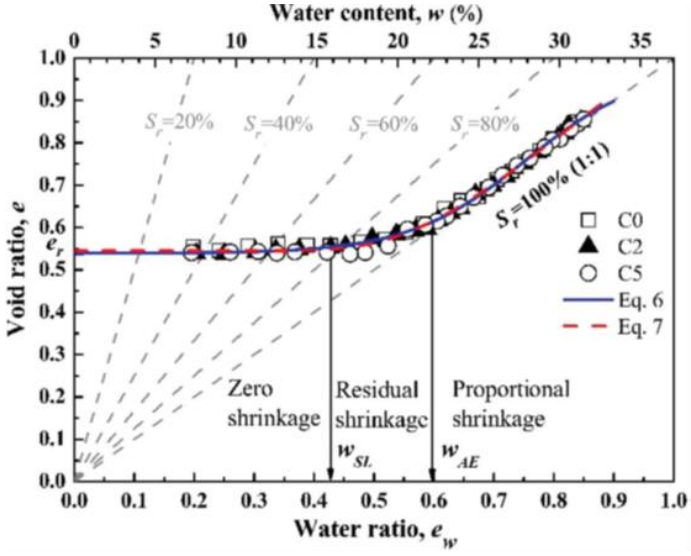

Figure 2-36: Shrinkage curves of low plastic soils amended with different contents of NaCl and the fitted curve with two shrinkage models (taken from Zhang et al. 2017).

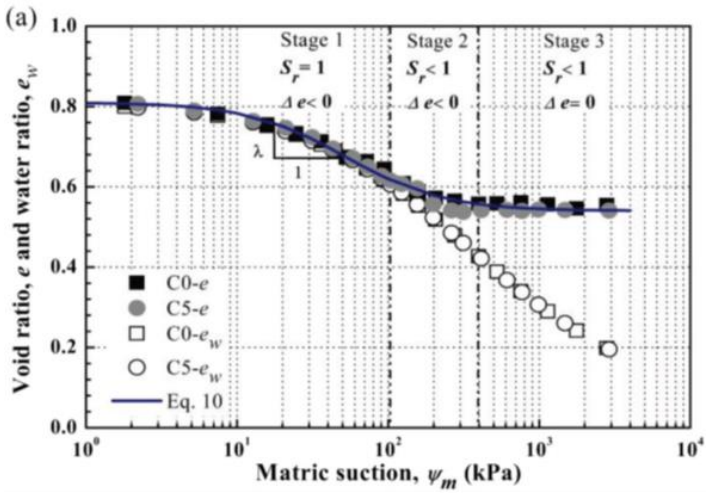

Figure 2-37: Relationship between void ratio and matric suction of NaCl amended soils (taken from Zhang et al. 2017).

Kananizadeh et al. (2011) have shown that the mixture of nanoparticles can effectively reduce the hydraulic conductivity of clays. Recently, the potential of nanoparticles including nano-CuO and γ-Al_2O_3 as an additive to control shrinkage was assessed by Coo et al. (2016). Coo et al. (2016) used a kaolin clay and two types of nanoparticles as additives. The two types of nanoparticles are insoluble in water and chemically stable. The kaolin samples with nanoparticles were compacted

and coated with wax to determine the volume of desiccated samples for shrinkage curve measurement. The fabric association between clay particles and nano-CuO was also observed with SEM imaging. Figure 2-38 shows the shrinkage curves, which indicated that a higher amount of nano-CuO could help to increase the shrinkage limit and final void ratio of clays. Similarly, γ-Al_2O_3 shows the same potential of reducing volume shrinkage as nano-CuO. The SEM images indicated that the clays with 6% nano-CuO had a more non-uniform and flocculated fabric compared with pure clays. Based on the test results, the nanoparticles are efficient to prevent excessive volume change of clays.

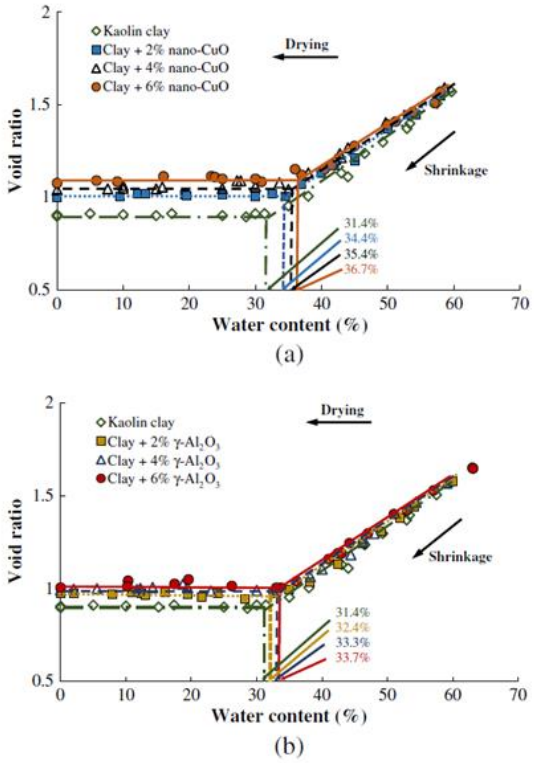

Figure 2-38: Shrinkage curves of clay amended with different contents of (a) nano-CuO, and (b) γ-Al_2O_3 (taken from Coo et al. 2016).

2.3.1.3 Advanced volume measurement in shrinkage test

As the conventional direct measurement methods are imprecise while the volume fluid replacement methods are destructive on specimen, some new technologies were developed, including volume determinations based on scanning (Jain et al. 2015; Sander and Gerke 2007; Wong et al. 2018) and photogrammetry (Li and Zhang 2019).

Wong et al. (2018) developed a procedure using three-dimension scanner to measure the volume of soil specimen. With three-dimensional scanner and related software, the three-dimensional point can be plotted. The three-dimensional point of soil specimen can be further edited and used to calculate the total volume. However, there was a little error of the calculated volume by scanning compared with the true volume. After several scanning of a certain object, a calibration factor was determined as follows:

$$Calibration\ factor(\alpha) = \frac{Scanned\ volume}{True\ volume} \tag{2-12}$$

Figure 2-39 shows the shrinkage curves for soils with low plastic, medium plastic and a high plastic, respectively, obtained from scanning methods. The shrinkage curves were then fitted with Fredlund shrinkage model (Fredlund et al. 2002). The agreements between the Fredlund model and experimental results are good.

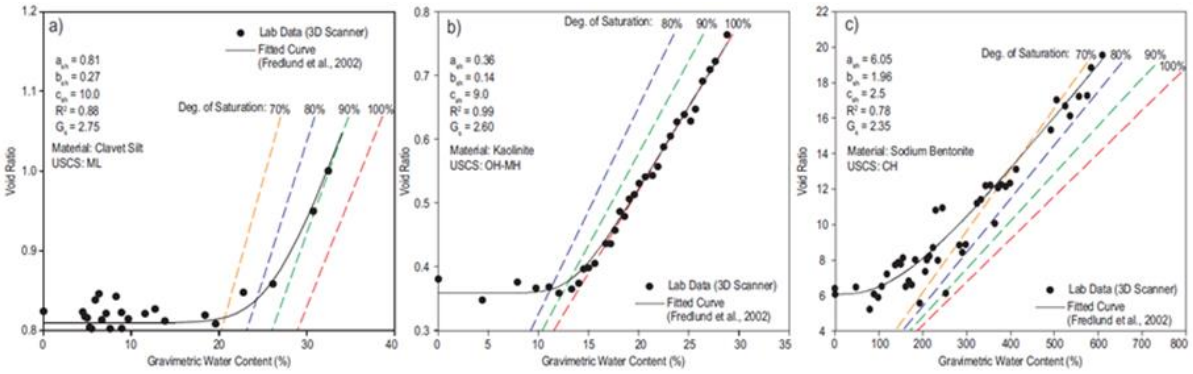

Figure 2-39: Comparison between shrinkage curves obtained with three-dimensional scanning method and fitted curve with Fredlund model from (a) a low-plasticity soil, (b) a medium-plasticity soil, and (c) a high-plasticity soil (taken from Wong et al. 2018).

As three-dimension scanner is expensive and its access is limited, Upreti and Leong (2018) took use of the photogrammetry methods by using a cellphone and available free software for three-dimensional modelling. They used the mixture of bentonite and kaolin as the test specimen. The conventional direct measurement method tests were also conducted for comparisons. Figure 2-40 shows the volumetric strain determined from photogrammetry method and manual method. The results indicated that measurement by three-dimensional modelling of photogrammetry was reliable.

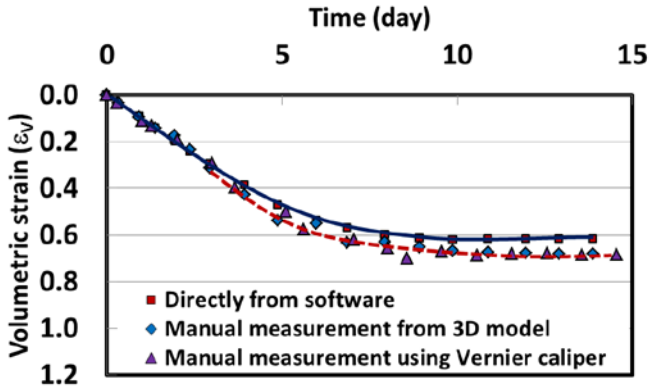

Figure 2-40: Comparison of the volumetric strain with time obtained from different measurement methods (taken from Upreti and Leong 2018).

2.3.2 Shrinkage model

The shrinkage properties of soils are generally associated with the soil water retention curves since void ratio e and matrix suction ψ can be linked in this way. For this purpose, several shrinkage models have been proposed (Peng and Horn 2005; Cornelis 2006b; Chen and Lu 2018; Crescimanno and Provenzano 1999; Leong and Wijaya 2015).

In soil mechanics, Fredlund model is easy and convenient to apply. The fitting parameters have certain physical meaning (Fredlund et al. 2002). Fredlund model is only applied to those unstructured soils which do not have the structural shrinkage phase. The model equation is based on the hyperbolic nature of the shrinkage curve. The proposed model is written as follows:

$$e(w) = a_{sh}\left[\frac{w^{c_{sh}}}{b_{sh}^{c_{sh}}} + 1\right] \tag{2-13}$$

where, a_{sh} equals to the minimum void ratio; b_{sh} equals to the slope of the line of tangency; c_{sh} equals to curvature of the residual shrinkage stage.

According to their definitions, a_{sh}/b_{sh} equals to G_s/S.

Figure 2-41 shows a comparison between some experimental results and fitting curves. A good agreement was obtained. Figures 2-42, 2-43 and 2-44 show the effect of some model parameters on the shrinkage behavior.

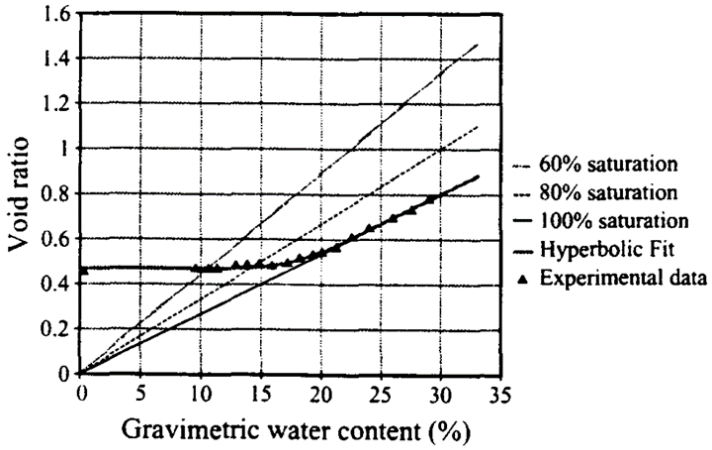

Figure 2-41: Comparison between shrinkage curves from experiment and proposed shrinkage equation (taken from Fredlund et al. 2002).

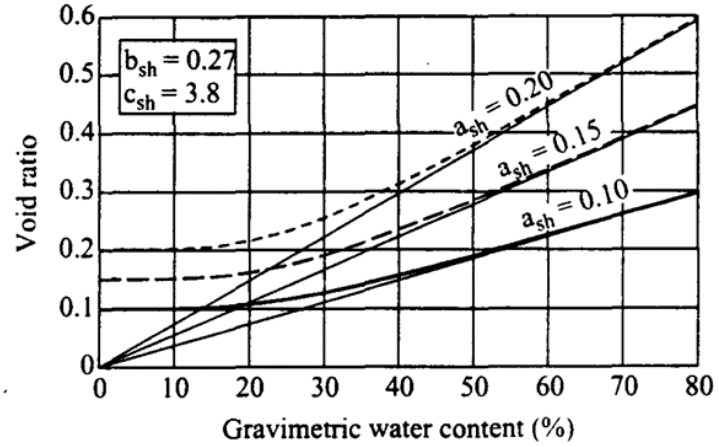

Figure 2-42: Variations of fitted shrinkage curves with different a_{sh} (taken from Fredlund et al. 2002).

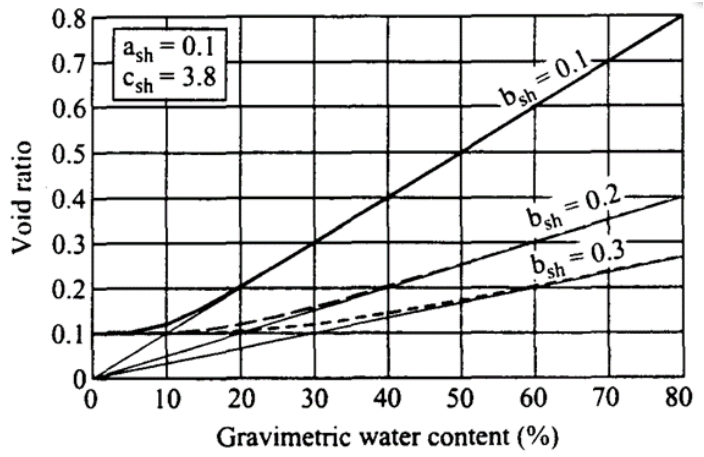

Figure 2-43: Variations of fitted shrinkage curves with different b_{sh} (taken from Fredlund et al. 2002).

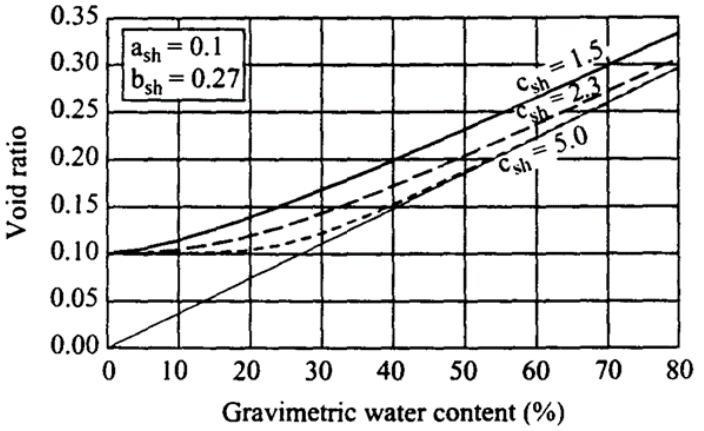

Figure 2-44: Variations of fitted shrinkage curves with different c_{sh} (taken from Fredlund et al. 2002).

The Fredlund model involves some drawbacks. For instance, the fitting parameters do not have clear and exact physical meaning. The model cannot be used to describe the structural shrinkage stage of structured soils. Gould et al. (2011) proposed a model composed of two parts:

$$e(w) = f(w,a) - f(w,b) - f(0,a) + f(0,b) + e_r \tag{2-14}$$

$$f(x,y) = -\frac{m}{\phi\pi}\langle \phi(x-y)\tan^{-1}[\phi(x-y)] - (1/2)\ln\{1+[\phi(x-y)]^2\}\rangle \tag{2-15}$$

where, w is water content; e is void ratio; a, b, e_r, m and φ are fitting parameters. Fitting parameters a and b affect the water content where the shrinkage curve's slope varies. Fitting parameter φ

controls the curvature of the segments around points *a* and *b*. Gould et al. (2011) also incorporated the net stresses in the shrinkage equation so that the void ratio could be derived with the water content and net stress of soils.

In soil science, some shrinkage models were also proposed between the void ratio and moisture ratio υ, which is defined as follows:

$$\upsilon = \frac{V_w}{V_s} \tag{2-16}$$

where V_w is the volume of water and V_s is the volume of solid.

McGarry and Malafant (1987) proposed a shrinkage model based on the S-shaped shrinkage curve:

$$e = e_0 + \frac{e_\upsilon}{1+exp[-\beta(\upsilon-\upsilon_i]} \tag{2-17}$$

where, e_υ is maximum void ratio range from the saturated condition to totally dry condition, υ_i is the moisture ratio at the inflection point and β is a slope parameter determined by AEV. Void ratio e_0 at $\upsilon = 0$ represents the lowest void ratio while $e_D = e_0+e_v$ is the upper asymptote.

This model has been approved to be appropriate for modelling the shrinkage curves containing the structural shrinkage stage (Crescimanno and Provenzano 1998).

Chertkov (2000, 2003) proposed a shrinkage model only applicable for the matrix of clay particles, expressed as follows:

$$e = \begin{Bmatrix} e_{min};\ \upsilon < \upsilon_{SL} \\ e_{min} + \mu(\upsilon - \upsilon_{SL})^2 \frac{\rho_w^2}{\rho_s};\ \upsilon_{SL} \le \upsilon \le \upsilon_{AE} \\ \upsilon;\ \upsilon > \upsilon_{AE} \end{Bmatrix} \tag{2-18}$$

where, e_{min} is the minimum void ratio; υ_{SL} is the moisture ratio at shrinkage limit; μ is a fitted model parameter; ρ_w and ρ_s are the density of water and density of soil particle; υ_{AE} is the moisture ratio at the suction of air entry value.

Cornelis et al. (2006b) proposed a shrinkage model which contains four parameters:

$$e = e_{min} + \gamma \left[\exp\left(\frac{-\xi}{\upsilon^\zeta}\right)\right] \tag{2-19}$$

where, e_{min} is the minimum void ratio for $\upsilon = 0$; γ, ζ and ξ are the model fitting parameters.

The fitted shrinkage model based on shrinkage tests can be used to determine soil's shrinkage, plastic and structural limits. However, this equation contains an implicit parameter ζ that reflects both the void ratio and swelling pressure. The determination of ζ requires a specific error minimization criterion. Other shrinkage models introduced in this section all involve explicit parameters that respectively represent one property of the curve and can be directly obtained from the shrinkage curve.

Leong and Wijaya (2015) proposed a model containing explicit parameters, which can capture different shrinkage curves including two, three and four segments shrinkage curve. The equation for two segments shrinkage curve is simplified as follows:

$$e(w) = e_{min} + \frac{G_s}{2S_0}\langle w + \frac{1}{k}\ln\left\{\frac{\cosh[k(w-SL')]}{\cosh(k..SL')}\right\}\rangle \quad (2\text{-}20)$$

where G_s is the specific gravity while S_0 is the initial degree of saturation. The parameter k is the curvature and can be calculated as:

$$k = \frac{2}{w_{AEV} - w_s} \quad (2\text{-}21)$$

where w_s is the shrinkage limit and w_{AEV} represents the water content corresponding air entry value.

Figure 2-45 shows a comparison between different fitted models. The Fredlund model has a higher coefficient of determination R^2 while the model by Leong and Wijaya also fits the measured shrinkage curve well.

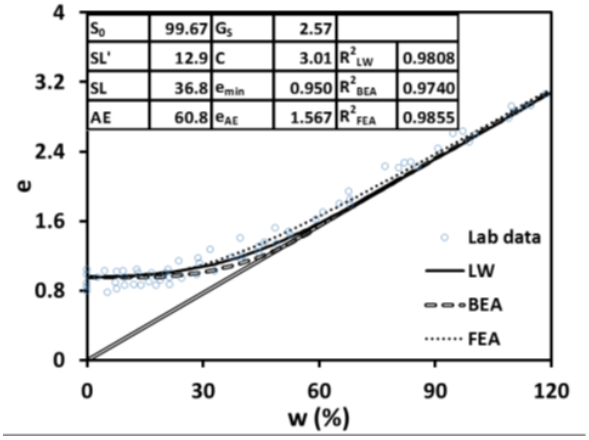

Figure 2-45: Comparison of shrinkage curves from lab data and three kinds of fitted shrinkage models (taken from Leong and Wijaya 2015).

Chen and Lu (2018) proposed another universal shrinkage model dividing the void ratio change into adsorption shrinkage void ratio e_a and capillary shrinkage void ratio e_{ca}:

$$e(\theta) = e_a(\theta) + e_{ca}(\theta) \tag{2-22}$$

$$e_a(\theta) = \frac{1}{2}\left[1 - \text{erf}\,(4\frac{\theta-\theta_{amax}^{SSC}}{\theta_{amax}^{SSC}})\right] \times c(\theta - \theta_{amax}^{SSC}) \tag{2-23}$$

where, erf () is the error function; θ_{amax}^{SSC} is the maximum adsorption volumetric water content; θ is the volumetric water content as υ and c is adsorption shrinkage rate.

$$e_{ca} = e_{ca0} + (e_s - e_{ca0} - e_a)\left[1 + \beta\frac{e_s-\theta}{\theta}\right]^{-\eta} \tag{2-24}$$

where, e_{ca0} is the void ratio at zero water content resulting from capillary shrinkage; e_s is the saturated void ratio; β and η are fitting parameters.

Figure 2-46 shows a conceptual illustration of shrinkage for clayey soil. The physical definitions of adsorption and capillary shrinkage void ratio are presented.

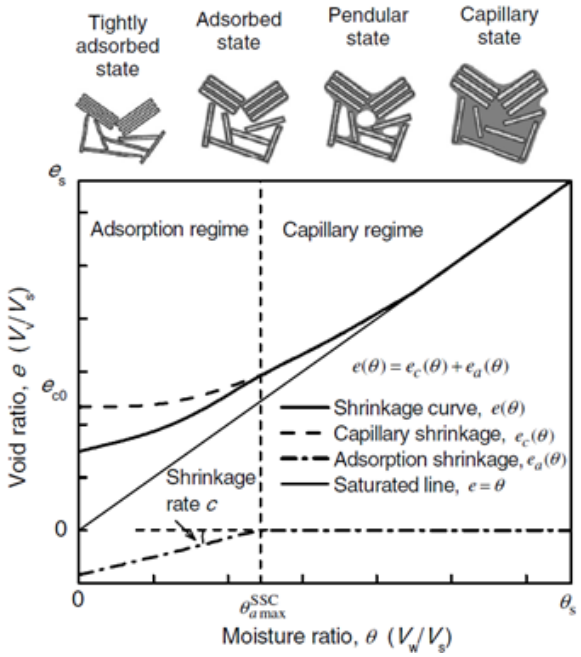

Figure 2-46: Conceptual illustration of shrinkage curve for clayey soil (taken from Chen and Lu 2018).

The model was then assessed with the shrinkage curves of non-structural and structural soils shown in Figure 2-47. The maximum adsorption water contents obtained respectively from soil water retention curve and shrinkage curve were very similar to each other.

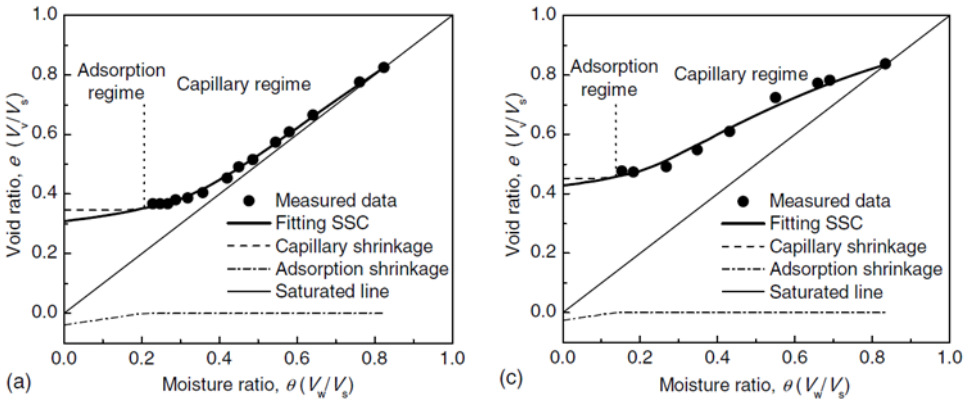

Figure 2-47: Comparison between measured shrinkage curve and fitted shrinkage curve by proposed shrinkage model for non-structured and structured clays (taken from Chen and Lu 2018).

2.3.3 Desiccation cracks in shrinkage

2.3.3.1 Desiccation cracking test

Desiccation cracks occur if the intrinsic stress exceeds the tensile strength of soil. The excessive intrinsic stress basically generates from the restrained boundary conditions like boundary frictions and adhesions, and different hydraulic gradient due to internal moisture distributions (Péron et al. 2009a). Since the cracking of soils will bring problems related to geotechnical, environmental and agricultural applications, the comprehensive understanding of the cracking formation mechanism and the crack propagations is necessary. Many field investigations on cracks of soil's surface have been reported (Konrad and Ayad 1997; Li and Zhang 2011) while more study on the crack morphology, cracking conditions and crack prevention should rely on the laboratory experiments with more details and accurate controlled conditions.

Nahlawin and Kodikara (2006) carried out a series of desiccation tests in a humidity chamber considering different layer thickness and relative humidity. In order to reduce the boundary friction, the mold walls were greased while the base was not covered by grease allowing the full adhesion

between soil and base. Then the number of cracks and cells divided by cracks were summarized during the test while the crack patterns were recorded. The variations of water content in specimen were obtained from both the top and bottom of specimen and water content at top was lower than that at bottom during most of the test. The effect of relative humidity on the desiccation rate was shown in Figure 2-48, which indicated that desiccation of specimen with lower relative humidity was faster. This phenomenon can be expected from the conclusions of Wilson et al. (1994) that the water evaporation rate is proportional to the relative humidity difference between the desiccation environment and soil pores at the evaporation surface. In order to analyze the desiccation rate quantitatively, a parameter termed desiccation coefficient was proposed between water content and time. The mathematical relation is:

$$(w - w_r) = (w_i - w_r)e^{-kt} \tag{2-25}$$

Hence,

$$\frac{dw}{dt} = -k(w - w_r) \tag{2-26}$$

where w is the water content at time t; w_i represents the initial water content and w_r is the residual water content finally. k is desiccation coefficient.

The desiccation rate dw/dt is proportional to the desiccation coefficient k.

The relationship between cracking water content and soil thickness is:

$$w_c = A\ln(d) + B \tag{2-27}$$

In the equation, A and B are constants fitted from experiment results; w_c is the water content at onset of cracking; d is the soil thickness.

The agreement between their proposed relation (Eq. 2-27) and experiment results is good according to the Figure 2-49.

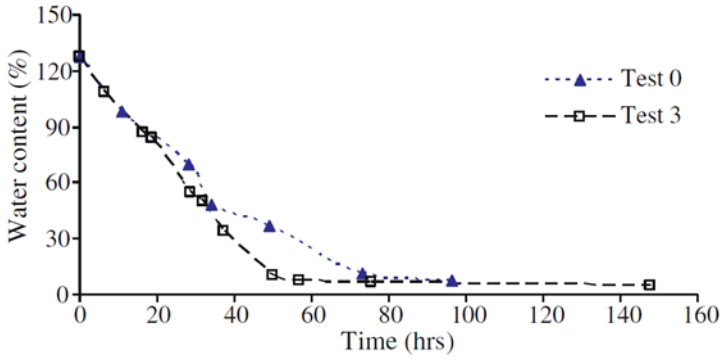

Figure 2-48: Variations of water content of two desiccation tests under different relative humidity (taken from Nahlawin and Kodikara 2006).

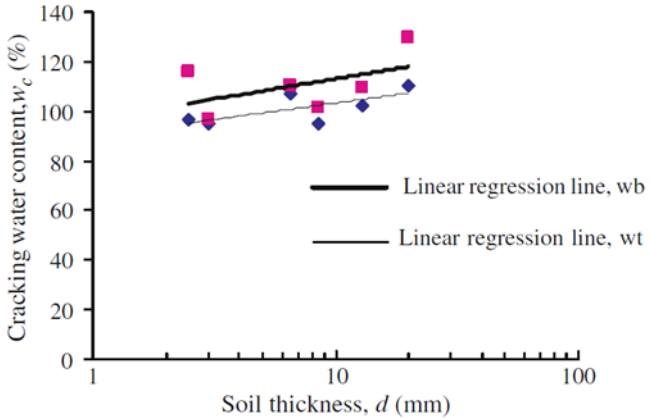

Figure 2-49: Cracking water content w_c versus soil thickness of slurry d (taken from Nahlawin and Kodikara 2006).

Tang et al. (2011) conducted a series of shrinkage tests with Romainville clay, which has caused a large amount of damages to buildings due to its swelling-shrinkage phenomenon. The relation between water content and elapsed time was shown in Figure 2-50, deriving the water evaporation rate versus time. The water evaporation rate R_e kept constant at the beginning of desiccation and then decreased abruptly when water content decreased under unsaturation onset water content w_{AEV}. After unsaturation, the sharp increase of matrix suction will bound the water molecules and slow down the evaporation.

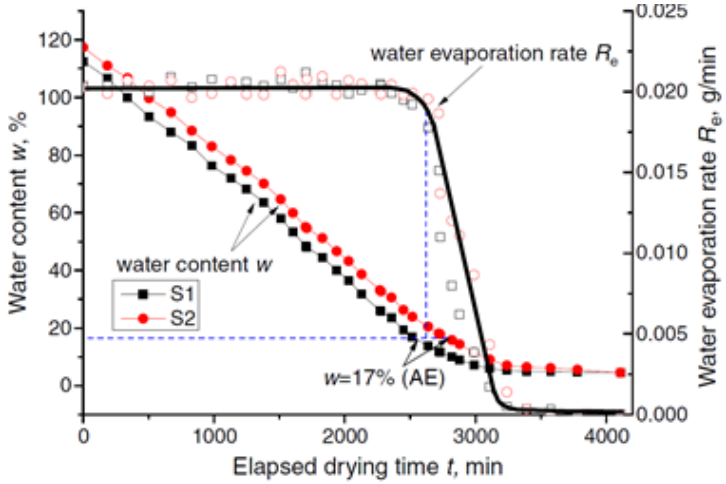

Figure 2-50: Variations of water content and water evaporation rate with time (taken from Tang et al. 2011).

2.3.3.2 Desiccation cracking modelling

By using discrete element method (DEM), the desiccation cracking of soil could be modelled to predict the initiation and development of cracks (Péron et al. 2009a; Guo et al. 2017; Amarasiri et al. 2011; Gui et al. 2016; Sima et al. 2014).

Sima et al. (2014) numerically reproduced the desiccation cracks in clay layer. They treated the clay soil as aggregates, which were represented by spherical grains. The macroscopic experimental results of shrinkage tests were conducted to obtain the required drying shrinkage kinetics which shown relationship between grain size and water content or drying time. The micro strength characteristics including tensile strength and elastic modulus were measured with the suction variation. With these relationships, the bond contact model of grains was realized. The DEM results were compared with the experiment results and fitted them well. Figure 2-51 shows the reproduction of varied surface crack ratio and other two crack parameters with water content.

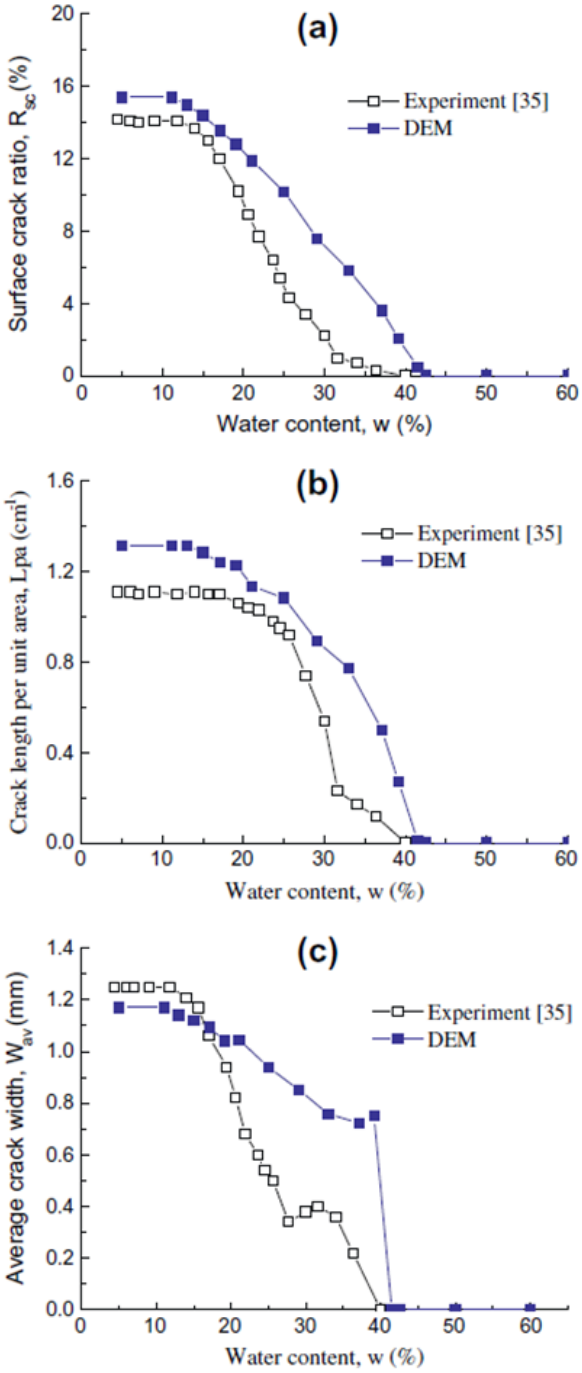

Figure 2-51: Comparison between variations of surface crack ratio, crack length per unit area and average crack width from experiment and DEM (taken from Sima et al. 2014).

2.4 Consolidation of soils

2.4.1 Consolidation theory

2.4.1.1 One-dimensional consolidation theory

Soil deformation upon external loading is generated by three parts: grain deformation, compression of fluid including air and water in void, and expelling of fluid from the void (Holts et al. 2011). For most cases, the grain deformation and compression of water and air can be considered as negligible (Terzaghi et al. 1996). The squeezing out of water is the main mechanism for soil's compressibility. When fine-grained soils undergo a loading, the rate of compression is dependent on the rate of water expelling. The process is called consolidation that relates effective stress, strain and time. Sand has a behavior very different from that of fine-grained soils. Sand has high permeability and the rate of drainage is very fast. The compression can occur immediately.

As a load is applied on a saturated soil, the pressure is taken by the pore water at the beginning, leading to the generation of excess pore water pressure equal to the applied pressure:

$$\Delta u = \Delta\sigma = u - u_0 \tag{2-28}$$

where u is the total pore water pressure and u_0 is hydrostatic pressure. With the water draining, Δu gradually decreases and settlement occurs.

By considering the continuity equation of one-dimensional flow and assuming constant hydraulic conductivity and small strain during the process of consolidation, the one-dimensional consolidation theory was proposed by Terzaghi (1925):

$$c_v \frac{\partial^2 u'}{\partial z^2} = \frac{\partial u'}{\partial t} \tag{2-29}$$

$$c_v = \frac{1}{\gamma_w}\frac{k}{m_v} \tag{2-30}$$

where c_v is coefficient of consolidation representing the rate of consolidation, u' is the excess pore water pressure, z represents a one-dimensional vertical coordinate, t is time, γ_w is the unit weight of water, k is the saturated hydraulic conductivity, m_v is the coefficient of volume compressibility.

2.4.1.2 One-dimensional finite strain consolidation theory

For large strain consolidation, the soil sample will undergo a large deformation with varied hydraulic conductivity and compressibility. These are not compatible with the assumption of Terzarghi's one-dimensional small strain consolidation theory. The nonlinear change of hydraulic conductivity and compressibility was considered by several researchers (Gibson et al. 1967; Lee and Sills 1979; Gibson et al. 1981; Pane and Schiffman 1985).

Gibson et al. (1967) developed a one-dimensional finite strain consolidation theory by incorporating the variation of compressibility and hydraulic conductivity. The second order partial differential equation is presented as:

$$\pm(G_s-1)\frac{d}{de}\left(\frac{k}{1+e}\right)\frac{\partial e}{\partial z}+\frac{1}{\gamma_w}\frac{\partial}{\partial z}\left(\frac{k}{1+e}\frac{d\sigma\prime}{de}\frac{\partial e}{\partial z}\right)+\frac{\partial e}{\partial t}=0 \tag{2-31}$$

where t is time; $\pm$ represents the direction of coordinate, + means the same direction with gravity while – means the opposite direction with gravity; G_s is the specific gravity of soil; z is the reduced material coordinate; k is hydraulic conductivity; σ' represents effective stress.

Lee and Sills (1979) proposed a finite strain consolidation equation in term of porosity in a Euler coordinate system with a moving boundary:

$$-\frac{\partial}{\partial x}\left[\frac{k(1+e)}{\gamma_w}\frac{d\sigma\prime}{de}\frac{\partial n}{\partial x}\right]-\left\{(G_s-1)\frac{d\left[k(1-n)^2\right]}{dn}-\frac{\partial q}{\partial n}\frac{d}{dn}\left[\frac{k(1-n)}{\gamma_w}\right]\right\}\frac{\partial n}{\partial x}+\frac{k}{\gamma_w}\frac{\partial^2 q}{(\partial x^2)(1-n)}=\frac{\partial n}{\partial t} \tag{2-32}$$

In the equation, q represents applied stress and n represents porosity while x is the convective vertical coordinate.

A finite strain governing equation combing the sedimentation and consolidation by introducing a parameter β in term of void ratio was developed by Pane and Schiffman (1985). The linked theory between sedimentation and consolidation is:

$$\sigma' = \beta(e)\sigma' + u \tag{2-33}$$

where β is an interaction coefficient which is a monotonic function in term of e; σ' and u are the effective stress and pore water pressure.

The finite strain consolidation theory is presented as follows (Pane and Schiffman 1985):

$$(\frac{\gamma_s}{\gamma_w}-1)\frac{d}{de}(\frac{k}{1+e})\frac{\partial e}{\partial z}+\frac{\partial}{\partial z}\left[\frac{k}{\gamma_w(1+e)}\beta\frac{d\sigma\prime}{de}\frac{\partial e}{\partial z}\right]+\frac{\partial}{\partial z}\left[\frac{k}{\gamma_w(1+e)}\frac{d\beta}{de}\sigma'\frac{de}{dz}\right]+\frac{\partial e}{\partial t}=0 \quad (2\text{-}34)$$

2.4.1.3 Self-weight consolidation theory

The analytical solution of self-weight consolidation with accreting sediments was firstly proposed by Gibson (1958). The time-thickness relationship was not considered in the governing equation. The moving boundary of top surface was considered while the hydraulic conductivity and compressibility were assumed constant. The governing equation of Gibson's solution is:

$$c_v\frac{\partial^2 u}{\partial x^2}=\frac{\partial u}{\partial t}-\gamma'\frac{dh}{dt} \quad (2\text{-}35)$$

where u is the pore water pressure, c_v is the coefficient of consolidation, x is the elevation of studied point from the base, t is the filling time and h represents the thickness of sediments at time t.

Sedimentation on an impervious base was investigated and two time-thickness relationships were combined with the former governing equations including $h = kt^{0.5}$ and $h = mt$. By considering $h = mt$, Gibson (1958) proposed the following governing equation to describe the variation of the pore water pressure during the slurry deposition on a pervious base:

$$u=-\gamma z\left(1+\frac{mz}{2c_v}\right)+\frac{\gamma m}{2c_v}(\pi c_v t)^{-\frac{1}{2}}\times\exp\left(-\frac{z^2}{4c_v t}\right)$$

$$\times\int_0^{\infty}\xi^2\coth\left(\frac{m\xi}{2c_v}\right)\sinh\left(\frac{z\xi}{2c_v t}\right)\exp\left(-\frac{\xi^2}{4c_v t}\right)d\xi \quad (2\text{-}36)$$

where u is the pore water pressure, γ is the unit weight of backfill, z is the height from the base of backfill, m is the filling rate, c_v is the coefficient of consolidation, t is the filling time and ξ is an arbitrary integration variable.

As the integral of Eq. (2-36) cannot be solved manually or with simple calculation tools. Zheng et al. (2018b) developed a solution by substituting the integral of Eq. (2-36) with a summation formula as follows:

$$u=-\gamma z\left(1+\frac{mz}{2c_v}\right)+\frac{2\gamma T c_v}{\sqrt{\pi}m}{h_0}^3\exp\left(-\frac{z^2m^2}{4Tc_v^2}\right)$$

$$\times\sum_{n=-\infty}^{\infty}\left\{n^2\coth\left(nh_0\sqrt{T}\sinh\left(\frac{zmnh_0}{c_v\sqrt{T}}\right)\exp(-n^2h_0^2)\right)\right\} \quad (2\text{-}37)$$

where n is a series number varying from -∞ to +∞, h_0 ($\leqslant 1$) is the step interval of y, T is the dimensionless time factor denoted by Gibson (1958) as follows:

$$T = \frac{m^2 t}{c_v} = \frac{mh}{c_v} \tag{2-38}$$

The similar mathematical operation has been done by Zheng et al. (2018a) on the Gibson (1958) solution for solving the pore water pressure during the slurry deposition on an impervious base. For both cases, the developed analytical solutions were validated by numerical results obtained by numerical modeling with Sigma/W.

The combined effects of self-weight consolidation and arching effect have been considered by Zheng et al. (2019, 2020) for estimating the total and effective stresses during the slurry deposition on a pervious base (Zheng et al. 2019) and impervious base (Zheng et al. 2020), respectively. For the case of slurry deposition on an impervious base, the vertical and horizontal total stresses are expressed as follows after considering both the arching and self-weight consolidation (Zhen et al. 2020):

$$\sigma_v = \sigma_v' + u + \gamma_w l = e^{-\frac{2Ktan\phi'}{B}l} \int_0^l \left(\gamma' + \frac{du}{dy}\right) e^{\frac{2Ktan\phi'}{B}l} dl + u + \gamma_w l \tag{2-39}$$

$$\sigma_h = \sigma_h' + u + \gamma_w l = k e^{-\frac{2Ktan\phi'}{B}l} \int_0^l (\gamma' + \frac{du}{dy}) e^{\frac{2Ktan\phi'}{B}l} dl + u + \gamma_w l \tag{2-40}$$

where σ_v and σ_h are vertical and horizontal total stresses, respectively; σ'_v and σ'_h are the vertical and horizontal effective stresses, respectively; u is the excess pore water pressure; γ_w and γ' are the unit weights of water and submerged backfill, respectively; l is the depth of the point in a mine stope considered in the solution; B is the width of the stope; y is the ordinate of the coordinate; K is the earth pressure coefficient; ϕ' is the effective internal friction angle of backfill.

Improvement can be made by considering a fully coupled equation, which should consider iteration and reciprocal effects between the process of consolidation and development of arching effect.

2.4.2 Consolidation test

2.4.2.1 Standard oedometer test

In order to acquire the constitutive relationship between void ratio and effective stress, Terzarghi (1927) firstly proposed the standard oedometer test to study the one-dimensional consolidation properties of soils. In oedometer test, increments of loading are applied on samples and the strain-time relationship can be obtained. In some cases, the hydraulic conductivity can also be measured after each loading. There are two types of oedometers used in laboratory, floating-ring oedometer and fixed-ring oedometer (Holtz et al. 2011) as shown in Figure 2-52:

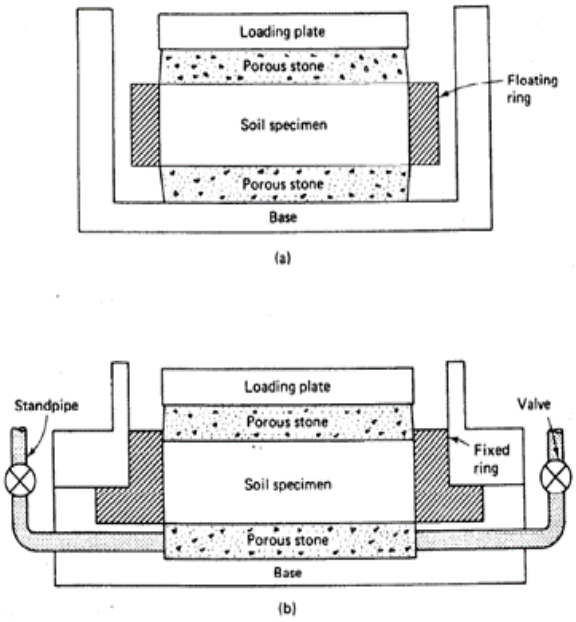

Figure 2-52: Schematic diagrams of (a) floating-ring oedometer, and (b) fixed-ring oedometer (taken from Holtz et al. 2011).

Since the compression occurs at the top and bottom in floating-ring oedometer, the ring friction is smaller than that in fixed-ring oedometer (Lambe 1951). However, the hydraulic conductivity can be measured in fixed-ring oedometer. In oedometer tests, the strain-time relationship can be obtained and the strain time curve can help to calculate c_v at each loading. With Casagrande's method (Casagrande and Fadum 1940), the vertical strain is plotted against the log time and the point where strain is half of the primary consolidation can be found, as shown in Figure 2-53. The

time at 50% primary consolidation is obtained. The coefficient of consolidation can then be calculated by the following equation:

$$c_v = \frac{TH_{D50}^2}{t} \tag{2-41}$$

where T is the time factor equal to 0.197 for 50% primary consolidation, H_{D50} is the drainage path length and t is the time with regard to 50% primary consolidation.

With Taylor's method (Taylor 1948), the strain is plotted against the square root of time. Then the time at strain equal to 90% primary consolidation can be obtained, as shown in Figure 2-54. c_v is calculated with the same equation as Eq. (2-41) while a different time factor is applied. Besides, H is half of the full specimen height when the specimen is two-sided drained while H is the full height for the specimen with one-sided drainage.

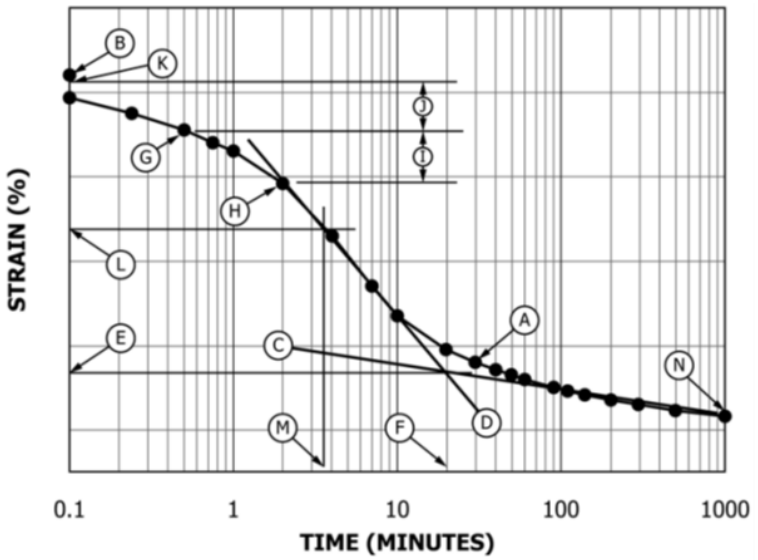

Figure 2-53: Time-deformation curve using log time method (taken from ASTM 2011).

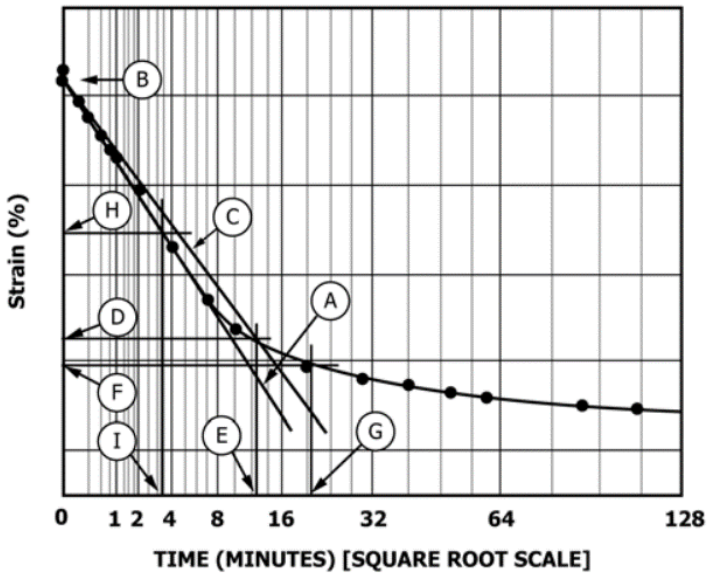

Figure 2-54: Time-deformation curve using square root of time method (taken from ASTM 2011).

2.4.2.2 Seepage induced consolidation test

The seepage induced consolidation test was firstly developed by Imai (1979), which is also called hydraulic consolidation test. The idea is to apply a downward hydraulic gradient at the specimen in slurry conditions and the seepage force will consolidate the specimen. With this method, the inaccurate applied load in conventional mechanical loading by wall friction can be overcome since the seepage force is constant. After the water having reached a steady flow state, the pore water pressure along the height will be measured with a needle piezometer. Then the specimen is cut into slices and the water content along height can be measured while the void ratio can be determined. The relationships of void ratio, vertical hydraulic conductivity and other consolidation parameters with the effective stress can be obtained. Figure 2-55 shows a conceptual illustration of seepage induced consolidation test with the distribution of water head. The main advantage of this test is that low effective stress range can be considered easily.

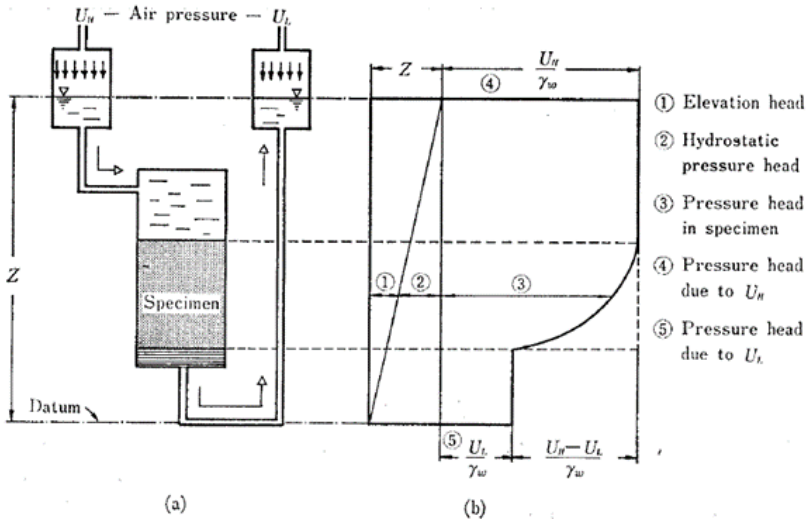

Figure 2-55: Conceptual illustration of (a) water flow caused by a constant water head difference, and (b) water head distribution throughout the system (taken from Imai 1979).

Abu-Hejleh (1996) improved the test method of Imai (1979) by dividing the experiment into three stages, which consist of measuring the void ratio without effective stress, measuring the PWP and specimen void ratio when flow is in steady condition. Fox and Baxter (1997) derived a relationship between total head, effective stress and pore water pressure with the discharge velocity. With this derivation, the test procedure of hydraulic conductivity test by Imai (1979) was simplified and only void ratio profile along height and discharge velocity were required, which could help derive other parameters including total head, effective stress and pore water pressure. Fox and Baxter (1997) then conducted the hydraulic consolidation tests and step-loading tests for comparison. The obtained e-σ and e-k relationships by hydraulic consolidation tests fitted well the results from step-loading consolidation test, as shown in Figure 2-56.

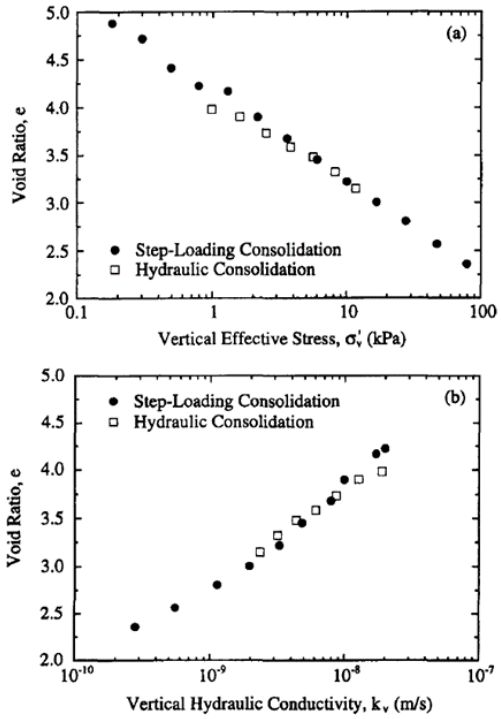

Figure 2-56: Comparison of (a) *e* versus log σ'_v, and (b) *e* versus log k_v from step-loading and hydraulic consolidation tests: (taken from Fox and Baxter 1997).

Tian et al. (2018) designed a seepage-induced consolidation test apparatus and conducted consolidation tests on a silty clay, a pure kaolin and a sandy silt. The obtained results of *e*-σ' curves were compared with those obtained by modified oedometer test method. A good agreement was obtained between them. The calculated hydraulic conductivity by oedometer test was also identical to those measured by seepage-induced consolidation test.

2.4.2.3 Large strain consolidation test

A large consolidometer was developed by O'Kelly (2009), as shown in Figure 2-57 for measuring the consolidation properties of highly organic soils. A floating-ring confining cell treated by lubricant was used to study the consolidation properties and hydraulic conductivity of organic soils. Figure 2-58 shows a comparison between *e*-logσ' obtained by the consolidometer with fixed-ring or floating-ring and that obtained by conventional oedometer test. The consolidation curve by floating-ring consolidometer fitted the result of oedometer test well while the consolidation curve by fixed-ring consolidometer was above the curve by oedometer test. The difference of consolidation curves comes from the larger boundary friction in fixed-ring consolidometer.

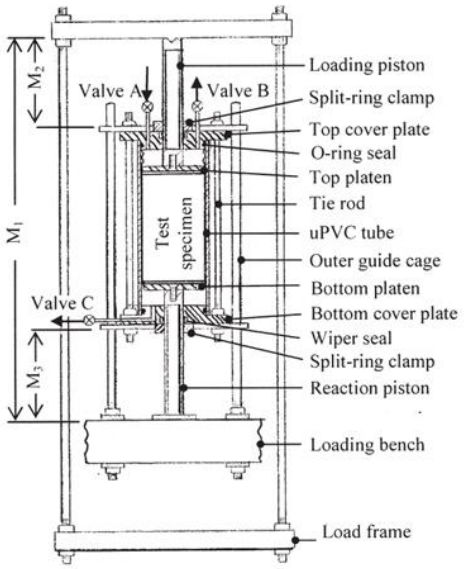

Figure 2-57: Schematic diagram of large consolidometer apparatus with a floating-ring confining cell (taken from O'Kelly 2009).

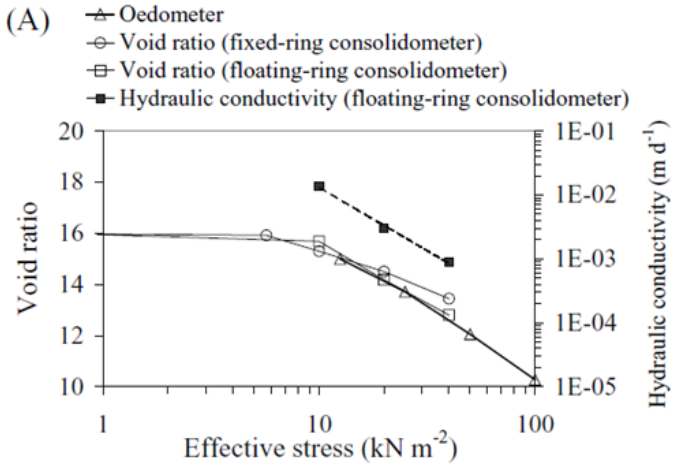

Figure 2-58: Comparison between the *e*-log*σ'* obtained from oedometer test, fixed-ring consolidometer and floating-ring consolidometer (taken from O'Kelly 2009).

He et al. (2017) conducted three tests with a slurry consolidometer by applying different loading sequences, including a constant rate of loading, an increasing rate of loading and step loading. These tests were simulated considering the wall friction development after sedimentation transferring to consolidation. Total stress and pore water pressure obtained from numerical

modelling of these slurry consolidometer tests fitted well with the measured results. The wall friction was decreased when diameter of consolidometer increased from 0.1 m to 0.3 m.

During the whole process of self-weight consolidation of tailings, desiccation may happen and should be taken into account along with the sedimentation and consolidation to estimate the stress state and water discharge in tailings. Shokouhi et al. (2018) conducted slurry consolidometer test and column test by considering the three processes. Their results showed that most of volume change in column test was induced by sedimentation, which accounts for 88% of total variation of void ratio. About 11% of variation of void ratio took place during consolidation while only 1% of void ratio change occurred in desiccation. The sedimentation process is the major factor controlling the volume change in column tests.

2.4.2.4 Sedimentation and self-weight consolidation test

For self-weight consolidation, the sedimentation-consolidation is the most significant period to investigate. Generally, sedimentation is a process during which the soil particles in a state of suspension. Figure 2-59 shows a schematic illustration of sedimentation and consolidation processes. In the flocculation stage and hindered settling zone of sedimentation stage, the particles have no contact with each other and thus the effective stress is zero (McRoberts and Nixon 1976). After the flow velocity in the suspension decreases sufficiently, the particles can settle down to the bottom and the grain contact generates in sediments with effective stress increasing like the consolidation zone in Figure 2-59 (Been and Sills 1981). With accreting sediments, the consolidation at the base will continue under the self-weight. The difficulty is to capture the transition between the sedimentation and consolidation. Numerous experimental investigations have been conducted to distinguish sedimentation from self-weight consolidation and have indicated that sedimentation and consolidation take place simultaneously in the process (Imai 1981; Dromer et al. 2004; Bonin et al. 2014; Zhang et al. 2017).

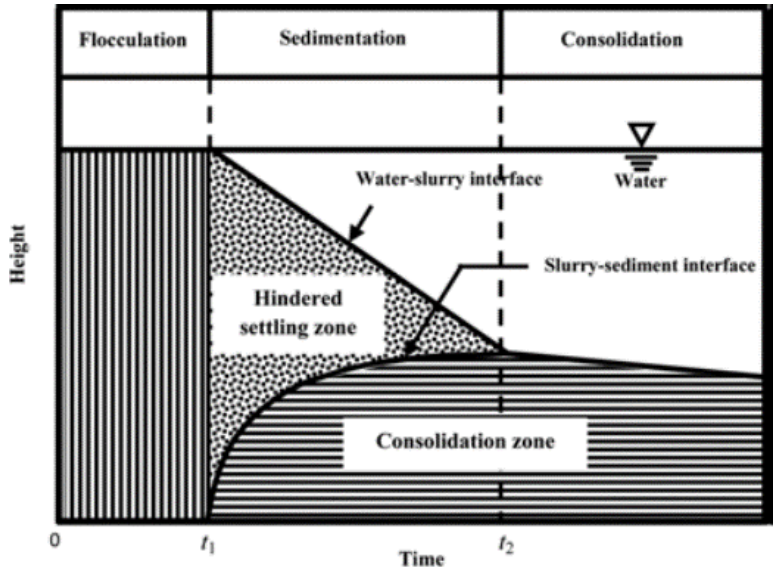

Figure 2-59: Schematic illustration of sedimentation and self-weight consolidation.

Been and Sills (1981) conducted a settling experiment and used X-rays to measure the density distribution along height, which was then used to derive the total stress distribution. The pore water pressure was also measured. The effective stress distribution was obtained. The variation of the void ratio distribution with time was given and the measured settlement and density profiles were compared with the calculated results.

Similarly, water content can be obtained by the measurement of density along the vertical direction. Dromer et al. (2004) developed a new testing system composed of an instrumented settling column and pressure transducers while the density was monitored by a gamma ray sensor unit. The density, pore water pressure and position of soil-water interaction were investigated in self-weight consolidation and forced consolidation. The interpretation of some parameters in the conventional consolidation equation and a unified theory for sedimentation and consolidation were given. The consolidation coefficient, compression coefficient and hydraulic conductivity of the sludge were estimated.

Dromer (2004) applied mechanical loading in the column consolidation tests. The friction between column walls and piston could affected the accuracy of the test results. Pedroni (2011) modified the column instrumentation of Dromer (2004) by applying a vertical hydraulic gradient rather than the external surcharge. Additional conventional tests including vane, fall cone test, permeability

tests and sedimentation tests were also conducted. The constitutive relations of *k-e* and *e-σ'* were obtained for a sludge deposition in tailings pond.

Imai (1981) developed a system for cutting the soil-water mixture into slices (Figure 2-60). The distribution of water content can be measured. Through the different water content distributions in the different zones, the distinction of three stages including floatation stage, settling stage and consolidation stage was determined. Imai (1981) also calculated the vertical effective stress and obtained the compression curve. However, the measurement of water content with slice cutting method was inaccurate and could be improved by other methods of measuring water content.

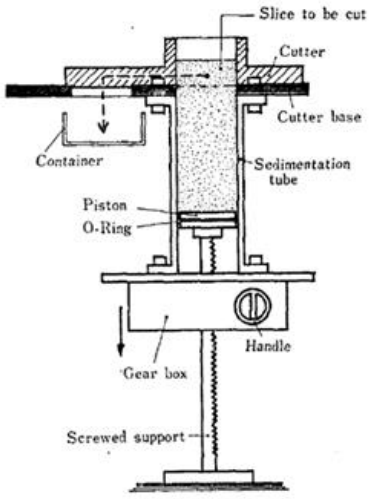

Figure 2-60: Schematic diagram of system for cutting a soil-water mixture into slices (taken from Imai 1981).

As the water content measurement in testing system of Imai depends on the quality of operation in cutting samples into layers, some researchers tried to improve the accuracy of measurement for water content profiles. A multilayer extraction sampling approach was developed by Zhang et al. (2017). With the sampling method, the extraction device can help to extract the slurry layer by layer and then the water content profile along the height of slurry can be measured more accurately. Through this method, the water content and velocity of soil particles can be determined. The velocity of soil particles, pore water pressure and water-slurry interface height with elapsed time can be obtained.

Bonin et al. (2014) investigated the settling and consolidation with the column test and consolidation tests in a consolidometer. Figure 2-61 shows the schematic diagram of the settling column.

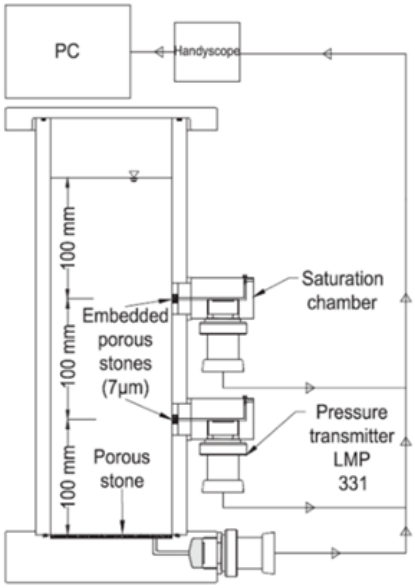

Figure 2-61: Schematic diagram of 300-mm-high settling column (taken from Bonin et al. 2014).

A one-dimensional piecewise-linear method proposed by Fox and Berles (1997) including a Lagrangian approach was applied to model the consolidation results. This model took into account large strain, self-weight effects, relative velocity between fluid and solid, and nonlinearity of consolidation properties. The relative velocity between fluid and solids was calculated based on the Darcy-Gersevanov law and principle of relative motion (Fox and Berles 1997). However, nonlinear constitutive relationships of k-e and e-σ' were obtained from the primary consolidation test at higher effective stress. The application of these constitutive relationships in numerical modelling of self-weight consolidation by Bonin et al. (2014) was unreasonable since the effective stress in self-weight consolidation is small. Nevertheless, a good agreement was still reached between the measurements and numerical results of evolved dissipation of excess pore water pressure and void ratio along vertical profile, as shown in Figures 2-62 and 2-63.

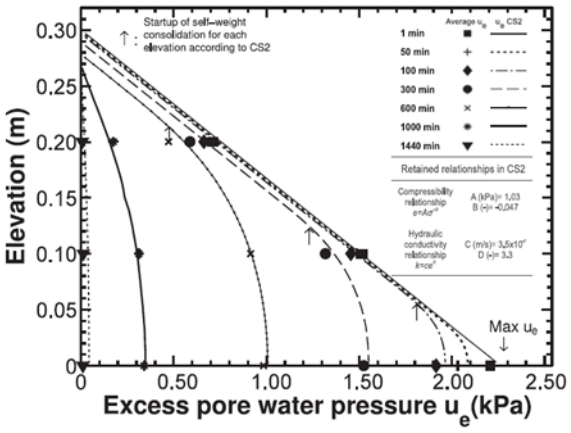

Figure 2-62: Profile of excess pore water pressure with elevation under different time (taken from Fox and Berles 1997).

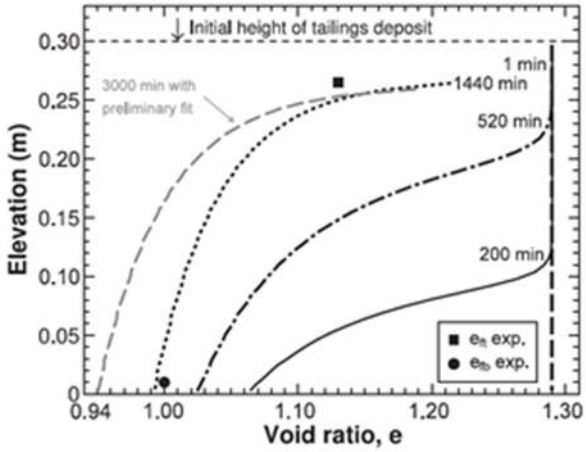

Figure 2-63: Profile of void ratio *e* with elevation under different time (taken from Fox and Berles 1997).

The effects of solid content of tailings on its self-weight consolidation behaviors were examined (Bonin et al. 2019). Bonin et al. (2019) conducted a series of self-weight consolidation tests of tailings with a wide range of solid contents from 50 to 72%. Total pore water pressure was measured with the pressure transmitters while the movement of tailings-water boundary was recorded in tests. Figure 2-64 shows the comparisons of experimental results of excess pore water pressure versus time and the simulated result by CS2 model.

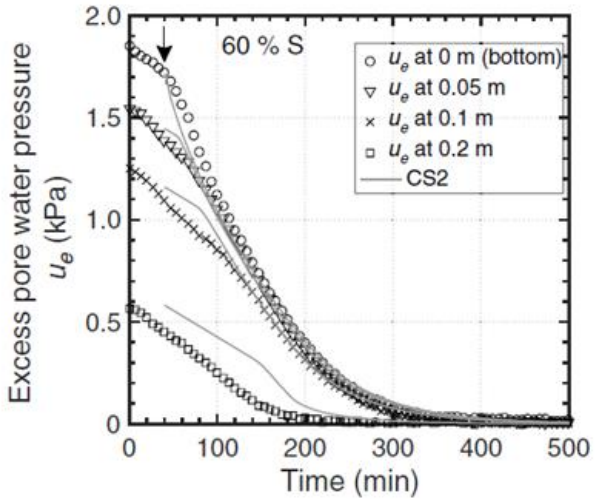

Figure 2-64: Excess pore water pressure versus time at different height with a 60% solid content (taken from Bonin et al. 2019).

The isochores of excess pore water pressure with time by measurement fit the numerical modeling well. From the experimental results, drained water amount and vertical strain decreased with the increase of initial solid content. According to the excess pore water pressure profile with time of slurry samples with different solid contents, the sedimentation can happen at low and high solid contents and end before the consolidation. The sedimentation and self-weight consolidation only take place simultaneously at low solid content varying from 65 to 68 %.

Li et al. (2013) designed a column test with only upward drainage focusing on the predicted equation of some hydraulic properties of slurried clay and compared them with the laboratory measurements including hydraulic conductivity, settlements, total density, void radio, excess pore water pressure and vertical effective stress. The instrumentations are quite simple and only need column and piezometer as shown in Figure 2-65.

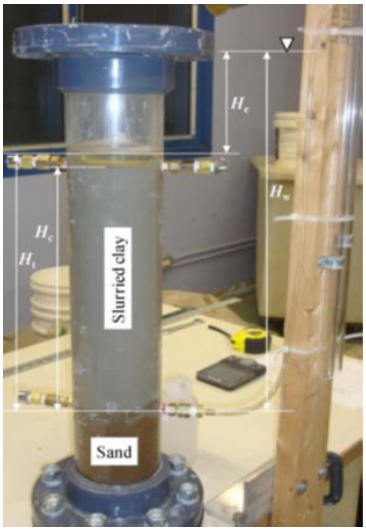

Figure 2-65: Photograph of the settling column and pressuremeter (taken from Li et al. 2013).

Saleh-Mbemba and Aubertin (2018) developed a new method to measure water content with moisture sensors by capturing the evolution of volumetric water content, volumetric strain, void ratio, settlement, and density at different height during self-weight consolidation. Figure 2-66 shows the calibration curve. With the measured moistures, the pore water pressure was obtained, as shown in Figure 2-67.

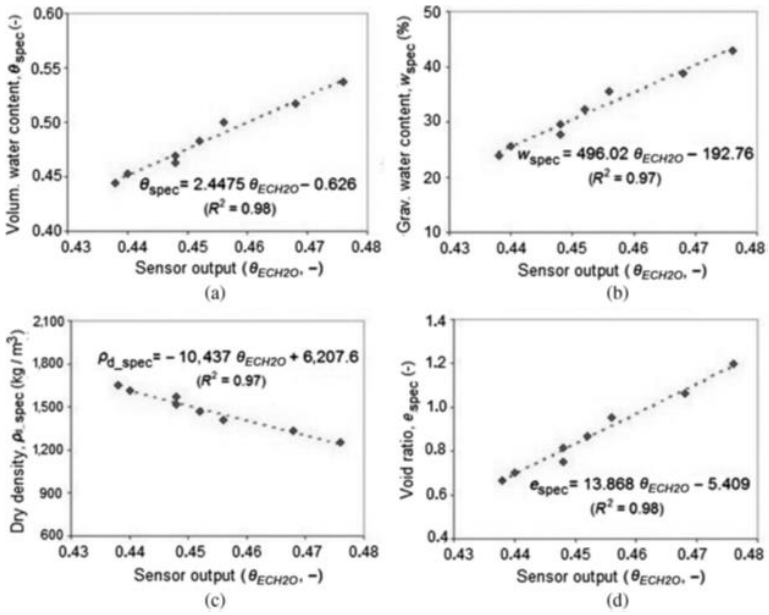

Figure 2-66: Calibration curves of the moisture sensors (taken from Saleh-Mbemba and Aubertin 2018).

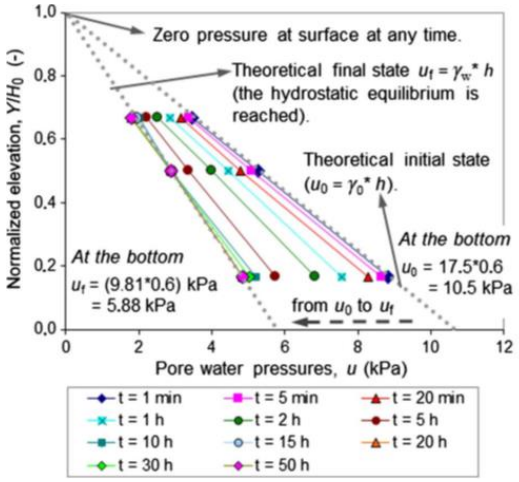

Figure 2-67: Pore water pressures *u* as functions of the normalized elevation (taken from Saleh-Mbemba and Aubertin 2018).

2.4.2.5 Consolidation test for CPB

For cemented paste backfill, the consolidation process is rather complicated due to the combined effects of arching effect in narrow stope, hydration of cement and self-weight effects. The research methodology of consolidation of cemented paste backfill should be adapted based on the conventional consolidation test. The evolutive hydration of cement should be considered in the research.

In order to investigate the consolidation mechanism of cemented paste backfill, Yilmaz and co-workers (Yilmaz et al. 2010; Yilmaz et al. 2015) have developed a test apparatus, called curing under applied pressure system and denoted as CUAPS, as shown in Figure 2-68 to investigate one-dimensional consolidation characteristics of cemented paste backfill. The apparatus can be applied to conduct one-dimensional consolidation test on CPB with the measurement of pore pressure, hydraulic conductivity under constant or changing axial load. The uniaxial compression test can be conducted after consolidation test. The compression index, recompression index, coefficient of consolidation, degree of consolidation can be obtained.

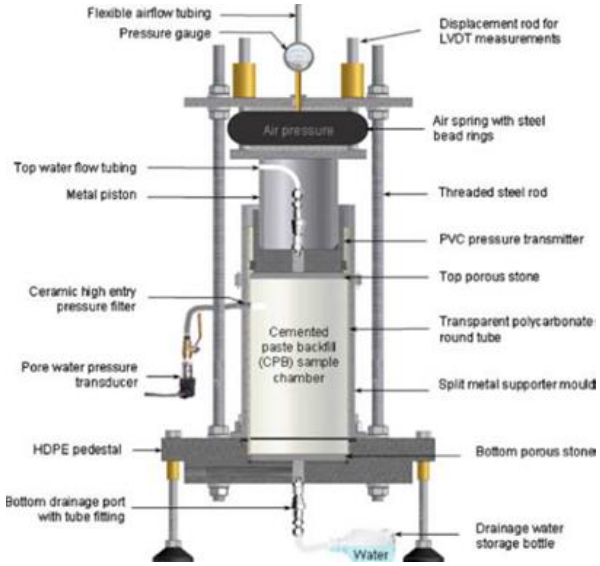

Figure 2-68: Schematic diagram of CUAPS (taken from Yilmaz et al. 2010).

Yilmaz et al. (2015) considered the influence of cementation on the compression curves and compressibility behavior. Obviously, with the increase of curing time, the compression resistance increases while the hydraulic conductivity and compression index decreases. Figure 2-69 shows the coefficient of consolidation with back-calculation of hydraulic conductivity and coefficient of compressibility. c_v decreased with curing time especially at the early period.

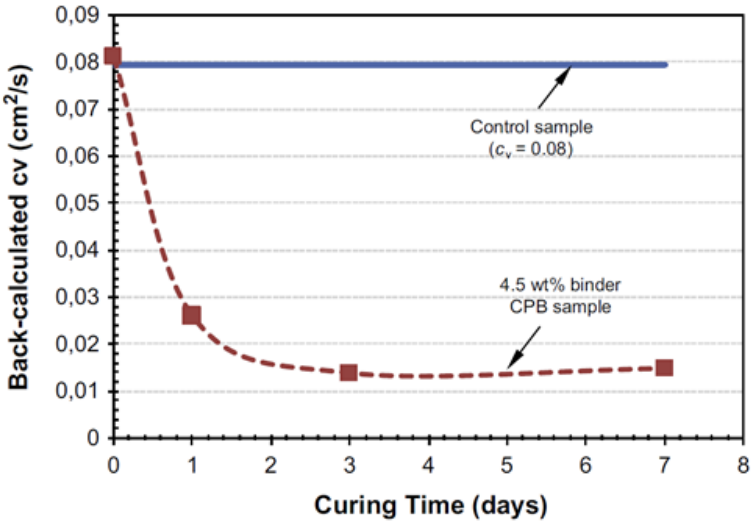

Figure 2-69: Variations of back-calculated c_v with curing time (taken from Yilmaz et al. 2015).

In other experiments, Yilmaz et al. (2008) estimated the coefficient of consolidation with square root of time of Taylor's method and then calculated the hydraulic conductivity based on values of

c_v and coefficient of compressibility a_v. Figure 2-70 shows the variations of final values for void ratio e, degree of saturation S_r, specific gravity G_s and water content w with different curing time.

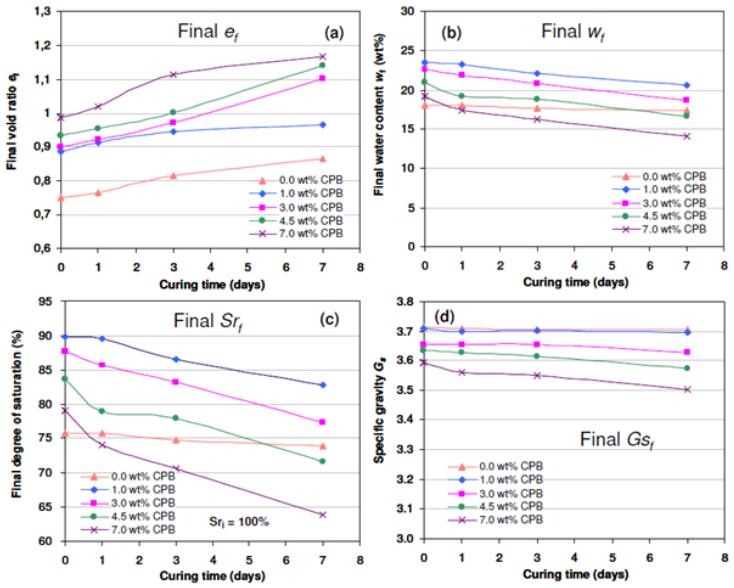

Figure 2-70: Variations of (a) final values of void ratio, (b) final water content, (c) final degree of saturation, and (d) final specific gravity of CPB with curing time (taken from Yilmaz et al. 2008).

Due to hydration of cement, the degree of saturation and water content decreased as predicted. the final void ratio also increased with curing time since the longer curing time with cement hydration leads to the decrease of compressibility. The strain, settlement, cumulative drainage water, and specific surface with different curing time and different binder contents were investigated and shown in Figure 2-71.

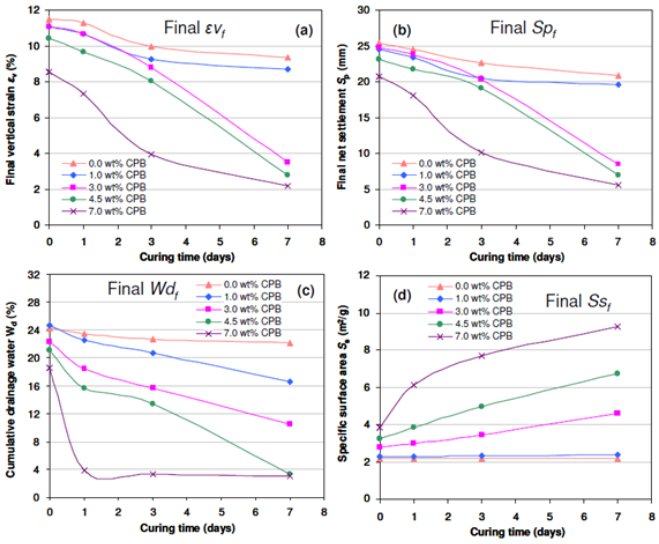

Figure 2-71: Variations of (a) final vertical strain, (b) final settlement, (c)cumulative drainage water, and (d) final specific surface of CPB with curing time (taken from Yilmaz et al. 2008).

The early period of self-weight consolidation with low effective stress cannot be reproduced in such a test with mechanical loading. Additionally, the friction of side wall should be considered since the height of the apparatus is twice long of the diameter. Such a considerable friction may affect the induced effective stress and then affect the initial excess pore water pressure, which will affect isochores of c_v.

Belem et al. (2016) conducted the high column tests to investigate the gravity-driven one-dimensional consolidation of cemented paste backfill. The different receipts of binder and different drainage scenarios were considered in the tests. The drainage scenarios were controlled by different configurations of geotextile draining seals and sealing joints, which categorized the drainage conditions into undrained condition, partially drainage and full lateral drainage shown in Figure 2-72.

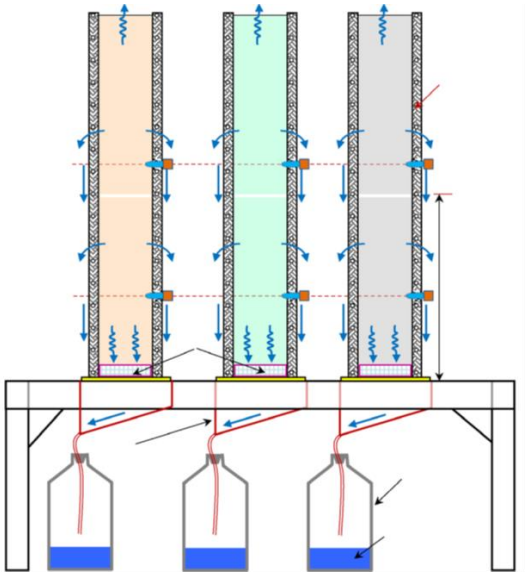

Figure 2-72: Schematic diagram of the three consolidation columns with different lateral drainage configurations (taken from Belem et al. 2016).

Drained water, settlement of backfill and pore water pressure were measured and shown in Figure 2-73.

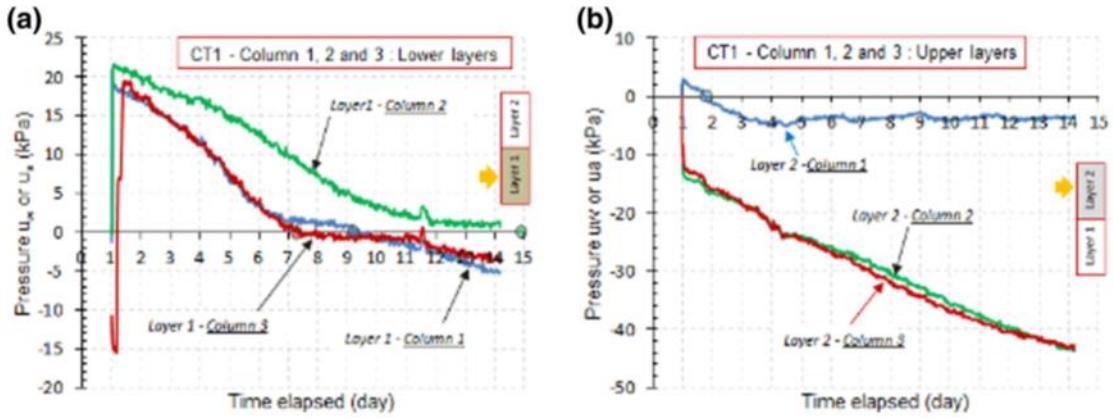

Figure 2-73: Pore water pressure dissipation of backfills in gravity-driven one-dimensional consolidation test (taken from Belem et al. 2016).

After fully consolidation and curing, the samples were cored and then tested with uniaxial compressive strength tests at different height. The effects of curing time and binder type on the evolution of volumetric strain, drainage of water and UCS after curing were investigated. The volumetric strain of CPB under different drainage scenarios indicated that in-situ cemented paste backfill behaved more similar to full lateral drainage or the partial lateral drainage.

Cement content and curing time are not the only influence factors which can affect consolidation behavior of CPB. Jamali (2012) investigated the effect of stress history on the one-dimensional consolidation behavior of CPB. The effects of different cement types and different contents as well as the load rate of applied pressure was mainly studied. For conventional consolidation test, several loading rates were assessed while the EM test was conducted at the same time to study the hydration process of cement-based materials. According to the experimental results, the onset of hydration progress takes place earlier with higher binder content as particle hydration bonds form faster in higher binder content. The hydration process was not affected by loading rate in CPB. In general, consolidation played a significant role in improving the stiffness in non-cemented and low-cement-content pastes, whereas hydration played a determining role in stiffness development in higher cement content pastes.

2.5 Chemical desiccation of CPB

When the cement reacts with water in cement hydration, the cement and water in reaction become hydrated products. During the process, volume of hydrated products is smaller than volume of reacted cement and water. Chemical shrinkage is the volume shrinkage in cement hydration, which equals to the volume decrease from reacted cement and water to hydrated products (Geiker and Knudsen 1982; Wild et al. 1998). Chemical shrinkage also exists in CPB.

Figure 2-74 shows the experimental instrumentation of Belem et al. (2010) to measure chemical shrinkage. The CPB and water were placed in a glass vial while the opening of the vial was sealed with a rubber stopper. A capillary tube was inserted in the mixture of CPB and water. The volume variation due to chemical shrinkage can thus be determined from the water table variation in capillary tube. The evaporation of water was prevented with the paraffin oil. The chemical shrinkage was measured with the elapsed time under different *w*/*c* ratios (ratio of water mass to cement mass). In addition to experimental measurement, the chemical shrinkage was incorporated with the consolidation and the effect of chemical shrinkage on pore pressure was studied (Wood and Doherty 2014). Cui and Fall (2017) also investigated the effect of chemical shrinkage on the volume change by incorporating the thermal, mechanical and hydraulic process.

Powers and Brownyard (1947) found that the mass of chemically combined water generally accounts for 23% of the mass of reacted cement with 28 days of curing. According to Locher (2006),

the non-evaporable water which constitutes the hydrated compounds only accounts for 12% of mass of reacted cement at the first three curing days. Therefore, the volume of chemical shrinkage only contributes to a very small portion of the total volume of CPB since the CPB has a high water content but low cement content (Helinski et al. 2007).

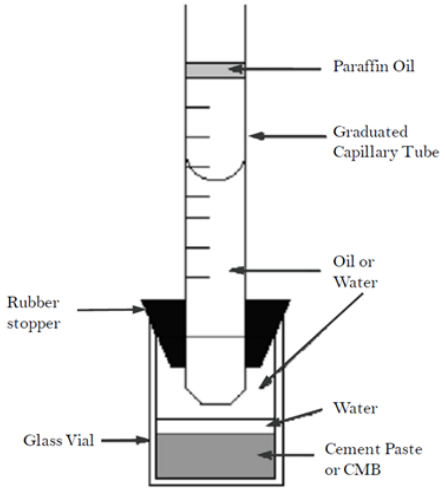

Figure 2-74: Schematic diagram of instrumentation to measure chemical shrinkage of hydrated CPB (taken from Belem et al. 2010).

The soil water retention curve (SWRC) of CPB was also studied by some researchers (Abdul-Hussain and Fall 2011; Suazo et al. 2016). The SWRC of CPB changes with time since the cement hydration will affect the micro-structure of CPB. Thus, the conventional measurement methods like pressure plate method and filter paper method cannot be used. Abdul-Hussain and Fall (2011) applied a device called dewpoint potentiometer to measure the SWRC of CPB with different degree of hydration under different cement contents. With hydration continuing, the matrix suction increases at the same volumetric water content.

CHAPTER 3 ARTICLE 1: AN ANALYTICAL SOLUTION TO ESTIMATE THE SETTLEMENT OF TAILINGS SLURRY DEPOSITED IN A CONTAINMENT STRUCTURE

Jiahao Qin, Jian Zheng, Li Li

Article submitted to *Engineering Geology* in April 2020.

Abstract: Every year, mining industry generates large amounts of tailings, which must be properly managed. A common practice is to transport and deposit the tailings slurry in tailings ponds. In recent decades, backfill is also increasingly used in underground mines by using tailings to fill the mined-out voids as it can bring several advantages, such as improved ground stability, increased ore recovery, and reduced the surface disposal of mine wastes. In both cases, an important concern is to have a good understanding of the settlement and volume variation of tailings slurry after the deposition. The settlement of tailings or backfill slurry is mainly associated with the processes of sedimentation, shrinkage, and self-weight consolidation, which have hardly been considered simultaneously in previous analytical solutions. In this paper, the three processes were reviewed first. The critical void ratio at the end of sedimentation is for the first time characterized through shrinkage test and considered to be equal to the unsaturation onset or air entry void ratio. A simple solution was proposed to evaluate the settlement and volume variation of tailings slurry after the deposition by considering the shrinkage (sedimentation) and self-weight consolidation. Its validity was then tested by experimental results obtained by physical model tests.

Key words: Shrinkage; Sedimentation; Consolidation; Settlement; Tailings pond; Mine stope

3.1 Introduction

To extract the valuable minerals from ore bodies, a large amount of mining wastes can be generated during the milling process. These mining wastes are tailings, which must be properly managed (Bussière et al. 2004; Wickland and Wilson 2005; Bolduc and Aubertin 2014; Yilmaz et al. 2014). Tailings are usually transported by pipes and deposited in tailings impoundments (Vick 1990; Bussière 2007). In recent decades, backfill made of tailings, water and binders has also been increasingly used in underground mines to fill mined-out voids (called stopes). This technology can bring several advantages, such as improved ground stability, increased ore recovery, and reduced surface disposal of mining wastes and environmental impacts (Hassani and Archibald 1998; Potvin et al. 2005; Benzaazoua et al. 2008; Yilmaz et al. 2008; Ghirian and Fall 2013; Yilmaz et al. 2015).

For tailings storage facilities and underground mine stopes, an important task is to have a good evaluation of the settlement and volume variation of tailings or backfill slurry after being placed in these confinement structures. This is critical to estimate the storage capacity and design the subsequent filling scheme for tailings storage facilities (TSF), finally help better optimize the life cycle management. For underground mine stopes, understanding the settlement and volume variation of backfill slurry is important to ensure a tight contact between the backfill and stope roof in cut-and-fill mining or to avoid excessive void space between the top surface of the backfill and the floor of over cut drift in sublevel mining. In the case of mine stopes backfilled with two pours (plug pour and final pour), the placement of plug pour much higher than the designed height results in a uselessly increase of cost due to the high cement content of plug. If the settled backfill of the plug pour is lower than the drift, an excessive pressure can be applied on the top part of the barricade during the pouring of the final pour, which is usually much higher than the plug pour. The barricade can fail near the upper portion due to internal local instability (Yang et al. 2017; Xu 2019[§]), resulting in undesirable consequences. This requires in turn a good understanding of the

[§] Xu, Y.H (2019) Personal communications.

mechanism, which determines the settlement and volume variation of tailings slurry after being placed in a TSF or underground mine stope.

When a tailings slurry is hydraulically deposited in a TSF or mine stopes, the tailings particles will move downward under the effect of gravity. The tailings slurry tends to become denser and expels the pore water out of the tailings. These trends can be limited due to the low permeability of the backfill slurry, leading to the generation of excess pore water pressure. At the very early stage after the placement of tailings or backfill slurry, grain-grain contacts are absent. With the dissipation of excess pore water pressure, the particles get closer to each other and the void spaces decrease. The tailings or backfill can become denser and the volume reduction is only due to the volume of expelled water. In this stage, the grain-grain contacts are absent and the dissipation of excess pore water pressure does not result in any generation of effective stresses. This phenomenon, known as sedimentation, has been observed in several laboratory and field measurements (Dromer et al. 2004; Thompson et al. 2012; Li et al. 2013; Bonin et al. 2019).

With further drainage and dissipation of the excess pore water pressure, the tailings particles can get into contact with each other. Any further dissipation of excess pore water pressure is unavoidably accompanied with the generation and increase of effective stresses. This process is called self-weight consolidation (Terzaghi et al. 1996; Holts et al. 2011).

While the sedimentation and self-weight consolidation are two processes closely related to the dissipation of excess pore water pressure in the depth of tailings or backfill slurry, another important process, called desiccation, is closely related to the increase of suction due to the unsaturation of tailings or backfill around the top surface. The settlement and volume variation of tailings or backfill slurry are thus determined by the processes of sedimentation, self-weight consolidation and shrinkage.

Over the years, the volume variation (settlement) of tailings or backfill slurry was mainly estimated by considering self-weight consolidation. A number of analytical solutions and experimental investigations have been reported to estimate the settlement of tailings slurry during and after the deposition in a tailings storage facility (TSF) (Gibson 1958; Davis and Raymond 1965; Gibson et al. 1967; Li et al. 2013; Saleh-Mbemba and Aubertin 2018; Zheng et al. 2018). For instance, Agapito and Bareither (2018) used a one-dimensional large-strain consolidation model to predict

the variation of tailings height and storage capacity of a TSF. Based on the Gibson (1958) model, Zheng et al. (2020a, 2020b) have proposed solutions to estimate the settlement and volume of drainage water of tailings slurry after being deposited in a TSF with permeable and impermeable bases. These solutions are usually nonlinear and require the measurements of several geotechnical parameters (e.g., the variation of void ratio, permeability, and consolidation coefficient with either depth or time), which need to be solved by finite elements or finite difference method. More importantly, the volume reduction of tailings or backfill slurry associated with the sedimentation in the early stage of deposition has hardly been evaluated. A solution has been proposed to estimate the settlement and volume variation of hydraulic backfill placed in underground mine stopes (Yang and Li 2017). The settlement and volume variation due to the consolidation has been neglected. Thus, the sedimentation together with consolidation has not been considered simultaneously in the estimation of settlement and volume variation of tailings or backfill slurry. The application of the existing solutions tends to underestimate the settlement and volume variation of tailings or backfill slurry during and after the deposition (McRoberts and Nixon 1976). This is particularly true for tailings slurry containing high water content and large amounts of fine particles, such as oil sand tailings.

In this paper, the processes of shrinkage, sedimentation and self-weight consolidation of slurried materials are first recalled. It will be seen that the required parameters for estimating the settlement and volume change associated with the process of sedimentation can be determined from shrinkage curves. The critical void ratio at the transition from sedimentation to consolidation can be considered to be equal to the unsaturation onset (i.e. air entry void ratio) on the shrinkage curve. A simple analytical solution was then proposed to evaluate the settlement and volume variation of tailings or backfill slurry by considering the combined effects of shrinkage and self-weight consolidation. The proposed solution was then verified by experimental results obtained by physical model tests.

3.2 Proposed solution to estimate the volume variation of the deposited tailings slurry

Figure 3-1 shows the shrinkage stages (Fig. 3-1a) and a typical shrinkage curve (Fig. 3-1b) of tailings of backfill slurry. In the initial stage, the slurry is oversaturated with an initial void ratio e_0.

It behaves as a heavy liquid without contact between the particles. During the normal shrinkage stage, the tailings particles get closer to each other with the expulsion of pore water and water loss due to evaporation. At the end of the normal shrinkage stage, the tailings particles start to touch each other. Even slight further water loss will lead to the replacement of pore water by air. The void ratio at this critical state is called unsaturation onset or air entry value (AEV) void ratio e_{AEV}. From this point, effective stresses associated with suction are generated and the residual shrinkage stage starts. With more water loss due to the evaporation, the suction and effective stresses become larger, leading to more volume decrease. This can last until a point at which the grain-grain contacts are tight enough and more loss of water does not result in any more significant volume reduction. The water content at this second critical point is called shrinkage limit w_s. From this point, the zero shrinkage stage starts with further loss of water due to evaporation while the void ratio remains almost constant. The void ratio at this stage is called final void ratio e_f (Fredlund et al. 2002; Saleh Mbamba et al. 2016).

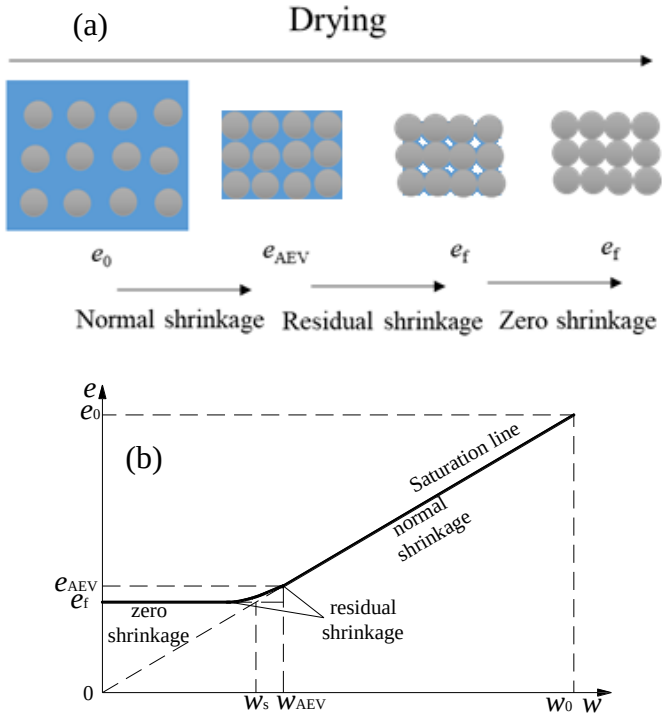

Figure 3-1: The processes of (a) physical presentation of shrinkage stages, and (b) typical shrinkage curve of tailings or backfill slurry (adapted from Marinho 2017).

Figure 3-2 shows the processes of sedimentation and self-weight consolidation (Fig. 3-2a) and a typical compression curve *e-σ'* (Fig. 3-2b) of tailings or backfill slurry. At the initial stage, the slurry is in a state of suspension without any contact between the particles. The initial void ratio is e_0 and the effective stress σ' is zero. Under the effect of self-weight of particles, the process of sedimentation starts and the particles settle and tend to become closer to each other. Nevertheless, the pore water pressure u in slurry equals to the total stress σ (= $\gamma_{sat} h_{tailings}$; γ_{sat} is the saturated unit weight of tailings while $h_{tailings}$ is the height of tailings slurry) according to effective stress theory. The height of settled tailings slurry and the excess pore water pressure u_e decrease without any generation of effective stress. When the space between the particles decreases to a critical state, in which the particles start to be in contact with each other, the process of sedimentation is completed. The void ratio reaches a critical value e_c. From this point, further dissipation of excess pore water will result in generation and increase of effective stresses, which in turn leads to volume reduction of the tailings or backfill. The process of self-weight consolidation starts.

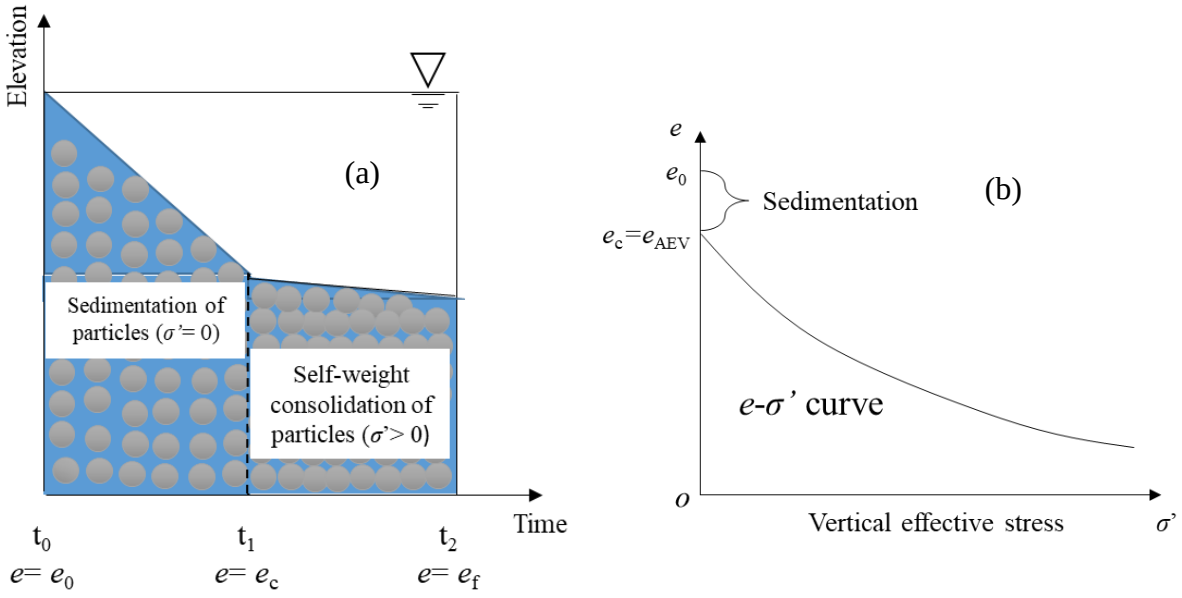

Figure 3-2: The processes of (a) physical presentation of sedimentation and self-weight consolidation (adapted from Zhang et al. 2017), and (b) typical compression curve *e-σ'* of tailings or backfill slurry.

If one compares Figure 3-1 and Figure 3-2, one can reach a common point between a shrinkage test (Fig. 3-1) and a self-weight consolidation test (Fig. 3-2). During the normal shrinkage stage

and the process of sedimentation, the tailings or backfill slurry is in a state of suspension. Effective stresses are absent. The volume reduction of tailings or backfill is equal to the volume of water loss due to the evaporation in the normal shrinkage stage and to the volume of expelled supernatant water in the process of sedimentation. Both processes end by the start of generation of effective stress. Further progress with more water loss or drainage will result in increase of effective stresses. It is thus reasonable to consider the critical void ratio at the end of sedimentation e_c to be equal to the unsaturation onset void ratio e_{AEV} of the shrinkage curve. After that, the slurry behaves as a real soil and consolidation occurs, which usually starts first from the bottom part of the slurry.

Assuming that a slurry is deposited in a confining structure with a horizontal cross-section area A. The slurry has an initial void ratio e_0, an initial height h_0, and a saturated unit weight γ_{sat}. The volume variation associated with the sedimentation can be estimated by considering the normal shrinkage stage of the shrinkage curve (e-w) shown in Fig. 3-1b. When the void ratio decreases from its initial value e_0 to the unsaturation onset void ratio e_{AEV}, the settlement (S_{ns}) and volume variation (V_{ns}) can be calculated as follows:

$$S_{ns} = \frac{e_0 - e_{AEV}}{e_0 + 1} h_0 \tag{3-1}$$

$$V_{ns} = \frac{e_0 - e_{AEV}}{e_0 + 1} V_0 \tag{3-2}$$

where V_0 is the initial volume of the slurry.

The volume variation associated with the consolidation can be estimated using the compression curve e-σ'. The initial void ratio for the process of consolidation corresponds to the critical void ratio at the end of sedimentation e_c (= e_{AEV}) while the initial height h_1 equals to ($h_0 - S_{ns}$). When the consolidation is completed, the vertical effective stress along the height of the tailings or backfill slurry can be calculated as:

$$\sigma' = (\gamma_{sat} - \gamma_w) \times (h_1 - x) \tag{3-3}$$

where γ_w (= 9.8 kN/m^3) is the unit weight of water, x is the elevation from the bottom of the tailings or backfill slurry ($0 \leq x \leq h_1$).

In Eq. 3-3, the height of tailings slurry after sedimentation rather than the consolidated height is used to calculate the settlement generated by consolidation. As the settlement due to sedimentation

accounts for the most of the total settlement (Shokouhi et al. 2018), the height after sedimentation should be close to the height of tailings slurry after consolidation. The use of the height of tailings slurry after sedimentation can thus be considered as a good approximation in the effective stress estimation presented in Eq. 3-3.

Eq. 3-3 is generally valid for the case of TSF, but leads to overestimation of the vertical effective stress for the case of backfilled stopes due to the neglect of possible arching effect.

The height of the tailings slurry h_1 can be divided into n layers with each layer having a thickness of $l_i = (h_1/n)$. With the obtained distribution of the vertical effective stress along the full height of the tailings or backfill, the void ratio variation for each layer can be obtained from the compression curve *e-σ'*. The settlement (S_c) and volume variation (V_c) caused by the consolidation can be calculated as follows:

$$S_c = \sum_{i=1}^{n} \frac{a_{vi}}{1+e_{AEV}} \sigma_i' l_i \tag{3-4}$$

$$V_c = \sum_{i=1}^{n} \frac{a_{vi}}{1+e_{AEV}} \sigma_i' l_i A \tag{3-5}$$

where a_{vi} is the coefficient of compressibility of tailings slurry at layer i, σ_i' is the average effective stress at layer i. The total settlement (S_t) and volume variation (V_t) induced by the sedimentation and consolidation can be calculated as follows:

$$S_t = S_{ns} + S_c = \frac{e_0 - e_{AEV}}{e_0+1} h_0 + \sum_{i=1}^{n} \frac{a_{vi}}{1+e_{AEV}} \sigma_i' l_i \tag{3-6}$$

$$V_t = V_{ns} + V_c = \frac{e_0 - e_{AEV}}{e_0+1} V_0 + \sum_{i=1}^{n} \frac{a_{vi}}{1+e_{AEV}} \sigma_i' l_i A \tag{3-7}$$

As an extreme case when the tailings slurry undergoes the full shrinkage phase with the void ratio decreases from e_0 to the final void ratio e_f, the settlement (S_{fs}) and volume variation (V_{fs}) can be calculated as follows:

$$S_{fs} = h_0 - \frac{e_f+1}{e_0+1} h_0 = \frac{e_0 - e_f}{e_0+1} h_0 \tag{3-8}$$

$$V_{fs} = V_0 - \frac{e_f+1}{e_0+1} V_0 = \frac{e_0 - e_f}{e_0+1} V_0 \tag{3-9}$$

Normally, one can expect that the value of S_{fs} is higher than that of S_t. Eqs. 3-6 and 3-7 can be used to estimate the settlement and volume reduction of slurry in underground mine stopes or for TSF

in regions like Canada while Eqs. 3-8 and 3-9 are more appropriate for evaluating the settlement and volume change of tailings slurry deposited in a TSF in arid or semi-arid regions.

3.3 Laboratory tests of settlement measurements

In this section, shrinkage and consolidation tests as well as the obtained shrinkage and compression curves of the tested tailings will be presented first. The settlement measurements of the tailings slurry placed in two plywood molds, one simulating a tailings pond and another for a mine stope, are then presented. The results can then be used to test the validity of the proposed solution.

3.3.1 Tested tailings

The tested tailings were collected from a mine in Northern Quebec, Canada. The specific gravity of the tailings solids was measured as G_s = 2.73. According to a sieve and hydrometer analysis, the grain size distribution curve of the used tailings is shown in Figure 3-3 with D_{10} = 3.3 μm, D_{30} = 14.2 μm, D_{60} = 43.2 μm, C_u = 13.02 (coefficient of uniformity), and C_c = 1.4 (coefficient of curvature). The saturated hydraulic conductivity k_{sat} was measured in the range of 1×10^{-6} to 5×10^{-6} m/s while the void ratio was between 0.46 and 0.83 (Rodet 2019). According to the Unified Soil Classification System, the tested tailings are classified as a low plastic silt ML.

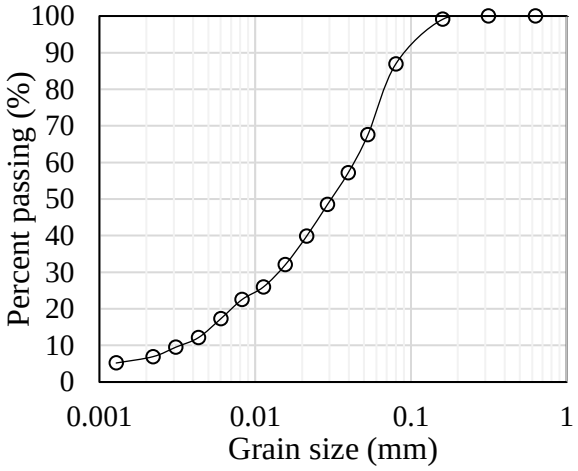

Figure 3-3: Grain size distribution curve of the tested tailings.

3.3.2 Shrinkage curve

Saleh-Mbemba et al. (2016) have shown that the final void ratio of a tailings slurry takes a value of 0.7 when the initial water content varies from 48.5 to 63.4%, but reduced to a value of 0.6 when the initial water content varies in the range of 33.5 to 40.0%. To further understand the shrinkage behavior of a tailings slurry, a series of shrinkage tests have been performed with PVC molds around 20 cm long, 3 cm wide and 5 cm high on a tailings slurry of different initial water contents. The details of instrumentation, test procedure and the test results are given in Qin (2020).

Figure 3-4 shows the shrinkage curves of the tailing slurry with initial water contents of 40%. From the figure, the air entry or unsaturation onset void ratio e_{AEV} and final void ratio e_f of the tailings slurry are 0.941 and 0.863, respectively.

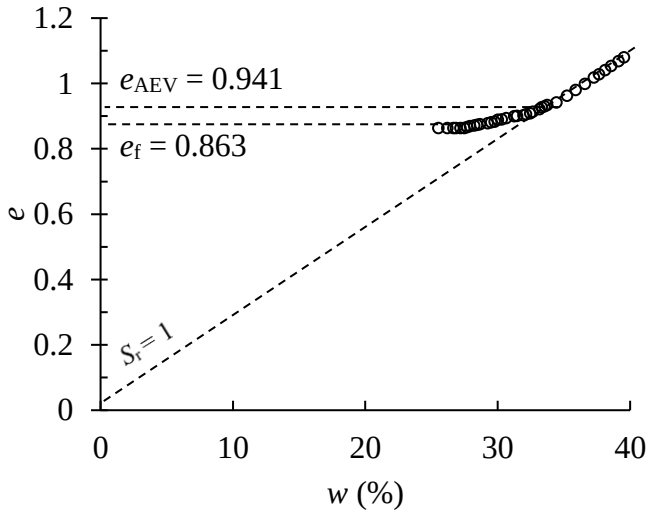

Figure 3-4: Shrinkage curves of the tailings slurry at initial water contents w_0.

3.3.3 Compression curve

The compression curve of the tailings slurry has been obtained by a standard oedometer consolidation test. Figure 3-5 shows a photograph of the instrumentation with an oedometer. The test instrumentation is composed of a steel load platen, a ring cell, a loading shaft, a displacement transducer and a weight. The tailings specimen was prepared with an initial water content of 38.17% and a void ratio of e_0 = 1.042 by thoroughly mixing the dry samples with deaired water. The tailings specimen was then placed in the cell with a light porous stone and a steel load platen added on top

of the tailings. As the tailings slurry has a high water content, the test was started by applying a very small load, equivalent to 1 kPa. Then, the load was increased with an increment ratio of 0.5 at each loading step. A new loading step began after a drainage period of 24 hours. The vertical displacement was recorded at a given interval.

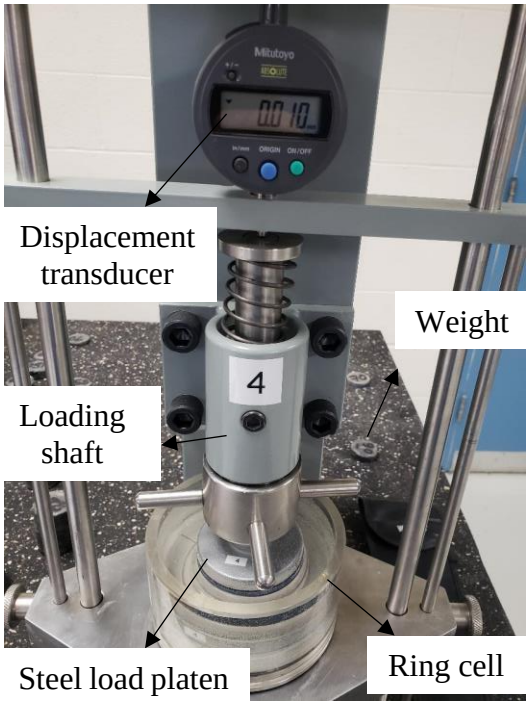

Figure 3-5: Photograph of the instrumentation for the oedometer test.

Figure 3-6a shows the compression curves *e*-logσ' of the tailings slurry. The compression index C_c of the tailings slurry is 0.055, a value that is within the range of 0.046 to 0.13, reported by Aubertin et al. (1996) for hard rock tailings. This value indicates that the tested tailings has a low compressibility.

It should be noted that additional consolidation tests with a column 43.5 cm high and 10 cm in diameter have been done. The details of instrumentation, test procedure and the results of the column consolidation tests are presented in Qin (2020). The results obtained with the standard oedometer tests agree well with the results obtained with the column consolidation tests.

From Figure 3-6a, one sees that the *e*-logσ' compression curve includes two phases, depending on the magnitude of the vertical effective stress. Figure 3-6b shows the *e*-σ' curve at low effective stress in the range of 0 to 9 kPa. This range is considered because the effective stress in the physical

model tests presented in Section 3.4 is quite small. The linear regression on these experimental results leads to a coefficient of compressibility of a_v = 0.0043 kPa^{-1}. This value will be used in Section 3.4 to apply the proposed solution (Eqs. 3-6 and 3-7) for calculating the settlement of backfill in the physical model tests.

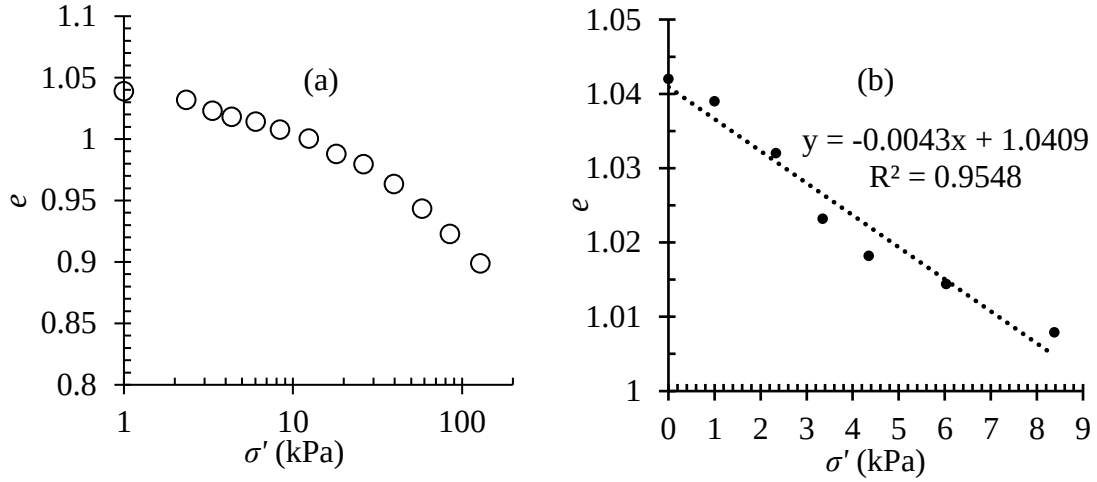

Figure 3-6: Compression curve of the tested tailings slurry: (a) full curve in the *e*-log*σ'* plane; (b) compression curve *e*-*σ'* in a range of low effective stresses.

3.3.4 Settlement and volume variation of tailings slurry

The settlement and volume variation of a tailing slurry placed in two plywood molds were measured. Figure 3-7 shows photographs of the two molds with tailings slurry deposition. The first one with an internal opening 79 cm long, 76 cm large and 18.26 cm high, called Mold 1, is used to simulate a tailings pond while the second one with an internal opening 76.2 cm high, 18.3 cm large and 42.4 cm long, called Mold 2 for simulating an underground mine stope. Mold 1 was smeared with sealant and the base was undrained. The inner walls of Mold 2 were covered by a layer of geomembrane first to prevent side drainage and evaporation and second to reduce the side-wall frictions and possible arching effect. The only possible drainage of tailings or backfill slurry in the two molds was upward. The tailings slurry was prepared at an initial water content of 40%. The tailings slurry has a density of 1.83 g/cm^3. The settlements of the tailing slurry in the two molds were measured with a Vernier caliper at an interval of 24 hours and the tests were ended when the thickness of the tailings slurry remained unchanged for 2 days.

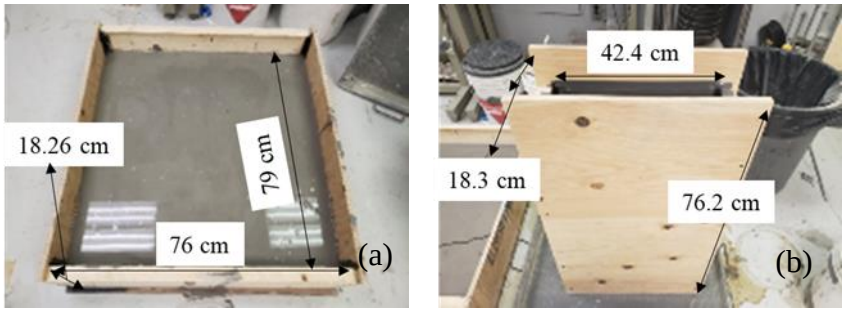

Figure 3-7: Photographs of (a) Mold 1 and (b) Mold 2, filled with a tailing slurry.

Figure 3-8 shows the variations of the thickness (Fig. 3-8a) and void ratio (Fig. 3-8b) of the tailings slurry in Mold 1 as a function of time. Most of the settlement occurred during the first six days. At the end of the test, the thickness of the tailings slurry decreased from 97.97 mm to 86.7 mm while the void ratio from 1.09 to 0.851. The final settlement of the tailings slurry is 11.27 mm, at which the cracks occurred at the surface top of the tailings and extended to depth.

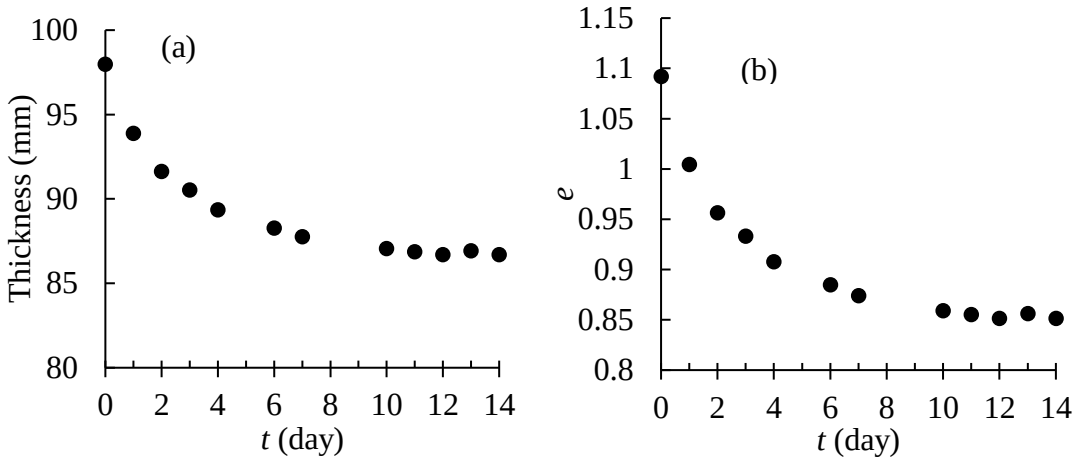

Figure 3-8: Variations of the (a) thickness and (b) void ratio of the tailings slurry in Mold 1 as a function of the drying time.

Figure 3-9 shows the variation of the thickness (Fig. 3-9a) and void ratio (Fig. 3-9b) of the tailings slurry deposited in Mold 2 as a function of time. Most of the settlement and void ratio variation occurred in the first day. At the end of the test, the thickness of the tailings slurry decreased from 71 cm to 65.62 cm while the void ratio from 1.092 to 0.933. The final settlement of the tailings slurry is 5.38 cm.

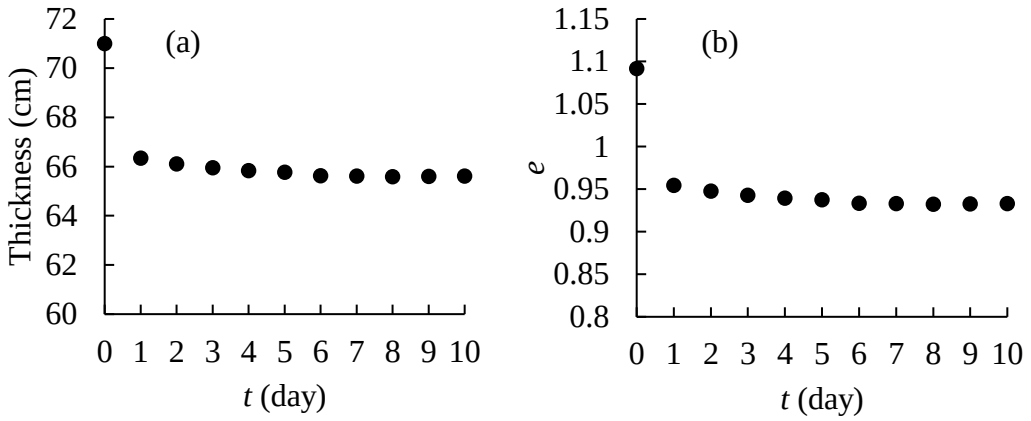

Figure 3-9: Variations of the (a) thickness and (b) void ratio of the tailings slurry in Mold 2 as a function of the drying time.

One notes that the settlement of the tailings slurry in Mold 1 (Fig. 3-8a) happened gradually while the major settlement of the backfill slurry in Mold 2 (Fig. 3-9a) occurred suddenly in the first day. In Mold 1, the volume variation of the tailings slurry was mainly controlled by evaporation, which took more time to finish. The thickness of tailings slurry decreased gradually. In Mold 2, water loss due to evaporation was negligible due to the larger thickness and small exposition surface. The settlement was mainly due to the sedimentation, which ended rapidly in the first day. In terms of strains (i.e. settlement over the initial thickness), both tests exhibit comparable values during the first day (4% for Mold 1 and 6.6% for Mold 2).

3.4 Verification of the proposed solution by experimental results

The tailings slurry deposited in Mold 1 has an initial void ratio e_0 of 1.09 and an initial height h_0 of 97.97 mm. The measured values of e_{AEV} and e_f of the tailings slurry are 0.941 and 0.863, respectively. The measured settlement at the end of the test is 11.3 mm. The tailings have become very dry with the formation of cracks on the top surface of the sample, Eq. 3-8 can be used to calculate the settlement as follows:

$$S_{fs} = \frac{e_0 - e_f}{e_0 + 1} h_0 = \frac{1.09 - 0.863}{1.09 + 1} \times 97.97\ mm = 10.641\ mm \quad (3\text{-}10)$$

This value is slightly smaller but quite close to the measured settlement of 11.3 mm. The slight difference can be attributed to the neglected volume of cracks and the possible unfinished residual

shrinkage stage in the shrinkage test. The latter can be confirmed by the stable void ratio of 0.851 at the end of the box test after 14 days of drying while the shrinkage test showed a final void ratio of e_f = 0.863. The proposed solution (Eqs. 3-8 and 3-9) can thus be considered as verified. It can be used to evaluate the settlement and volume change of tailings slurry deposited in a TSF in arid or semi-arid regions.

The settlement of tailings slurry in Mold 1 is also calculated by applying Eq. 3-6. The obtained S_t is smaller than S_{fs}. This is because the water content of sample in Mold 1 at end of the test was quite low. The suction was expected to be as high as 10^2 to 10^4 kPa according to the soil water retention characteristics of hard rock tailings (Aubertin et al. 2003). The high suction at low water content can lead to more volume change than that associated with self-weight consolidation.

For the tailings slurry deposition test with Mold 2, the tailings slurry has an initial void ratio e_0 = 1.092 and an initial height h_0 = 71 cm. The saturated unit weight of the tailings slurry is γ_{sat} = 17.93 kN/m^3 based on its density of 1.83 g/cm^3. The measured values of e_{AEV} and e_f are 0.941 and 0.863, respectively. The settlement of the tailings slurry at the end of sedimentation can be calculated as follows:

$$S_{ns} = \frac{e_0 - e_{AEV}}{e_0 + 1} h_0 = \frac{1.092 - 0.941}{1.092 + 1} \times 71\ cm = 5.06\ cm \tag{3-11}$$

The initial height of the tailings sample for the process of consolidation is then obtained as $h_1 = h_0 - S_{ns}$= 65.94 cm. At the end of the drainage and consolidation, the vertical effective stress in the slurried tailings can be calculated by Eq. (3-3) as follows:

$$\sigma' = (\gamma_{sat} - \gamma_w) \times (h_1 - x) = (17.934\ kN/m^3 - 9.8\ kN/m^3) \times (h_1 - x)$$

$$= 8.134\ kN/m^3 \times (h_1 - x) \tag{3-12}$$

By dividing the tailings height into 20 layers. the settlement caused by the consolidation can be calculated with Eq. (3-4) as follows:

$$S_c = \sum_{i=1}^{n} \frac{a_{vi}}{1 + e_{AEV}} \sigma_i' l_i = 0.39\ cm \tag{3-13}$$

where the coefficient of compressibility a_{vi} = 0.0043 kPa^{-1} was obtained by compression curve e-σ' shown in Figure 3-6(b).

These results confirm that the total settlement of this test is mainly due to the settlement of sedimentation, further explaining the quick settlement shown in Fig. 3-9a.

The total settlement of the tailings slurry is then obtained as follows:

$$S_t = S_{ns} + S_c = 5.45\ cm \tag{3-14}$$

This value is very close to but slightly higher than the measured settlement of 5.38 cm. The proposed solution (Eqs. 3-6 and 3-7) can thus be used to estimate the volume variation or settlement of tailings or backfill slurry placed in underground mine stopes or TSF in the regions where water balance is positive.

The slight overestimation of the total settlement by applying the proposed solution can be explained by several aspects. For instance, geomembrane was applied on the internal walls of the box to reduce interface friction. The efficiency of friction reduction by applying geomembrane between the backfill and walls is unknown (Zheng et al. 2020c). The possible fill-wall interface friction can have effect to prevent the settlement of the backfill. In addition, the shrinkage of the backfill slurry was probably not yet completed due to the large thickness and small exposition surface. This can be confirmed by the fact that the stable void ratio of 0.933 at the end of the box test after drying for 14 days is higher than the e_f (=0.863) at the end of the shrinkage tests.

3.5 Discussions

In this study, a simple analytical solution was proposed to estimate the settlement and volume variation of tailings slurry by considering the combined effects of shrinkage and self-weight consolidation. The proposed analytical solution was then verified by laboratory tests results. It thus constitutes a simple and useful tool to evaluate the settlement and volume variation of tailings slurry deposited in TSF or underground mine stopes. However, it should be noted that the proposed solution and laboratory tests contain some limitations.

For example, the settlement was calculated with the shrinkage (sedimentation) first and then the self-weight consolidation. In practice, there is no such a clear boundary between these two processes. With the coarse particles, the process of sedimentation can be completed more quickly than with the fine particles, resulting in more accumulation of coarse particles and formation of a soil skeleton at the bottom part (Been and Sills 1981) while the fine particles still remain in a state

of suspension. The processes of sedimentation and self-weight consolidation can thus take place simultaneously along the whole height of the tailings slurry (Imai 1981). Nevertheless, this does not affect the validity of the proposed solutions developed for estimating the settlement and volume variation of the final state of tailings slurry. More work is necessary to take into account these aspects if the evolution of the settlement and volume variation needs to be evaluated.

It should be noted that the initial void ratio of the compression curve shown in Figure 3-6 is higher than the unsaturation onset void ratio shown in Figure 3-4. This is abnormal because they are expected to be identical or at least very close to each other. The very possible reason is that the prepared samples for the consolidation test was not fully saturated while the drainage and consolidation process during the first initial loadings was not completed, resulting in measured void ratios higher than the actual values. More consolidation tests are necessary. Nevertheless, it is expected that the slope of the compression curve should not change significantly.

In this study, the proposed solution was developed by considering a uniform shrinkage along the height of tailings slurry. In practice, segregation can take place during the sedimentation process. Coarse particles settle down faster and accumulate at the bottom of the tailings slurry, resulting in non-uniform material along the full height of the tailings slurry (Bonin et al. 2014; Dalcé et al. 2019). The proposed solution can still be used by dividing the tailings slurry height into sufficient number of layers. More work is required to obtain the required parameter distribution.

In this study, arching effect was neglected in the estimation of vertical effective stresses. In the laboratory tests, a layer of geomembrane was applied over the inner walls to reduce the interface friction and arching effect. This is not representative of the field condition along the fill-rock wall interfaces in underground mine stopes. In practice, the rock walls of mine stopes can be rough. Arching effect can be significant and should be taken into account in the effective stress estimation for the process of consolidation (Aubertin et al. 2003; Thompson et al. 2012; Zheng et al. 2019). The vertical effective stress profile of backfill slurry will then become nonlinear. More work is necessary to take into account the effect of arching effect in the estimation of the settlement by consolidation.

In this study, the solution was proposed for tailings slurry and uncemented backfill. In practice, cemented backfill is usually used to fill underground mine stopes. The hydration and cementation

of cemented backfill can significantly affect the unsaturation onset void ratio and final void ratio compared to uncemented backfill (Helinski et al. 2007; Wood and Doherty 2014; Qin 2020). More work is required to take into account this aspect in the future.

In this study, only two physical model tests were conducted. The experimental results were used to verify the proposed solutions. More experimental work is necessary by using different geometries and materials.

Finally, cracks were observed on the top surface of the tailings slurry deposited in Mold 1 at the end of the tests, as shown in Figure 3-10. This indicates again the full shrinkage of the tailings slurry placed in Mold 1. More work is required to consider this aspect in the future.

Figure 3-10: Photograph of the tailings slurry in Mold 1 with the formation of cracks on the top surface at the end of the tests.

3.6 Conclusions

A simple analytical solution is proposed in this paper to estimate the settlement and volume variation of tailings slurry, deposited in a TSF or underground mine stope. It is the first time that the combined effects of shrinkage and consolidation were considered in the analytical solution to evaluate the settlement and volume variation of tailings slurry. The critical void ratio at the end of sedimentation is for the first time characterized through shrinkage test and considered to be equal to the unsaturation onset or air entry void ratio. To verify the proposed solution, the shrinkage and consolidation tests were conducted first to obtain the required parameters. Tailings slurry deposition tests were then conducted with two molds, one to simulate a tailings pond and the other

for underground mine stope. Good agreements were obtained between the measured settlements and those predicted by applying the proposed analytical solution. As shrinkage tests are simple and easy to do, the proposed solution can be considered as a simple and useful tool for the practitioners to evaluate the settlement and volume variation of tailings slurry, placed in TSF or underground mine stope, at least in the preliminarily stage of projects.

Acknowledgements

The authors would like to acknowledge the financial support from the Natural Sciences and Engineering Research Council of Canada (NSERC 402318), Fonds de recherche du Québec—Nature et Technologies (FRQNT 2015-MI- 191676), Mitacs Elevate Postdoctoral Fellowship (IT12573), and industrial partners of the Research Institute on Mines and the Environment (RIME UQAT-Polytechnique; http://rime-irme.ca/).

3.7 References

Agapito, L. A., Bareither, C. A., 2018. Application of a one-dimensional large-strain consolidation model to a full-scale tailings storage facility. Miner. Eng. 119, 38-48.

Aubertin, M., Bussiere, B., Chapuis, R. P., 1996. Hydraulic conductivity of homogenized tailings from hard rock mines. Can. Geotech. J. 33, 470-482.

Aubertin, M., Li, L., Arnoldi, S., Belem, T., Bussière, B., Benzaazoua, M., Simon, R., 2003. Interaction between backfill and rock mass in narrow stopes. Soil Rock Mech Am. 1, 1157-1164.

Aubertin, M., Mbonimpa, M., Bussière, B. Chapuis, R.P., 2003 A model to predict the water retention curve from basic geotechnical properties. Can. Geotech. J., 40(6): 1104-1122.

Been, K., Sills, G. C., 1981. Self-weight consolidation of soft soils: an experimental and theoretical study. Géotechnique 31, 519-535.

Benzaazoua, M., Bussière, B., Demers, I., Aubertin, M., Fried, É., Blier, A., 2008. Integrated mine tailings management by combining environmental desulphurization and cemented paste backfill: Application to mine Doyon, Quebec, Canada. Miner. Eng. 21, 330-340.

Bolduc, L. F., Aubertin, M., 2014. Numerical investigation of the influence of waste rock inclusions on tailings consolidation. Can. Geotech. J. 51, 1021-1032.

Bonin, M. D., Nuth, M., Dagenais, A. M., Cabral, A. R., 2014. Experimental study and numerical reproduction of self-weight consolidation behavior of thickened tailings. J. Geotech. Geoenviron. Eng. 140, 04014068.

Bonin, M., Cabral, A., Nuth, M., 2019. Examination of the effects of solids content on thickened gold mine tailings sedimentation and self-weight consolidation. Geotech. Test. J. 42, 1493-1517.

Bussière, B., 2007. Colloquium 2004: Hydrogeotechnical properties of hard rock tailings from metal mines and emerging geoenvironmental disposal approaches. Can. Geotech. J. 44, 1019-1052.

Bussière, B., Benzaazoua, M., Aubertin, M., Mbonimpa, M., 2004. A laboratory study of covers made of low-sulphide tailings to prevent acid mine drainage. Environ. Geol. 45, 609-622.

Dalcé, J. B., Li, L., Yang, P. Y., 2019. Experimental study of uniaxial compressive strength (UCS) distribution of hydraulic backfill associated with segregation. Minerals 9, 147.

Davis, E. H., Raymond, G. P., 1965. A non-linear theory of consolidation. Geotechnique 15, 161-173.

Dromer, J. B., Aubertin, M., Kennedy, G., Pedroni, L., Bussière, B., 2004. A new testing system to investigate the sedimentation and consolidation of sludge and slurry. In: 57th Annual Conference of the Canadian Geotechnical Society. pp. 16-23.

Fredlund, M. D., Wilson, G. W., Fredlund, D. G., 2002. Representation and estimation of the shrinkage curve. In: Proceedings of the 3rd International Conference on Unsaturated Soils. pp. 145-149.

Ghirian, A., Fall, M., 2013. Coupled thermo-hydro-mechanical–chemical behaviour of cemented paste backfill in column experiments. Part I: physical, hydraulic and thermal processes and characteristics. Eng. Geol. 164, 195-207.

Gibson, R. E., 1958. The progress of consolidation in a clay layer increasing in thickness with time. Géotechnique 8, 171-182.

Gibson, R. E., England, G. L., Hussey, M. J. L., 1967. The theory of one-dimensional consolidation of saturated clays: I. finite non-linear consolidation of thin homogeneous layers. Géotechnique 17, 261-273.

Hassani, F., Archibald, J. (Eds.), 1998. Mine backfill. CIM, Canada.

Helinski, M., Fourie, A., Fahey, M., Ismail, M., 2007. Assessment of the self-desiccation process in cemented mine backfills. Can. Geotech. J. 44, 1148-1156.

Holtz, R. D., Kovacs, W. D., Sheahan, T. C., 1981. An introduction to geotechnical engineering. Pearson, London, UK.

Imai, G., 1981. Experimental studies on sedimentation mechanism and sediment formation of clay materials. Soils Found. 21, 7-20.

Li, L., Alvarez, I. C., Aubertin, J. D., 2013. Self-weight consolidation of slurried deposition: tests and interpretation. Int. J. Geotech. Eng. 7, 205-213.

Marinho, F. A. M., 2017. Fundamentals of soil shrinkage. In: Proceedings of the Pan Am Unsaturated Soils Conference. pp. 198-222.

McRoberts, E. C., Nixon, J. F., 1976. A theory of soil sedimentation. Can. Geotech. J. 13, 294-310.

Potvin, Y., Thomas, E., 2005. Handbook on mine fill. Australian Centre for Geomechanics, Perth.

Qin, J. H., 2020. Analytical and experimental evaluation of the settlement and volume variation of tailings slurry deposited in containment structures. Master thesis, École Polytechnique de Montréal, Canada.

Rodet, J., 2019. Caractérisation hydrogéotechnique des déchets miniers dans les mines d'Eléonore. Montreal, Canada.

Saleh-Mbemba, F., Aubertin, M., Mbonimpa, M., Li, L., 2016. Experimental characterization of the shrinkage and water retention behaviour of tailings from hard rock mines. Geotech. Geol. Eng. 34, 251-266.

Saleh-Mbemba, F., Aubertin, M., 2018. Characterization of self-weight consolidation of fine-grained mine tailings using moisture sensors. Geotech. Test. J. 41, 543-554.

Shokouhi, A., Zhang, C., Williams, D. J., 2018. Settling, consolidation and desiccation behaviour of coal tailings slurry. Mining Technol. 127(1), 1-11.

Terzaghi, K., Peck, R. B., Mesri, G., 1996. Soil Mechanics in Engineering Practice. John Wiley & Sons, New York, USA.

Thompson, B. D., Bawden, W. F., Grabinsky, M. W., 2012. In situ measurements of cemented paste backfill at the Cayeli Mine. Can. Geotech. J. 49, 755-772.

Vick, S. G., 1990. Planning, Design, and Analysis of Tailings Dams. BiTech Publishers. B.C., Canada.

Wickland, B. E., Wilson, G. W., 2005. Self-weight consolidation of mixtures of mine waste rock and tailings. Can. Geotech. J. 42, 327-339.

Wood, D. M., Doherty, J. P., 2014. Coupled chemical shrinkage and consolidation: some benchmark solutions. Transp. Porous Media 105, 349-370.

Yang, P., Li, L., 2017. Evolution of water table and pore-water pressure in stopes with submerged hydraulic fill. Int. J. Geomech, 17(9), 04017052.

Yilmaz, E., Belem, T., Benzaazoua, M., 2014. Effects of curing and stress conditions on hydromechanical, geotechnical and geochemical properties of cemented paste backfill. Eng. Geol. 168, 23-37.

Yilmaz, E., Belem, T., Bussière, B., Benzaazoua, M., 2008. Consolidation characteristics of early age cemented paste backfill. In: Proceedings of the 61st Canadian Geotechnical Conference and the 9th Joint CGS/IAH-CNC Groundwater Conference, Edmonton, Canada.

Yilmaz, E., Belem, T., Bussière, B., Mbonimpa, M., Benzaazoua, M., 2015. Curing time effect on consolidation behaviour of cemented paste backfill containing different cement types and contents. Constr. Build. Mater. 75, 99-111.

Zhang, N., Zhu, W., He, H., Lv, Y., 2017. Experimental study on sedimentation and consolidation of soil particles in dredged slurry. KSCE J. Civ. Eng. 21, 2596-2606.

Zheng, J., Li, L., Mbonimpa, M., Pabst, T., 2018. An analytical solution of Gibson's model for estimating the pore water pressures in accreting deposition of slurried material under one-dimensional self-weight consolidation. Part I: pervious base. Indian Geotech. J. 48, 72-83.

Zheng, J., Li, L., Li, Y. C., 2019. Total and effective stresses in backfilled stopes during the fill placement on a pervious base for barricade design. Minerals 9, 38.

Zheng, J., Li, L., Li, Y. C., 2020a. Solutions to estimate the excess PWP, settlement and volume of draining water after slurry deposition. Part I: impervious base. Environ. Earth Sci. 79, 124.

Zheng, J., Li, L., Li, Y. C., 2020b. Solutions to estimate the excess PWP, settlement and volume of draining water after slurry deposition. Part II: pervious base. Under review by Environ. Earth Sci.

Zheng, J., Li, L., Daviault, M. 2020c. An experimental study on the effectiveness of lubricants in reducing the sidewall friction. Int J Geomech (accepted with changes, March 2020).

CHAPTER 4 ARTICLE 2: EXPERIMENTAL STUDY OF THE SHRINKAGE BEHAVIOR OF CEMENTED PASTE BACKFILL

Jiahao Qin, Jian Zheng, Li Li

Article submitted to *Construction and Building Materials* in April 2020.

Abstract: Cemented paste backfill (CPB) is largely used in underground mining stopes around the world. When a CPB is placed in a stope, an important task is to estimate the settlement associated with the shrinkage and self-weight consolidation of the CPB. This is closely related to the volume management to ensure the stability of barricades and tight contacts between the backfill and stope roof. Over the recent years, a few studies have been published on the shrinkage and self-weight consolidation of tailings. There is little study on the shrinkage of CPB. To fill this gap, a series of shrinkage tests have been conducted on CPB with different cement contents, including zero cement content (uncemented paste backfill; uCPB). The results show that the shrinkage response of CPB is very different from that of uCPB. At a given initial water content, CPB exhibits a shorter normal shrinkage stage than uCPB. The unsaturation onset water content and void ratio, shrinkage limit and final void ratio of CPB are generally higher than those of uCPB. At a given cement content, the shrinkage behavior of CPB and uCPB is significantly influenced by the initial water content.

Key words: Cemented paste backfill; Shrinkage; Evaporation; Underground mine stopes; Volume variation

4.1 Introduction

Cemented paste backfill (CPB) made of full (all sizes of particles) tailings is widely used in underground mines to increase ore recovery, reduce mineral dilution and improve ground stability. This technique allows the maximum reuse of mine tailings in underground stopes. The surface disposal of mine tailings can thus be minimized, resulting in a better preservation of environment (Bussière 2007; Ercikdi et al. 2015; Yilmaz et al. 2015).

When a slurried backfill is placed in a stope, an important task is to evaluate the required volume of slurried backfill to fully fill a given stope and ensure a tight contact between the backfill and stope roof. When the top surface of placed backfill is used as part of drift floor, it is critical to well estimate the volume of backfill slurry in the mine stopes to avoid creation of excessive void between the top surface of the settled backfill and the floor of over cut drift used as passing way of vehicles and workers. When the stope is filled in two stages (i.e., plug pour and final pour), a critical concern is how to ensure the final surface of the plug pour reaches the designed level (usually 2 to 3 meters higher than the roof level of access drift in which the barricade is built to retain the backfill in place). A too much higher plug pour than the access drift leads to a useless increase of binder consumption. With a plug pour lower than the roof level of access drift, excessive pressures can exercise on the top part of the barricade during the final pour, resulting in undesirable consequence associated with internal local instability near the upper portion of the barricade (Yang et al. 2016, Xu 2019[§]).

In order to estimate the required volume of backfill to fully fill an underground stope, one has to perform shrinkage tests to obtain some required parameters (Qin 2020). In fact, when a backfill slurry is placed in a stope, excess pore water pressure can be generated (Gibson 1958; Zheng et al. 2018a, 2018b). The particles of the backfill are not in contact and the effective stresses are zero. The volume reduction of the backfill is mainly associated with the dissipation of excess pore water pressure. The water consumption due to cement hydration is negligible for CPB as mentioned by Helinski et al. (2007) and also shown later in this paper. The volume reduction of the backfill is

[§] Xu, Y.H. (2019) Personal communications.

thus equal to the volume of water drainage. This process is known as “sedimentation” (Ahmed and Siddiqua 2014). The process of sedimentation is completed when the grain-grain contacts of the backfill slurry start. The void ratio at the end of sedimentation is called “sedimentation end void ratio”, which has been shown to correspond to the unsaturation onset void ratio of shrinkage curve (Qin 2020). It is thus important to have a good understanding of the shrinkage behavior of CPB.

Over the years, studies have been mainly given on the shrinkage response of fine-grained soils, such as silt and clayey soils (e.g., Crescimanno and Provenzano 1999; Albrecht and Benson 2001; Boivin et al. 2004; Péron et al. 2009). The shrinkage response of cemented clays was analyzed by Omidi et al. (1994) while the shrinkage behavior of cemented dredged sludge was studied by Zhang et al. (2010) and Hu and Zhao (2015). A few works have been conducted to investigate the shrinkage properties of uncemented tailings (e.g., Qiu and Sego 2001; Rodríguez 2006; Fisseha et al. 2007; Rodríguez et al. 2007; Saleh-Mbemba et al. 2016; Simms et al. 2017) or the chemical shrinkage associated with the hydration of cement (Walske 2014; Wood and Doherty 2014; Ghirian and Fall 2015; Cui and Fall 2017; Walske and Doherty 2018). The shrinkage behavior of CPB has never been investigated.

In this study, a brief review on soil shrinkage is given first. The results of a series of laboratory shrinkage tests on CPB are then presented. The influence of cement content and initial water content on the shrinkage behavior of CPB is then analyzed.

4.2 Theory of soil shrinkage

Shrinkage refers to the volume reduction as a function of water loss, mostly due to evaporation (Terzarghi 1925; Bowles 1984; Fredlund 2002; Leong and Wijaya 2015). It is generally described as the variation of void ratio e as a function of water content by mass w. The resulting curve is called shrinkage curve (Fredlund et al. 2002).

Shrinkage can generally be divided into four stages: structural shrinkage, normal shrinkage, residual shrinkage, and zero shrinkage (Peng and Horn 2013). The structural shrinkage is closely related to the large inter-aggregate pores and biological tubular pores in structured soils or soils with biological activity (Wijaya et al. 2015). It is generally absent in disturbed and loose non-aggregated specimen, such as tailings (Cornelis et al. 2006).

Figure 4-1 schematically shows a typical shrinkage curve of loose and disturbed unstructured soils (Marinho 2017). In the stage of normal shrinkage, the specimen always remains saturated with a degree of saturation S_r = 100% despite the decrease in water content by mass. The water content w progressively decreases from its initial value w_0 to a critical value, called unsaturation onset water content (w_{AEV}) corresponding the matrix suction equal to air entry value (AEV), below which unsaturation starts. The void ratio e varies linearly with the variation of w; the slope equals to G_s/S_r (i.e. $\Delta e/\Delta w = G_s/S_r$; G_s is the specific gravity) because the volume (and void ratio) change is totally generated by the grain-grain approach associated with the loss of water by drying or evaporation.

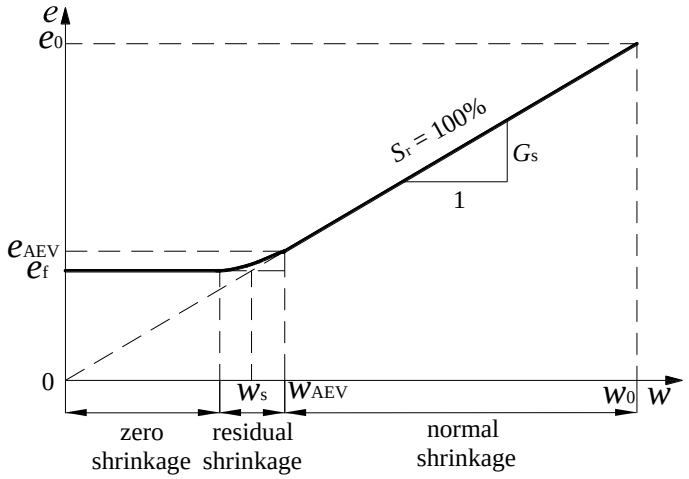

Figure 4-1: A typical shrinkage curve of loose and disturbed unstructured slurried soils (adapted from Marinho 2017).

When the water content further decreases to a degree smaller than the unsaturation onset water content w_{AEV}, the shrinkage curve becomes nonlinear and the slope decreases significantly with further water loss because grain-grain contacts begin and air starts to replace the inter-granular voids initially occupied by water. The unsaturation associated with capillarity generates suction, which in turn leads to contraction (i.e. desiccation) of the specimen. Nevertheless, the volume change of the specimen is smaller than the volume loss of water. This stage is called residual shrinkage (Peng et al. 2005).

Zero shrinkage is the final stage of the drying process, in which the grain-grain contacts become very tight. No significant deformation occurs to the specimen even though more water in inter-granular voids is replaced by air. Subsequently, the void ratio remains unchanged despite further

loss of water. The shrinkage curve becomes a quasi-horizontal line in the *e*–*w* plane, which intersects the *y* axis at the minimum (final) void ratio e_f (see Fig. 4-1). The water content at the intersection between the saturation line (S_r = 100%) and the horizontal line of zero shrinkage stage is called shrinkage limit w_s (Marinho 1994; Fredlund et al. 2002).

Over the years, several methods have been used to obtain a precise measurement of volume change associated with water loss, and subsequently the shrinkage curve. These include direct measurement method, volume replacement method, and non-contact method (Li et al. 2019). The direct measurement method is to directly measure the volume change of soil samples by using length measurement devices, such as Vernier calipers and LVDT (Péron et al. 2009; Saleh-Mbemba et al. 2016). This method is non-destructive, fast and easy to execute while the accuracy of measurement depends on the operator. The volume replacement method includes wax coated method, balloon method, and mercury replacement method (Prakash et al. 2009; Tang et al. 2011; Gapak et al. 2017). Due to the destructive effect on specimens and the evaporation of poisonous mercury, the volume replacement method is not suggested. The non-contact method is another non-destructive method that makes use of 3D scanner and high-resolution image techniques to obtain accurate measurement of volume (Sander and Gerke 2007; Hobbs et al. 2014; Jain et al. 2015; Upreti and Leong 2018; Wong et al. 2019). Its application depends on the availability of the required equipment and is thus limited. In this study, the direct measurement method is adopted due to its simplicity.

4.3 Shrinkage tests of cemented tailings

4.3.1 Tested tailings and cement

The CPB is made of tailings, cement and water. The tailings used in this study were collected from a hard rock mine in Quebec, Canada. Before sample manipulation, the tailings were stored in sealed barrels. The specific gravity of the tailings was measured to be G_s = 2.73. The grain size distribution of the used tailings was analyzed through sieve and hydrometer tests. Figure 4-2 shows the grain size distribution curve of the tested tailings with D_{10} = 3.3 μm, D_{30} = 14.2 μm, D_{60} = 43.2 μm, C_u = 13.02 (coefficient of uniformity), and C_c = 1.4 (coefficient of curvature). It can be classified as low plastic silt ML according to the Unified Soil Classification System (USCS; Holtz and Kovacs

1981). As the tested tailings contain 40% of fine particles smaller than 20 μm, the requirement of at least 15% of fine particles smaller than 20 μm defined in Potvin et al. (2005) for a backfill to be considered as a paste backfill is largely satisfied. The saturated hydraulic conductivity k_{sat} was measured to range from 1×10^{-6} to 5×10^{-6} m/s while the void ratio from 0.46 to 0.83 (Rodet 2019). These values are somewhat higher than typical values of tailings (Bussière 2007). Ordinary Portland cement type 10 was used as the binder material with a specific gravity of 3.15.

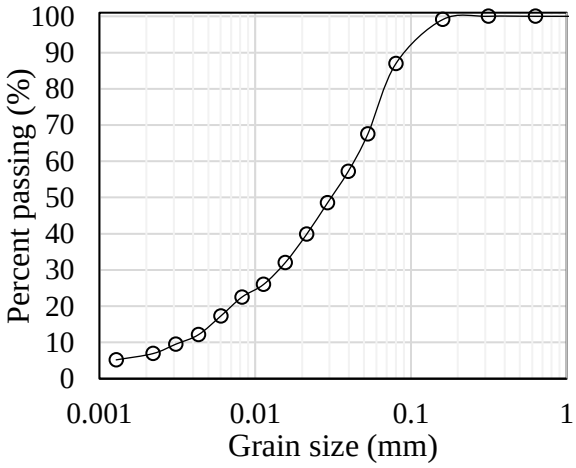

Figure 4-2: Grain size distribution curve of the tested tailings.

The CPB were obtained by mixing a given mass of oven-dried tailings, a given mass of de-aired water and a given mass of ordinary Portland cement in a bowl. The initial (gravimetric) water contents w_0 are 40, 50, 60, 80, and 100% (or 71.4, 66.7, 62.5, 55.6 and 50% in terms of initial solid contents by mass, S_0), respectively. These solid contents may not completely meet the requirement of typical CPB. This reflects the use of CPB in practice where more water than the requirement of CPB has to be added to facilitate the transportation of the backfill by pipes. The CPB were prepared with cement contents C_0 of 3, 5, and 7%, respectively. These cement contents are in the range of commonly used CPB in underground mines in Canada (Kesimal et al. 2005; Fall et al. 2007). Uncemented paste backfill (uCPB) has also been tested for the sake of comparison. After the mixing process, the CPB specimens were vibrated for 30 seconds to remove any air bubbles in the slurry.

4.3.2 Instrumentation and testing procedures

The testing instrumentation was inspired from that of Péron et al. (2009) and Saleh-Mbemba et al. (2016). Figure 4-3 shows a photograph of the testing instrumentation, which consists of a PVC mold having an internal opening 199.8 mm long, 30.0 mm large and 50.2 mm high, a balance (accuracy: 0.1 g) and a Vernier caliber (accuracy: 0.01 mm). In this study, two more PVC molds have been used, one having an internal opening 205.9 mm long, 31.1 mm large and 50.0 mm high and another having an internal opening of 199.9 mm long, 29.7 mm large and 50.1 mm. In order to prevent sticking between the specimen and the inside walls of the mold, the base and lateral walls of the mold were first applied with a thin layer of silicone grease and then covered by a layer of Teflon. The measured dimensions of the internal opening above are the dimensions after Teflon and grease are applied. This treatment is necessary and efficient to avoid cracking of the cemented tailings during the shrinkage.

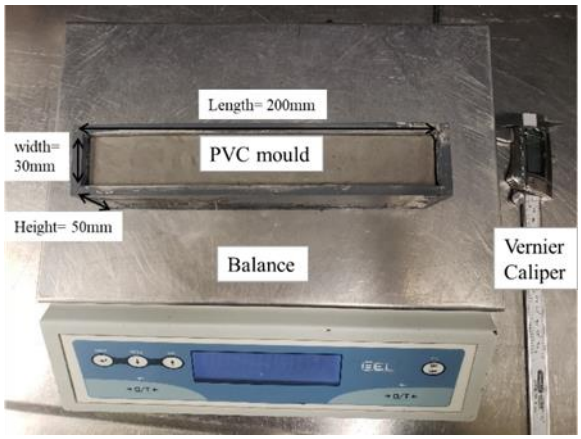

Figure 4-3: Photograph of the testing instrumentation with a Vernier caliper and a testing mold placed on a balance.

The tests started by measuring the mass and sizes of the internal opening of the empty mold having its internal walls and base applied with grease and Teflon. A prepared tailings specimen was then manually placed in the mold with a flat spoon until the mold was filled up with specimen. During the placement, the mold was gently tapped on the four sides to eliminate any air bubbles between the fill and side walls. A soil knife and a wet towel were used to carefully remove the excess material on top of the mold. The initial total mass of each sample (M_{t0}) was measured while the initial volume (V_0) was determined from the sizes of the internal opening covered with grease and

Teflon. The initial total mass of solids ($M_{s0.tot}$) and initial mass of water (M_{w0}) are calculated from the initial water content (w_0) and total mass (M_{t0}) as follows:

$$M_{s0.tot} = \frac{M_{t0}}{1+w_0} \tag{4-1}$$

$$M_{w0} = M_{t0} - M_{s0.tot} \tag{4-2}$$

The initial masses of cement solids ($M_{S0.c}$) and tailings solids ($M_{S0.tail}$) can then be calculated as follows from the cement content (C_0):

$$M_{s0.c} = M_{s0.tot} C_0 \tag{4-3}$$

$$M_{s0.tail} = M_{s0.tot} - M_{s0.c} \tag{4-4}$$

The initial total volume of solids (including tailings and cement), $V_{S0.tot}$, is obtained as follows:

$$V_{s0.tot} = \frac{M_{s0.tail}}{\rho_{tailings}} + \frac{M_{s0.c}}{\rho_{cement}} \tag{4-5}$$

where $\rho_{tailings}$ (= 2730 kg/m^3) and ρ_{cement} (= 3150 kg/m^3) are the densities of the tailings solid and cement solid, respectively.

The initial void ratio e_0 is then obtained as follows:

$$e_0 = \frac{V_0 - V_{s0.tot}}{V_{s0.tot}} \tag{4-6}$$

Table 4-1 shows the samples prepared for the shrinkage tests.

Table 4-1: Parameters of the prepared specimens at the initial state.

C_0 (%)	w_0 (%)	S_0 (%)	V_0 (cm^3)	M_{t0} (g)	M_{w0} (g)	$M_{S0.c}$ (g)	$M_{S0.tail}$ (g)	$M_{S0.tot}$ (g)	e_0
0	40	71.4	320.7	587.5	167.9	0.0	419.6	419.6	1.09
0	50	66.7	301.2	512.9	171.0	0.0	341.9	341.9	1.37
0	60	62.5	297.6	493.1	184.9	0.0	308.2	308.2	1.64
0	80	55.6	301.2	430.7	191.4	0.0	239.3	239.3	2.18
0	100	50.0	301.2	439.5	219.8	0.0	219.8	219.8	2.73
3	40	71.4	301.2	551.2	157.5	11.8	381.9	393.7	1.10
3	50	66.7	320.7	554.5	184.8	11.1	358.6	369.7	1.37
3	60	62.5	320.7	531.1	199.2	10.0	322.0	331.9	1.64
3	80	55.6	320.7	495.8	220.4	8.3	267.2	275.4	2.19
3	100	50.0	320.7	470.1	235.1	7.1	228.0	235.1	2.74
5	40	71.4	320.7	582.2	166.3	20.8	395.1	415.9	1.10

5	50	66.7	301.2	516.2	172.1	17.2	326.9	344.1	1.37
5	60	62.5	297.6	495.2	185.7	15.5	294.0	309.5	1.65
5	80	55.6	301.2	465.1	206.7	12.9	245.5	258.4	2.20
5	100	50	301.2	442.1	221.1	11.1	210.0	221.1	2.75
7	40	71.4	297.6	538.6	153.9	26.9	357.8	384.7	1.10
7	50	66.7	297.6	513.8	171.3	24.0	318.6	342.5	1.38
7	60	62.5	301.2	497.2	186.5	21.8	289.0	310.8	1.65
7	80	55.6	297.6	459.2	204.1	17.9	237.3	255.1	2.20
7	100	50	297.6	436.4	218.2	15.3	202.9	218.2	2.76

The drying process of the filled mold took place under an ambient environment with a room temperature of 20° C (±3° C) and relative humidity between 30 and 50%[☼]. At predetermined time intervals, the mass of the filled mold was measured. The mass loss of water and the new water content can then be determined. In the meantime, the length and width of the specimen were directly measured with the Vernier caliper while the thickness was obtained by subtracting the measured settlement from the initial thickness. Each dimension was determined by averaging five measurements at different positions. The volume and void ratio variation of the specimen can then be calculated. The interval between two successive measurements was generally 1 h during the first day and increased to longer time from the second days. The tests were ended when the total volume of the specimen became unchanged for 2 days. The specimen was then withdrawn from the mold and placed in the oven at a temperature of 250° C for 24 h. The total mass of solids $M_{sf.tot}$ was then measured. The shrinkage curve can then be obtained by plotting the variation of the void ratio as a function of the water content.

4.4 Test results and interpretation

Figure 4-4 shows the shrinkage curves of the tested CPB with different cement contents when the initial gravimetric water content w_0 is 100 (Fig. 4-4a), 80 (Fig. 4-4b), 60 (Fig. 4-4c), 50 (Fig. 4-4d) and 40% (Fig. 4-4e), respectively. The test results of uCPB has also been plotted on the figure for the sake of comparison. In all cases, the shrinkage curves show a linear variation between the void

[☼] Values taken from Saleh-Mbemba et al. (2016)

ratio and water content, following the saturation line during the normal shrinkage stage. These results are similar to those obtained on tailings by Rodríguez (2006) and Saleh-Mbemba et al. (2016). After then, the shrinkage curves exhibit a short residual shrinkage stage. These results are similar to those shown in Rodríguez (2006), but different from those reported by Saleh-Mbemba et al. (2016) who showed that the residual shrinkage stage was almost absent and the shrinkage curves were almost bilinear curve. This difference can be partly explained by the difference in the gradation and soil water retention characteristics of tested tailings. However, more work is necessary to fully understand the different shrinkage behaviors of different materials. After the residual shrinkage stage, a zero-shrinkage stage ($e = e_f$) is observed on the tested tailings, as shown by Rodríguez (2006) and Saleh-Mbemba et al. (2016).

At a given initial water content w_0, the shrinkage curves of CPB and uCPB follow the same saturation line (S_r = 100%) with a slope equal to G_s/S_r in the normal shrinkage stage. For the case of w_0 = 50% as shown in Fig. 4-4d, slight differences can be observed between the shrinkage curves of CPB and that of uCPB. This is probably due to some errors or disturbance associated with some renovation work around the laboratory. In all cases, the CPB exhibits shorter normal shrinkage stage than the uCPB. The unsaturation onset water content (w_{AEV}) and void ratio (e_{AEV}) as well as the shrinkage limit (w_s) and final void ratio (e_f) of the CPB are much larger than those of uCPB. They generally increase as the cement content increases even though the increasing rates are not homogeneous when the initial water content changes from 100 to 40%. These results are similar to those reported by Omidi et al. (1994) on cemented clays with a cement content of 3 to 12% and those presented by Zhang et al. (2010) on the shrinkage of cemented dredged sludge with a water content of 70% to 140% and a cement content of 0 to 20%. The results clearly indicate the occurrence of hydration during the shrinkage tests with the CPB.

When cement meets water, a chemical reaction process known as hydration starts. According to Locher (2006), small quantities of ettringite and calcium hydroxide are generated at the very beginning. The CPB may become stiffer, but without generation of any cohesion. This stage can last 4 to 6 hours. After this first stage of induction, the reaction accelerates. Long fibers up to 2 m long can be generated as long as the required spaces are available. With further hydration, a network of short, strip-shaped calcium silicate particles can be formed after 24 hours. The resulting microstructure can exhibit a certain strength even though the porosity still remains quite high,

which was also found in SEM analysis and pore structure study by Ouellet et al. (2008). As the tested CPB has high initial void ratios and low cement contents, the development of long fibers and microstructure network can freely develop and occupy more space. When the shrinkage reaches the onset point of unsaturation, the stiff and strength fibers and microstructure network resist the volume contraction associated with the suction, resulting higher final void ratios and shrinkage limits than the uCPB.

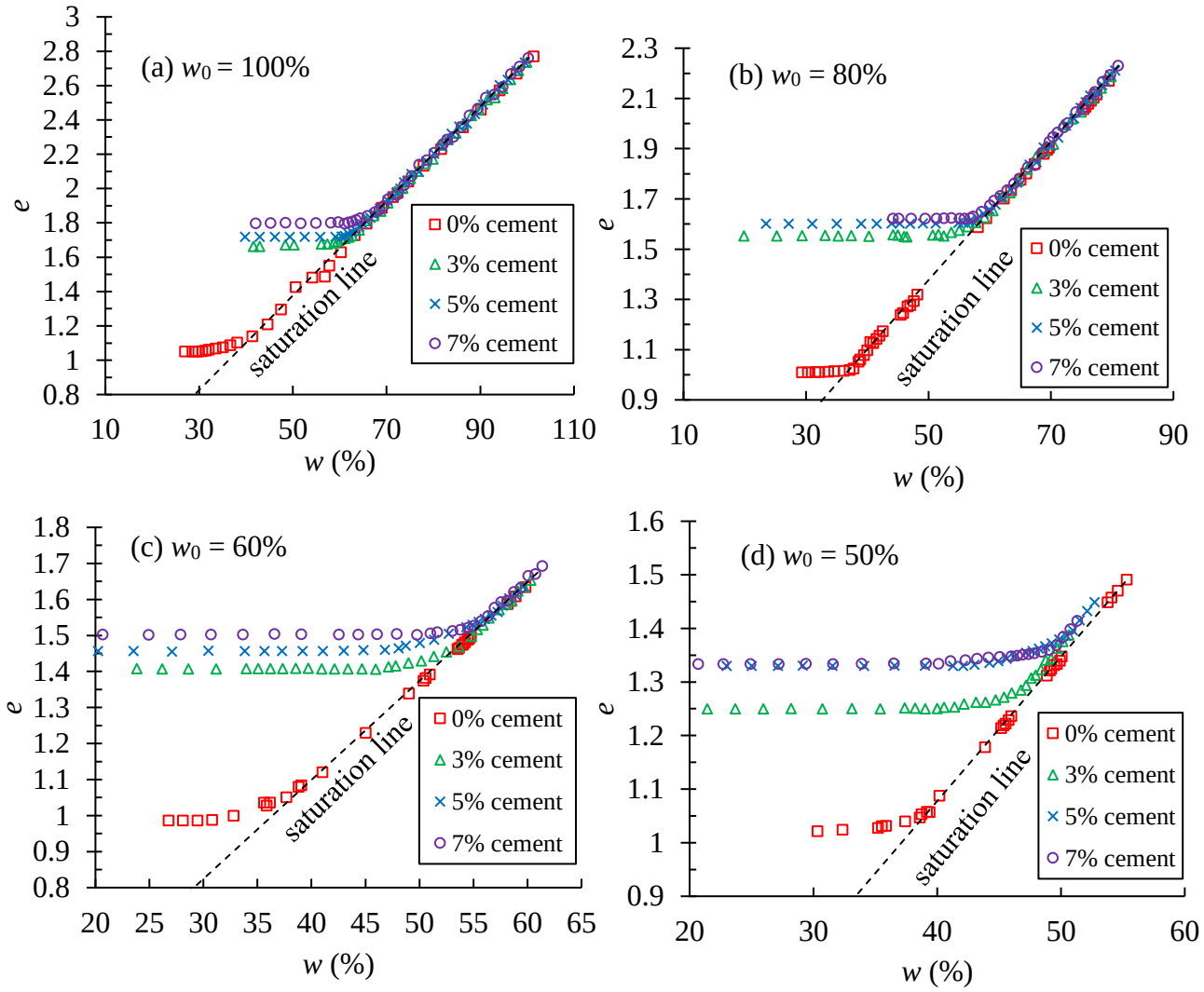

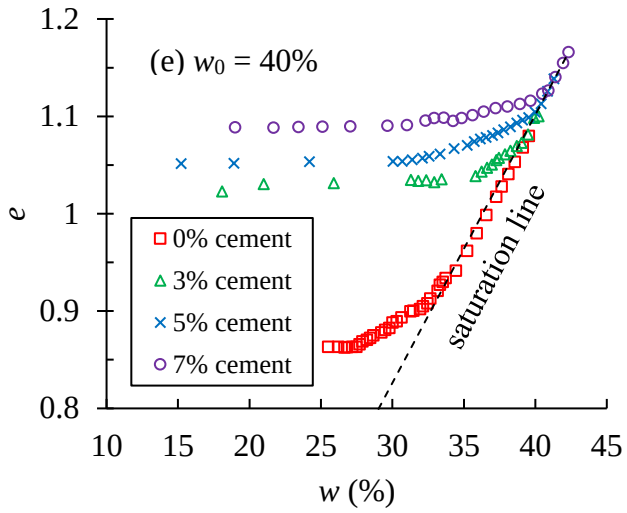

Figure 4-4: Shrinkage curves of uncemented and cemented tailings with different cement contents under the initial water content of (a) 100%, (b) 80%, (c) 60%, (d) 50%, and (e) 40%.

Theoretically, the cementation and hydration of CPB consume pore water and transform a portion of free water into bonded water, resulting in high final void ratio and shrinkage limit. It is thus interesting to compare the final total masses of solids (including the bounded water and the initial total masses of tailings and cement) at the end of each shrinkage test ($M_{Sf.tot}$) with the initial total masses of solids ($M_{S0.tot}$).

Table 4-2 shows the total masses of solids at the beginning ($M_{S0.tot}$) and end ($M_{Sf.tot}$) of each shrinkage test. The shrinkage parameters, including the unsaturation onset water content (w_{AEV}) and void ratio (e_{AEV}) as well as the shrinkage limit (w_s) and final void ratio (e_f), are also presented in the table.

Table 4-2: Parameters of the tested CPB and uCPB at different stages of shrinkage.

C_0 (%)	w_0 (%)	e_0	$M_{S0.c}$ (g)	$M_{S0.tail}$ (g)	$M_{S0.tot}$ (g)	$M_{Sf.tot}$ (g)	w_{AEV} (%)	e_{AEV}	w_s (%)	e_f
0	40	1.09	0.0	419.6	419.6	421.0	37.4	1.02	31.5	0.86
0	50	1.37	0.0	341.9	341.9	330.2	38.6	1.05	37.4	1.02
0	60	1.64	0.0	308.2	308.2	308.5	37.7	1.03	36.3	0.99
0	80	2.18	0.0	239.3	239.3	240.0	37.8	1.03	37.0	1.01
0	100	2.73	0.0	219.8	219.8	218.2	41.4	1.13	38.5	1.05
3	40	1.10	11.8	381.9	393.7	393.1	39.1	1.07	37.5	1.03
3	50	1.37	11.1	358.6	369.7	368.1	46.8	1.28	45.6	1.25
3	60	1.64	10.0	322.0	331.9	331.3	53.7	1.47	51.5	1.41

3	80	2.19	8.3	267.2	275.4	275.7	59.2	1.62	56.6	1.55
3	100	2.74	7.1	228.0	235.1	235.2	62.7	1.72	60.6	1.66
5	40	1.10	20.8	395.1	415.9	412.0	39.5	1.09	38.3	1.05
5	50	1.37	17.2	326.9	344.1	338.0	50.4	1.38	48.4	1.33
5	60	1.65	15.5	294.0	309.5	310.3	56.7	1.56	53.0	1.46
5	80	2.20	12.9	245.5	258.4	257.7	62	1.7	58.2	1.6
5	100	2.75	11.1	210.0	221.1	221.6	64.2	1.76	62.6	1.72
7	40	1.10	26.9	357.8	384.7	378.4	40.9	1.13	39.6	1.09
7	50	1.38	24.0	318.6	342.5	339.5	49.6	1.37	48.4	1.33
7	60	1.65	21.8	289.0	310.8	308.1	55.7	1.53	54.6	1.5
7	80	2.20	17.9	237.3	255.1	253.7	62.9	1.73	58.8	1.62
7	100	2.76	15.3	202.9	218.2	217.9	67.6	1.86	65.4	1.8

For the case of uCPB, the total masses of solids at the end ($M_{Sf.tot}$) and beginning ($M_{S0.tot}$) of each shrinkage test are very close to each other. These results indicate that the mass measurements and the test procedure are reliable.

When the cement content C_0 was 7%, the total mass of solids at the end ($M_{Sf.tot}$) of each shrinkage test is even smaller than that at the beginning ($M_{S0.tot}$). This is because the cement content C_0 was high and the bond generated at the end of each shrinkage test between the CPB samples and Teflon became quite strong. Care had to be given to recover all the sample of each test. Loss of material was unavoidably generated.

When the CPB has a cement content C_0 of 3% or 5%, the total masses of solids at the end ($M_{Sf.tot}$) and beginning ($M_{S0.tot}$) of each shrinkage test are very close to each other. These results indicate the water consumption and bonded water are negligible during the curing process of the CPB. Similar results have been reported by Helinski et al. (2007), who indicated that the amount of water consumption by hydration and chemical shrinkage can be negligible for high water content and low cement content CPB. If one evaluates the degree of cementation and hydration of CPB based on the consumption of water, one probably concludes that the cementation and hydration are absent during the two or three days of shrinkage. In fact, the combined water during the hydration can be divided into evaporable and non-evaporable. The non-evaporable water represents the chemically bounded water, which is combined with cement and transferred into hydrated compounds. It does not evaporate or separate from the hydrated compound even under high temperature. The non-

evaporable water during the first three days of curing only represents 12% of cement (Locher 2006). Table 4-3 shows the measured and expected final masses of solids at the end of each shrinkage tests of two or three days. The variation of solid mass in specimens should show the mass of non-evaporable water. One can see that the measured and expected values are very close to each other. The negligible amount of non-evaporable water consumption during the shrinkage tests of two or three days cannot be taken as a reliable indicator of hydration.

Table 4-3: Measured and expected final total masses of solids at the end of each shrinkage test for the CPB having cement contents of 3 and 5%, respectively.

C_0 (%)	w_0 (%)	$M_{S0.c}$ (g)	$M_{S0.tail}$ (g)	$M_{S0.tot}$ (g)	$M_{Sf.tot}$ (g)	
					Measured	Expected
3	40	11.8	381.9	393.7	393.1	395.1
3	50	11.1	358.6	369.7	368.1	371.0
3	60	10.0	322.0	331.9	331.3	333.1
3	80	8.3	267.2	275.4	275.7	276.4
3	100	7.1	228.0	235.1	235.2	235.9
5	40	20.8	395.1	415.9	412.0	418.4
5	50	17.2	326.9	344.1	338.0	346.2
5	60	15.5	294.0	309.5	310.3	311.4
5	80	12.9	245.5	258.4	257.7	259.9
5	100	11.1	210.0	221.1	221.6	222.4

Figure 4-5 shows the shrinkage curves (*e*-*w*) of Figure 4-4 for different initial water contents when the initial cement content C_0 is 0 (Fig. 4-5a), 3 (Fig. 4-5b), 5 (Fig. 4-5c) and 7% (Fig. 4-5d), respectively. For uCPB (C_0 = 0%), the shrinkage curves of different initial water contents follow the same saturation line in the normal shrinkage stage. However, the final void ratio and shrinkage limit increase as the initial water content increases.

With CPB, the influence of initial water content on the shrinkage behavior becomes more pronounced. The shrinkage limit and final void ratio increase as the initial water content increases. At a given cement content, the grain-grain spacing of a specimen with a higher initial water content can be larger. The development of long fibers and network microstructure can be freer and more complete. This can explain the larger final volume and larger final void ratio of the specimen at the end of each shrinkage test.

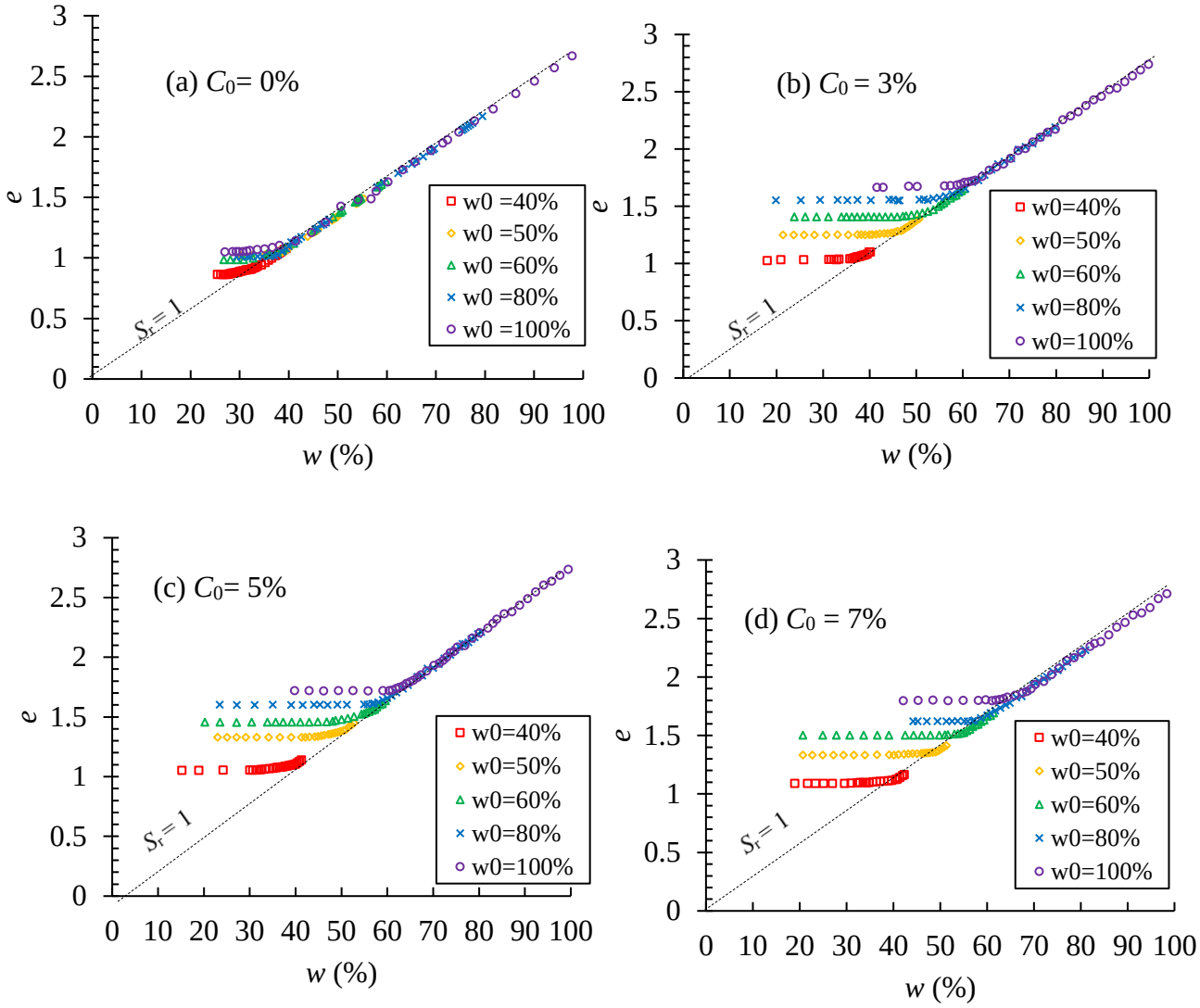

Figure 4-5: Shrinkage curves of tailings with different initial water contents under the cement content of (a) 0%, (b) 3%, (c) 5%, and (d) 7%.

Figure 4-6 shows the variations of the shrinkage limit (Fig. 4-6a) and final void ratio (Fig. 4-6b) as a function of cement content under different initial water contents. The uCPB shows the lowest shrinkage limit, which is in the range of 30% to 40%. At a given initial water content, the cement content of CPB has only a slight effect on the shrinkage limit. The value of w_s increases slightly as the cement content increases from 3 to 7%. At a given cement content, the shrinkage limit of CPB can be significantly influenced by the initial water content. A higher initial water content results in a higher shrinkage limit. Similarly, the uCPB shows the lowest final void ratio, compared to the CPB. At a given initial water content, the final void ratio of CPB increases slightly as the cement

content increases from 3 to 7%. At a given cement content, higher initial water content leads to higher final void ratio.

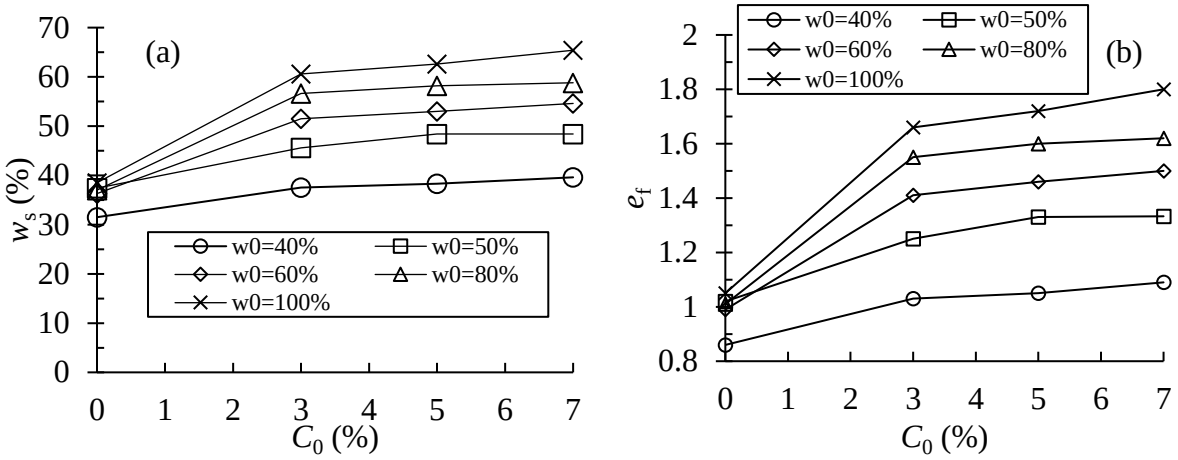

Figure 4-6: Variations of (a) shrinkage limit w_s and (b) final void ratio e_f as a function of cement content under different initial water contents.

Figure 4-7 shows the variation of unsaturation onset water content w_{AEV} (Fig. 4-7a) and void ratio e_{AEV} (Fig. 4-7b). One can see that the values of w_{AEV} and e_{AEV} for CPB are higher than those of uCPB. The mechanism to explain these results is the same as that of shrinkage limit and final void ratio. At a given cement content, the values of w_{AEV} and e_{AEV} for CPB increase significantly as the initial water content increases. However, the values of w_{AEV} and e_{AEV} for CPB at a given initial water content increase only slightly as the cement content increases.

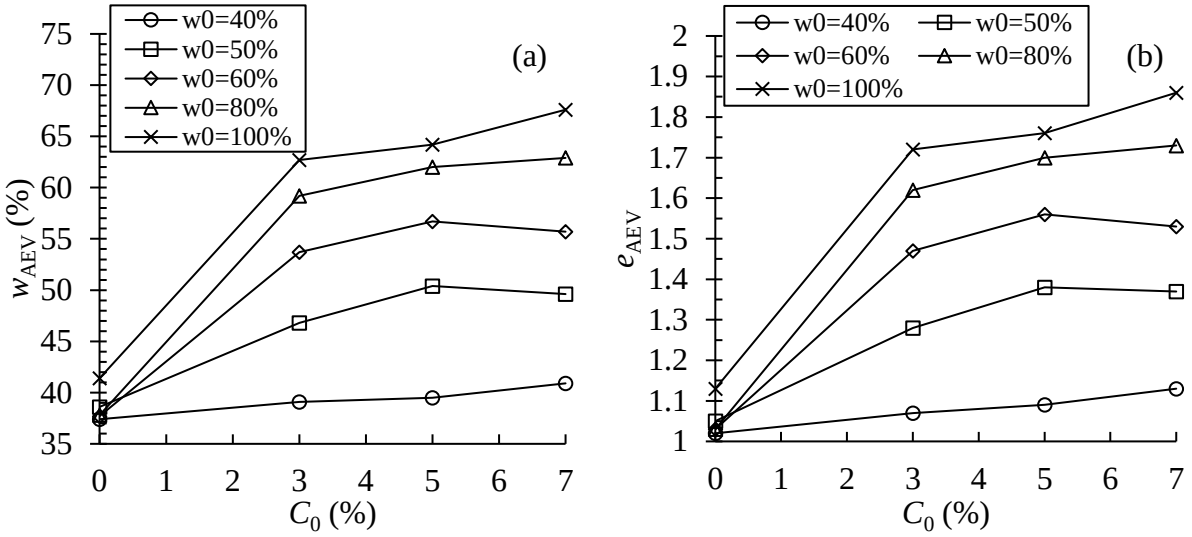

Figure 4-7: Variations of (a) w_{AEV} and (b) e_{AEV} as a function of cement content under different initial water contents.

4.5 Discussion

The molds used in this study are 200 mm long, 30 mm large, and 50 mm deep. These sizes were chosen to study the volume change properties of CPB and uCPB only associated with water loss by evaporation. The geometry of the mold is not representative of mine stopes. However, large dimension testing molds, especially in depth, should be avoided. Otherwise, the processes of segregation, self-weight consolidation and arching effect may take place during the shrinkage tests. This may render the results interpretation very complex. Moreover, a very thick sample may not only need longer time to evaporate, but also result in dried sample near the top surface and saturated sample near the base (Nahlawi and Kodikara 2006).

In this study, the drainage and evaporation were only possible in the upward direction. In practice, lateral drainage can take place in a mine stope through the surrounding fractured rock walls (Belem et al. 2016) or permeable barricades (Rankine 2005). The lateral drainage can accelerate the water loss and increase the volumetric shrinkage rate (ratio of decreased volume to initial volume). More work is required to consider more representative drainage conditions.

In this study, the shrinkage tests were conducted with only one type of tailings and binder. More work is required to consider different tailings and binders (e.g., slag or lime) in the future work.

When shrinkage tests were conducted without applying lubricants or plastic film on the base and inner walls of the mold, cracks would appear during the shrinkage tests, as shown in Figure 4-8. Cracking can be avoided when the mold is treated with grease and Teflon. More work is required to consider the influence of cracks on the shrinkage behavior in the future.

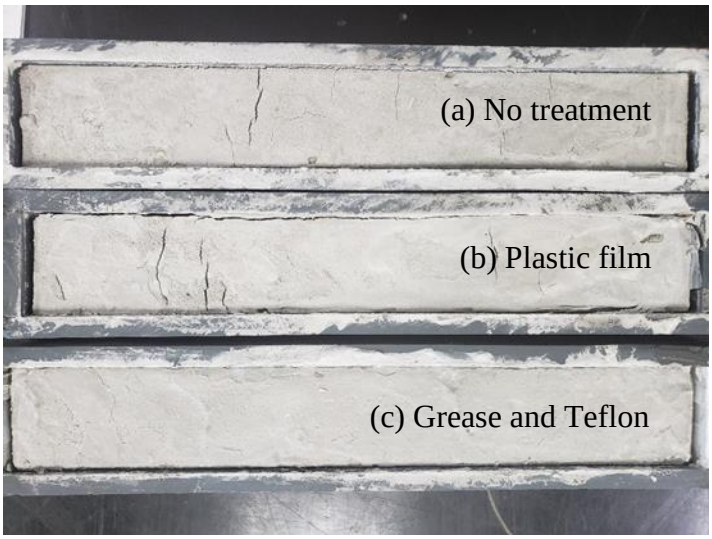

Figure 4-8: Photograph of different crack patterns of CPB with different boundary conditions: (a) no treatment, (b) applying with plastic film, and (c) applying with grease and Teflon.

4.6 Conclusion

The shrinkage behaviors of CPB and uCPB have been investigated. The shrinkage behavior of CPB is very different from that of uCPB. The normal shrinkage stage of the CPB is much shorter than that of uCPB. The unsaturation onset water content and void ratio, shrinkage limit, and final void ratio of CPB are higher than those of uCPB. The shrinkage curves of CPB can be significantly influenced by the initial water content. At a given cement content, the unsaturation onset water content and void ratio, shrinkage limit and final void ratio of CPB increase significantly as initial water content increases. However, the shrinkage behavior of CPB is only slightly influenced by the cement content. At a given initial water content, the increase of cement content from 3% to 7% can only lead to slight increase in unsaturation onset water content, void ratio, shrinkage limit, and final void ratio.

Acknowledgements

The authors would like to acknowledge the financial support from the Natural Sciences and Engineering Research Council of Canada (NSERC 402318), Fonds de recherche du Québec—Nature et Technologies (FRQNT 2015-MI- 191676), Mitacs Elevate Postdoctoral Fellowship (IT12572), and industrial partners of the Research Institute on Mines and the Environment (RIME UQAT-Polytechnique; http://rime-irme.ca/).

4.7 References

Ahmed SI and Siddiqua S. (2014) A review on consolidation behavior of tailings. *International Journal of Geotechnical Engineering*, 8(1): 102-111.

Albrecht BA and Benson CH. (2001) Effect of desiccation on compacted natural clays. *Journal of Geotechnical and Geoenvironmental Engineering*, 127(1): 67-75.

Belem T, El Aatar O, Bussière B and Benzaazoua M. (2016) Gravity-driven 1-D consolidation of cemented paste backfill in 3-m-high columns. *Innovative Infrastructure Solutions*, 1(1): 37.

Boivin P, Garnier P and Tessier D. (2004) Relationship between clay content, clay type, and shrinkage properties of soil samples. *Soil Science Society of America Journal*, 68(4): 1145-1153.

Bowles JE. (1984) Physical and geotechnical properties of soils. New York: McGraw-Hill.

Bussière B. (2007) Colloquium 2004: Hydrogeotechnical properties of hard rock tailings from metal mines and emerging geoenvironmental disposal approaches. *Canadian Geotechnical Journal*, 44(9): 1019-1052.

Cornelis WM, Corluy J, Medina H, Diaz J, Hartmann R, Van Meirvenne M and Ruiz ME (2006) Measuring and modelling the soil shrinkage characteristic curve. *Geoderma*, 137(1-2): 179-191.

Crescimanno G and Provenzano G. (1999) Soil shrinkage characteristic curve in clay soils: measurement and prediction. *Soil Science Society of America Journal*, 63(1): 25-32.

Cui L and Fall M. (2017) Multiphysics model for consolidation behavior of cemented paste backfill. *International Journal of Geomechanics*, 17(3): 04016077.

Ercikdi B, Külekci G and Yılmaz T. (2015) Utilization of granulated marble wastes and waste bricks as mineral admixture in cemented paste backfill of sulphide-rich tailings. *Construction and Building Materials*, 93: 573-583.

Fall M, Belem T, Samb S and Benzaazoua M. (2007) Experimental characterization of the stress–strain behaviour of cemented paste backfill in compression. *Journal of Materials Science*, 42(11): 3914-3922.

Fisseha B, Glancy T and Simms P. (2007) The influence of the initial degree of saturation on the shrinkage curve of silts. *Proc. of 8th Joint IAH-CNC and CGS Groundwater Specialty Conference and 60th Canadian Geotechnical Conference*, Ottawa, Ontario, Canada, (p. 21-24).

Fredlund MD, Wilson GW and Fredlund DG. (2002) Representation and estimation of the shrinkage curve. *Proc. of 3rd International Conference on Unsaturated Soils*, (p. 145-149).

Gapak Y, Das G, Yerramshetty U and Bharat TV. (2017) Laboratory determination of volumetric shrinkage behavior of bentonites: A critical appraisal. *Applied Clay Science*, 135: 554-566.

Ghirian A and Fall M. (2015) Coupled behavior of cemented paste backfill at early ages. *Geotechnical and Geological Engineering*, 33(5): 1141-1166.

Gibson RE (1958) The progress of consolidation in a clay layer increasing in thickness with time. *Géotechnique*, 8(4):171–182

Helinski M, Fourie A, Fahey M and Ismail M. (2007) Assessment of the self-desiccation process in cemented mine backfills. *Canadian Geotechnical Journal*, 44(10): 1148-1156.

Hobbs PRN, Jones LD, Kirkham MP, Roberts P, Haslam EP and Gunn DA. (2014) A new apparatus for determining the shrinkage limit of clay soils. *Géotechnique*, 64(3): 195-203.

Holtz RD, Kovacs WD and Sheahan TC. (1981) An introduction to geotechnical engineering (Vol. 733). Englewood Cliffs, NJ: Prentice-Hall.

Hu X and Zhao Z. (2015) Experimental study of drying shrinkage of solidified dredged material. *Journal of Hohai University*, 43: 39-43.

Jain S, Wang YH and Fredlund DG. (2015) Non-Contact sensing system to measure specimen volume during shrinkage test. *Geotechnical Testing Journal*, 38(6): 936-949.

Kesimal A, Yilmaz E, Ercikdi B, Alp I and Deveci H. (2005) Effect of properties of tailings and binder on the short-and long-term strength and stability of cemented paste backfill. *Materials Letters*, 59(28): 3703-3709.

Leong EC and Wijaya M. (2015) Universal soil shrinkage curve equation. *Geoderma*, 237-238: 78-87.

Li L, Zhang X and Li P. (2019) Evaluating a new method for simultaneous measurement of soil water retention and shrinkage curves. *Acta Geotechnica*, 14(4): 1021-1035.

Locher FW. (2006) Cement: Principles of production and use. Düsseldorf: Verlag Bau+Technik GmbH.

Marinho FAM. (1994) Shrinkage behavior of some plastic clays. *Ph. D. Thesis*. University of London, London, UK.

Marinho FAM. (2017) Fundamentals of soil shrinkage. *Proc. of the Pan Am Unsaturated Soils Conference*. Dallas, Texas, USA, (p. 198-222).

Nahlawi H and Kodikara JK. (2006) Laboratory experiments on desiccation cracking of thin soil layers. *Geotechnical and Geological Engineering*, 24(6): 1641-1664.

Omidi GH, Prasad TV, Thomas JC and Brown KW. (1996) The influence of amendments on the volumetric shrinkage and integrity of compacted clay soils used in landfill liners. *Water, Air, and Soil Pollution*, 86(1): 263-274.

Ouellet S, Bussière B, Aubertin M and Benzaazoua M. (2008) Characterization of cemented paste backfill pore structure using SEM and IA analysis. *Bulletin of Engineering Geology and the Environment*, 67(2): 139-152.

Peng X and Horn R. (2005) Modeling soil shrinkage curve across a wide range of soil types. *Soil Science Society of America Journal*, 69(3): 584-592.

Peng XH and Horn R. (2013) Identifying six types of soil shrinkage curves from a large set of experimental data. *Soil Science Society of America Journal*, 77(2): 372-381.

Péron H, Hueckel T, Laloui L and Hu LB. (2009) Fundamentals of desiccation cracking of fine-grained soils: experimental characterisation and mechanisms identification. *Canadian Geotechnical Journal*, 46(10): 1177-1201.

Potvin Y and Thomas E. (2005) Handbook on mine fill. Perth: Australian Centre for Geomechanics.

Prakash K, Sridharan A, Baba J and Thejas H. (2009) Determination of shrinkage limit of fine-grained soils by wax method. *Geotechnical Testing Journal*, 32(1): 86-89.

Qin JH. (2020) Analytical and experimental evaluation of the settlement and volume variation of tailings slurry deposited in containment structures. *Master thesis*. École Polytechnique de Montréal, Montreal, Canada.

Qiu Y and Sego DC. (2001) Laboratory properties of mine tailings. Canadian Geotechnical Journal, 38(1): 183-190.

Rankine KJ. (2005) An investigation into the drainage characteristics and behaviour of hydraulically placed mine backfill and permeable minefill barricades, *Ph. D. Thesis*. James Cook University, Townsville, Australia.

Rodet J. (2019) Caractérisation hydrogéotechnique des déchets miniers dans les mines d'Eléonore. Unpublished manuscirpt, École Polytechnique de Montréal, Montreal, Canada.

Rodríguez R. (2006) Hydrogeotechnical characterization of a metallurgical waste. *Canadian Geotechnical Journal*, 43(10): 1042-1060.

Rodríguez R, Sánchez M, Ledesma A and Lloret A. (2007) Experimental and numerical analysis of desiccation of a mining waste. *Canadian Geotechnical Journal*, 44(6): 644-658.

Saleh-Mbemba F, Aubertin M, Mbonimpa M and Li L. (2016) Experimental characterization of the shrinkage and water retention behaviour of tailings from hard rock mines. *Geotechnical and Geological Engineering*, 34(1): 251-266.

Sander T and Gerke HH. (2007) Noncontact shrinkage curve determination for soil clods and aggregates by three-dimensional optical scanning. *Soil Science Society of America Journal*, 71(5): 1448-1454.

Simms P, Soleimani S, Mizani S, Daliri F, Dunmola A, Rozina E and Innocent-Bernard T. (2017) Cracking, salinity and evaporation in mesoscale experiments on three types of tailings. *Environmental Geotechnics*, 6(1): 3-17.

Tang CS, Shi B, Liu C, Suo WB and Gao L. (2011) Experimental characterization of shrinkage and desiccation cracking in thin clay layer. *Applied Clay Science*, 52(1-2): 69-77.

Terzaghi K. (1925) Principles of soil mechanics: I – Phenomena of cohesion of clays. *Engineering News-Record*, 95(19): 742-746

Upreti K and Leong EC. (2018) Measurement of soil shrinkage curve using photogrammetry. *Proc. of 2nd Pan American Conference of Unsaturated Soils*, Dallas, Texas, USA, (p. 71-80).

Walske M. (2014) An experimental study of cementing paste backfill. *Ph. D. Thesis*. University of Western Australia, Perth, Australia.

Walske ML and Doherty J. (2018) Incorporating chemical shrinkage volume into Gibson's solution. *Canadian Geotechnical Journal*, 55(6): 903-908.

Wijaya M, Leong EC and Rahardjo H. (2015) Effect of shrinkage on air-entry value of soils. *Soils and Foundations*, 55(1): 166-180.

Wong JM, Elwood D and Fredlund DG. (2019) Use of a three-dimensional scanner for shrinkage curve tests. *Canadian Geotechnical Journal*, 56(4): 526-535.

Wood DM and Doherty JP. (2014) Coupled chemical shrinkage and consolidation: some benchmark solutions. *Transport in Porous Media*, 105(2): 349-370.

Yang, PY, Li, L, Aubertin, M, Brochu-Baekelmans, M, and Ouellet, S. (2017) Stability analyses of waste rock barricades designed to retain paste backfill. *International Journal of Geomechanics*, 17(3), 04016079.

Yilmaz E, Belem T, Bussière B, Mbonimpa M and Benzaazoua M. (2015) Curing time effect on consolidation behaviour of cemented paste backfill containing different cement types and contents. *Construction and Building Materials*, 75: 99-111.

Zhang CL, Zhu W and Fan GJ. (2010) Shrinkage properties of cement solidified sludge with high water content. *Journal of Hohai University (Natural Sciences)*, (38)3: 295-299.

Zheng J, Li L, Mbonimpa M and Pabst T. (2018a) An analytical solution of gibson's model for estimating the pore water pressures in accreting deposition of slurried material under one-dimensional self-weight consolidation. Part I: pervious base. *Indian Geotechnical Journal*, 48(1): 72-83.

Zheng J, Li L, Mbonimpa M and Pabst T. (2018b) An analytical solution of Gibson's model for estimating pore water pressures in accreting deposition of slurried material under one-dimensional self-weight consolidation. Part II: impervious base. *Indian Geotechnical Journal*, 48(1): 188-195.

CHAPTER 5 DISCUSSIONS

In this thesis, two analytical solutions have been proposed to evaluate the settlement and volume variation of tailings or backfill slurry after being placed in a tailings pond or underground mine stope by considering the shrinkage, sedimentation and weight consolidation. The proposed analytical solutions have been verified by experimental results obtained by physical model tests in laboratory. The good agreements between the analytical and experimental results indicate that the proposed solutions can be used to evaluate the settlement and volume variation of tailings or backfill slurry deposited in tailings ponds or underground mine stopes. In addition, experimental study was conducted to investigate the shrinkage behavior of cemented paste backfill with different initial water contents and cement contents. However, it should be noted that the experimental and analytical studies presented in Chapter 3 and 4 contain some limitations, which will be summarized as follows:

In the proposed solutions developed to evaluate the settlement and volume variation of tailings or backfill slurry, the settlement induced by sedimentation or shrinkage was first calculated by considering the void ratio reduces to the unsaturation onset void ratio e_{AEV}. After that, the settlement due to consolidation begins. In practice when a backfill slurry is placed in a mine stope, the coarser particles settle down faster, resulting in earlier grain-grain contacts near the bottom while the fine particles can remain longtime on the top part in a state of suspension. Segregation takes place, resulting in non-uniform distribution of tailings particles along the full height (Dalcé et al. 2019). In the future, more work is required to take into account the occurrence of segregation as well as the simultaneous occurrence of sedimentation and consolidation along the full height of the tailings or backfill slurry.

In this study, the initial void ratio of the compression curve was higher than the unsaturation onset void ratio e_{AEV}. This is abnormal because they should be very close to each other. Besides, it is difficult to understand or explain the two-phase consolidation curve as the tailings slurry did not submit to any preconsolidation. These are probably attributed to the not fully saturated samples and inadequate operation during the first steps of loading in the consolidation tests. In the future, more consolidation tests are required to verify these abnormal results.

Arching effect is neglected in the application of the proposed solutions to interpret the experimental results of physical model tests. This can be appropriate for a tailings slurry deposited in a tailings

pond with a large horizontal dimension. For backfill deposited in a mine stope, the occurrence of arching effect along the interfaces between the backfill and rock walls can slow down the consolidation and reduce the settlement (Aubertin et al. 2003; Li and Aubertin 2008). The neglect of arching effect could lead to an overestimate of the effective stresses and subsequently an overestimate of the settlement due to consolidation. More work is required to consider the arching effect in the future work.

The proposed solutions were proposed by considering one-layer deposition of tailings or backfill slurry. In the field conditions, tailings are always deposited layer by layer in the TSF. Several scenarios are possible. For instance, if the interval between layer and layer depositions is very short, the tailings slurry can be considered as an accreting layer with the possible sedimentation and consolidation during the thickness increase (Gibson 1958). If the interval between layer and layer depositions is very long, the sedimentation and consolidation of previous layers can thus be considered as completed. A new layer can be considered as a surcharge. Settlements due to consolidation of previous layers can be calculated while the settlement of the fresh layer can be estimated by applying the proposed solution (Eq. 3-6). For intermediate cases, the problem can become very complex. In all cases, more work is necessary to develop a more elaborate solution that can be used to evaluate the settlement and volume variation of tailings or backfill slurry after taking into account the field conditions.

In this study, the proposed solutions have been verified by physical model tests on uncemented tailings and paste backfill. In underground mines, paste backfill is always cemented. The shrinkage tests on cemented paste backfill have shown that the addition of cement can significantly influence the unsaturation onset void ratio. To apply the proposed solution for estimate the settlement and volume variation of cemented paste backfill, the required parameters (e_f, e_{AEV}) of cemented paste backfill have been obtained by shrinkage tests. More work is required to test the validity of the proposed solutions for estimating the settlement and volume variation of cemented paste backfill. This requires to do consolidation tests on cemented paste backfill to obtain the coefficient of compressibility a_v (Yilmaz et al. 2008). Physical model tests on cemented paste backfill with settlement measurement are also necessary.

During the volume variation tests, cracks were observed on the top surface of the tailings slurry deposited in the mold simulating a tailings pond. The influence of the cracks on the settlement and

volume variation of the tailings slurry was neglected during the result interpretation by applying the proposed solution. More work is required to develop a solution for estimating the settlement and volume variation of tailings slurry after taking into account the formation of cracks.

The proposed solutions to evaluate the settlement of tailings slurry have been verified by laboratory test results. It could be interesting to test its validity in field condition.

In this study, the normal shrinkage stage of shrinkage tests is similar to the sedimentation process of self-weight consolidation tests. Based on this, the void ratio of end sedimentation was considered as equal to the unsaturation onset void ratio. This hypothesis needs to be verified by performing self-weight consolidation tests and shrinkage tests. The self-weight consolidation tests should be done with the measurements of total stresses and pore water pressure.

The shrinkage tests were conducted in molds of 200 mm long, 30 mm large and 50 mm high. This geometry is not representative of a mine stope. The small height is designed to facilitate the evaporation and ensure the completion of the shrinkage tests in a reasonable period. Moreover, it can minimize the possibility of segregation and influence of consolidation during the shrinkage tests.

In the physical model tests, the drainage and evaporation were only allowed in the upward direction. The base and side walls of the molds were impermeable. In practice, the rockmass walls of mine stopes usually contain some fractures (Belem et al. 2016). Barricades are usually built with permeable materials or with draining pipes (Rankine 2005). Lateral drainage can thus take place, accelerate the water loss and increase the shrinkage and drainage rate. More experimental work is required by considering more representative drainage conditions.

The shrinkage tests were only conducted with one kind of tailings with the addition of Portland cement. Previous studies have shown that the grain size distribution of tailings and mineralogy of binder can influence the shrinkage responses and cementation rate of cemented paste backfill. More work is required to conduct shrinkage tests with different tailings and binders in the future.

The solid contents of the tested cemented paste backfill range from 50 to 71.4%. These values are smaller than the required solid contents of cemented paste backfill. In practice, it is very difficult to respect the solid content requirement of paste backfill, at which the backfill is unsaturated and cohesive (due to suction). More water than the requirement of paste backfill has to be added to

facilitate the transportation by pipes. In the future, shrinkage tests can be conducted with more representative cemented paste backfill.

In this study, the experimental results obtained by shrinkage tests conducted by applying a layer of grease and Teflon in the inner walls of the mold have been presented. This instrumentation was to reduce the sidewall frictions and minimize the possibility of cracking. Cracks were clearly observed on the top surface of the backfill at the end of the shrinkage tests conducted by using a layer of plastic or without applying any lubricants in the mold. The sticking between the backfill and mold walls can lead to the formation of cracks. More work is required to investigate the influence of the formation of cracks on the shrinkage responses of cemented paste backfill.

It can be interesting to obtain the soil water retention curve of cemented paste backfill, which relates water content and matrix suction. In residual shrinkage stage, the void ratio variation with increase of matrix suction is similar to the void ratio decrease with effective stress increase of consolidation. This hypothesis needs to be verified by experimental results.

The shrinkage test of cemented paste backfill is also associated with the evaporation rate of cemented paste backfill. The evaporation rate of cemented paste backfill is expected to be influenced by the cement content, tailings type and so on. More work is required to investigate the evaporation characteristics of cemented paste backfill and uncemented tailings.

The explanation to the decreased shrinkage by cement hydration is based on the theory in concrete and cement base materials with higher cement content. The expected development of microstructure network by long fibers in cement hydration and the increased stiffness should be assessed with more tests like scanning electron microscope (SEM) tests.

CHAPTER 6 CONCLUSIONS AND RECOMMANDATIONS

6.1 Conclusions

This thesis first proposed an analytical solution to estimate the settlement and volume variation of the tailings or backfill slurry after being placed in a tailings pond or underground mine stope by considering the combined effects of shrinkage, sedimentation and consolidation. For the requirement of settlement estimation in backfilled stope, the shrinkage response of cemented paste backfill was investigated and the effect of cement content and initial water content was studied.

In Chapter 3, the analytical and experimental studies conducted to investigate the settlement and volume variation of the tailings or backfill slurry after being placed in a tailings pond or underground mine stope have been presented. The main conclusions are summarized as follows:

- The normal shrinkage phase of shrinkage tests plays the same role as the sedimentation of self-weight consolidation tests on the volume decrease of slurry. The critical void ratio of the transition from sedimentation to consolidation is for the first time regarded as the void ratio at the onset of unsaturation of shrinkage curve.
- Analytical solutions have been proposed to estimate the settlement and volume variation of tailings or backfill slurry after being deposited in tailings ponds or underground mine stopes. One solution is for underground mine stopes or TSF in non-arid regions while the other for TSF in arid or semi-arid regions.
- The combined effects of sedimentation, shrinkage and consolidation are for the first time considered in analytical solutions to evaluate the settlement and volume variation of tailings slurry.
- The proposed solutions have been applied to estimate the settlements obtained by two physical model tests, one simulating a tailings pond and another simulating an underground mine stope. The good agreements between the measured settlements and those predicted by applying the proposed solutions indicate the validity of the proposed solutions.
- The proposed solutions can thus be considered as a simple and useful tool for the practitioners to estimate the settlement and volume variation of tailings or backfill slurry

deposited in tailings ponds or underground mine stopes at least in the preliminarily stage of projects.

In Chapter 4, the shrinkage tests performed on cemented paste backfill have been presented. The cemented paste backfill samples are prepared with different initial water contents and cement content. The shrinkage response of the cemented paste backfill is compared with that of the uncemented paste backfill. The main conclusions are summarized as follows:

- Shrinkage tests considering the evaporation are, for the first time, conducted on cemented paste backfill.
- The shrinkage response of cemented paste backfill is very different from that of uncemented paste backfill. The cemented past backfill samples show shorter normal shrinkage phase and higher shrinkage parameters (e.g., unsaturation onset water content and void ratio, shrinkage limit, and final void ratio) than the uncemented paste backfill.
- The shrinkage properties of uncemented paste backfill are less affected by the initial water content and the variations of final void ratio and unsaturation onset void ratio with varied initial water contents are quite small, which are similar to results of Saleh-Mbemba et al. (2016).
- At a given initial water content, the shrinkage of the cemented paste backfill is only slightly influenced with the increase of cement content.
- At a given cement content, the shrinkage of cemented paste backfill is significantly influenced by initial water content. This response is different from that of uncemented paste backfill.
- The test results show that the variation of solid mass of cemented paste backfill before and after the shrinkage tests is negligible. Water consumption in cement hydration is negligible for most used cemented paste backfill.

6.2 Recommendations

In addition to the results presented in the thesis, more work is required to obtain a good understanding of the shrinkage response of the cemented paste backfill and the settlement and

volume variation of the tailings or backfill slurry after being deposited in a tailings pond or underground mien stope.

- The proposed solution calculates the settlement driven by the sedimentation first and then the self-weight consolidation. In practice, these two processes may take place simultaneously in the tailings or backfill slurry. More work is required to improve the proposed solution by considering this aspect.
- More oedometer tests should be performed by ensuring saturation of tested samples and waiting long enough for every step of loading.
- The proposed solutions were proposed by considering a uniform material along the height of the tailings or backfill slurry. More work is required to divide the tailings slurry into sufficient number of layers and apply the proposed solutions for each layer.
- More work is required to take into account the arching effect in the proposed solutions to estimate the settlement of backfill slurry in underground mine stope.
- When the mine stope is filled with cemented paste backfill, the occurrence of cement hydration can impact the shrinkage response and parameters of the backfill slurry. More work is required to consider the influence of cement hydration in the proposed solution.
- More work is required to consider the accreting deposition of tailings in tailings pond in the proposed solutions.
- The formation of cracks should be taken into account in the proposed solutions, especially in the case of tailings slurry deposited in the tailings pond.
- More physical model tests considering different geometries and materials are required to further validate the proposed solutions.
- The validity of the proposed solutions in field conditions should be assessed with data of field measurements.
- More shrinkage tests need to be conducted with different kinds of tailings or binders.
- More shrinkage tests are required with cemented paste backfill having more representative solid contents.

- More work is required to conduct the shrinkage tests by considering lateral drainage.
- The desiccation tests only considering the evaporation characteristics of cemented paste backfill and uncemented tailings are required to study the variation of water content and void ratio of cemented paste backfill or uncemented tailings with elapsed time.
- Measuring soil water retention characteristics of cemented paste backfill is required to verify the similarity between the void ratio variation under increase of effective stress and increase of matrix suction.
- Consolidation tests and physical model tests on cemented paste backfill are required to test the validity of proposed solutions for the settlement and volume variation of cemented paste backfill.

BIBLIOGRAPHY

Abu-Hejleh AN, Znidarčić D and Barnes BL. (1996) Consolidation characteristics of phosphatic clays. *Journal of Geotechnical Engineering*, 122(4): 295-301.

Abdul-Hussain N and Fall M. (2011) Unsaturated hydraulic properties of cemented tailings backfill that contains sodium silicate. *Engineering Geology*, 123(4): 288-301.

Agapito LA and Bareither CA. (2018) Application of a one-dimensional large-strain consolidation model to a full-scale tailings storage facility. *Minerals Engineering*, 119: 38-48.

Ahmed SI and Siddiqua S. (2014) A review on consolidation behavior of tailings. *International Journal of Geotechnical Engineering*, 8(1):102–111

Albrecht BA and Benson CH. (2001) Effect of desiccation on compacted natural clays. *Journal of Geotechnical and Geoenvironmental Engineering*, 127(1): 67-75.

Álvarez-Valero AM, Sáez R, Pérez-López R, Delgado J and Nieto JM. (2009) Evaluation of heavy metal bio-availability from Almagrera pyrite-rich tailings dam (Iberian Pyrite Belt, SW Spain) based on a sequential extraction procedure. *Journal of Geochemical Exploration*, 102(2): 87-94.

Amarasiri AL, Kodikara JK and Costa S. (2011) Numerical modelling of desiccation cracking. *International Journal for Numerical and Analytical Methods in Geomechanics*, 35(1): 82-96.

ASTM 427-04. (2008). Test method for shrinkage factors of soils by the mercury method. *ASTM International*, West Conshohocken, PA, USA.

ASTM 2435. (2011). Standard test methods for one-dimensional consolidation properties of soils using incremental loading. *ASTM International*, West Conshohocken, PA, USA.

Aubertin M, Bussiere B and Chapuis RP. (1996) Hydraulic conductivity of homogenized tailings from hard rock mines. *Canadian Geotechnical Journal*, 33(3): 470-482.

Aubertin M, Li L, Arnoldi S, Belem T, Bussière B, Benzaazoua M and Simon R. (2003) Interaction between backfill and rock mass in narrow stopes. *Soil and rock America*, 1: 1157-1164.

Aubertin M, Mbonimpa M, Bussière B and Chapuis RP. (2003) A model to predict the water retention curve from basic geotechnical properties. *Canadian Geotechnical Journal*, 40(6): 1104-1122.

Barbour SL, Wilson GW and St-Arnaud LC. (1993) Evaluation of the saturated–unsaturated groundwater conditions of a thickened tailings deposit. *Canadian Geotechnical Journal*, 30(6): 935-946.

Barron RA. (1948) Consolidation of fine-grained soils by drain wells. *Transactions of the American Society of Civil Engineers*, 113: 718–742.

Been K and Sills GC. (1981) Self-weight consolidation of soft soils: an experimental and theoretical study. *Géotechnique*, 31(4): 519-535.

Belem T and Benzaazoua M. (2004) An overview on the use of paste backfill technology as a ground support method in cut-and-fill mines. *Proc. of the 5th International Symposium on Ground support in Mining and Underground Construction*, Perth, Australia, (p. 28-30).

Belem T and Benzaazoua M. (2008) Design and application of underground mine paste backfill technology. *Geotechnical and Geological Engineering*, 26(2): 147-174.

Belem T, El Aatar O, Bussière B and Benzaazoua M. (2016) Gravity-driven 1-D consolidation of cemented paste backfill in 3-m-high columns. *Innovative Infrastructure Solutions*, 1(1): 37.

Belem T, Fourie AB and Fahey M. (2010) Measurement of volume change in cemented mine backfills at early ages. *Proc. of 1st International Seminar on the Reduction of Risk in the Management of Tailings and Mine Waste*, Perth, Australia, (p. 449-462).

Benzaazoua M, Bussière B, Demers I, Aubertin M, Fried É and Blier A. (2008) Integrated mine tailings management by combining environmental desulphurization and cemented paste backfill: Application to mine Doyon, Quebec, Canada. *Minerals Engineering*, 21(4): 330-340.

Blight G. (2009) Geotechnical engineering for mine waste storage facilities. UK: Taylor & Francis.

Bolduc F and Aubertin M. (2014) Numerical investigation of the influence of waste rock inclusions on tailings consolidation. *Canadian Geotechnical Journal*, 51(9): 1021-1032.

Boivin P, Garnier P and Tessier D. (2004) Relationship between clay content, clay type, and shrinkage properties of soil samples. *Soil Science Society of America Journal*, 68(4): 1145-1153.

Bonin MD, Cabral A and Nuth M. (2019) Examination of the effects of solids content on thickened gold mine tailings sedimentation and self-weight consolidation. *Geotechnical Testing Journal*, 42(6): 1493-1517.

Bonin MD, Nuth M, Dagenais AM and Cabral AR. (2014) Experimental study and numerical reproduction of self-weight consolidation behavior of thickened tailings. *Journal of Geotechnical and Geoenvironmental Engineering*, 140(12): 04014068.

Bowles JE. (1984) Physical and Geotechnical Properties of Soils. New York: McGraw-Hill.

Burritt RL and Christ KL. (2018) Water risk in mining: Analysis of the Samarco dam failure. *Journal of Cleaner Production*, 178: 196-205.

Bussière B. (2007) Colloquium 2004: Hydrogeotechnical properties of hard rock tailings from metal mines and emerging geoenvironmental disposal approaches. *Canadian Geotechnical Journal*, 44(9): 1019-1052.

Bussière B, Benzaazoua M, Aubertin M and Mbonimpa M. (2004) A laboratory study of covers made of low-sulphide tailings to prevent acid mine drainage. *Environmental Geology*, 45(5): 609-622.

Byrne P, Hudson-Edwards KA, Bird G, Macklin MG, Brewer PA, Williams RD and Jamieson HE. (2018) Water quality impacts and river system recovery following the 2014 Mount Polley mine tailings dam spill, British Columbia, Canada. *Applied Geochemistry*, 91: 64-74.

Casagrande A and Fadum RE. (1940) Notes on soil testing for engineering purposes. *Harvard Soil Mechanics, Series No. 8*, Cambridge, Mass, USA.

Chen P and Lu N. (2018) Generalized equation for soil shrinkage curve. *Journal of Geotechnical and Geoenvironmental Engineering*, 144(8): 04018046.

Chertkov VY. (2000) Modeling the pore structure and shrinkage curve of soil clay matrix. *Geoderma*, 95(3): 215-246.

Chertkov VY. (2003) Modelling the shrinkage curve of soil clay pastes. *Geoderma*, 112(1): 71-95.

Clayton S, Grice TG and Boger DV. (2003) Analysis of the slump test for on-site yield stress measurement of mineral suspensions. *International Journal of Mineral Processing*, 70(1): 3-21.

Coo JL, So ZPS and Ng CWW. (2016) Effect of nanoparticles on the shrinkage properties of clay. *Engineering Geology*, 213: 84-88.

Cornelis WM, Corluy J, Medina H, Díaz J, Hartmann R, Van Meirvenne M and Ruiz ME. (2006a) Measuring and modelling the soil shrinkage characteristic curve. *Geoderma*, 137(1): 179-191.

Cornelis WM, Corluy J, Medina H, Hartmann R, Van Meirvenne M and Ruiz ME. (2006b) A simplified parametric model to describe the magnitude and geometry of soil shrinkage. *European Journal of Soil Science*, 57(2): 258-268.

Crescimanno G and Provenzano G. (1999) Soil shrinkage characteristic curve in clay soils: Measurement and prediction. *Soil Science Society of America Journal*, 63(1): 25-32.

Cui L and Fall M. (2017) Multiphysics model for consolidation behavior of cemented paste backfill. *International Journal of Geomechanics*, 17(3): 04016077.

Dalcé JB, Li L and Yang P. (2019) Experimental study of uniaxial compressive strength (UCS) distribution of hydraulic backfill associated with segregation. *Minerals*, 9(3): 147.

Dash SK and Hussain M. (2015) Influence of lime on shrinkage behavior of soils. *Journal of Materials in Civil Engineering*, 27(12): 04015041.

Davies MP. (2002) Tailings impoundment failures are geotechnical engineers listening? *Geotechnical news-Vancouver-*, 20(3): 31-36.

Davis EH and Raymond GP. (1965) A non-linear theory of consolidation. *Géotechnique*, 15(2): 161-173.

Dromer J, Aubertin M, Kennedy G, Pedroni L and Bussière B. (2004) A new testing system to investigate the sedimentation and consolidation of sludge and slurry. *Proc. of the 57th Canadian Geotechnical Conference*, Quebec, Canada, (p. 16-23).

Edraki M, Baumgartl T, Manlapig E, Bradshaw D, Franks DM and Moran CJ. (2014) Designing mine tailings for better environmental, social and economic outcomes: a review of alternative approaches. *Journal of Cleaner Production*, 84: 411-420.

Ercikdi B, Külekci G and Yılmaz T. (2015) Utilization of granulated marble wastes and waste bricks as mineral admixture in cemented paste backfill of sulphide-rich tailings. Construction and Building Materials, 93: 573-583.

Fahey M, Helinski M and Fourie A. (2009) Some aspects of the mechanics of arching in backfilled stopes. *Canadian Geotechnical Journal*, 46(11): 1322-1336.

Fall M, Belem T, Samb S and Benzaazoua M. (2007) Experimental characterization of the stress–strain behaviour of cemented paste backfill in compression. *Journal of Materials Science*, 42(11): 3914-3922.

Fall M, Benzaazoua M and Saa EG. (2008) Mix proportioning of underground cemented tailings backfill. *Tunnelling and Underground Space Technology*, 23(1): 80-90.

Fisseha B, Glancy T and Simms P. (2007) The influence of the initial degree of saturation on the shrinkage curve of silts. *Proc. of the 8th Joint IAH-CNC and CGS Groundwater Specialty Conference and 60th Canadian Geotechnical Conference*, Ottawa, Ontario, Canada, (p. 21-24).

Fourie AB, Blight GE and Papageorgiou G. (2001) Static liquefaction as a possible explanation for the Merriespruit tailings dam failure. *Canadian Geotechnical Journal*, 38(4): 707-719.

Fox PJ and Baxter CD. (1997) Consolidation properties of soil slurries from hydraulic consolidation test. *Journal of Geotechnical and Geoenvironmental Engineering*, 123(8): 770-776.

Fox PJ and Berles JD. (1997) CS2: a piecewise-linear model for large strain consolidation. *International Journal for Numerical and Analytical Methods in Geomechanics*, 21(7): 453-475.

Fredlund DG and Xing A. (1994) Equations for the soil-water characteristic curve. *Canadian Geotechnical Journal*, 31(4): 521-532.

Fredlund MD, Wilson GW and Fredlund DG. (2002) Representation and estimation of the shrinkage curve. *Proc. of the 3rd International Conference on Unsaturated Soils*, Lisse, Netherlands, (p. 145-149).

Fujiyasu Y and Fahey M. (2000) Experimental study of evaporation from saline tailings. *Journal of Geotechnical and Geoenvironmental Engineering*, *126*(1): 18-27.

Gapak Y, Das G, Yerramshetty U and Bharat TV. (2017) Laboratory determination of volumetric shrinkage behavior of bentonites: A critical appraisal. *Applied Clay Science*, 135: 554-566.

Geiker M and Knudsen T. (1982) Chemical shrinkage of Portland cement pastes. *Cement and Concrete Research*, 12(5): 603-610.

Ghirian A and Fall M. (2014) Coupled thermo-hydro-mechanical–chemical behaviour of cemented paste backfill in column experiments: Part II: Mechanical, chemical and microstructural processes and characteristics. *Engineering Geology*, 170: 11-23.

Ghirian A and Fall M. (2015) Coupled behavior of cemented paste backfill at early ages. *Geotechnical and Geological Engineering*, 33(5): 1141-1166.

Gibson RE. (1958) The progress of consolidation in a clay layer increasing in thickness with time. *Géotechnique*, 8(4): 171-182.

Gibson RE, England GL and Hussey MJL. (1967) The theory of one-dimensional consolidation of saturated clays: I. finite non-linear consolidation of thin homogeneous layers. *Géotechnique*, 17(3): 261-273

Gibson RE, Schiffman RL and Cargill KW. (1981) The theory of one-dimensional consolidation of saturated clays. II. finite nonlinear consolidation of thick homogeneous layers. *Canadian Geotechnical Journal*, 18(2): 280-293.

Gould SJF, Kodikara J, Rajeev P, Zhao XL and Burn S. (2011) A void ratio – water content – net stress model for environmentally stabilized expansive soils. *Canadian Geotechnical Journal*, 48(6): 867-877.

Grice AG. (2001) Recent minefill developments in Australia. *Proc. of the 7th International Symposium on Mining with Backfill*, Seattle, USA, (p. 351-357).

Gui YL, Zhao ZY, Kodikara J, Bui HH and Yang SQ. (2016) Numerical modelling of laboratory soil desiccation cracking using UDEC with a mix-mode cohesive fracture model. *Engineering Geology*, 202: 14-23.

Guo Y, Han C and Yu X. (2017) Laboratory characterization and discrete element modeling of shrinkage and cracking in clay layer. *Canadian Geotechnical Journal*, 55(5): 680-688.

Hansbo S. (1979) Consolidation of clay by bandshaped prefabricated drains. *Ground Engineering*, 12(5).

Hassani F and Archibald J. (1998) Mine backfill. Montreal: Canadian Institute of Mine, Metallurgy and Petroleum.

He W, Williams D and Shokouhi A. (2017) Numerical study of slurry consolidometer tests taking into account the influence of wall friction. *Computers and Geotechnics*, 91: 39-47.

Helinski M, Fourie A, Fahey M and Ismail M. (2007) Assessment of the self-desiccation process in cemented mine backfills. *Canadian Geotechnical Journal*, 44(10): 1148-1156.

Holtz RD, Kovacs WD and Sheahan TC. (2011) An introduction to geotechnical engineering. London: Pearson.

Holtz RD, Kovacs WD and Sheahan TC. (1981) An introduction to geotechnical engineering. Englewood Cliffs, NJ: Prentice-Hall.

Hobbs PRN, Jones LD, Kirkham MP, Roberts P, Haslam EP and Gunn DA. (2014) A new apparatus for determining the shrinkage limit of clay soils. *Géotechnique*, 64(3): 195-203.

Hu X and Zhao Z. (2015) Experimental study of drying shrinkage of solidified dredged material. *Journal of Hohai University*, 43: 39-43.

Hughes PB, Pakalnis R, Hitch M and Corey G. (2010) Composite paste barricade performance at Goldcorp Inc. Red Lake Mine, Ontario, Canada. *International Journal of Mining, Reclamation and Environment*, 24(2): 138-150.

ICOLD U. (1996) Monitoring of tailings dams – review and recommendations (Bulletin 104). *International Commission on Large Dams*, Paris.

Imai G. (1979) Development of a new consolidation test procedure using seepage force. *Soils and Foundations*, 19(3): 45-60.

Imai G. (1981) Experimental studies on sedimentation mechanism and sediment formation of clay materials. *Soils and Foundations*, 21(1): 7-20.

Jain S, Wang Y and Fredlund D. (2015) Non-contact sensing system to measure specimen volume during shrinkage test. *Geotechnical Testing Journal*, 38(6): 936-949.

Jamali-Firouz-Abadi M. (2012) Effect of binder content and load history on the one-dimensional compression of Williams mine cemented paste backfill. *Master Thesis*. University of Toronto, Toronto, Canada.

James M, Aubertin M, Wijewickreme D and Wilson GW. (2011) A laboratory investigation of the dynamic properties of tailings. *Canadian Geotechnical Journal*, 48(11): 1587-1600.

Jaouhar E, Aubertin M and James M. (2011) Effect of mine waste rock inclusions on the consolidation of tailings. *Proc. of the Pan-Am CGS Geotechnical Conference*, Toronto, Canada.

Jayasree PK, Balan K, Peter L and Nisha KK. (2015) Shrinkage characteristics of expansive soil treated with coir waste. *Indian Geotechnical Journal*, 45(3): 360-367.

Jeeravipoolvarn S, Scott JD and Chalaturnyk RJ. (2009) 10 m standpipe tests on oil sands tailings: long-term experimental results and prediction. *Canadian Geotechnical Journal*, *46*(8): 875-888.

Jehring MM and Bareither CA. (2016) Tailings composition effects on shear strength behavior of co-mixed mine waste rock and tailings. *Acta Geotechnica*, 11(5): 1147-1166.

Kananizadeh N, Ebadi T, Khoshniat SA and Mousavirizi SE. (2011) The positive effects of nanoclay on the hydraulic conductivity of compacted Kahrizak clay permeated with landfill leachate. *CLEAN–Soil, Air, Water*, 39(7): 605-611.

Kesimal A, Yilmaz E, Ercikdi B, Alp I and Deveci H. (2005) Effect of properties of tailings and binder on the short-and long-term strength and stability of cemented paste backfill. *Materials Letters*, 59(28): 3703-3709.

Konrad JM and Ayad R. (1997) Desiccation of a sensitive clay: field experimental observations. *Canadian Geotechnical Journal*, 34(6): 929-942.

Kossoff D, Dubbin WE, Alfredsson M, Edwards SJ, Macklin MG and Hudson-Edwards KA. (2014) Mine tailings dams: characteristics, failure, environmental impacts, and remediation. *Applied Geochemistry*, 51: 229-245.

Krisdani H, Rahardjo H and Leong EC. (2008) Effects of different drying rates on shrinkage characteristics of a residual soil and soil mixtures. *Engineering Geology*, 102(1): 31-37.

Krosley L, Likos W and Lu N. (2003) Alternative encasement materials for clod test. *Geotechnical Testing Journal*, 26(4): 461-463.

Lambe TW (1951) Soil testing for engineers. New York: Wiley.

Landriault D. (1995) Paste backfill mix design for Canadian underground hard rock mining. *Proc. of the 97th Annual General Meeting of CIM*, Halifax, Nova Scotia.

Lee K and Sills G. (1979) A moving boundary approach to large strain consolidation of a thin soil layer. *Proc. of the 3rd International Conference on Numerical Methods in Geomechanics*, Aachen, Germany, (p. 163-173).

Leong EC and Wijaya M. (2015) Universal soil shrinkage curve equation. *Geoderma*, 237-238: 78-87.

Li JH and Zhang LM. (2011) Study of desiccation crack initiation and development at ground surface. *Engineering Geology*, 123(4): 347-358.

Li L. (2014) Analytical solution for determining the required strength of a side-exposed mine backfill containing a plug. *Canadian Geotechnical Journal*, 51(5): 508-519.

Li L, Alvarez IC and Aubertin JD. (2013) Self-weight consolidation of slurried deposition: tests and interpretation. *International Journal of Geotechnical Engineering*, 7(2): 205-213.

Li L and Aubertin M. (2012): A modified solution to assess the required strength of exposed backfill in mine stopes. *Canadian Geotechnical Journal*, 49(8): 994-1002.

Li L and Aubertin M. (2011) Limit equilibrium analysis for the design of backfilled stope barricades made of waste rock. *Canadian Geotechnical Journal*, 48(11): 1713-1728.

Li L and Yang P. (2015) A numerical evaluation of continuous backfilling in cemented paste backfilled stope through an application of wick drains. *International Journal of Mining Science and Technology*, 25(6): 897-904.

Li L and Zhang X. (2019) A new approach to measure soil shrinkage curve. *Geotechnical Testing Journal*, 42(1): 1-18.

Li L. (2014) Generalized solution for mining backfill design. *International Journal of Geomechanics*, 14(3): 04014006.

Liu G, Li L, Yang X and Guo L. (2018) Required strength estimation of a cemented backfill with the front wall exposed and back wall pressured. *International Journal of Mining and Mineral Engineering*, 9(1): 1-20.

Locher FW. (2006) Cement: Principles of production and use. Düsseldorf: Verlag Bau+Technik GmbH.

Lottermoser B. (2003) Mine water. In Mine Wastes. Berlin: Springer.

Marinho FAM. (1994) Shrinkage behaviour of some plastic soils. *Ph.D. Thesis*. University of London, London, UK.

Marinho FAM. (2017) Fundamentals of soil shrinkage. *Proceedings of the Pan Am Unsaturated Soils Conference*, Dallas, Texas, USA, (p. 198-222).

Marston A. (1930) The theory of external loads on closed conduits in the light of the latest experiments (Bulletin 96). Iowa Engineering Experiment Station, Ames, Iowa.

Martin T and McRoberts E. (1999) Some considerations in the stability analysis of upstream tailings dams. *Proc. of the 6th International Conference on Tailings and Mine Waste*, Rotterdam, Netherlands, (p. 287-302).

Mbonimpa M, Aubertin M, Maqsoud A and Bussière B. (2006) Predictive model for the water retention curve of deformable clayey soils. *Journal of Geotechnical and Geoenvironmental Engineering*, 132(9): 1121-1132.

McGarry D and Malafant KWJ. (1987) The analysis of volume change in unconfined units of soil. *Soil Science Society of America Journal*, 51(2): 290-297.

McRoberts EC and Nixon JF. (1976) A theory of soil sedimentation. *Canadian Geotechnical Journal*, 13(3): 294-310.

Mishra PN, Scheuermann A, Bore T and Li L. (2019) Salinity effects on soil shrinkage characteristic curves of fine-grained geomaterials. *Journal of Rock Mechanics and Geotechnical Engineering*, 11(1): 181-191.

Mitchell RJ, Olsen RS and Smith JD. (1982) Model studies on cemented tailings used in mine backfill. *Canadian Geotechnical Journal*, 19(1): 14-28.

Mittal HK and Morgenstern NR. (1976) Seepage control in tailings dams. *Canadian Geotechnical Journal*, 13(3): 277-293.

Morris PH. (2002) Analytical solutions of linear finite-strain one-dimensional consolidation. *Journal of Geotechnical and Geoenvironmental Engineering*, 128(4): 319-326.

Nahlawi H and Kodikara JK. (2006) Laboratory experiments on desiccation cracking of thin soil layers. *Geotechnical and Geological Engineering*, 24(6): 1641-1664.

O'Kelly BC. (2009) Development of a large consolidometer apparatus for testing peat and other highly organic soils. *Suoseura*, 60(1–2): 23–36.

Omidi GH, Prasad TV, Thomas JC and Brown KW. (1996) The influence of amendments on the volumetric shrinkage and integrity of compacted clay soils used in landfill liners. *Water, Air, and Soil Pollution*, 86(1): 263-274.

Ouellet S, Bussière B, Aubertin M and Benzaazoua M. (2008) Characterization of cemented paste backfill pore structure using SEM and IA analysis. *Bulletin of Engineering Geology and the Environment*, 67(2): 139-152.

Palu MC and Julien PY. (2019) Modeling the sediment load of the Doce River after the Fundão tailings dam collapse, Brazil. *Journal of Hydraulic Engineering*, 145(5): 05019002.

Pane V and Schiffman RL. (1985) A note on sedimentation and consolidation. *Géotechnique*, 35(1): 69-72.

Peng X and Horn R. (2005) Modeling soil shrinkage curve across a wide range of soil types. *Soil Science Society of America Journal*, 69(3): 584-592.

Peng XH and Horn R. (2013) Identifying six types of soil shrinkage curves from a large set of experimental data. *Soil Science Society of America Journal*, 77(2): 372-381.

Péron H, Delenne JY, Laloui L and El Youssoufi MS. (2009a) Discrete element modelling of drying shrinkage and cracking of soils. *Computers and Geotechnics*, 36(1): 61-69.

Péron, H. Hueckel T, Laloui L and Hu LB. (2009b) Fundamentals of desiccation cracking of fine-grained soils: experimental characterisation and mechanisms identification. *Canadian Geotechnical Journal*, 46(10): 1177-1201.

Péron H, Laloui L, Hueckel T and Hu L. (2006) Experimental study of desiccation of soil. *Proc. of the 4th International Conference on Unsaturated Soils*, Virginia, USA, 1073-1084.

Potvin Y, Thomas E and Fourie A. (2005) Handbook on mine fill. Perth: Australian Centre for Geomechanics.

Powers TC and Brownyard TL. (1947) Studies of the physical properties of hardened Portland cement paste (Bulletin 22). *Research Laboratory of Portland Cement Association*, Skokie, Illinois, USA.

Prakash K, Sridharan A, Baba J and Thejas H. (2009) Determination of shrinkage limit of fine-grained soils by wax method. *Geotechnical Testing Journal*, 32(1): 86-89.

Qiu Y and Sego DC. (2001) Laboratory properties of mine tailings. *Canadian Geotechnical Journal*, 38(1): 183-190.

Rankine KJ. (2005) An investigation into the drainage characteristics and behaviour of hydraulically placed mine backfill and permeable minefill barricades. *Ph. D. Thesis*. James Cook University, Townsville, Australia.

Rankine R, Pacheco M and Sivakugan N. (2007) Underground mining with backfills. *Soils and Rocks*, 30(2): 93-101.

Reeve MJ, Hall DGM and Bullock P. (1980) The effect of soil composition and environmental factors on the shrinkage of some clayey British soils. *Journal of Soil Science*, 31(3): 429-442.

Rico M, Benito G, Salgueiro AR, Díez-Herrero A and Pereira HG. (2008) Reported tailings dam failures: a review of the European incidents in the worldwide context. *Journal of Hazardous Materials*, 152(2): 846-852.

Rodet J. (2019) Caractérisation hydrogéotechnique des déchets miniers dans les mines d'Eléonore. Unpublished manuscript, Montreal, Canada.

Rodríguez R. (2006) Hydrogeotechnical characterization of a metallurgical waste. *Canadian Geotechnical Journal*, 43(10): 1042-1060.

Rodríguez R, Sánchez M, Ledesma A and Lloret A. (2007) Experimental and numerical analysis of desiccation of a mining waste. *Canadian Geotechnical Journal*, 44(6): 644-658.

Saad B and Mitri H. (2010) Staged construction analysis of surface tailings disposal facilities. *International Journal of Mining, Reclamation and Environment*, 24(1): 44-63.

Saleh-Mbemba F and Aubertin M. (2018) Characterization of self-weight consolidation of fine-grained mine tailings using moisture sensors. *Geotechnical Testing Journal*, 41(3): 543-554.

Saleh-Mbemba F, Aubertin M, Mbonimpa M and Li L. (2010) A new testing procedure to assess shrinkage of paste tailings. *Proc. of the 13th International Seminar on Paste and Thickened Tailings*, Perth, Australia, (p. 495-504).

Saleh-Mbemba F, Aubertin M, Mbonimpa M and Li L. (2016) Experimental characterization of the shrinkage and water retention behaviour of tailings from hard rock mines. *Geotechnical and Geological Engineering*, 34(1): 251-266.

Sander T and Gerke HH. (2007) Noncontact shrinkage curve determination for soil clods and aggregates by three-dimensional optical scanning. *Soil Science Society of America Journal*, 71(5): 1448-1454.

Shokouhi A, Zhang C and Williams DJ. (2018) Settling, consolidation and desiccation behaviour of coal tailings slurry. *Mining Technology*, 127(1): 1-11.

Shrestha BK, Tannant DD, Proskin S, Reinson J and Greer S. (2008) Properties of cemented rockfill used in an open pit mine. *Proc. of the 61st Canadian Geotechnical Conference*, Edmonton, Canada, (p. 609-616).

Sima J, Jiang M and Zhou C. (2014) Numerical simulation of desiccation cracking in a thin clay layer using 3D discrete element modeling. *Computers and Geotechnics*, 56: 168-180.

Simms P, Soleimani S, Mizani S, Daliri F, Dunmola A, Rozina E and Innocent-Bernard T. (2017) Cracking, salinity and evaporation in mesoscale experiments on three types of tailings. *Environmental Geotechnics*, 6(1): 3-17.

Sivakugan N, Rankine RM, Rankine KJ and Rankine KS. (2006) Geotechnical considerations in mine backfilling in Australia. *Journal of Cleaner Production*, 14(12-13): 1168-1175.

Soares L, Arnez F and Hennies WT. (2000) Major causes of accidents in tailing dam due to geological and geotechnical factors. *Proc. of the Mine Planning and Equipment Selection – International Symposium*, (p. 371–376).

Strachan C. (2002) Review of tailings dam incident data. *Mining Environment Management*, 7(9).

Stone KJL, Randolph MF, Toh S and Sales AA. (1994) Evaluation of consolidation behavior of mine tailings. *Journal of Geotechnical Engineering*, 120(3): 473-490.

Suazo G, Fourie A and Doherty J. (2016) Experimental study of the evolution of the soil water retention curve for granular material undergoing cement hydration. *Journal of Geotechnical and Geoenvironmental Engineering*, 142(7): 04016022.

Tang CS, Shi B, Cui YJ, Liu C and Gu K. (2012) Desiccation cracking behavior of polypropylene fiber–reinforced clayey soil. *Canadian Geotechnical Journal*, 49(9): 1088-1101.

Tang CS, Shi B, Liu C, Suo WB and Gao L. (2011) Experimental characterization of shrinkage and desiccation cracking in thin clay layer. *Applied Clay Science*, 52(1): 69-77.

Tariq AUR and Durnford DS. (1993) Soil volumetric shrinkage measurements: a simple method. *Soil Science*, 155(5): 325-330.

Taylor DW. (1948) Fundamentals of soil mechanics. New York: Jonh Wiley and Sons.

Terzaghi K. (1925) Principles of soil mechanics: I – Phenomena of cohesion of clays. Engineering News-Record, 95(19): 742-746

Terzaghi K, Peck RB and Mesri G. (1996) Soil mechanics in engineering practice. New York: John Wiley and Sons.

Thompson BD, Bawden WF and Grabinsky MW. (2012) In situ measurements of cemented paste backfill at the Cayeli Mine. *Canadian Geotechnical Journal*, 49(7): 755-772.

Tian Z, Bareither CA and Scalia J. (2020) Development and assessment of a seepage-induced consolidation test apparatus. *Geotechnical Testing Journal*, 43(4).

Umezaki T and Kawamura T. (2013) Shrinkage and desaturation properties during desiccation of reconstituted cohesive soil. *Soils and Foundations*, 53(1): 47-63.

Upreti K and Leong EC. (2018) Measurement of soil shrinkage curve using photogrammetry. *Proc. of the 2nd Pan American Conference of Unsaturated Soils*, Dallas, Texas, (p. 71-80).

Van Genuchten MT. (1980) A closed-form equation for predicting the hydraulic conductivity of unsaturated soils 1. *Soil Science Society of America Journal*, 44(5): 892-898.

Van Niekerk HJ and Viljoen MJ. (2005) Causes and consequences of the Merriespruit and other tailings-dam failures. *Land Degradation & Development*, 16(2): 201-212.

Vick SG. (1990) Planning, design, and analysis of tailings dams. B.C.: BiTech.

Walske M. (2014) An experimental study of cementing paste backfill. *Ph.D. thesis*. University of Western Australia, Perth, Australia.

Walske ML and Doherty J. (2018) Incorporating chemical shrinkage volume into Gibson's solution. *Canadian Geotechnical Journal*, 55(6): 903-908.

Wang Z, Xu SF and Wang GC. (2012) Study of early strength and shrinkage properties of cement or lime solidified soil. *Energy Procedia*, 16: 302-306.

Wang Z, Xu SF, Yan LL, Guo P and Chen Q. (2011) Shrinkage properties of cement solidified sludge with high water content. *Advanced Materials Research*, 168-170: 1496-1500.

Wickland BE and Wilson GW. (2005) Self-weight consolidation of mixtures of mine waste rock and tailings. *Canadian Geotechnical Journal*, 42(2): 327-339.

Wickland BE, Wilson GW, Wijewickreme D and Klein B. (2006) Design and evaluation of mixtures of mine waste rock and tailings. *Canadian Geotechnical Journal*, 43(9): 928-945.

Wijaya M, Leong EC and Rahardjo H. (2015) Effect of shrinkage on air-entry value of soils. *Soils and Foundations*, 55(1): 166-180.

Wild S, Khatib JM and Roose LJ. (1998) Chemical shrinkage and autogenous shrinkage of Portland cement—metakaolin pastes. *Advances in Cement Research*, 10(3): 109-119.

Williams DJ. (1992) Co-disposal of coal mine tailings and coarse reject: a promising new technique. *Australian Geomechanics Journal*, (July): 50-55.

Wilson GW, Fredlund DG and Barbour SL. (1994) Coupled soil-atmosphere modelling for soil evaporation. *Canadian Geotechnical Journal*, 31(2): 151-161.

Wong JM, Elwood D and Fredlund DG. (2019) Use of a three-dimensional scanner for shrinkage curve tests. *Canadian Geotechnical Journal*, 56(4): 526-535.

Wood DM and Doherty JP. (2014) Coupled chemical shrinkage and consolidation: some benchmark solutions. *Transport in Porous Media*, 105(2): 349-370.

Yang P and Li L. (2015) Investigation of the short-term stress distribution in stopes and drifts backfilled with cemented paste backfill. *International Journal of Mining Science and Technology*, 25(5): (p. 721-728).

Yang P and Li L. (2017) Evolution of water table and pore-water pressure in stopes with submerged hydraulic fill. *International Journal of Geomechanics*, 17(9): 04017052.

Yang P, Li L and Aubertin M. (2017) A new solution to assess the required strength of mine backfill with a vertical exposure. *International Journal of Geomechanics*, 17(10): 04017084.

Yang P, Li L, Aubertin M, Brochu-Baekelmans M and Ouellet S. (2017) Stability analyses of waste rock barricades designed to retain paste backfill. *International Journal of Geomechanics*, 17(3): 04016079.

Yilmaz E, Belem T, Benzaazoua M. (2014) Effects of curing and stress conditions on hydromechanical, geotechnical and geochemical properties of cemented paste backfill. *Engineering. Geology*. 168: 23-37.

Yilmaz E, Belem T, Benzaazoua M and Bussière B. (2010) Assessment of the modified CUAPS apparatus to estimate in situ properties of cemented paste backfill. *Geotechnical Testing Journal*, 33(5): 351-362.

Yilmaz E, Belem T, Bussière B and Benzaazoua M. (2008) Consolidation characteristics of early age cemented paste backfill. *Proc. of the 61st Canadian Geotechnical Conference and the 9th Joint CGS/IAH-CNC Groundwater Conference*, Edmonton, Canada, (p. 797-804).

Yilmaz E, Belem T, Bussière B, Mbonimpa M and Benzaazoua M. (2015) Curing time effect on consolidation behaviour of cemented paste backfill containing different cement types and contents. *Construction and Building Materials*, 75: 99-111.

Yilmaz E and Fall M. (2017) Paste Tailings Management. Berlin: Springer.

Zhang CL, Zhu W and Fan GJ. (2010) Shrinkage properties of cement solidified sludge with high water content. *Journal of Hohai University (Natural Sciences)*, (38)3: 295-299.

Zhang N, Zhu W, He H and Lv Y. (2017) Experimental study on sedimentation and consolidation of soil particles in dredged slurry. *KSCE Journal of Civil Engineering*, 21(7): 2596-2606.

Zhang Y, Ye W, Chen Y and Chen B. (2017) Impact of NaCl on drying shrinkage behavior of low-plasticity soil in earthen heritages. *Canadian Geotechnical Journal*, 54(12): 1762-1774.

Zheng J, Li L, Mbonimpa M and Pabst T. (2018a) An analytical solution of Gibson's model for estimating pore water pressures in accreting deposition of slurried material under one-dimensional self-weight consolidation. Part II: impervious base. *Indian Geotechnical Journal*, 48(1): 188-195.

Zheng J, Li L, Mbonimpa M and Pabst T. (2018b) An analytical solution of Gibson's model for estimating the pore water pressures in accreting deposition of slurried material under one-dimensional self-weight consolidation. Part I: pervious base. *Indian Geotechnical Journal*, 48(1): 72-83.

Zheng J, Li L and Li Y. (2019) Total and effective stresses in backfilled stopes during the fill placement on a pervious base for barricade design. *Minerals*, 9(1).

Zheng J, Li L and Li Y. (2020a) Solutions to estimate the excess PWP, settlement and volume of draining water after slurry deposition. Part I: impervious base. *Environmental Earth Sciences*, 79: 124.

Zheng J, Li L and Li Y. (2020b) Solutions to estimate the excess PWP, settlement and volume of draining water after slurry deposition. Part II: pervious base. *Environmental Earth Sciences*.

Zheng, J., Li, L., Daviault, M. (2020c) An experimental study on the effectiveness of lubricants in reducing the sidewall friction. *ASCE – International Journal of Geomechanics* (accepted with changes, March 2020).

APPENDIX A ADDITIONAL RESULTS RELATED TO CHAPTER 3

A.1 Column consolidation test

Two sets of column consolidation tests were conducted for a comparison with the standard oedometer test. The used slender column has a height of 43.5 cm and an inner diameter of 10 cm. The experimental setup, experimental procedures and results are presented below.

A.1.1 Experimental setup and procedures

The compression curve of the tailings slurry was also measured with the slurry consolidometer test conducted in a slender column with a height of 43.5 cm and a diameter of 10 cm. Figure A-1 shows the photograph (Fig. A-1a) and schematic diagram (Fig. A-1b) of the column consolidation testing instrumentation, which is composed of a column, a load platen, a LVDT, three PWP sensors (PWP1, PWP2 and PWP3), a load cell, a loading frame and a data acquisition system. The geotextile was used at the top and bottom of the tailings specimen to prevent the migration of the tailings and the geotextile was saturated before the test. Moreover, the inner wall of the slender column is coated with a layer of grease to reduce the wall friction. The settlement of the tailings was measured with a LVDT while the pore water pressures were monitored by the PWP sensors installed along the height of the column at three different heights. The load cell was used to measure the pressure applied by the load frame added on the load platen.

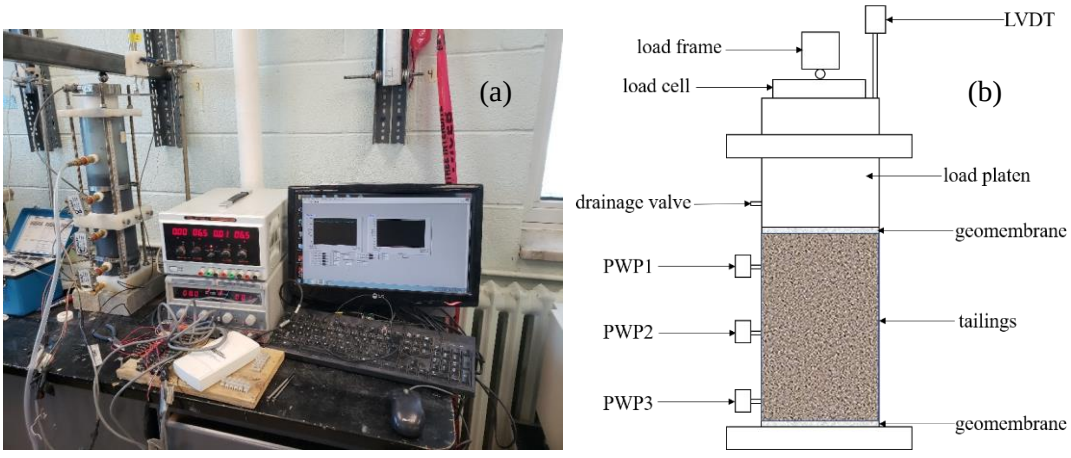

Figure A-1: (a) Photograph, and (b) Schematic diagram of the instrumentation for column consolidation tests.

Before the test, the LVDT and PWP sensors were calibrated with a power supply and the calibration curves are given in Figure A-2, showing the LVDT and PWP sensors function well.

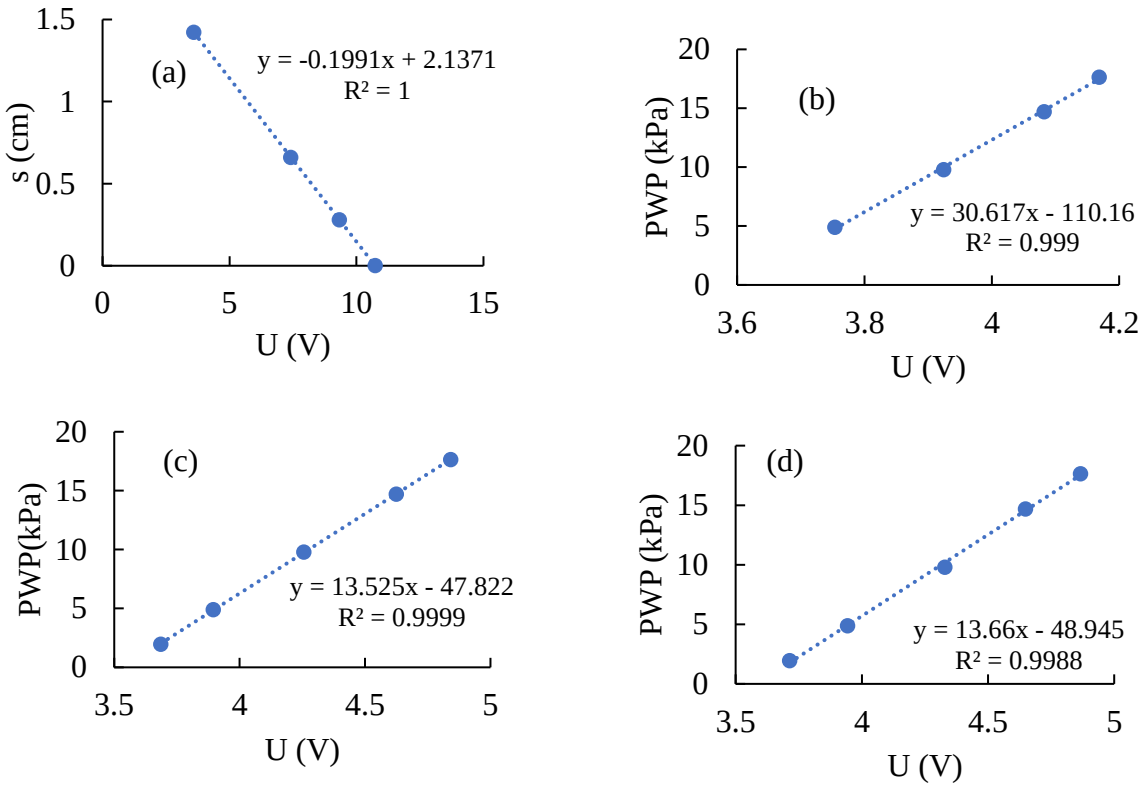

Figure A-2: Calibration curves of (a) LVDT, (b) PWP1, (c) PWP2, and (d) PWP3.

After we obtained the calibration curves of used LVDT and PWP sensors, two specimens were prepared with initial water contents of 38.76% and 38.15% by thoroughly mixing the dry tailings with deaired water and then placed in the slender column. After placed in column, the tailings were left for settling without any loading. After 24 hours, the settling was finished and the first loading of the plastic platen was applied to the top of tailings, where a geotextile was placed already. After the settlement from LVDT became stable and the second loading of loading frame and load cell was put at the top of plastic loading platen. Afterwards, the subsequent load was applied by weights. In addition to the settlement measurement by LVDT, a tape was also used to measure the settlement for comparison. With the test finished, the water content of samples is measured.

A.1.2 Results of column consolidation test

The *e*-log*σ'* compression curves of two column consolidation tests and oedometer test are compared in Figure A-3 and the result from column consolidation tests fit well with stand oedometer test especially at the range of low effective stress. However, the void ratio of compression curves by column consolidation test is seen to be higher when effective stress exceeds 40 kPa, which indicates that the wall friction of slender column affects the compression properties of tailings. The compression index C_c of 0.041 and 0.037 from column consolidation tests is smaller than that obtained from oedometer test.

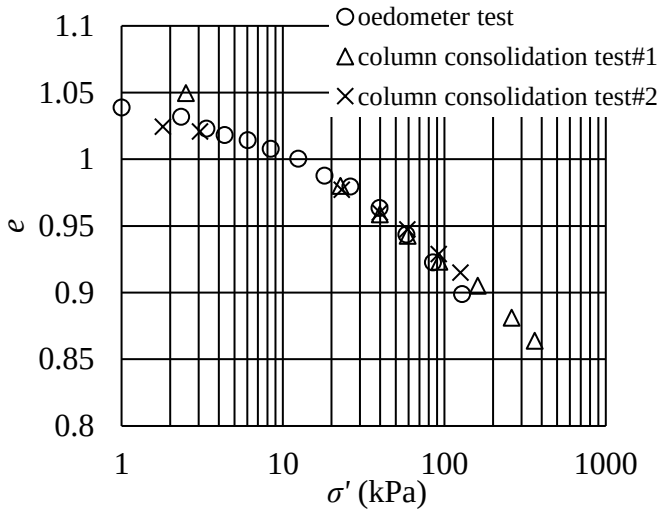

Figure A-3: *e*-log*σ'* compression curves of column consolidation tests and oedometer test.

Figure A-4 shows the ratio between the pore water pressure change Δu and change of applied pressure $\Delta\sigma$ at PWP 2 and PWP 3 in column consolidation test #2, which represents the transferring of applied pressure at the samples' different positions. The ratio ranges from 0.85 to 1 when the applied pressure is lower than 40 kPa while decreases a lot under higher applied pressure. When the applied pressure exceeds 40 kPa, the transferring of applied pressure decreases a lot and this could explain the difference of compression curve with different methods at high effective stress.

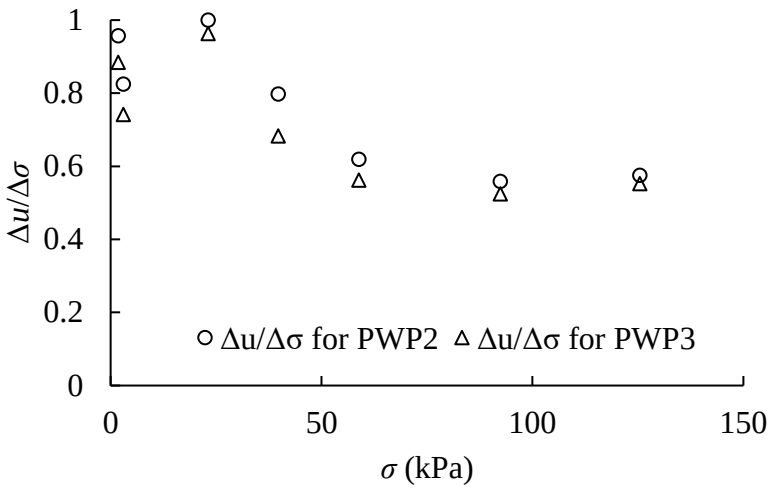

Figure A-4: Relationship between $\Delta u/\Delta\sigma$ and effective stress σ at position of PWP2 and PWP3 in column consolidation test #2.

A.2 Time-settlement curve of consolidation tests

A.2.1 Time-settlement curve of column consolidation test #1

Figure A-5, A-6 and A-7 show the time-settlement curves under normal time, log time and square root of time of each loading step in first column consolidation test.

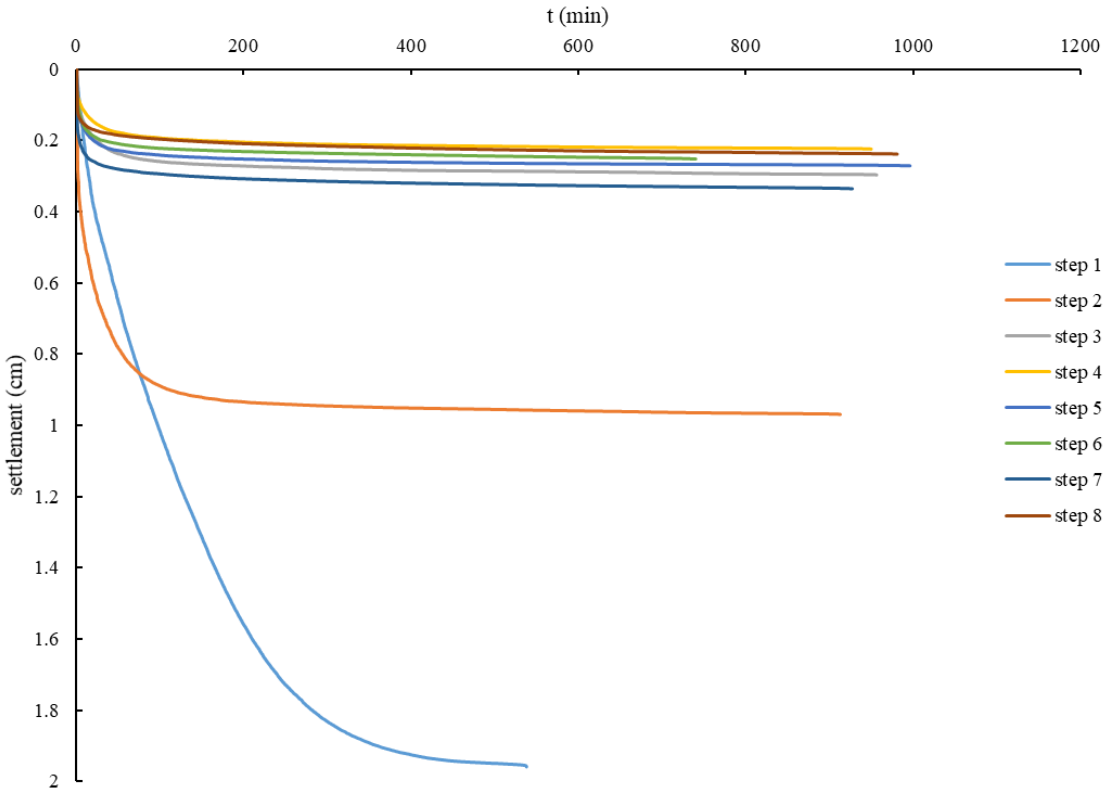

Figure A-5: Time-settlement curve after each loading step for column consolidation test #1.

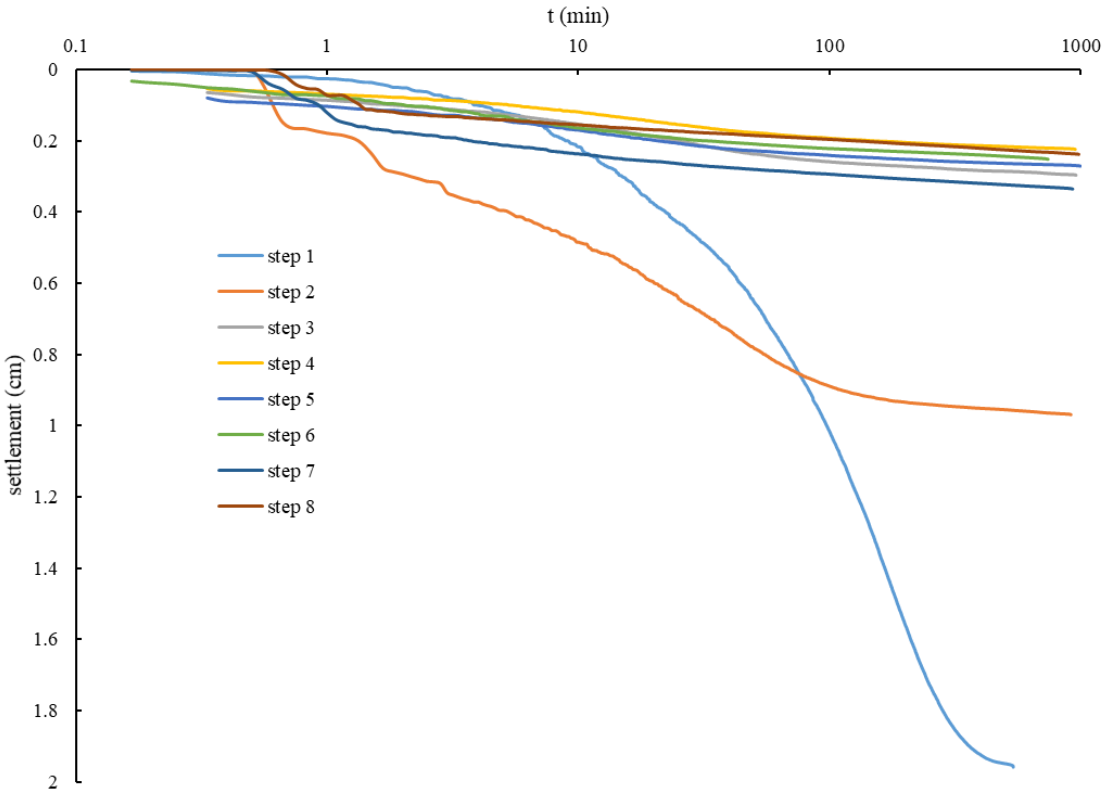

Figure A-6: Time-settlement curve using log time method after each loading step for column consolidation test #1.

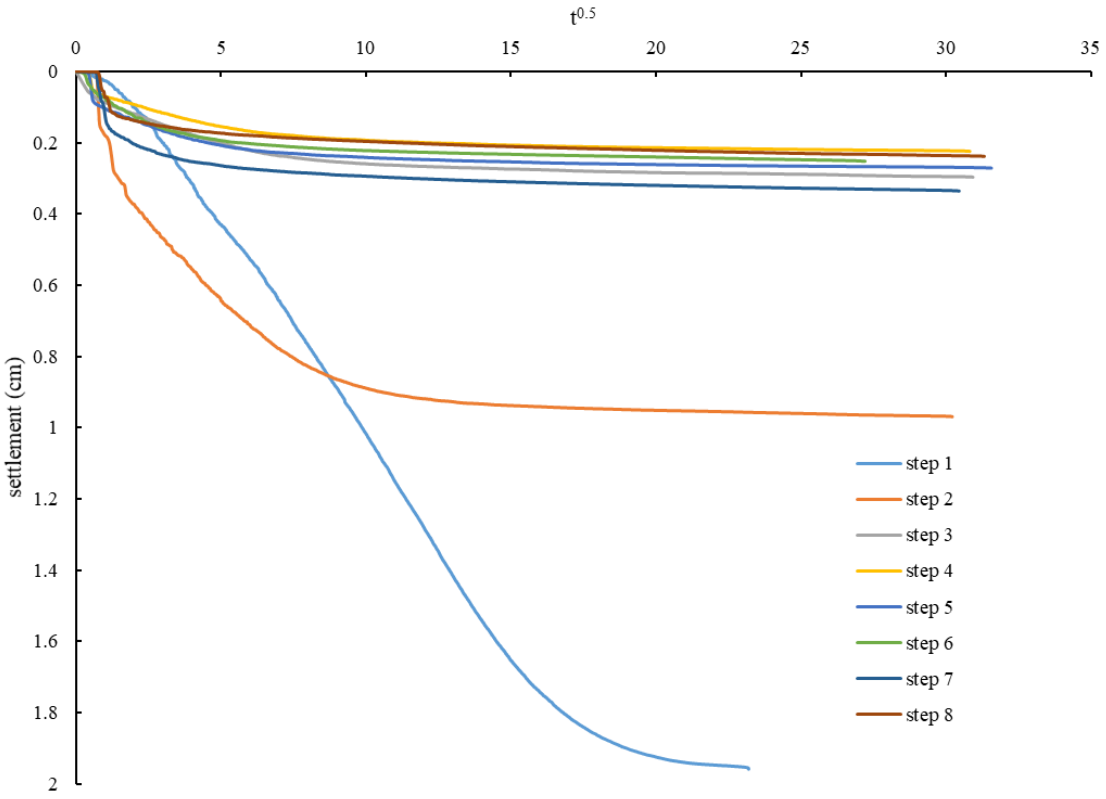

Figure A-7: Time-settlement curve using square root of time method after each loading step for column consolidation test #1.

A.2.2 Time-settlement curve of column consolidation test #2

Figure A-8, A-9 and A-10 show the time-settlement curves under normal time, log time and square root of time of each loading step in second column consolidation test.

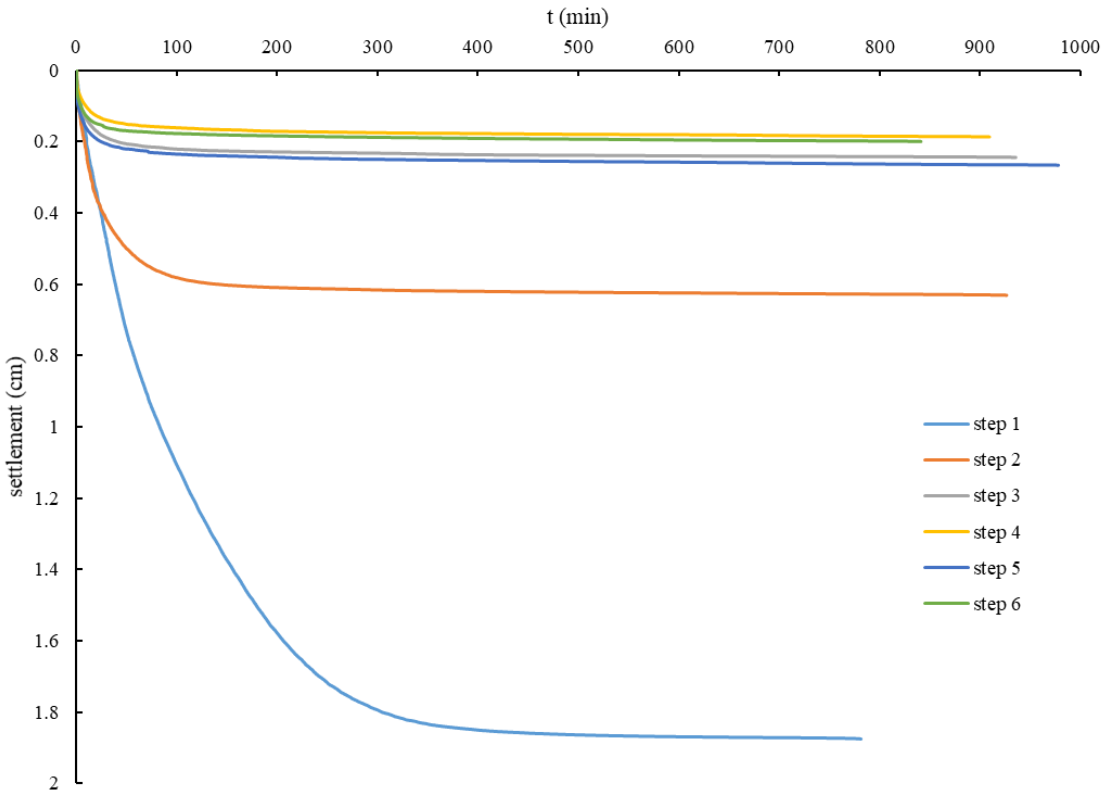

Figure A-8: Time-settlement curve after each loading step for column consolidation test #2.

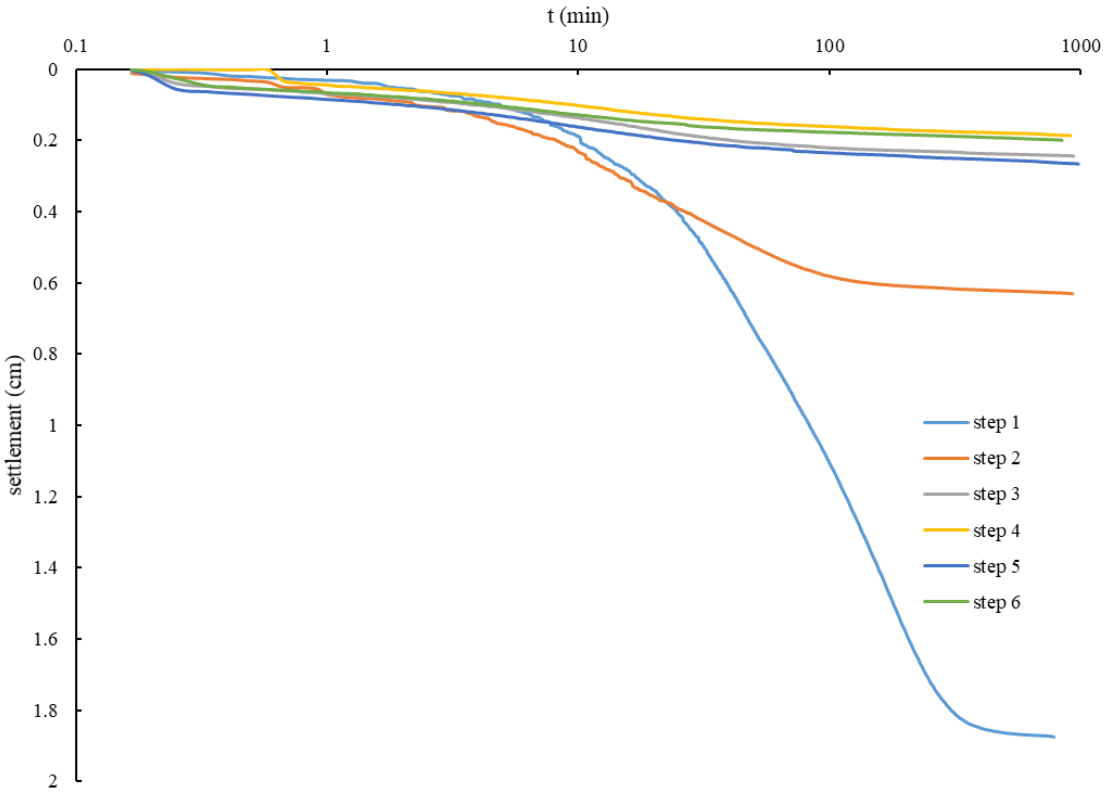

Figure A-9: Time-settlement curve using log time method after each loading step for column consolidation test #2.

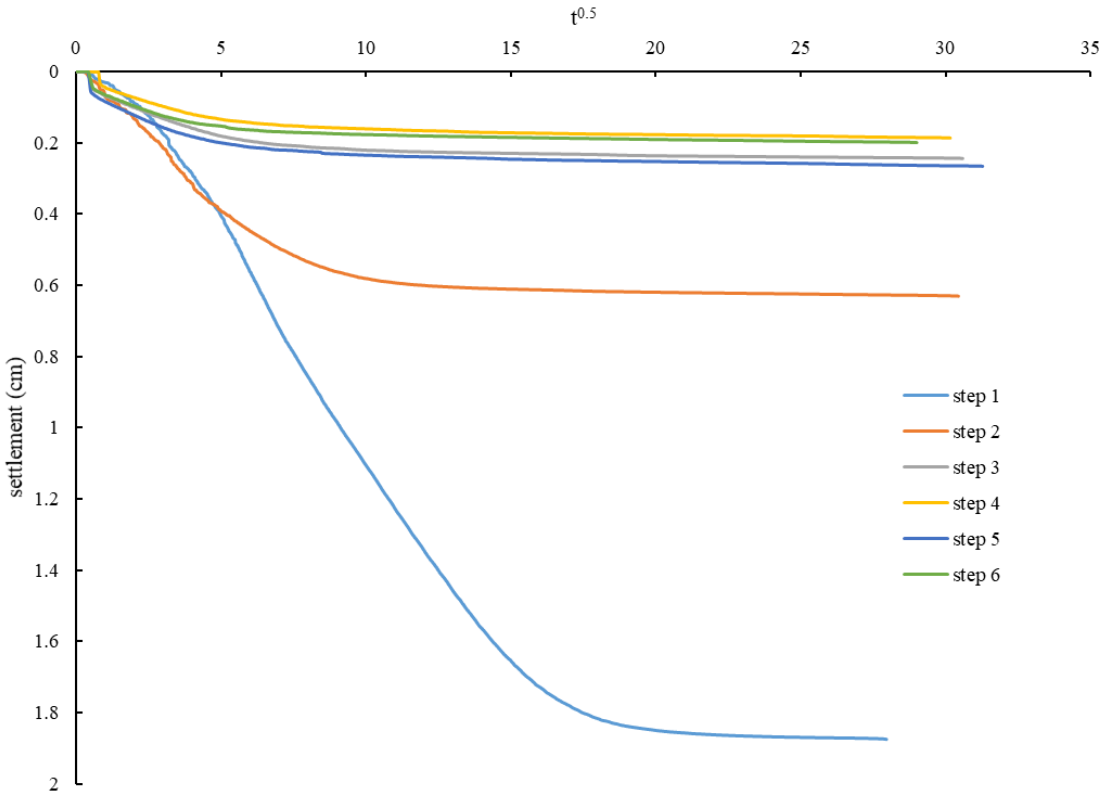

Figure A-10: Time-settlement curve using square root of time method after each loading step for column consolidation test #2.

A.2.3 Time-settlement curve of oedometer test

Figure A-11, A-12 and A-13 show the time-settlement curves under normal time, log time and square root of time of each loading step in oedometer test.

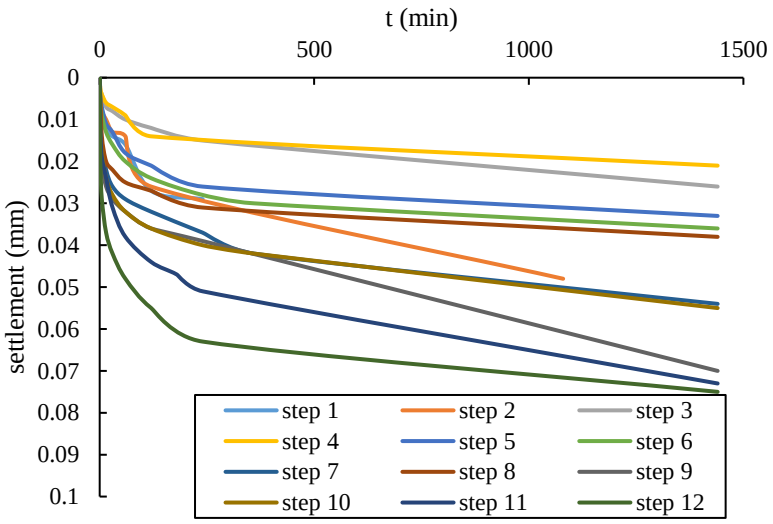

Figure A-11: Time-settlement curve after each loading step for oedometer test.

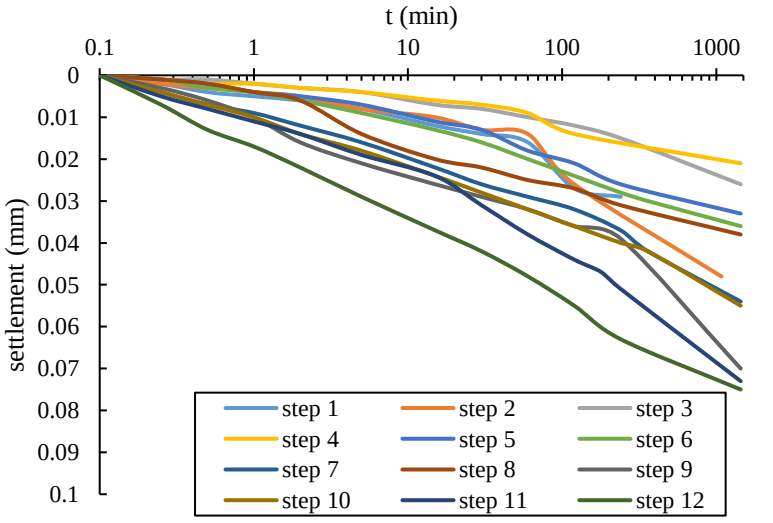

Figure A-12: Time-settlement curve using log time method after each loading step for oedometer test.

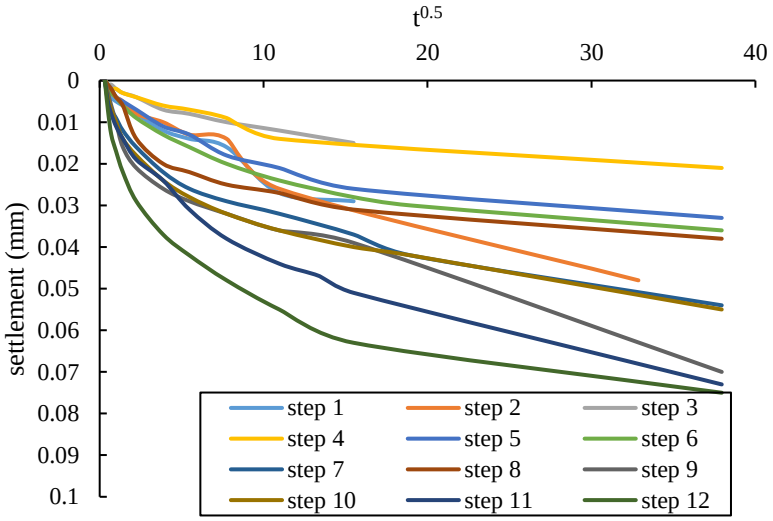

Figure A-13: Time-settlement curve using square root of time method after each loading step for oedometer test.

A.3 Consolidation parameters of consolidation tests

A.3.1 Consolidation parameters of column consolidation test #1

Figure A-14 and A-15 respectively show the variation of coefficient of compressibility a_v, coefficient of volume compressibility m_v with the applied effective stress σ' while the variation of coefficient of consolidation c_v and saturated hydraulic conductivity k_{sat} with void ratio is shown in Figure A-16 and A-17.

The calculations of these consolidation parameters at load step i are based on the equations below:

$$a_{vn} = \frac{e_{n-1} - e_n}{\sigma'_n - \sigma'_{n-1}} \quad \text{(A-1)}$$

$$m_{vn} = \frac{a_{vn}}{1+e_0} \quad \text{(A-2)}$$

$$c_{vn} = \frac{T_v H_n^2}{t_n} \quad \text{(A-3)}$$

$$k_{satn} = \gamma_w m_{vn} c_{vn} \quad \text{(A-4)}$$

Where the c_{vn} is calculated with Taylor's time square root method and time factor T_v equals to 0.848. Since the drainage is upward only, the drainage length H_n is the height of the sample at the step i. t_n is determined from the corresponding time at 90% of consolidation in Figure A-5.

a_v and m_v decrease with effective stress increased according to Figure A-14 and A-15, which is reasonable since the stiffness increases with decreased compressibility as effective stress increases. Figure A-16 indicates that the coefficient of consolidation gradually decreases with time, showing that the rate of consolidation decreases. The value of c_v is between 0.034 to 0.119 cm^2/s, which fits the typical values of 5×10^{-2} to 1×10^{-1} cm^2/s for tailings with similar void ratio (Mittal and Morgenstern 1975). The back-calculated hydraulic conductivity k_{sat} decreases with decreased void ratio and ranges from 4.82×10^{-5} to 6.77×10^{-4} m/s.

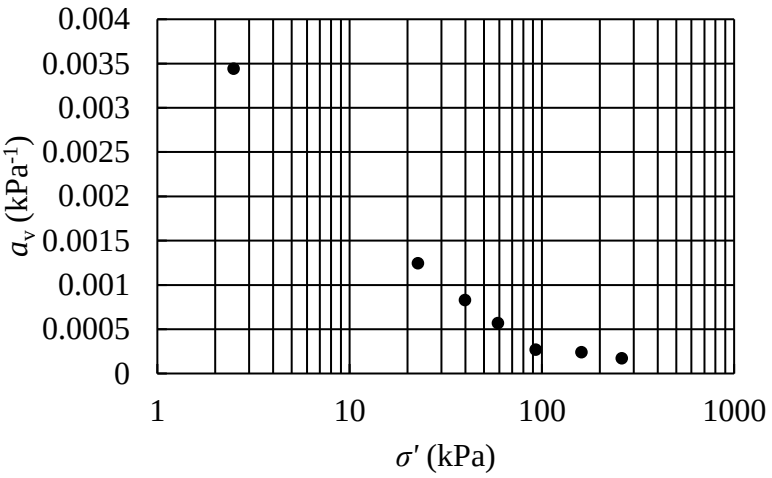

Figure A-14: Variations of coefficient of compressibility a_v with axial effective stress σ' for column consolidation test #1.

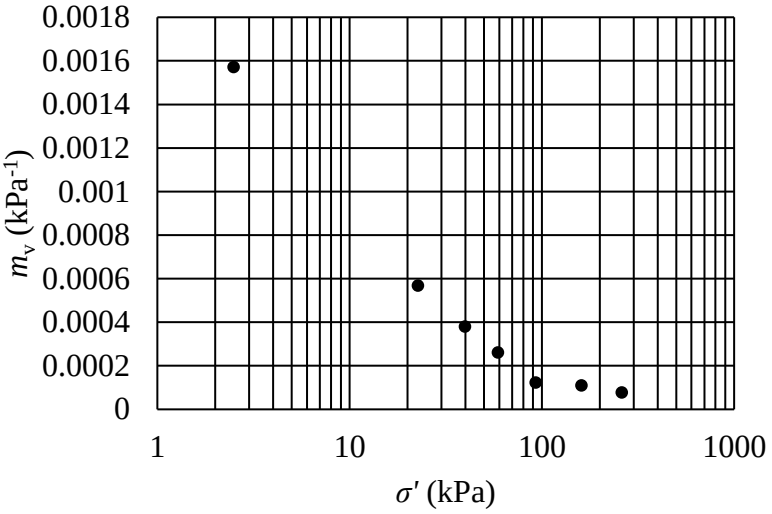

Figure A-15: Variations of coefficient of volume compressibility m_v with axial effective stress σ' for column consolidation test #1.

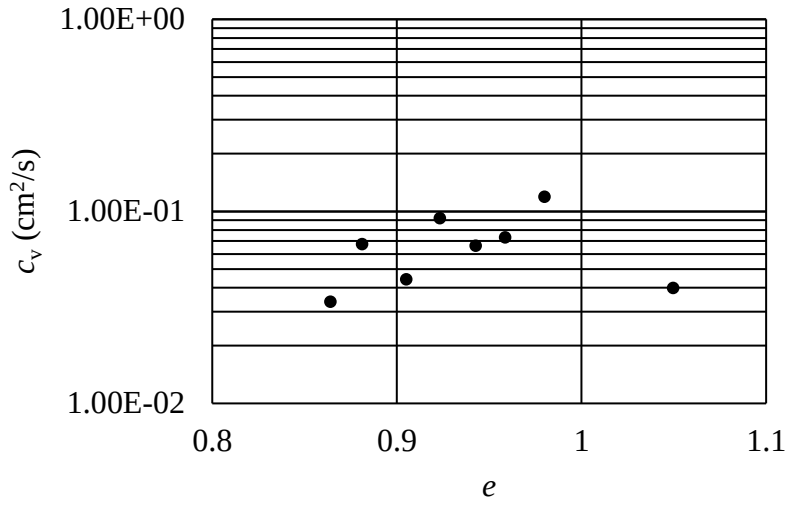

Figure A-16: Variations of coefficient of consolidation c_v with void ratio e for column consolidation test #1.

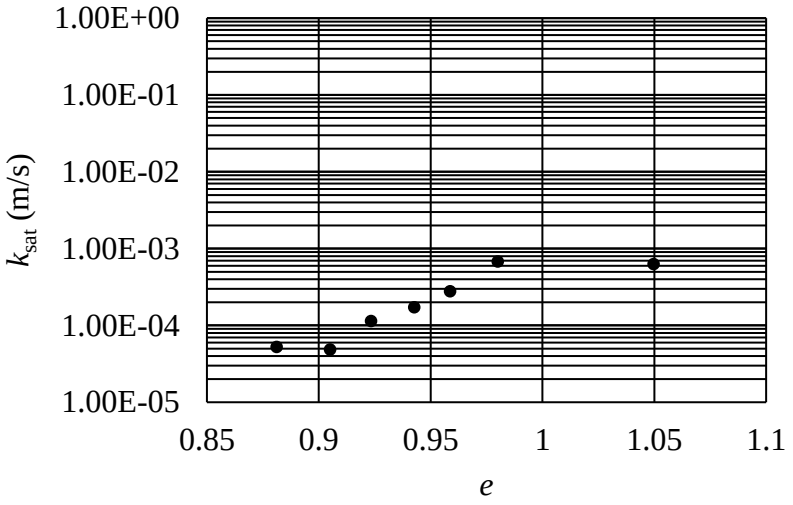

Figure A-17: Variations of saturated hydraulic conductivity k_{sat} with void ratio e for column consolidation test #1.

A.3.2 Consolidation parameters of column consolidation test #2

Figure A-18 and Figure A-19 show the variations of a_v and m_v with effective stress while a_v ranges from 4.2×10^{-4} kPa^{-1} to 2.8×10^{-3} kPa^{-1} and m_v is between 1.9×10^{-4} kPa^{-1} and 1.3×10^{-3} kPa^{-1}. These two parameters from the second column consolidation test is close to those from the first test.

Figure A-20 shows that the coefficient of consolidation c_v ranges from 7.5×10^{-2} to 2.3×10^{-1} cm^2/s, which is similar to the range of c_v in the first test. The variation trend of k_{sat} is reasonable since the water flow is reduced by decreased void.

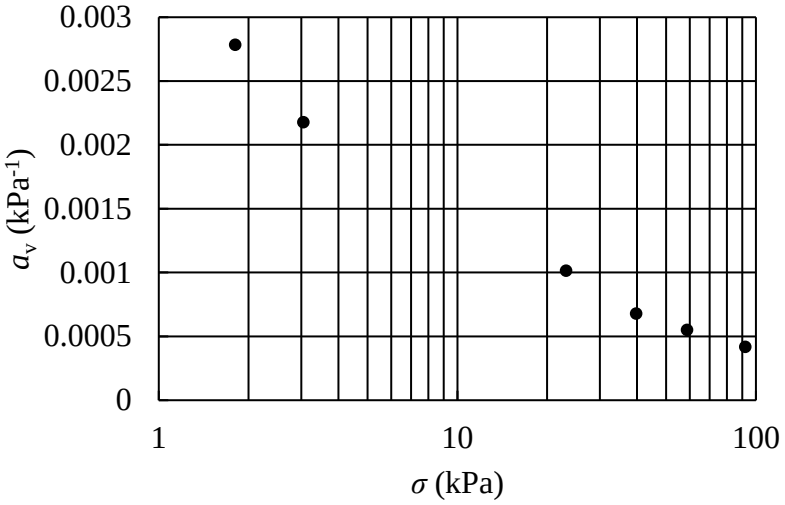

Figure A-18: Variations of coefficient of compressibility a_v with axial effective stress σ' for column consolidation test #2.

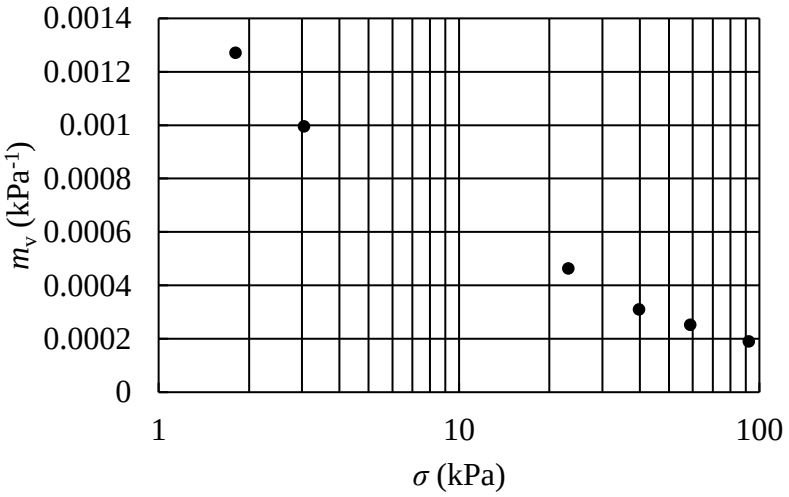

Figure A-19: Variations of coefficient of volume compressibility m_v with axial effective stress σ' for column consolidation test #2.

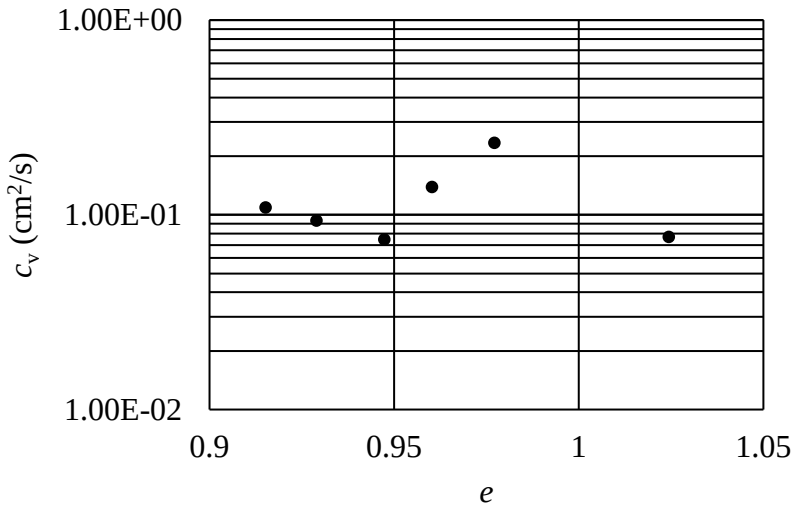

Figure A-20: Variations of coefficient of consolidation c_v with void ratio e for column consolidation test #2.

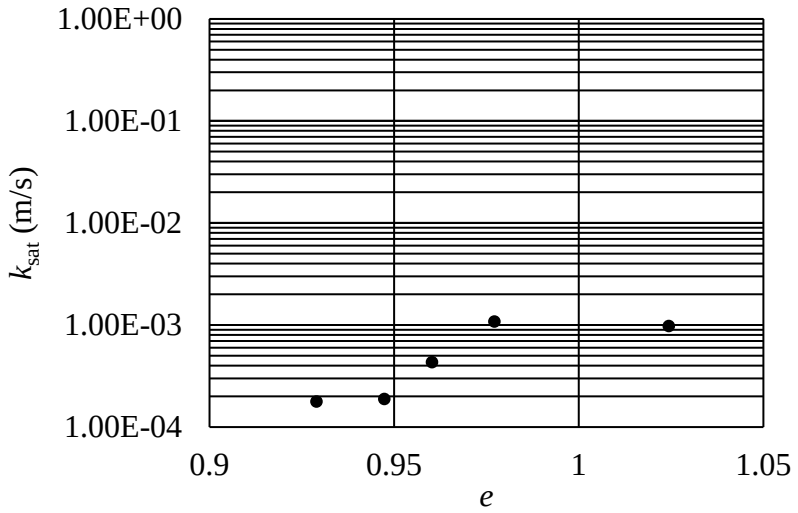

Figure A-21: Variations of saturated hydraulic conductivity k_{sat} with void ratio e for column consolidation test #2.

A.3.3 Consolidation parameters of oedometer test

Figure A-22 and A-23 shows the variations of a_v decreasing from 8.7×10^{-3} to 5.5×10^{-4} kPa^{-1} and m_v decreasing from 4.3×10^{-3} to 2.7×10^{-4} kPa^{-1} with effective stress increasing, which are quite close to those obtained from column consolidation test and indicate the validity of oedometer test.

Obtained c_v is ranged from 2.35 to 6.5×10^{-3} cm^2/s. ksat by back-calculation is about 4.1 to 8.8×10^{-6}m/s at void ratio between 0.92 to 1.008, which fits the result by Rodet (2019).

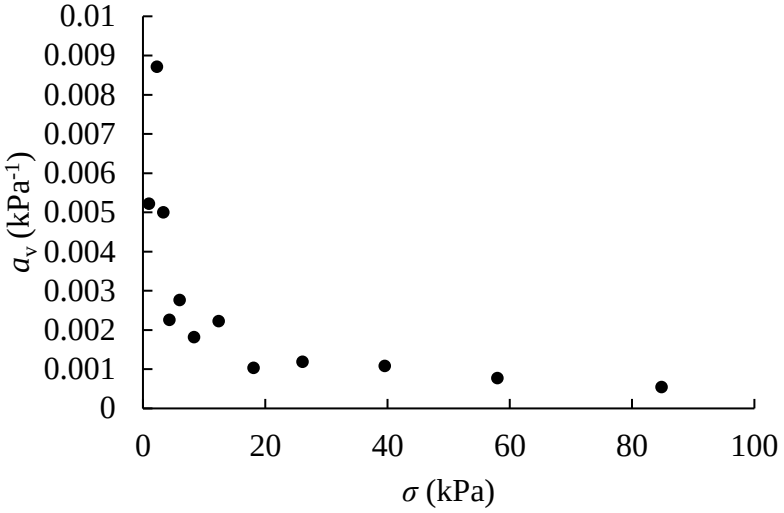

Figure A-22: Variations of coefficient of compressibility a_v with axial effective stress σ' for oedometer test.

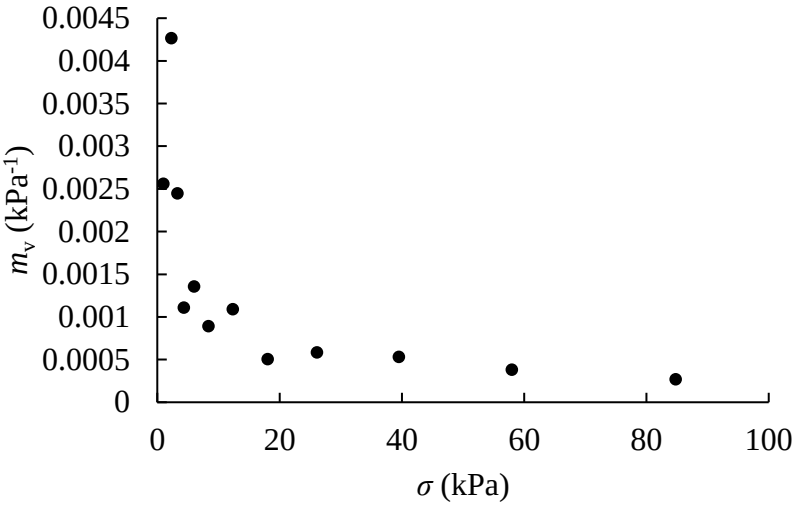

Figure A-23: Variations of coefficient of volume compressibility m_v with axial effective stress σ' for oedometer test.

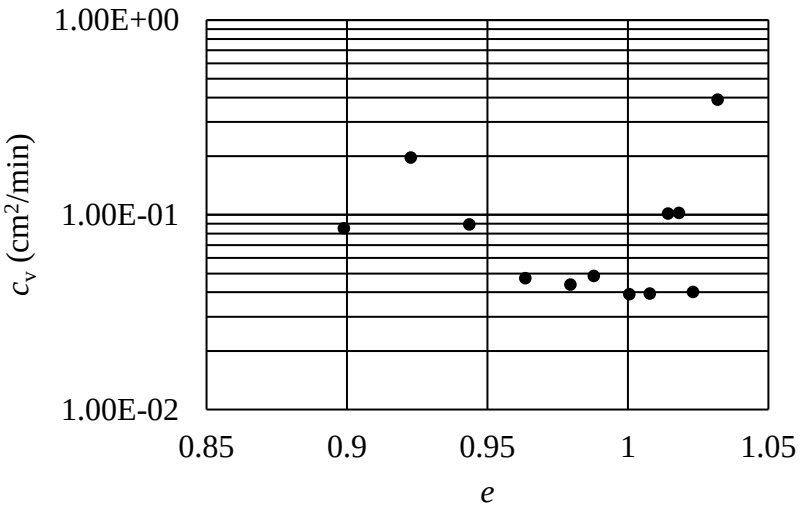

Figure A-24: Variations of coefficient of consolidation c_v with void ratio e for oedometer test.

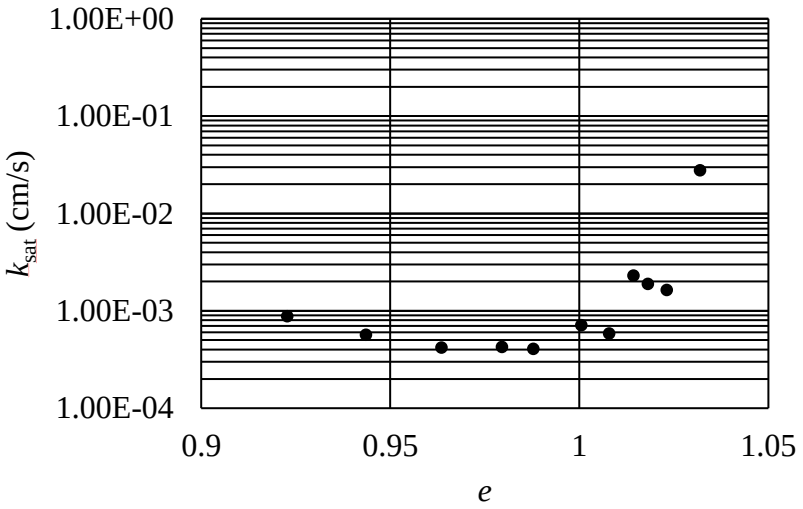

Figure A-25: Variations of saturated hydraulic conductivity k_{sat} with void ratio e for oedometer test.

APPENDIX B ADDITIONAL RESULTS RELATED TO CHAPTER 4

B.1 Calibration of shrinkage curves by the Fredlund model

A number of mathematical models have been proposed to describe the shrinkage curve. These models usually contain several fitting parameters, which have or have no physical meanings (McGarry and Malafant 1987; Tariq and Durnford 1993; Peng and Horn 2005; Chen and Lu 2018). Among them, the Fredlund model is commonly used due to its simplicity. It is expressed as follow (Fredlund et al. 2002):

$$e_w = a_{sh}[\frac{\omega^{c_{sh}}}{b_{sh}^{c_{sh}}} + 1]^{1/c_{sh}} \quad \text{(B-1)}$$

where a_{sh} is the minimum void ratio, e_f; b_{sh} is the shrinkage limit; c_{sh} is the curvature of the residual shrinkage stage; and a_{sh}/b_{sh} is equal to G_s/S_r, which is a constant value for a specific soil. This means b_{sh} can be determined once the minimum void ratio e_f is a known value.

The Fredlund shrinkage model is used to fit the obtained shrinkage curves in Chapter 4 due to its simple mathematical form and valid physical meanings for the fitting parameters. Figure B-1 shows an example of the curve fitting of the shrinkage curve obtained for CPB with 3% cement content and 80% initial water content. The curve fitting was conducted with nonlinear regression algorithm in the Solver® built in Microsoft Excel.

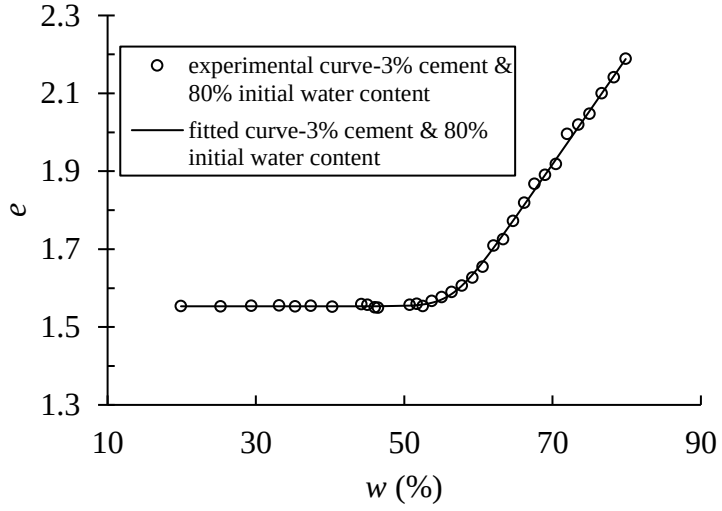

Figure B-1: An example of curve fitting of the shrinkage curve obtained for CPB specimen with cement content of 3% and initial water content of 80%.

Table B-1 shows the fitting parameters of the obtained shrinkage curves for the tailings specimens by using the Fredlund model. As explained previously, the fitting parameter a_{sh} represents the final void ratio (e_f). Variation of a_{sh} is seen to be consistent with the variation of e_f shown in Chapter 4. The parameter b_{sh} represents the slope of line of tangency, which can be an indicator of the shrinkage limit (w_s). Table B-1 shows that the variation of b_{sh} is also consistent with the variation of w_s shown in Chapter 4. The values of R (correlation coefficient) and RMSE (root mean squared error) indicate the agreement between the experimental results and the used model. A good agreement requires the value of R to be as close as possible to 1 and the value of RMSE to be as small as possible. The high values of R (>0.99) and low values of RMSE (<0.01) in Table B-1 indicate that the Fredlund model can be used to fit the obtained shrinkage curves of CPB in this study. The obtained fitting parameters along with Eq. (B-1) can then be used in the numerical modeling to estimate the shrinkage response of the uCPB and CPB. It can also be used with the soil water retention curve to describe the volume (void ratio) variation versus the suction.

Table B-1: The obtained fitting parameters of shrinkage curves by using the Fredlund model.

Specimen	Fitting Parameters			Statistical Parameters	
	a_{sh}	b_{sh}	c_{sh}	R	RMSE
w_0= 40%, C_0 = 0% cement	0.8634	0.3151	18.4829	0.9981	0.0049
w_0= 50%, C_0 = 0% cement	1.0210	0.3740	71.5398	0.9990	0.0173
w_0= 60%, C_0 = 0% cement	0.9861	0.4184	3.33038	0.9958	0.0001
w_0= 80%, C_0 = 0% cement	1.0097	0.3726	33.4840	0.9999	0.0123
w_0= 100%, C_0 = 0% cement	1.0510	0.3850	14.5836	0.9996	0.0158
w_0= 40%, C_0 = 3% cement	1.0280	0.3742	23.5153	0.9904	0.0063
w_0= 50%, C_0 = 3% cement	1.2500	0.4562	40.2004	0.9966	0.0039
w_0= 60%, C_0 = 3% cement	1.4077	0.5137	33.7888	0.9989	0.0041
w_0= 80%, C_0 = 3% cement	1.5532	0.5669	30.5485	0.9994	0.0071
w_0= 100%, C_0 = 3% cement	1.6640	0.6073	29.8483	0.9996	0.0098
w_0= 40%, C_0 = 5% cement	1.0463	0.3819	20.3496	0.9808	0.0077

w_0= 50%, C_0 = 5% cement	1.3300	0.4842	30.7849	0.9928	0.0050
w_0= 60%, C_0 = 5% cement	1.4960	0.5446	56.9437	0.9985	0.0034
w_0= 80%, C_0 = 5% cement	1.6025	0.5834	44.1909	0.9997	0.0059
w_0= 100%, C_0 = 5% cement	1.7195	0.6259	48.1659	0.9998	0.0072
w_0= 40%, C_0 = 7% cement	1.0885	0.3953	28.7380	0.9715	0.0072
w_0= 50%, C_0 = 7% cement	1.3333	0.4841	37.7877	0.9746	0.0060
w_0= 60%, C_0 = 7% cement	1.4627	0.5311	24.5191	0.9964	0.0063
w_0= 80%, C_0 = 7% cement	1.6221	0.5890	40.0078	0.9996	0.0059
w_0= 100%, C_0 = 7% cement	1.7978	0.6528	44.5208	0.9995	0.0103

B.2 Volume shrinkage rate (ε_v)

Volumetric shrinkage rate is commonly used to capture the degree of volume shrinkage as it can eliminate the effects of the initial void ratio. The volumetric shrinkage rate ε_v can be expressed as follows (Tang et al. 2011):

$$\varepsilon_v = \frac{V_0 - V_f}{V_0} \times 100\% \quad \text{(B-2)}$$

Figure B-2 shows the variation of the volumetric shrinkage rate of CPB and uCPB as a function of the cement content when the initial water content varies from 40% to 100%. For uCPB, the value of volumetric shrinkage rate is always higher than the CPB as the cement hydration products tend to fill the inner voids and limit the volume variation. The value of ε_v is closely related to the initial water content. Higher initial water content means higher void ratio and compressibility, resulting in higher volume variation and value of ε_v.

When the cement is added, the volumetric shrinkage rates first decrease as cement content increases from 0% to 3% and then remain almost constant with the further increase of the cement content from 3% to 7%. These results are consistent with the obtained shrinkage curves shown in Chapter 3. In addition, the effect of cement on ε_v are similar to those reported by Zhang et al. (2010) for cemented dredged sludge, which also showed decrease of the volumetric shrinkage rate due to the increased cement content (Zhang et al. 2010).

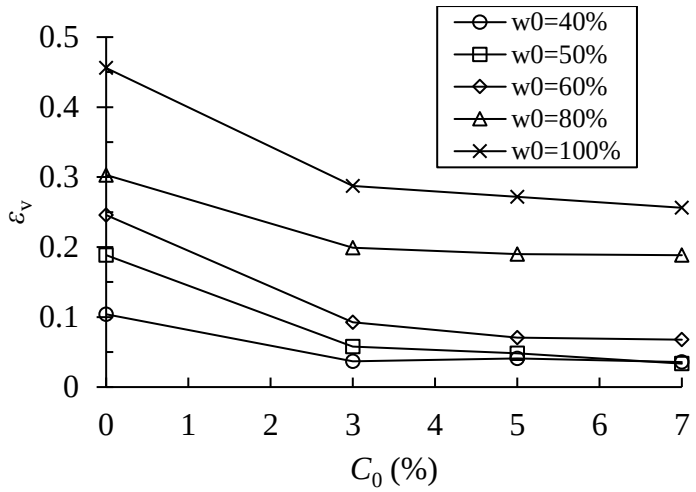

Figure B-2: Variations of the volumetric shrinkage rate ε_v as a function of the cement content under different initial water contents.

B.3 Evolution of water content and void ratio

B.3.1 Water content (*w*) versus time (*t*)

Figure B-3 shows the variation of water content *w* with time *t* (h) for different cement contents when the given initial water content is 100, 80, 60, 50 and 40%, respectively. In all cases, one sees that the water content *w* decreases quickly at the beginning. The decrease rate gradually decreases with more time of drying. The constant water decrease rate has also been found in tailings' desiccation (Simms et al. 2017) and clay (Nahlawi and Kodikara 2006; Tang et al. 2011). According to evaporation test of Wilson et al. (1994), the decrease rate of *w* includes constant zone, falling rate zone and final stabilized zone in which constant decrease rate comes from the same temperature and relative humidity RH as well as the saturated state at beginning. The CPB with higher cement content shows a slightly slower decrease of water content with time increase. The result indicates the consumption of water by hydration could not be dominant factor, otherwise the water decrease rate could be influenced obviously at the initial of desiccation. The variation of water content decrease rate by cement content could be caused by the decrease of hydraulic conductivity (Fall et al. 2009) and finer pore structure due to cementation bond between grains. According to research of Fall et al. (2009) the decrease of hydraulic conductivity is not very obvious in the first few days and this could be the reason why decrease rate of *w* is less affected by cement content.

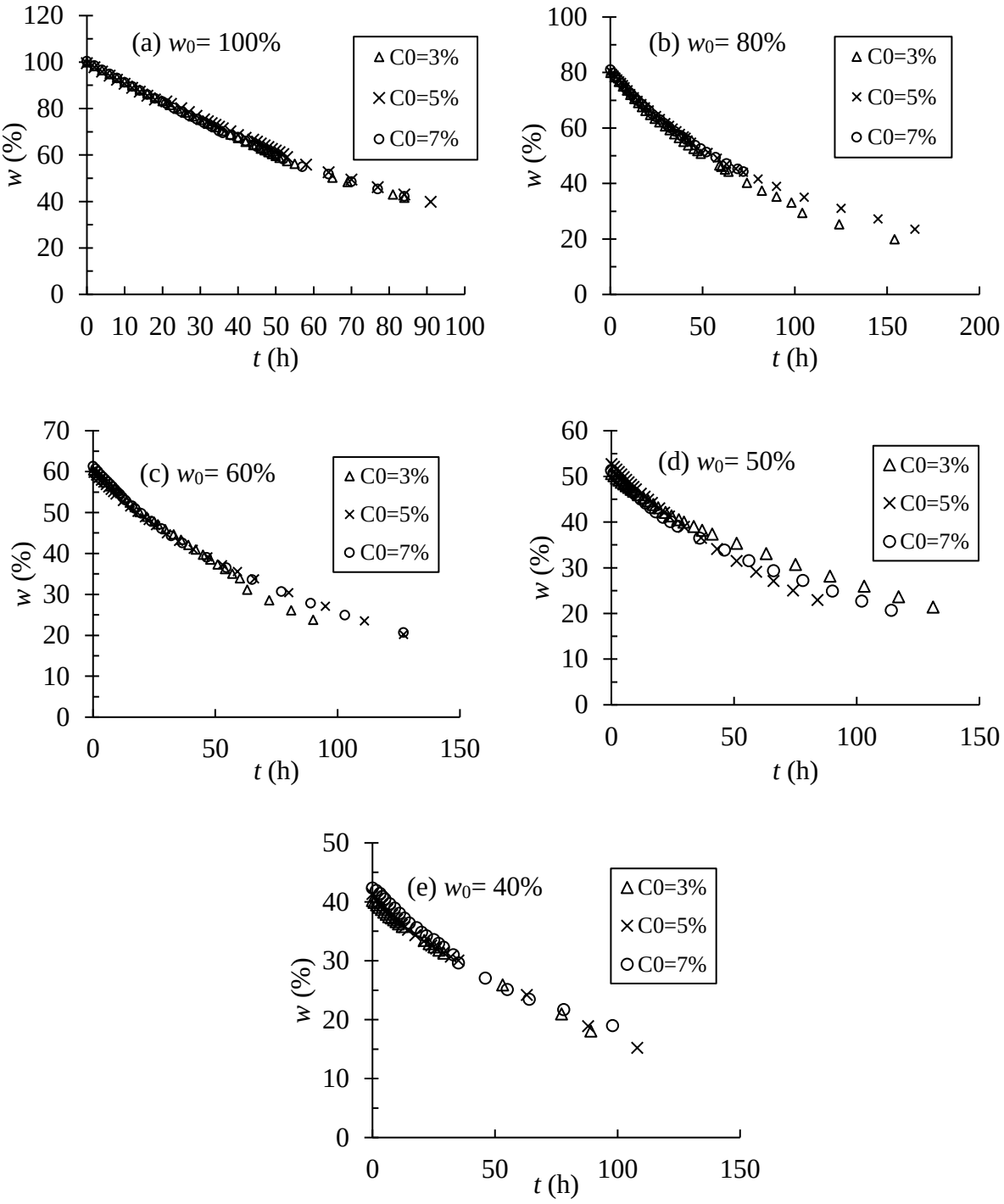

Figure B-3: Water content *w* versus desiccation time *t* with different cement contents under initial water content of (a) 100%, (b) 80%, (c) 60%, (d) 50%, and (e) 40%.

Figure B-4 shows the relationship of *w* versus *t* with different initial water contents at a given cement content. CPB with w_0 from 60% to 80% shows the same and almost constant decrease rate

of *w* at the initial stage. The same decrease rate at beginning is reasonable since the water ponding firstly occurs at the top of CPB and the water evaporation from ponded water is the same. The CPB with low w_0 of 40% and 50% does not show the ponded water and the water evaporation is much slower and the water content decrease stabilizes soon due to the rapid transferring to unsaturation. After constant rate zone, the decrease of *w* gradually slows and CPB with initial low water content enters the falling rate zone sooner. Compared with desiccation of clay, the effect of suction on the decrease rate of *w* is quite obvious and the water content decrease slows down rapidly (Tang et al. 2011). But for CPB, the developed suction preventing water evaporation is much smaller and therefore leads to a gradually decrease of evaporation rate.

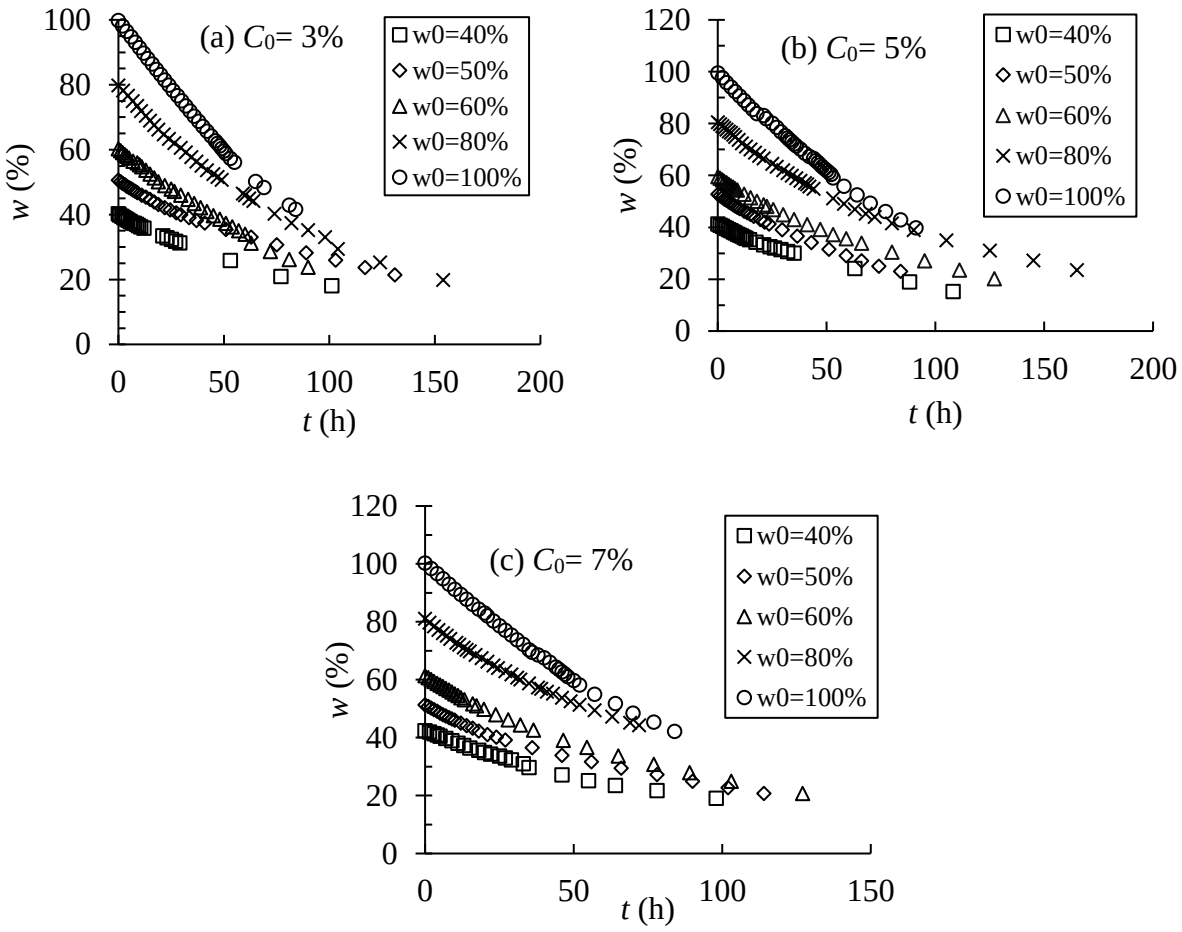

Figure B-4: Water content *w* versus desiccation time *t* with different initial water contents under cement content of (a) 3%, (b) 5%, and (c) 7%.

B.3.2 Void ratio (*e*) versus time (*t*)

According to the measurement of time, the variation of *e* and *w* with elapsed time is investigated, which can help to capture the time-dependent behavior of volume shrinkage by evaporation. Figure B-5 shows the variation of void ratio *e* with time under different cement contents at the given initial water content. For CPB with high initial water content like 80% and 100%, the decrease rate of void ratio is slightly affected by the cement content and keeps constant, indicating the low range of cement contents has less influence on the evaporation under high-water content. For low range of water content from 40% to 60%, the decrease rate of void ratio will decrease soon, which is obviously caused by the rapid unsaturation of these low-water content specimen. In all specimens, the higher cement content is seen to accelerate the void ratio's decrease to final void ratio, which can be explained that the CPB with higher cement content can obtain higher resistance to deformation sooner during evaporation and this has been discussed in the Chapter 4.

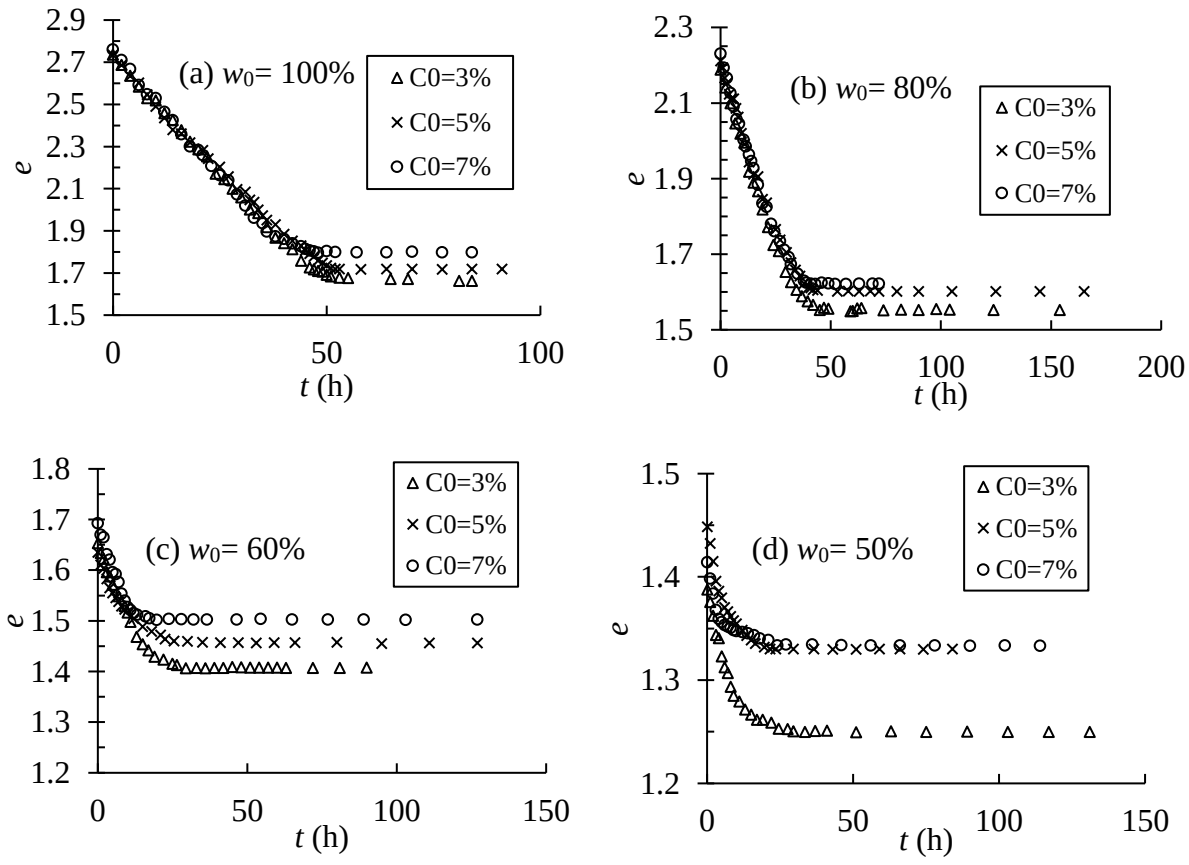

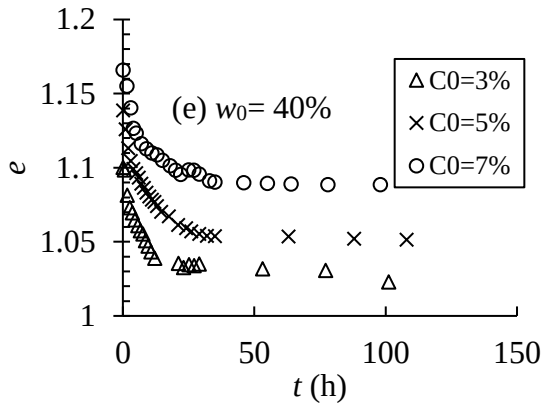

Figure B-5: Void ratio *e* versus desiccation time *t* for CPB with different cement contents under initial water content of (a) 100%, (b) 80%, (c) 60%, (d) 50%, and (e) 40%.

Figure B-6 shows relationship of *e* versus *t* under different initial water content for a given cement content. CPB with higher initial water content undergoes longer time to the stabilization of void ratio. The CPB with high water content having a more dispersive grain spacing and loose structure requires more time to obtain the enough resistance and grain contact to resist the deformation under capillary suction. The decrease rate of *e* at initial stage for CPB at w_0 = 60% to 100% is the same, which actually comes from the same decrease rate of *w* due to $e = wG_s$ in saturation stage.

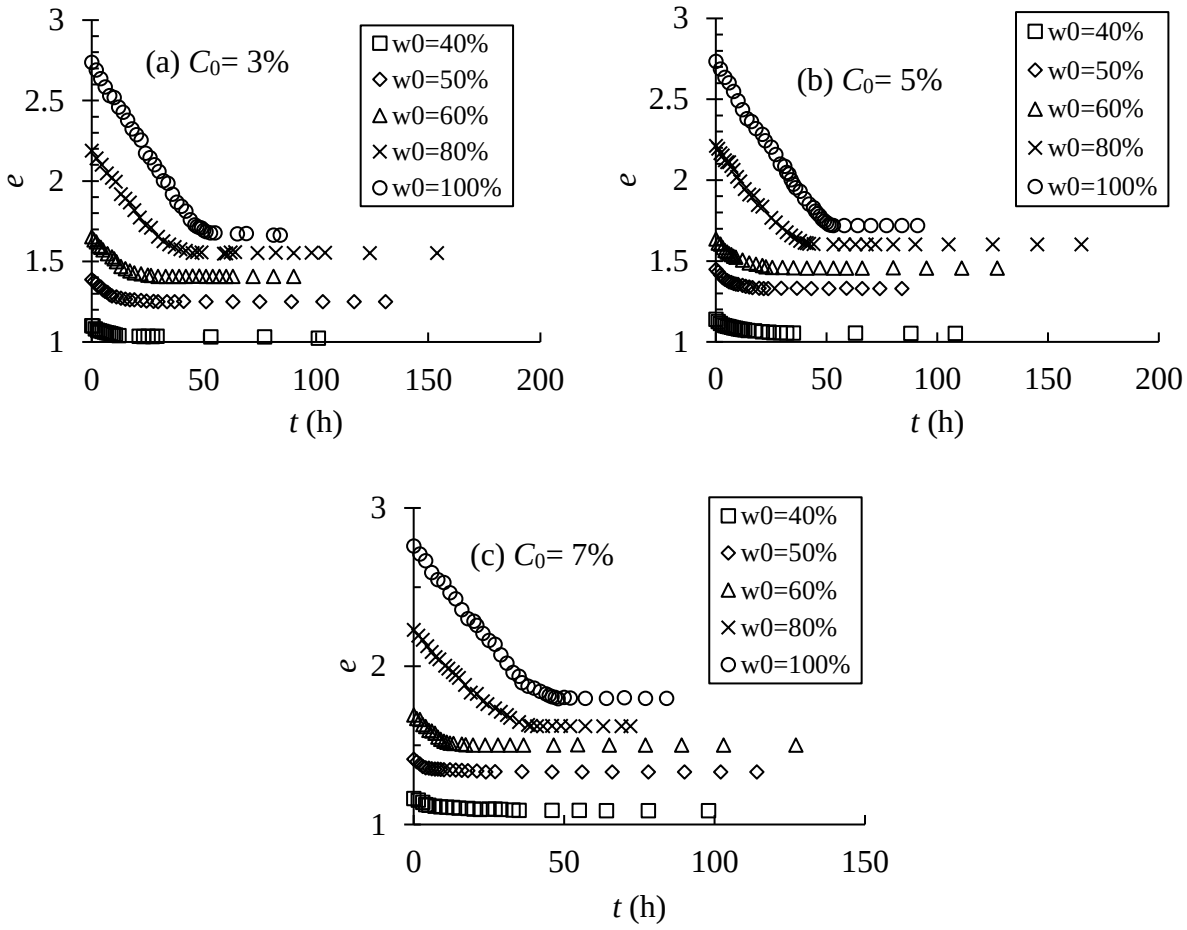

Figure B-6: Void ratio e versus desiccation time t with different initial water contents under cement content of (a) 3%, (b) 5%, and (c) 7%.

B.4 Results of shrinkage tests of CPB after 12 hours' curing

The CPB after 12 hours' curing was also studied for the shrinkage behavior. The shrinkage curves and corresponding shrinkage parameters are given as the Chapter 4. The interpretation of the experimental results will not be presented since the variations of shrinkage curves and shrinkage parameters are similar to those of CPB without curing time.

B.4.1 Shrinkage curves

Figure B-7 shows the shrinkage curves of CPB after 12h curing with varied cement content under the given initial water content.

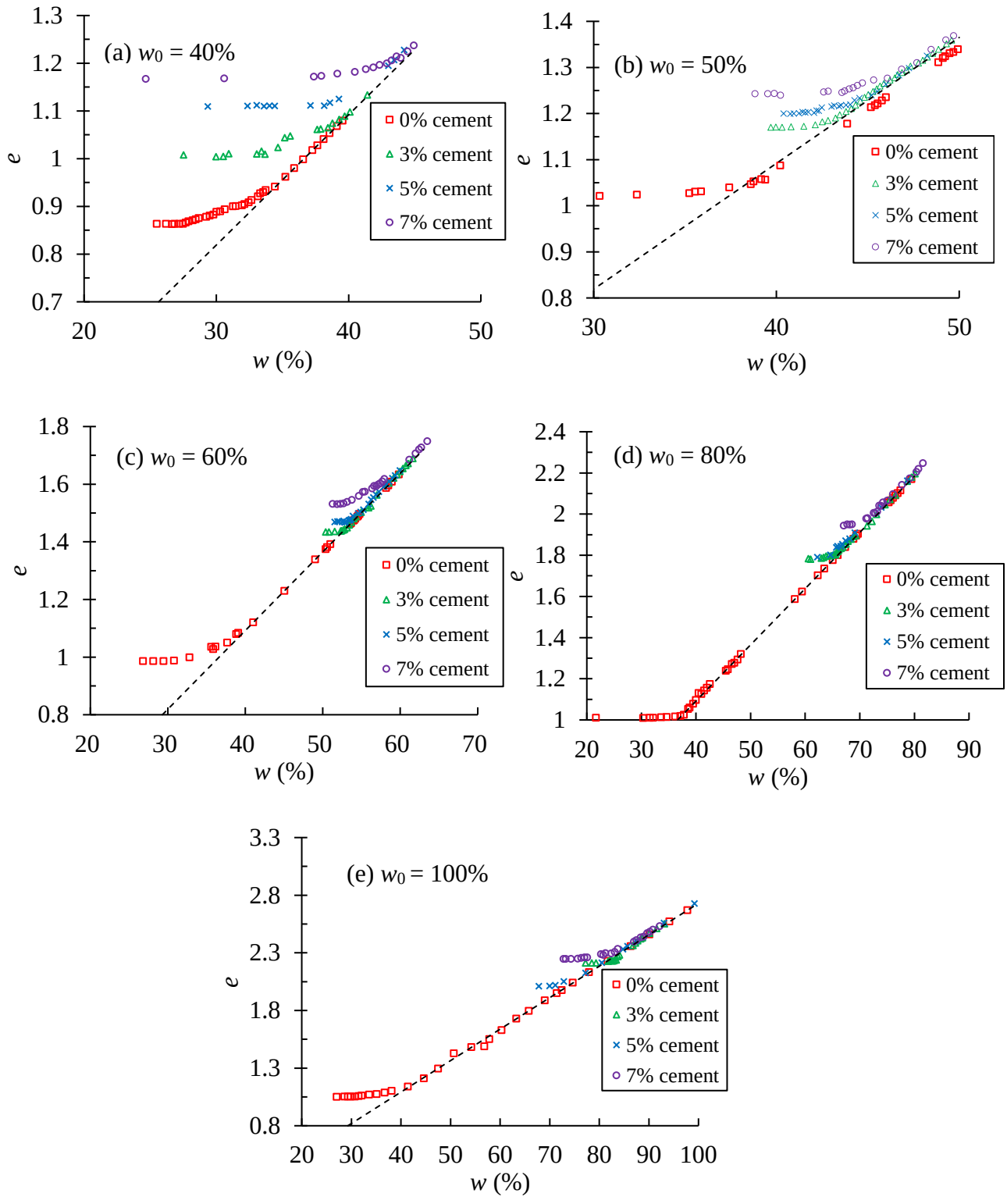

Figure B-7: Shrinkage curves of uncemented and cemented tailings with different cement contents under the initial water content of (a) 40%, (b) 50%, (c) 60%, (d) 80%, and (e) 100%.

Figure B-8 shows the shrinkage curves of CPB after 12h curing with varied initial water content under the given cement content.

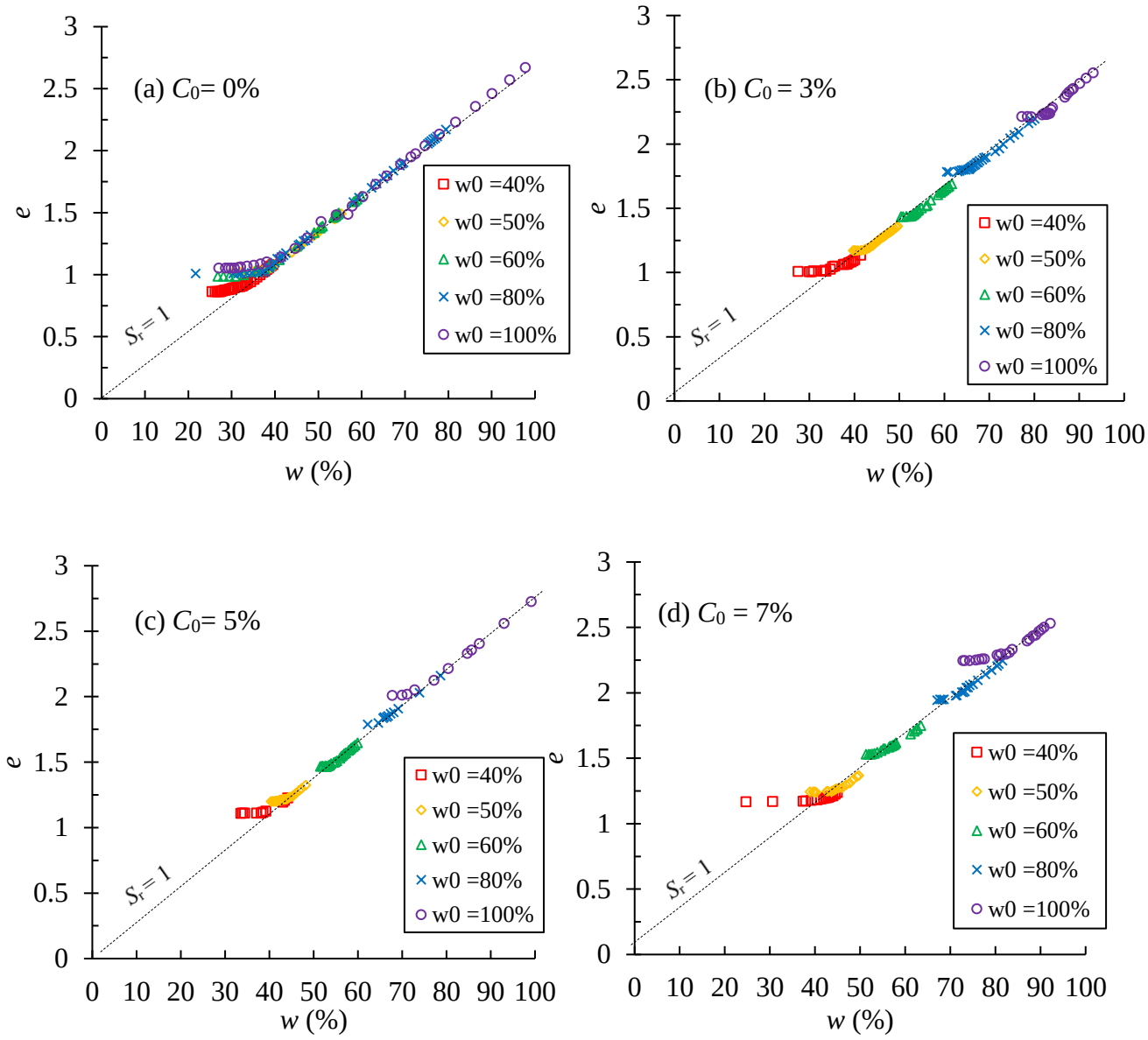

Figure B-8: Shrinkage curves of tailings with different initial water contents under the cement content of (a) 0%, (b) 3%, (c) 5%, and (e) 7%.

B.4.2 Shrinkage parameters

Table B-2 shows the shrinkage parameters determined from the shrinkage curves of CPB with 12h curing.

Table B-2: Parameters of the prepared CPB with curing and calculated from the shrinkage tests.

Targeted *iwc* (%)	Obtained *iwc* (%)	C_0 (%)	w_s (%)	w_{AEV} (%)	Δw (%)	e_0	e_f	Δe
40%	38.97	3	34.24	36.10	4.73	1.07	0.94	0.13
50%	49.59	3	42.72	43.81	6.87	1.36	1.17	0.19
60%	61.63	3	52.35	52.31	9.28	1.69	1.43	0.26
80%	80.11	3	65.08	65.55	15.03	2.20	1.78	0.42
100%	99.16	3	73.19	77.23	25.97	2.73	2.01	0.72
40%	44.20	5	40.39	44.44	3.81	1.23	1.11	0.12
50%	48.24	5	43.69	45.20	4.55	1.33	1.20	0.13
60%	59.95	5	53.48	53.67	6.47	1.65	1.47	0.18
80%	78.69	5	65.16	68.11	13.53	2.16	1.79	0.37
100%	101.27	5	80.72	81.78	20.55	2.78	2.21	0.57
40%	44.93	7	42.38	39.00	2.55	1.24	1.17	0.07
50%	49.70	7	45.12	46.86	4.58	1.37	1.24	0.13
60%	63.49	7	55.60	57.69	7.89	1.75	1.53	0.22
80%	81.57	7	70.56	72.57	11.01	2.25	1.94	0.31
100%	102.86	7	81.55	83.13	21.31	2.83	2.25	0.58

Shrinkage limit (w_s) *and final void ratio* (e_f)

Figure B-9 shows the variations of w_s and e_f with cement content under given initial water content. The effect of cement content on the shrinkage limit and final void ratio of CPB with 12h curing is similar to that on CPB without curing.

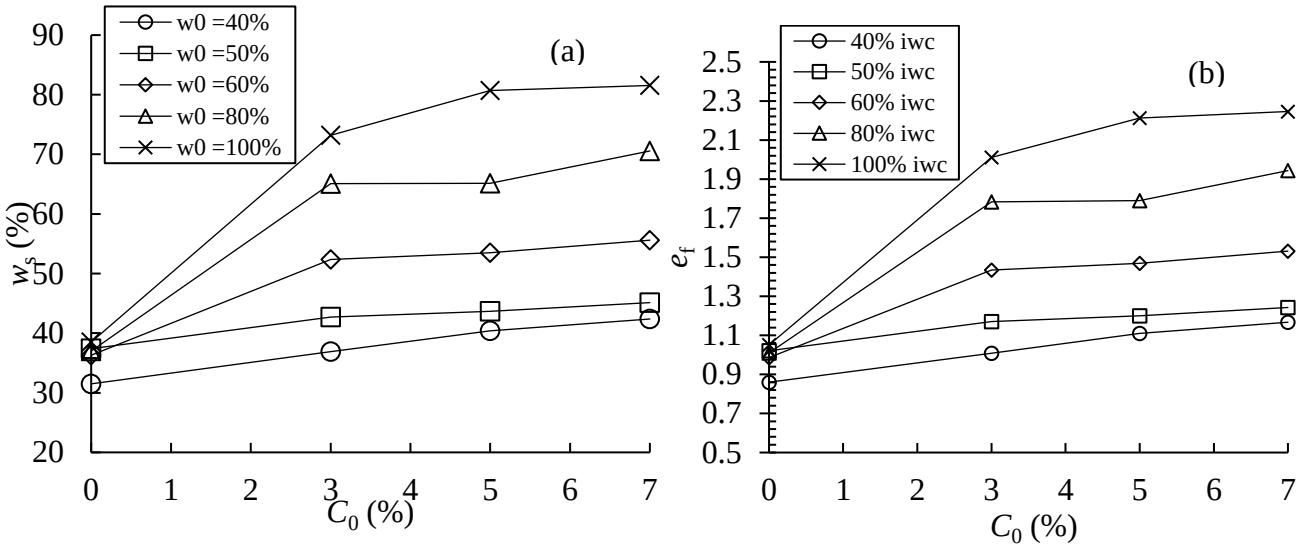

Figure B-9: Variations of (a) the shrinkage limit w_s, and (b) final void ratio e_f as a function of the cement content under different initial water content.

Volumetric shrinkage rate (ε_v)

Figure B-10 shows the variations of volumetric shrinkage rate for CPB with curing time as cement content increases and the slight effect of increased cement content on ε_v is similar to CPB without curing.

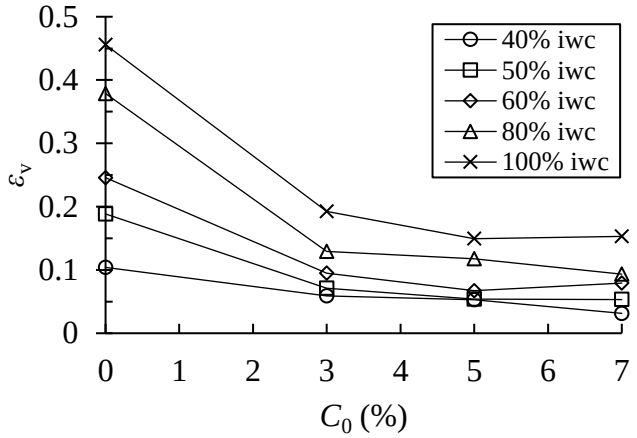

Figure B-10: Variations of the volumetric shrinkage rate as a function of the cement content under different initial water contents.

desaturation onset water content (w_{AEV})

Figure B-11 shows the variations of desaturation onset water content w_{AEV} with initial water content or with cement content.

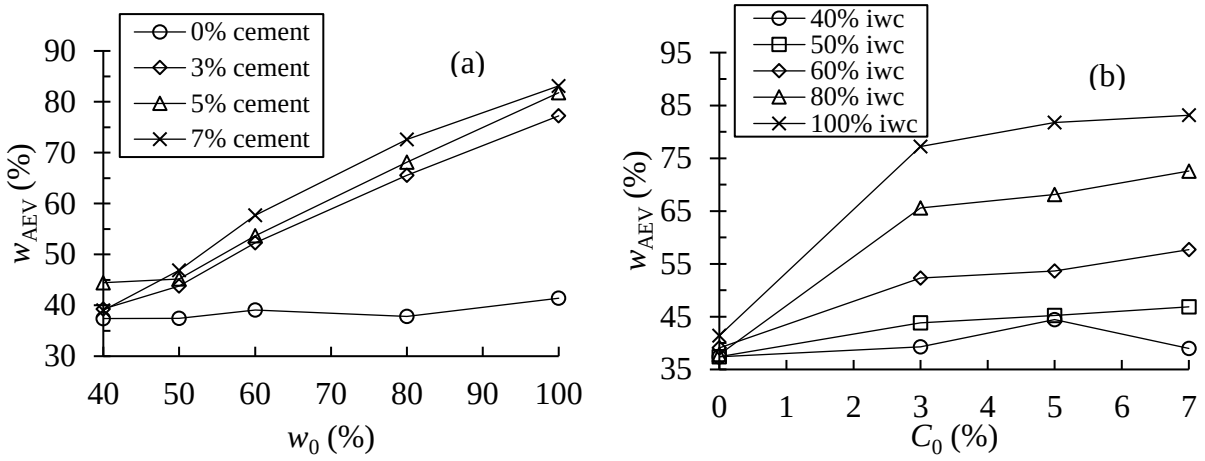

Figure B-11: (a) Variations of the w_{AEV} as a function of the initial water content under different cement contents; (b) Variation of the w_{AEV} as a function of the initial cement content under different initial water contents.

B.4.3 Comparison between shrinkage curves of CPB with and without 12 hours' curing

To investigate the effect of cement hydration on the shrinkage response of CPB, the CPB were placed in the mold and cured for 12 hours without water evaporation by sealing the mold with plastic sheets. The experimental procedures were identical to that explained in Chapter 4. Figure B-12 shows the shrinkage curves of the tailings specimens without curing and cured for 12 hours, with different initial water content under the cement content of 5% (Figure B-12(a)) and 7% (Figure B-12(b)). The results show that the 12 hours of curing can significantly influence the shrinkage response of the cemented tailings with high water content of 80% and 100%, resulting in shorter normal shrinkage stage and higher shrinkage parameters for cured tailings specimens. This influence can be more obvious for tailings with higher cement content (7%). For tailings with relative low water content of 40%, 50%, and 60%, the 12 hours of curing only slightly influence the shrinkage response, resulting in similar normal shrinkage stage and shrinkage parameters between the cured and uncured CPB. The curing time of 12 hours allows the rapid development of hydration products and stiffness increase, then the growing effect of restraining the shrinkage.

It is obvious that the CPB with higher initial water content undergo a larger volume decrease and therefore are more easily affected by the cement hydration. On the contrary, specimen with lower initial water content shows the slight variation since its void ratio decrease is relatively small.

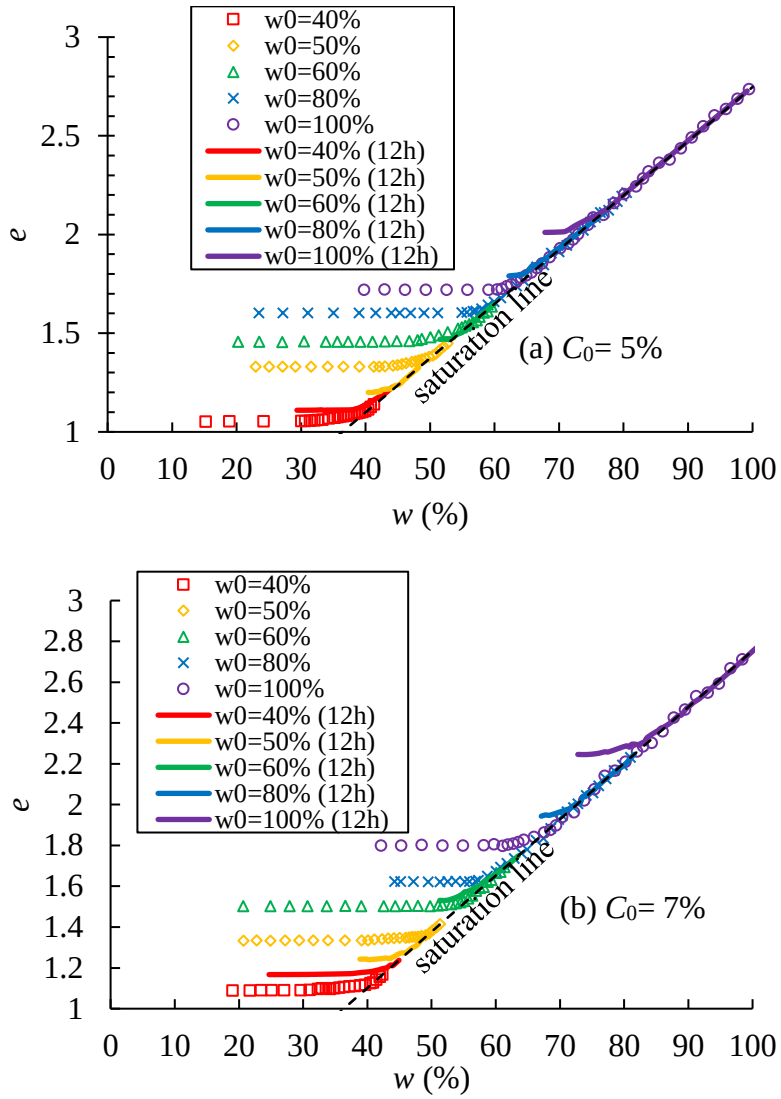

Figure B-12: Shrinkage curves of CPB with different water contents under the cement content of (a) 5% and (b) 7%, cured for 12 hours and without curing.